Spectroscopic and Functional Characterization of the Heme Proteins Nitrophorin 4, Nitrophorin 7, and Selected Site-Directed Mutants: Studies of Their Nitrite Reactivity and of the Ferroheme Forms

Inaugural-Dissertation

zur

Erlangung des Doktorgrades der

Mathematisch-Naturwissenschaftlichen Fakultät

der Heinrich-Heine-Universität Düsseldorf

vorgelegt von

Chunmao He

aus **Chenzhou, P.R.China**

Mülheim an der Ruhr, December 2011

Aus dem Max-Planck-Institut für Bioanorganische Chemie, Mülheim an der Ruhr

Gedruckt mit der Genehmigung der
Mathematisch-Naturwissenschaftlichen Fakultät der
Heinrich-Heine-Universität Düsseldorf

Referent: Prof. Dr. Wolfgang Lubitz
Koreferent: Prof. Dr. Henrike Heise

Tag der mündlichen Prüfung: 13.12.2011

Acknowledgements

The work presented here would not have been possible without the enormous support from the following people.

First of all, I would like to thank Professor Dr. Wolfgang Lubitz for his kind support of this project and being my supervisor. Professor Dr. Henrike Heise is also acknowledged for being the co-supervisor of my PhD study, and her critically reading of this thesis.

Dr. Markus Knipp, who guided me through the whole project, is such a nice tutor showing me not only how experiments are running, but also how interesting it is to run the experiments. His broad scientific background and attitudes towards science have great influence on this work and also on me in developing my way of doing science.

Mrs. Johanna J. Taing is gratefully acknowledged for her endless and beautiful work on the expression of the nitrophorins, which made my life much easier in the lab. We always had trainees and students from time to time in the lab, namely Mr. Fabian Kalveram, Ms. Alina Steinbach, Ms. Robyn L. Kosinsky, and Mrs. Katrin Wrede. Their contributions to this work should also be acknowledged.

Dr. Hideaki Ogata is gratefully acknowledged for his nice work on the crystallization of nitrophorins, without which most of our work would be much more difficult. Dr. Koji Nishikaw and Ms. Yvonne Brandenburger joined his team later on. I would also like to thank Dr. Martin Fuchs (Swiss Light Source at Paul Scherrer Institut), who helped us measuring the combined diffraction and UV/vis absorption spectra on the crystals of NP4(L130R).

Dr. Maria-Eirini Pandelia and Mr. Ian McPherson (University of Oxford) are gratefully acknowledged for their critically reading of part of this thesis. Mr. Thomas Lohmiller is gratefully acknowledged for his translation of the abstract into zusammenfassung.

The technical assistance from Mr. Jan Hanis, Mrs. Marion Stapper, Mr. Leslie Currell, Mrs. Gudrun Klihm, Mr. Frank Reikowski, and Mr. Norbert Dickmann was essential to my experimental work.

I would like to thank Mrs. Gülümse Koç, Mrs. Rita Gröver, Mrs. Birgit Deckers and Mr. Stephan Kempkes who helped me with the office and personnel cases, so that adaption to Germany became much easier.

We had a long time collaboration with Professor Dr. Cristiano Viappiani (University of Parma, Italy) and his team (Dr. Stefania Abbruzzeti, Dr. Stefano Bruno, and Mr. Alessandro Tinozzi) on the laser flash photolysis of the CO complexes. I would like to thank them for their kindness during my stay in Parma.

Finally, my dad and mom not only gave me my life, brought me up, more importantly they also show me how to be a kind human being with their examples. They always provide me a warm, safe, and supportive harbor. My wife Juan Liu is always there listening to me, giving suggestions to me, and accompanying me.

Zusammenfassung

Hämproteine sind sehr wichtig für lebende Organismen, wo sie an verschiedenen metabolischen Funktionen wie Katalyse, Elektronentransfer sowie der Erkennung und dem Transport gasförmiger Moleküle beteiligt sind. Nitrophorine (NP) bilden eine Familie von Ferrihäm *b*-Proteinen aus dem Speichel des blutsaugenden Insekts *Rhodnus prolixus*. Diese Hämproteine sequestrieren und stabilisieren NO, das von der Stickstoffmonoxid-Synthase (NOS) in den Endothelialzellen der Speicheldrüsen produziert wird. Während das Insekt Blut saugt, injiziert es gleichzeitig seinen Speichel in das Gewebe des Opfers, wo das an das Häm-Eisen koordinierte NO freigesetzt wird. Es existieren mindestens fünf Isoformen innerhalb der NP-Proteinfamilie, NP1-4 und NP7. Von diesen ist NP7 am wenigsten gut untersucht, obwohl es äußerst interessant im Hinblick auf seine einzigartige Phospholipidmembran-Bindefähigkeit und seine, verglichen mit den anderen NP sehr verschiedene Häm-Bindestelle ist. Daher behandelt diese Arbeit insbesondere NP7, wenngleich zu Vergleichszwecken auch NP4 untersucht wurde, da es die am besten charakterisierte Isoform ist und hochaufgelöste Strukturen davon existieren. Wo nötig, wurden sequenzspezifisch mutierte Proteinvarianten von NP4 und NP7 hergestellt und verwendet.

Erst kürzlich wurde die Hypothese aufgestellt, dass NP auch katalytische Eigenschaften besitzen. In der vorliegenden Arbeit wurde NO_2^- als Substrat von NP4 und NP7 in Betracht gezogen. Obwohl es oft vorwiegend als physiologisch unerwünschte Verbindung angesehen wird, ist NO_2^- in großen Mengen (500 nM – 10 µM) im menschlichen Blutplasma und Gewebe vorhanden. Vor Kurzem wurde es als die häufigste intravaskuläre Speicherform von NO beschrieben. Nach Inkubation von NO_2^- mit NP4 oder NP7 bei neutralem pH wurde beobachtet, dass NO gebildet wird und das andere Produkt als NO_3^- identifiziert. Die Stöchiometrie wurde als die der Nitrit-Disproportionierungsreaktion

bestimmt. Durch Absorptions- und EPR-Spektroskopie wurde außerdem gezeigt, dass NP4 und NP7 in Anwesenheit des NO- Reaktanden Phenyl-4,4,5,5-tetramethylamidazolin-1-oxyl-3-oxid (PTIO) als Katalysatoren dieser Reaktion wirken, da mehrere Formelumsätze möglich sind.

Um den Reaktionsmechanismus zu verstehen, wurden die Ausgangskomplexe von NO_2^- mit NP4 und NP7 mittels UV/Vis Absorptionsspektroskopie, Resonanz-Raman- (RR-), EPR-Spektroskopie und Stopped-Flow-Kinetik untersucht. Diese Studien ergaben zusammen mit kristallografischen Untersuchungen von Wildtyp-NP4-NO_2^- einen η^1-N-Bindungsmodus, wie er für die meisten NO_2^--Komplexe von Ferrihäm-Modellen und -Proteinen typisch ist. In einer anderen Versuchsreihe wurde eine Proteinmutante durch Austausch von Leuzin-130 in der distalen Häm-Bindestelle von NP4 gegen eine Arginin-Seitenkette erzeugt. Verglichen mit wildtyp-NP4 zeigte diese Mutante eine sehr viel geringere Reaktivität gegenüber NO_2^-. Der signifikanteste Unterschied dabei ist, dass das Netzwerk von Wassermolekülen, das im Wildtyp Aspartat-30 mit NO_2^- verbindet, in NP4(L130R) unterbrochen ist. Es wird angenommen, dass Aspartat-30 einen außergewöhnlich hohen pK_a (5,6 – 7,4) besitzt. Daher erscheint es plausibel, dass Aspartat-30 als Protonendonor dient, der essentiell für die Nitrit-Disproportionierungsreaktion ist. Dies wird zusätzlich durch eine weitere Proteinmutante NP4(D30N), die ebenfalls eine verringerte Reaktivität gegenüber NO_2^- aufweist, gestützt.

Überraschenderweise zeigt die Röntgenkristallstruktur von NP4(L130R), gemessen bei 100 K, eine Koordination von Arginin-130 zum Häm-Zentrum, wohingegen UV/Vis-, RR- und EPR-Spektren, die sowohl bei Raumtemperatur als auch in gefrorener Lösung aufgenommen wurden, einen sechsfach koordinierten High-Spin- (6cHS-) Häm-Komplex mit Wasser als sechstem Liganden ergaben. Durch dosisabhängige Röntgenbestrahlung von Kristallen, die mittels Mikroabsorptionsspektroskopie beobachtet wurden, konnte gezeigt werden, dass das Ferrihäm schon durch eine sehr niedrige Dosis (0.45 MGy)

der Röntgenstrahlung reduziert wird. Daher wird eine Koordination von Arginin-130 an das Ferrohäm bei niedriger Temperatur vorgeschlagen, was zusätzlich durch das RR-Spektrum bei 77 K des chemisch reduzierten Proteins, unterstützt wird das ein sechsfach koordiniertes Low-Spin- (6cLS-) Häm zeigte. NP4(L130R) ist somit das erste Beispiel einer Koordination von Arginin an ein Metalloporphyrin.

Der Fe^{II}-Oxidationszustand der NP wurde ebenfalls untersucht. Obwohl nicht der natürliche Oxidationszustand, rückte er vor Kurzem in den Fokus, als das Fe^{II}–CO-Derivat als isoelektronisches Modell für den $\{FeNO\}^6$-Komplex herangezogen wurde, zum Beispiel in FT-IR- und Laserblitzlichtphotolyse-Experimenten. Zunächst jedoch wurde der Effekt des routinemäßig benutzten Reduktionsmittels $Na_2S_2O_4$ auf die Disulfide der NP untersucht. Im Überschuss eingesetztes $Na_2S_2O_4$ ist in der Lage, die Disulfidbrücken zu öffnen, wie durch ^{13}C-NMR-Spektroskopie, Reversed-Phase-Chromatographie und Massenspektrometrie nachgewiesen wurde. Ferro-NP4 und -NP7 und ihre NO-Komplexe wurden dann mittels UV/Vis- und RR-Spektroskopie im Detail charakterisiert. Überraschenderweise wurde nur im Fall von NP7 beobachtet, dass die Reduktion zum Aufbrechen der Fe^{II}–N_{His}–Bindung führt. Weiter wurden die Häm-Bindestellen der Proteinmutanten NP4(D70A), NP2(V24E), NP7(E27V) und NP7(E27Q) sowie mit symmetrischem Häm rekonstituiertes NP7 charakterisiert. Wie sich dadurch herausstellte, liegt die Ursache für die geschwächte Fe^{II}–His60–Bindung in der dichten räumlichen Anordnung der Reste Glu27, Phe43 und His60 in der proximalen Häm-Bindestelle von NP7, wodurch ein Druck auf die Fe–N–Bindung hervorgerufen wird.

Insgesamt zeigt die vorliegende Studie, dass NP4 und NP7 die ersten Beispiele von Ferrihäm-Komplexen sind, die die NO_2^-–Disproportionierungsreaktion bei neutralem pH katalysieren. Dies erweitert die ohnehin sehr umfangreiche Chemie von Häm-Modellen und -Proteinen weiter. Darüber hinaus zeigte sich die einzigartige Beschaffenheit der Häm-Bindestelle von NP7 im Aufbrechen der proximalen Fe–His–Bindung in Folge der

Reduktion des Eisens zu Fe^{II}. Im Fall des Ferrohäm-Proteins lösliche Guanylylcyclase (sGC), die der wichtigste Sensor für NO in Säugern ist, bricht die Fe^{II}–His–Bindung in Folge der Bindung von NO, wodurch die Signaltransduktion eingeleitet wird. Leider steht die Struktur von sGC nicht zur Verfügung und der Mechanismus, durch den Fe^{II}–His gespalten wird, ist nicht vollständig verstanden. Die vorliegende Studie zeigt, dass sterische Spannung zusammen mit weiteren Faktoren, von denen der wichtigste sicherlich der negative *trans* Effekt von NO ist, eine bedeutende Rolle bei diesem Vorgang spielen mögen.

Abstract

Heme proteins are very important for living organisms where they are involved in all kinds of metabolic functions including catalysis, electron transfer, and gaseous molecule sensing and transportation. Nitrophorins (NPs) comprise a family of ferriheme *b* proteins from the saliva of the blood sucking insect *Rhodnus prolixus*. These heme proteins sequester and stabilize NO that is produced from the nitric oxide synthase (NOS) present in the endothelial cells of the salivary gland. When sucking blood, the insect concomitantly injects the saliva into the victim's tissue where the coordinated NO on the heme iron is released. There are at least five isoforms in the NP family, NP1-4 and NP7. Of these, NP7 is the least studied although the most exciting isoform with respect to its unique phospholipid membrane binding ability and its very different heme pocket compared to the other NPs. Therefore, this thesis has an emphasis on NP7. However, NP4 is also studied in comparison since it is the best characterized isoform and high resolution structures are available. Where required, site-directed mutant proteins of NP4 and NP7 were engineered and applied.

It was recently hypothesized that NPs may also have catalytic properties. In the present study, NO_2^- was considered a substrate for NP4 and NP7. Although often thought about predominantly as a physiologically undesired compound, NO_2^- is present in large quantities (500 nM – 10 μM) in the blood plasma and tissue of humans. Recently, it was proposed to resemble the largest intravascular storage form of NO. Upon incubation of NO_2^- with NP4 or NP7 at neutral pH, it was observed that NO is formed and the other product was identified as NO_3^-. The final stoichiometry was elucidated as the nitrite disproportionation reaction. It was further shown by absorbance and EPR spectroscopy that in the presence of the NO scavenger phenyl-4,4,5,5-tetramethylamidazoline-1-oxyl 3-

oxide (PTIO) NP4 and NP7 act as catalysts for this reaction because several turn overs are possible.

In order to understand the reaction mechanism, the initial NO_2^- complexes of NP4 and NP7 were investigated by UV/vis absorption spectroscopy, resonance Raman (RR), EPR spectroscopy, and stopped-flow kinetics. These studies together with the crystallographic investigations of wild-type NP4–NO_2^- revealed an η^1-N binding mode, which is typical for most of the NO_2^- complexes of ferriheme models and proteins. In another attempt, a mutant protein was engineered by exchanging Leucine-130 in the distal heme pocket of NP4 with an Arginine residue. This mutant shows a much lower reactivity towards NO_2^- compared to wild-type NP4. The most significant difference is that the water network connecting Aspartate-30 with NO_2^- in the wild-type is disrupted in NP4(L130R). Aspartate-30 is estimated to have an unusually high pK_a (5.6 - 7.4). It is, therefore, feasible to assume that Aspartate-30 may serve as a proton donor that is critical for the nitrite disproportionation reaction. This is further supported by another mutant protein NP4(D30N) that shows also a decreased reactivity toward NO_2^-.

Surprisingly, the X-ray crystal structure of NP4(L130R) determined at 100 K reveals an Arginine-130 coordination to the heme center where UV/vis, RR, and EPR spectra recorded both at room temperature and in frozen solutions show a six-coordinate high spin (6cHS) heme complex with water as the sixth ligand. It was shown through dose-dependent X-ray irradiation on crystals observed by micro-absorbance spectroscopy that the ferric heme is readily reduced by a very low dose (0.45 MGy) of X-ray irradiation. It is, therefore, proposed that Arginine-130 coordinates to the ferrous heme at low temperature. This was further supported by the RR spectrum of the chemically reduced protein at 77 K, which showed a six-coordinate low spin (6cLS) heme. Thus, NP4(L130R) represents the first example of an Arginine coordination to a metalloporphyrin.

The ferrous oxidation state of NPs has been also studied. Although it is not the native oxidation state, it came recently into focus when the Fe^{II}-CO derivative was used as a isoelectronic model for the $\{FeNO\}^6$ complex, for example in FT-IR and laser flash photolysis experiments. The first issue addressed was the effect of the routinely used reducing agent $Na_2S_2O_4$ on the disulfides of NPs. An excess amount of $Na_2S_2O_4$ is able to open the disulfides as has been identified by ^{13}C NMR spectroscopy, reversed phase chromatography, and mass spectrometry. Ferrous NP4 and NP7 and their NO complexes were then characterized in detail by UV/vis and RR spectroscopy. Surprisingly, it was observed that only in the case of NP7 reduction leads to the breakage of the Fe^{II}–N_{His} bond. Further characterizations were carried out on the heme pocket mutant proteins NP4(D70A), NP2(V24E), NP7(E27V), and NP7(E27Q) as well as NP7 reconstituted with symmetric heme. As a result, the spatial arrangement of the residues Glutamate-27, Phenylalanine-43, and Histidine-60 in the proximal heme pocket of NP7 is the reason for the weakened Fe^{II}–His60 bond through steric tension.

In conclusion, the present study demonstrates NP4 and NP7 being the first examples of ferric hemes that promote the NO_2^- disproportionation reaction at neutral pH. This further expands the very diverse chemistry of heme models and proteins. Moreover, the very unique property of the heme pocket of NP7 was manifested in the breakage of the proximal Fe-His bond upon reduction of the iron to Fe^{II}. In case of the ferroheme protein soluble guanylate cyclase (sGC), which is the key sensor for NO in mammals, the Fe^{II}-His bond breaks upon NO binding and, thus, initiates signal transduction. Unfortunately, the structure of sGC is not available and the mechanism by which the Fe^{II}-His is cleaved is not fully understood. The present study shows that steric tension in combination with other factors, the most important of which certainly is the negative *trans* effect of NO, may play an important role in that event.

Table of Content

Table of Content

Chapter 1. Introduction

1.1. Nitrophorins

The saliva of blood-sucking insects contains a vast variety of substances that help animals obtain a sufficient blood meal. When pumped into the tissue during a meal, these substances inhibit blood coagulation, widen the blood vessels, and suppress the immune response.[1,2] The "kissing bug" *Rhodnius prolixus* has a salivary nitrovasodilator,[3] which comprises a unique class of heme proteins.[4,5] They act as nitric oxide (NO) storage and delivery systems and have thus been named nitrophorin (*greek*: nitro = NO, phorin = carrier).[6] In its adult phase, *R. prolixus* expresses at least four nitrophorins (NPs), designated NP1-4 in the order of their abundance.[6,7] There are five instar nymphal stages before *R. prolixus* reaches its adult phase.[8] Another two NPs, designated NP5 and NP6, were identified mainly in the juvenile stages.[9] The latest member of the NP family, NP7, was identified in a cDNA library created from salivary glands of the fifth instar nymphs.[10,11] However, the protein has not been isolated from the insects.

The amino acid sequences of NP1-4 fall into two pairs, as shown in Figure 1. NP1 and NP4 share 91% amino acid sequence identity, while NP2 and NP3 share 78%.[12] NP7 has a sequence identity of 41% to NP1, 60% to NP2, 61% to NP3, and 42% to NP4, respectively.[13] The three-dimensional structures of NP1,[14] NP2,[15] and NP4[16-19] have been determined by X-ray crystallography. The overall structures of nitrophorins are similar to each other and the structure of NP2 is presented as an example in Figure 2. The structure comprises an 8-stranded *β*-barrel that is characteristic of the protein fold of lipocalins. Lipocalins are a family of proteins with a surprisingly low amino acid sequence identity, which are found in all types of living organisms and serve a variety of functions

including hormone and lipid transport, coloration, and enzymatic activity (Table 1).[20,21] In the NPs, the cofactor heme *b* is bound to the protein *via* a His ligand on the open site of the β-barrel, leaving the sixth coordination site available to bind external ligands. The structure has four Cys residues that form two disulfides, which is characteristic of lipocalins.[20,21]

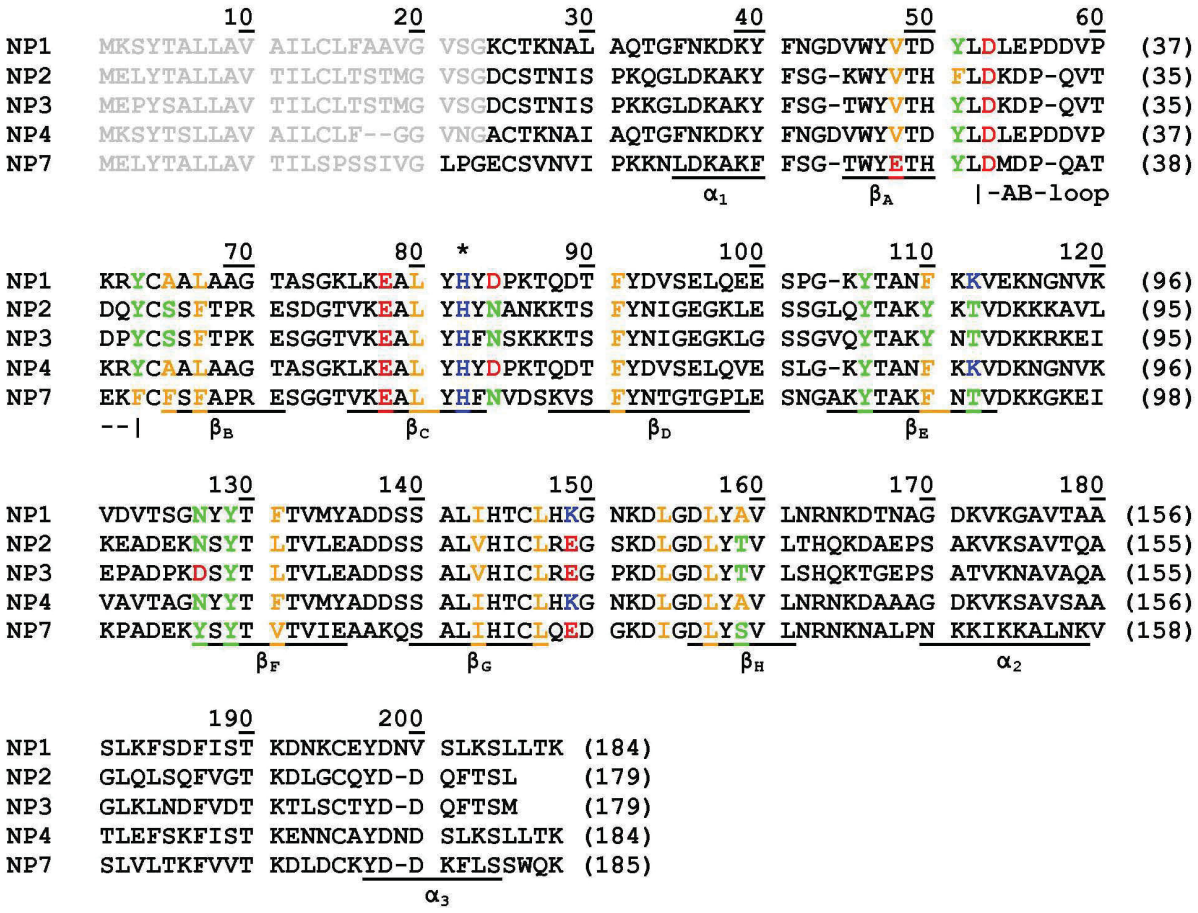

Figure 1. Amino acid sequence alignment of *R. prolixus* NP1 (Uni-Port entry Q26239), NP2 (Uni-Port entry Q26241), NP3 (Uni-Port entry Q94733), NP4 (Uni-Port entry Q94734), and NP7 (Uni-Port entry Q6PQK2). Signal sequences for secretion are colored gray. The amino acid residue numbering given at the end of each line is for the truncated forms throughout this thesis. The proximal His is indicated with an asterisk (*). The secondary structure elements, α-helices (α) and β-sheets (β), are given on the basis of the crystal structure of NP2 (PDB code 1EUO) and the homology model of NP7.[22]

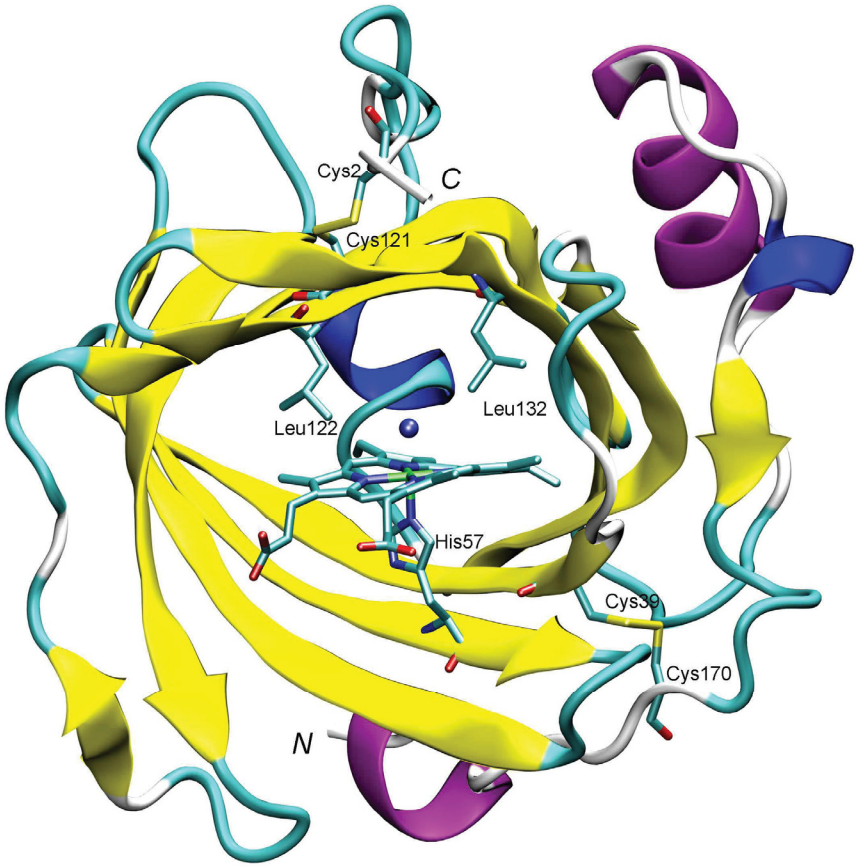

Figure 2. X-ray crystal structure of NP2 from *R. prolixus* with NH_3 as proximal heme ligand (PDB code 1EUO).[15] The N– and C–termini are designated with italic letters. The four Cys residues, the two Leu residues pointing toward the heme plane, the heme cofactor, and the proximal His57 are presented as stick models.

Table 1. Selected examples of lipocalin proteins.

Lipocalin	Residues	Disulfide	pI	Ligand	Ref.
AGP[a]	183	2	4.97		23-25
ApoD[b]	169	2	5.7	progesterone, arachidonic acid	26-28
C8γ[c]	182	1	8.67		29,30
GLY[d]	162	2	6.02		31,32
α_1m[e]	183	1	6.68	heme	33-35
NGAL[f]	178	1	9.77	enterobactin	36,37
OBP[g]	155	1	7.44		38,39
PGDS[h]	168	1	8.63	prostaglandin D	40
RBP[i]	183	3	5.42	all-trans retinol	41,42
Tlc[j]	158	1	5.2	stearic acid, palmitic acid, cholesterol	43,44

[a] α_1-Acid glycoprotein. [b] Apolipoprotein D. [c] Complement factor 8γ chain. [d] Glycodelin. [e] α_1-Microglobulin. [f] Neutrophil gelatinase associated lipocalin. [g] Odorant-binding protein. [h] Lipocalin-type prostaglandin D synthase. [i] Retinol-binding protein. [j] Tear lipocalin.

As has been mentioned previously, the biological function of NPs is to store and transport NO, which is accomplished in the ferric oxidation state. NO, which is produced by a nitric oxide synthase (NOS) enzyme in the gland endothelium,[45-47] forms very stable complexes with NPs in the salivary gland ($\{FeNO\}^6$)[48†]. Upon injection into the victim's blood,[49,50] the drastic pH change to ~ 7.4 induces a conformational change of the NP structure so that the affinity of NO is decreased by 1-2 orders of magnitude.[15,16,51] Together with the large dilution into the blood stream, this facilitates the release of NO.

It should be mentioned that unlike metMb and metHb the ferric oxidation state in NPs is preserved against the so-called "auto-reduction" upon binding of NO (see *Chapter 1.3.2*). The reduction potential of NPs (e.g., -303 mV vs SHE at 28 °C, pH 7.5 for NP1)[52] is much lower compared to that of horse Mb (~0 mV vs SHE at 28 °C, pH 7.5).[52,53] The stabilization of the ferric oxidation state is accomplished by several carboxylates around the heme pocket and a ruffled heme geometry induced by two Leu residues that point toward the heme plane (Figure 2).[54,55] This feature of NPs is crucial for their function as NO transporters, since an Fe^{II}–NO ($\{FeNO\}^7$) complex with dissociation constants in the picomolar range, would be too stable to allow the effective dissociation of NO upon injection into the victim's blood.[56]

1.2. The physiology of nitric oxide

1.2.1. Sources of nitric oxide in biology

Historically, NO has been considered a poison gas to humans even at very low doses (e.g., inhaled ≥ 80 ppm, methemoglobinemia).[57,58] However, it was realized in the 1980s that humans are capable of synthesizing NO for immune defense and signaling.[59-61] In

[†]According to the notation of *Enemark and Feltham*, the superscript represents the number of electrons (5 *d* electrons from Fe, and 1 π electron from NO), but the charge distribution is usually ambiguous.

1992, it was selected as “molecule of the year” by the journal *Science*[62] and shown to be a central signaling molecule in the cardiovascular system by Ignarro, Furchgott, and Murad,[63-65] who jointly won the Nobel Prize in Physiology or Medicine in 1998. In mammals, NO is synthesized by NO synthase (NOS), which belongs to the cytochrome P450 type of enzymes, using L-arginine and molecular oxygen as substrates (Figure 3).[66] Recently, NO_2^- was identified as a source for NO in mammals, however, the mechanism by which the one-electron reduction is achieved is not clear. It is believed, though, that it may occur through both enzymatic and non-enzymatic pathways.[67-70] In bacteria, nitrite reductases (NiR) also convert nitrite to NO, which will be discussed in detail in *Chapter 1.4.3.1*. Considering the presence of bacteria in the mouth and gut of vertebrates, this pathway is also of importance for the biology and medicine of humans.

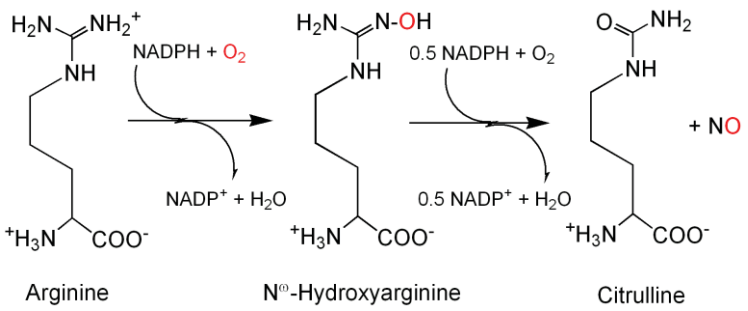

Figure 3. NOS-enzyme catalyzed NO synthesis from L-Arg.

1.2.2. The physiological function of nitric oxide in the cardiovascular system

The primary and initially recognized effect of NO in the cardiovascular system is mediated through activation of soluble guanylate cyclase (sGC) and the subsequent formation of guanosine 3’,5’-cyclic monophosphate (cGMP),[71-74] which then causes smooth muscle relaxation, inhibits vascular smooth muscle cell growth, and prevents platelet aggregation and adherence of neutrophils to endothelial cells.[75] Although the structure of sGC is currently not available, it is generally accepted that a heme cofactor in the β sub-

unit‡ is essential for the sensing of NO,[76,77] which subsequently leads to the weakening of the Fe^{II}–N_{His} bond due to the so-called negative *trans* effect of NO. As a result, a 5-coordinate (5c) nitrosyl complex of sGC is formed according to Figure 4.[78,79]

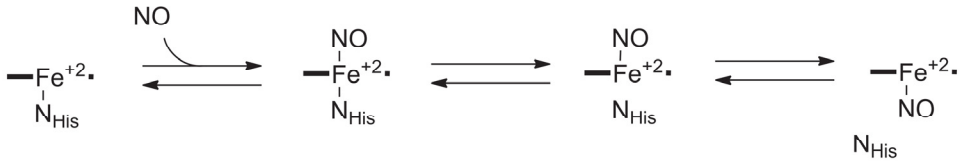

Figure 4. Mechanism of binding of NO to sGC. Reprinted with permission from He, C., Neya, S., Knipp, M. *Biochemistry* 2011, *50*, 8559-8575. Copyright 2011 American Chemistry Society.

Only few examples of proteins that break their Fe^{II}–N_{His} bond upon NO coordination at neutral pH are known, i.e., CO-oxidation activator protein (CooA), PAS-A§ domain of the mammalian circadian protein CLOCK (CLOCK PAS-A), the heme NO/oxygen-binding (H-NOX) domains of *Thermoanaerobacter tengcongensis*,[80] and cytochrome *c*' from various species.[81-83] In particular, cytochrome *c*' proteins, which originate from bacteria yet no function is known, have been studied in the past as models for sGC. A great advantage is the availability of crystallographic structures of the protein from *Alcaligenes xylosoxidans*, often termed AXCP.[84] As shown in Figure 5 and also through mutagenesis studies, an Arginine residre (Arg124) provides the key stabilizing effect through H-bonding to the coordinated NO.[84] However, from the recently reported energy optimized homology model of the human sGC heme domain**,[85] there is no such H-bonding residue in the distal pocket to stabilize the 5c NO complex. Thus, the mechanism, by which the 5c NO complex of sGC is formed and stabilized might not be same like in AXCP.

‡ sGC is a heterodimer comprised of a α and a β subunit.
§ The PAS domain is a protein domain contained in many signaling protein where it functions as a signal sensor. It was named after the three proteins in which it occurs: period circadian protein, aryl hydrocarbon receptor nuclear translocator protein, and single-minded protein.
** The homology model was based on *Ns*H-NOX (PDB code 2O09).

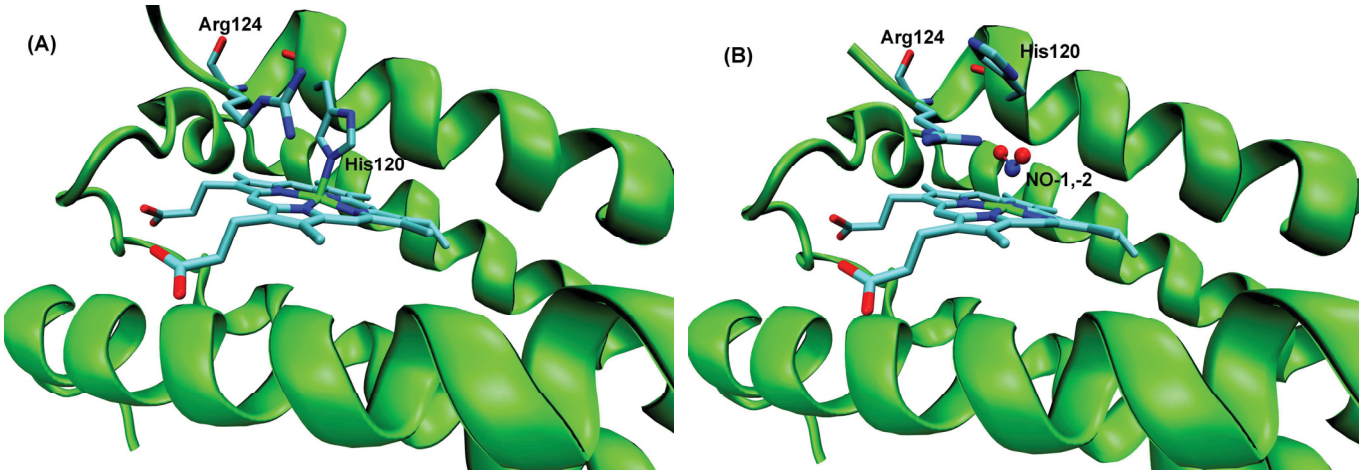

Figure 5. X-ray crystal structure of unliganded (PDB code 1E84) (A) and NO-bound (PDB code 1E85) (B) cytochrome *c*' from *Alcaligenes xylosoxidans* (AXCP) structures. Two NO orientations were solved and indicated as NO-1,-2.

1.3. Interaction of nitric oxide with model heme compounds and heme proteins

1.3.1. Nitric oxide coordination to model heme compounds and heme proteins

NO coordinates to both ferrous and ferric hemes *via* the nitrogen atom. Vibrational spectroscopy is an important technique to study heme nitrosyl complexes because the spectra contain information about the oxidation state, spin state, and coordination number of the iron atom (see *Chapter 1.5.1*). In the case of ferric heme nitrosyl complexes, i.e. $\{FeNO\}^6$, they are not accessible to EPR spectroscopy. Resonance Raman (RR) and Infrared (IR) spectroscopy are generally used for the selective assignment of the stretching frequencies of ν_{Fe-NO}, δ_{Fe-N-O}, and ν_{N-O}, respectively, *via* isotopic labelling. Table 2 summarizes the crystallographic and vibrational data of the selected examples of heme nitrosyl complexes. In the case of 5c $\{FeNO\}^7$ the ν_{Fe-NO} is in the range of 520-540 cm^{-1}, ν_{N-O} is in the range of 1660-1700 cm^{-1} and the angle of Fe–N–O is usually bent at ~ 140°, whereas for 6-coordinate (6c) $\{FeNO\}^7$ the ν_{Fe-NO} is in the range of 550-570 cm^{-1}, ν_{N-O} is in the range of 1610-1640 cm^{-1}. Interestingly, the ν_{Fe-NO} of $\{FeNO\}^6$ is usually at

~600 cm^{-1}, which is larger than that of {FeNO}^{7} (520-570 cm^{-1}), indicating a stronger Fe–NO bond in ferric heme nitrosyl complexes. In contrast, the Fe–NO bond is thermodynamically much stronger in ferrous heme nitrosyl complexes as inferred from their equilibrium constants K_{eq} (10^{11} - 10^{15} M^{-1} for {FeNO}^{7}) *vs*. 10^3 -10^9 M^{-1} for {FeNO}^{6}).[22,86] A new excitation state, high spin (HS) Fe^{III} antiferromagnetically coupled to NO (S = 2), has been suggested from the calculated potential energy surfaces; upon elongation of the Fe–NO bond, the complex becomes 5c HS with the proximal imidazole (ImH) and the $NO^{\bullet}$ (radical) is antiferromagnetically coupled to Fe^{III}.[87] This state is responsible for the thermodynamic weakening of the Fe–NO bond and the smaller K_{eq} in the case of ferric heme nitrosyl complexes. As such, NO forms a strong Fe–NO bond (from spectroscopy), yet, it is a weak ligand to the ferric hemes (from thermodynamics).[87,88]

Table 2. Crystallographic and vibrational features for selected heme nitrosyl complexes

Heme–NO complexes	Fe–NO (Å)	N–O (Å)	∠Fe–N–O (°)	ν_{Fe-NO}	ν_{N-O}	Ref.
		5c Fe^{II}–NO				
Fe^{II}(OEP)–NO	1.72	1.17	144	522	1671	89,90
Fe^{II}(TPP)–NO	1.74	1.16	144	532	1697	91,92
α-Hb^{II}–NO[a]	1.74	1.1	145			93
sGC^{II}–NO[b]				525	1677	78
AXCP–NO[c]	2.03	1.16	125	526	1661	84,94
		6c Fe^{II}–NO				
Fe^{II}(TPP)(MI) –NO	1.75	1.18	138	563	1630	95,96
$hhMb^{II}$–NO[d]	1.87	1.20	144	558	1613	97-99
Hb^{II}–NO[a]	1.74	1.1	145	553	1615	93,100
hHO-1[e]	1.64	1.14	138	566		101,102
FixLH[f]	1.76	1.14	154	568	1634	103,104
		Fe^{III}–NO				
[Fe^{III}(OEP)(NO)](ClO_4)	1.64	1.11	177	611	1868	105,106
$NP4^{III}$–NO (pH 5.6)[g]	1.69	1.09	159	590	1904	107-109
HRP^{III}–NO[h]				604	1903	110
hHO-1[e]				596	1918	111

[a] Horse hemoglobin. [b] From bovine lung. [c] *Alcaligenes xylosoxidans* cytochrome *c*'. [d] From horse heart. [e] Human heme oxygenase-1. [f] The heme-binding domains of *Bradyhizobium japonicum* FixL. [g] Nitrophorin-4. [h] Horseradish peroxidase.

Fe^{II}–CO is isoelectronic to {FeNO}^{6} and ν_{Fe-CO} can be readily detected as a band of moderate intensity at ~500 cm^{-1} in RR spectra. As indicated in Figure 6a, the CO heme complexes show well-behaved anti-correlations, which is the expected variation in back-

bonding. The extent of backbonding is influenced by polarization of the bound CO in the heme pocket.[112] For example, horseradish peroxidase (HRP) usually has high ν_{Fe-CO}/ν_{C-O} pairs along the Mb-line due to the polarity induced by the positively charged Arg residue in the distal pocket (Figure 6a).[113] In the case of Mb, replacing of the distal His64, which provides a weak H-bond to the bound CO, with a non-polar Leu residue moves the ν_{Fe-CO}/ν_{C-O} pair down along the Mb-line (Figure 6a).[114]

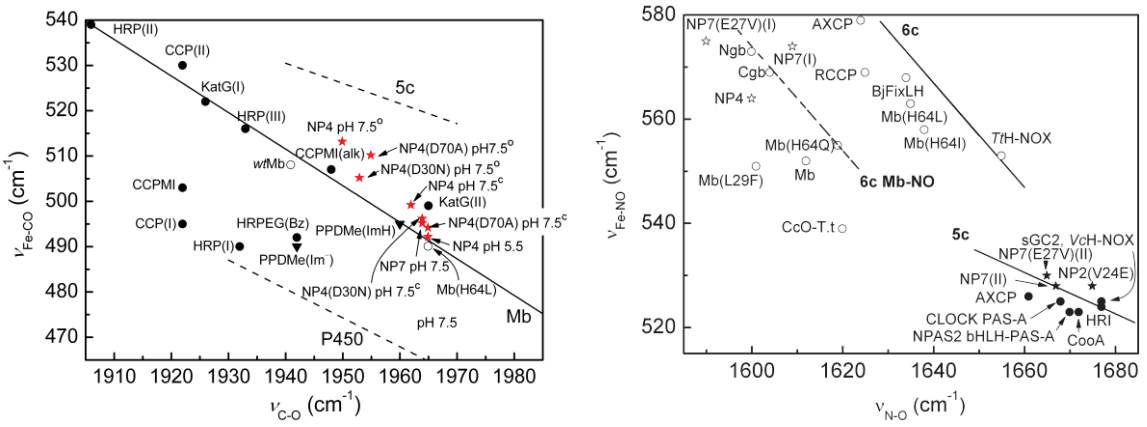

Figure 6. (a) Left, ν_{Fe-CO}/ν_{C-O} correlation plot for the data from heme protein Fe^{II}–CO complexes. Manuscript in preparation. (b) Right, ν_{Fe-NO}/ν_{N-O} anti-correlation plot for the data from heme protein {FeNO}^{7} complexes. Reprinted with permission from He, C., Neya, S., Knipp, M. *Biochemistry* 2011, *50*, 8559-8575. Copyright 2011 American Chemistry Society.

In the case of 5c ferrous NO heme proteins, as can be seen from Table 2, the ν_{Fe-NO} and ν_{N-O} show the expected inverse correlation (Figure 6b). 6c ferrous NO/His heme proteins show a very scattered behavior from the ideal line of model hemes compared to 5c complexes[115] and 6c Fe^{II}–CO complexes (Figure 6a).[116] This deviation has been attributed to the perturbation of the Fe–N–O angle, which is predicted ~ 140° based on calculations (Figure 7). The His64 residue in Mb provides H-bonding to the NO and can potentially enhance the Fe^{III}–NO^- character.[115] This was further supported by the mutants, Mb(H64I) and Mb(H64L), for which the pairs of ν_{Fe-NO}/ν_{N-O} are closer to the normal 6c line (Figure 6b).[99,117] Neuroglobin (Ngb) and cytoglobin (Cgb) have a similar distal His

like Mb, and the distal Cu^{+} in cytochrome c oxidase (CcO) creates a similar situation. Thus, many of the 6c nitrosyl heme proteins fall on an alternate line that is parallel to the line of model hemes (dashed line in Figure 6b). As already mentioned, this can be attributed to the stabilization of the Fe^{III}–NO^{-} character by H-bonding to NO. As a consequence, the angle ∠(Fe–N–O) is expected to be significantly small than 140° (Figure 7). It should be mentioned, that in a recent study using nuclear resonance vibrational spectroscopy (NRVS) the traditional ν_{Fe-NO} was proposed to be better described as δ_{Fe-N-O}.[88] It reflects both angles and bond lengths and may account for the bad anticorrelation observed in the case of the ferroheme nitrosyl complexes.

Unlike CO that coordinates to the heme in only an approximately linear configuration the angle of Fe–N–O can vary between 180° – 120°. One possible explanation for this is that the character of Fe–N–O ranges from that of a nitrosyl cation (NO^{+}) where considerable charge has transferred to the metal, to that of a nitrosyl anion (NO^{-}) in which case the charge transfer is in the opposite direction.[86,118] The possible tautomers are summarized in Figure 7, in the case of NO^{+}, the Fe–N–O angle is ~ 180° and the antibonding electron is transferred to the Fe d_{z^2} orbital leading to the shortening of the Fe–NO bond. While in the case of NO^{-} the Fe–N–O angle is bent at ~ 120°, the two electrons occupy the NO π^* orbital resulting in a double bond N=O^{-} and a lengthening of the Fe–NO bond.[115]

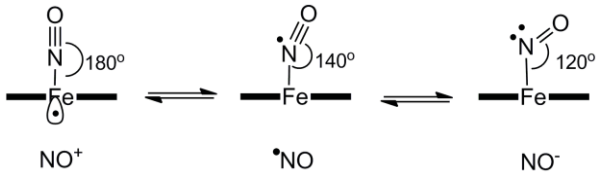

Figure 7. Valence isomers of the nitrosyl ferrous heme complex, adapted from ref 115.

1.3.2. Reductive nitrosylation of ferriheme proteins

In contrast to NPs, most ferric heme proteins like metMb can be readily reduced by excess NO, which is a consequence of the much higher reduction potential (Table 2 in

Chapter 8.1). Figure 8 depicts the proposed mechanism. Interestingly, it was found that nitrite is not only the reaction product (Figure 8) but also catalyzes the reductive nitrosylation of metHb, metMb, and ferriheme model compounds in aqueous solution.[119-121] The proposed mechanism will be discussed in *Chapter 1.4.3.3*.

$$\text{metMb-NO} + \text{OH}^- \xrightarrow{k_{OH}} \text{Mb} + \text{HNO}_2$$

$$\text{HNO}_2 + \text{OH}^- \rightleftharpoons \text{NO}_2^- + \text{H}_2\text{O}$$

$$\text{Mb} + \text{NO} \xrightarrow{k_{NO}} \text{Mb-NO}$$

Figure 8. Reductive nitrosylation of metMb, adapted from ref 122.

1.4. Interaction of nitrite with model heme compounds and heme proteins

NO_2^- has been recognized predominantly as an undesired compound in the food chain with potentially carcinogenic effects,[123] or as a "dead end" product of endogenous NO metabolism. Its role in human physiology had been neglected until very recently.[67,124,125] NO_2^- has now been proposed to play an important physiological role in signaling, blood flow regulation, and hypoxic NO homeostasis.[126] The concentration of NO_2^- in the plasma and tissue is remarkably high (0.5 µM - 10 µM).[125] NO_2^- can be converted to NO *via* one-electron reduction and it is proposed that enzymes such as Hb, Mb, and xanthine oxidoreductase,[††] are involved under physiological or pathological hypoxic conditions.[126] NO_2^- is also a key player in the global nitrogen cycle, which proceeds *via* heme proteins in various bacteria and funghi.[127,128] Many microbial species use denitrification to gain energy for their cell growth under anaerobic conditions.[127,129,130] Denitrification is the four-step five-electron reduction of NO_3^- to N_2 involving four enzymes Eq. (1) (NaR, nitrate reductase; NiR, heme cd_1 nitrite reductase; NoR, nitric oxide reductase; N_2OR, nitrous oxide reductase):

[††]Xanthine oxidoreductase is a molybdenum-containing enzyme.

$$NO_3^- \xrightarrow{NaR} NO_2^- \xrightarrow{NiR} NO \xrightarrow{NoR} N_2O \xrightarrow{N_2OR} N_2 \qquad (1)$$

1.4.1. Some basics about nitrite chemistry

NO_2^- is the conjugate base of nitrous acid Eq. (2), its pK_a has been recently re-determined as 3.16 at 25 ℃. [131]

$$HNO_2 \rightleftharpoons H^+ + NO_2^- \qquad (2)$$

The redox chemistry of NO_2^- in aqueous solution is strongly pH dependent, for example the one-electron reduction of NO_2^- to NO requires two H^+ Eq. (3) and (4). The standard reduction potential of NO_2^- to NO can range from 0.99 V (vs. SHE) at pH 0 to -0.46 V (vs. SHE) at pH 14 depending on the pH.[132]

$$HNO_2 + H^+ + e^- \rightarrow NO + H_2O, \qquad E = 0.99 \text{ V (vs. SHE)} \qquad (3)$$

$$NO_2^- + H_2O + e^- \rightarrow NO + 2OH^- \qquad E = -0.46 \text{ V (vs. SHE)} \qquad (4)$$

NO_2^- is unstable at low pH and undergoes a disproportionation reaction according to the following equation (the rate of NO production for 1 mM nitrite at pH 3.0 and 25° is ~ 10^{-7} M s^{-1})[133]:

$$3NO_2^- + 2H^+ \rightleftharpoons 2NO + NO_3^- + H_2O \qquad (5)$$

Although the full mechanism of the nitrite disproportionation has yet to be elucidated, the first step of this reaction was proposed to be the protonation of the nitrite ion (compare Eq. (2) and *Chapter 8.1*).

1.4.2. Nitrite coordination to heme complexes

Three monodentate types of NO_2^- binding modes to heme complexes have been identified so far (Figure 9). A fourth case can be imagined, but has not been reported for a porphyrin, which is the η^2-*O*,*O*-bidentate. It is, though, found for the Cu-containing nitrite reductase.[127]

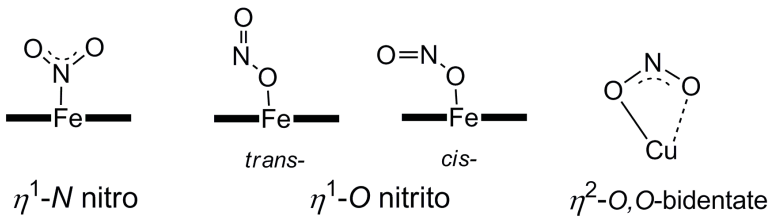

Figure 9. Crystallographically determined binding modes of nitrite to heme proteins and copper-containing nitrite reductase.

DFT calculations reveal that the η^1-N nitro form is only slightly more stable than the η^1-O nitrito form by about 7 kcal mol^{-1},[67] suggesting that the nitrito form is energetically also feasible. However, almost all of the crystallographically characterized NO_2^- complexes (both synthetic models and heme proteins) are N-bound.[134-138] The rare exception is the "picket fence" porphyrin complex $[Fe(TpivPP)(NO_2)(NO)]^-$, which has two crystalline forms, one shows the nitro-nitrosyl structure, the other is disordered because of the presence of both nitrite binding modes (30% of nitrito form).[135] Thus, it was surprising when Richter-Addo and co-workers solved the structures of the NO_2^- complexes of metMb and metHb, both of which exhibiting the nitrito form.[97,139] Comparison with the distal pocket mutant proteins metMb(H64V) and metMb(H64V/V67R) reveals that the distal H-bond donating His residue dictates the nitrito binding mode.[140] Very recently, the X-ray crystal structure of the NO_2^- complex of chlorite dismutase (Cld) from *Dechloromonas aromatica* has been solved, which also shows a nitrito binding mode, where nitrite is stabilized through the H-bonding of an arginine residue (Arg184).[141] Figure 10

summarizes the available X-ray crystal structures of nitrite complexes with heme proteins.

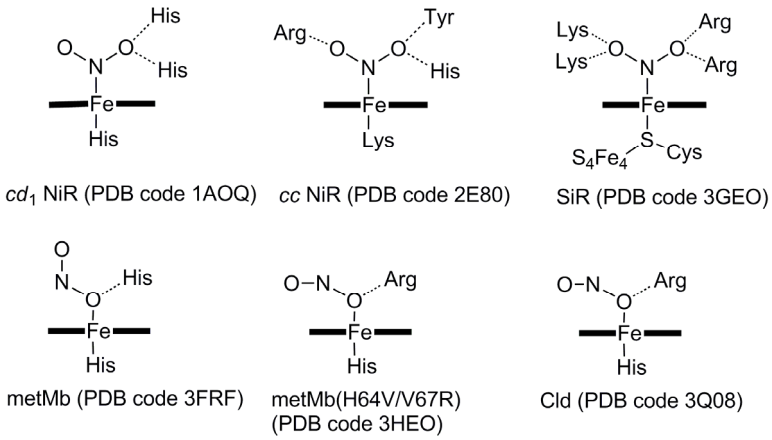

Figure 10. X-ray crystal structures of nitrite complexes with heme proteins. cd_1 NiR, cytochrome cd_1 nitrite reductase; cc NiR, cythchrome *c* NiR; SiR, sulfite reductase; Cld, chlorite dismutase.

1.4.3. Reactions of nitrite with heme complexes

1.4.3.1. One-electron reduction of nitrite by bacterial nitrite reductase

The one-electron reduction of NO_2^- to NO is a key step in the global nitrogen cycle.[127,128] Two types of bacterial NiR have been found so far, cytochrome cd_1 NiR (cd_1 NiR) and cytochrome *c* NiR (ccNiR).

cd_1 NiR is a bifunctional enzyme that catalyzes the one-electron reduction of NO_2^- to NO in the nitrogen cycle and the four-electron reduction of O_2 to H_2O.[127] This enzyme is homo-dimeric, each subunit has a heme *c* and a heme d_1, both of which undergo heme ligand-switching during the reaction according to Figure 11.[137]

The other type of enzymes is the cc NiR which catalyzes the six-electron reduction of NO_2^- to NH_4^+ without the release of potential intermediates Eq. (1).[136] However, the first step is the one-electron reduction of NO_2^- to NO. The X-ray structures of ccNiR from *Sulfurospirillum deleyianum*[142] and *Wolinella succinogenes*[143] contain a multiheme *c* en-

zyme, in which the heme cofactor is covalently linked to the protein *via* two Cys residues. The X-ray crystal structure of the NO_2^- complex with cc NiR reveals a η^1-N nitrite binding mode (Figure 10).

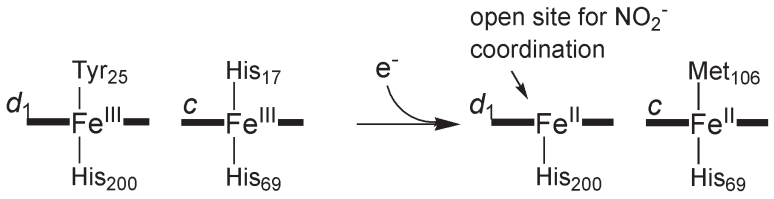

Figure 11. Heme ligand-switching upon reduction of *cd*$_1$ NiR from *Thiosphaera pantotropha*, the heme d_1 becomes 5c HS and the His_{17} residue is replaced by Met_{106} in heme *c*.

1.4.3.2. One-electron reduction of nitrite by hemoglobin in mammals

The NO_2^- reducing reactivity of Hb was first discovered by Brooks in 1937, who found metHb and NO as products upon incubation of Hb with NO_2^- Eq. (6).

$$NO_2^- + Hb + 2H^+ \longrightarrow NO + metHb + H_2O \qquad (6)$$

$$NO + Hb \rightleftharpoons HbNO \qquad (7)$$

The reaction kinetics and product distribution have since been characterized by several groups,[144,145] where the ratio of metHb : HbNO is found to be ~ 1 : 1.[145] In the red blood cells (RBC), the concentration of Hb is in huge excess compared to that of nitrite. How could the coordinated NO possibily escape the RBC since it forms a very stable complex with Hb Eq. (7) (K_{eq} = 10^{10}-10^{11} M^{-1})?[146] A solution was recently proposed that would include the formation of N_2O_3 *via* a nitrite anhydrase reaction of metHb. N_2O_3 might be able to escape the cell membrane by diffusion.[67] In this case it could serve as an NO equivalent upon decomposition Eq. (8). However, the validity of this N_2O_3 pathway *in vivo* raises question and has yet to be confirmed.

$$N_2O_3 \rightarrow NO + NO_2 \qquad (8)$$

1.4.3.3. Nitrite catalyzes the reductive nitrosylation of ferriheme complexes.

As was already mentioned in *Chapter 1.3.2*, two mechanisms have been proposed for the nitrite catalyzed reductive nitrosylation of ferriheme complexes that are presented in Figure 12.[119] The key event for the inner sphere pathway (Figure 12, left) is the nucleophilic attack of nitrite on the $\{FeNO\}^6$ moiety,[147] which resembles a reaction that also occurs with other nucleophiles, e.g., H_2O and OH^-. The other pathway involves an initial electron transfer step (Figure 12, right). The oxidation of nitrite to NO_2 is energetically unfavorable, however, the NO_2 formed would be rapidly trapped by excess NO which reacts further. It was also observed that the rate constant follows the reduction potential of the ferriheme nitrosyl complexes[119] (Table 2 in *Chapter 8.1*) and this further supports the latter oxidation-reduction mechanism.

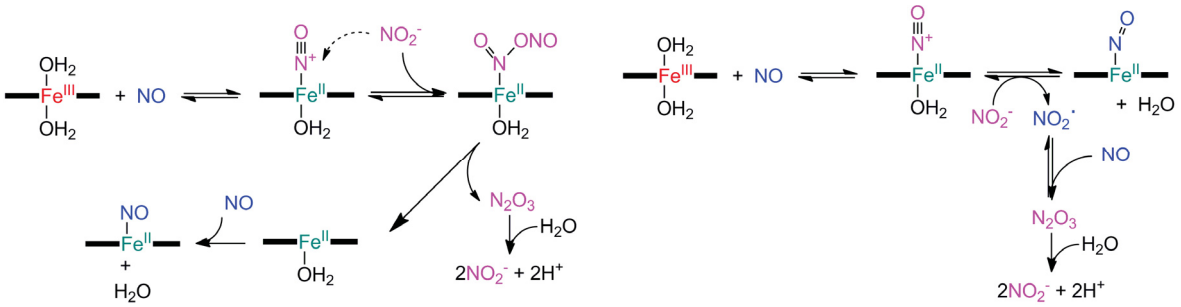

Figure 12. Proposed mechanism for nitrite catalysis of reductive nitrosylation of the bisaquo ferriheme model complexes.[119] (a) Left, inner sphere pathway. (b) Right, electron transfer pathway.

1.4.3.4. Oxygen-atom-transfer reaction of nitrite

For ferric heme complexes, the oxygen-atom-transfer (OAT) reaction of the coordinated NO_2^- has been reported in both aqueous[148] and nonaqueous[149-151] media according to Eq. (9).

$$Fe^{III}(Por)NO_2^- + \mathbf{S} \rightarrow Fe^{II}(Por)(NO) + \mathbf{S}O \qquad (9)$$

In near-neutral aqueous solution, the substrate **S** represents 3,3′,3″- phosphinidynetris (benzenesulfonic acid) trisodium (TPPTS), dimethyl sulfide (DMS), cysteine, and GSH.[148] In the case of the biological relevant compound cysteine, the product has been identified as the disulfide CysS–SCys or the sulfenic acid [CysS(O)H],[148] where the latter may be significant with respect to the appearance of CysS(O)H in some proteins as post translational modifications, which has particular importance in redox-mediated signal transduction.[152,153]

1.5. Experimental methods

Resonance Raman (RR) and electron paramagnetic resonance (EPR) spectroscopy are very powerful techniques for the investigation of the electronic structure and properties of various metal centers in biological systems. During this thesis, both methods were, besides many other spectroscopic, chromatographic, and biochemical techniques, applied and the obtained results represent a fundamental basis for the conclusions drawn herein.

1.5.1. Resonance Raman spectroscopy

Molecular vibrational frequencies typically fall in the infrared (IR) region of the electromagnetic spectrum. Transitions corresponding to vibrationally excited states can therefore be measured by the direct absorption of light in the IR region. However, these transitions can principally also be accessed *via* an inelastic scattering process (Raman process), in which the energy is acquired from a photon of higher energy (Figure 13). Since the first discovery of the Raman effect in 1928 by Sir C. V. Raman,[154] Raman spectroscopy has provided data on the vibrational frequencies of various molecules and is usually complementary to IR spectra. Unlike IR spectra, which are dominated by anti-

symmetric stretching and deformation modes, signals obtained in Raman spectroscopy usually originate from symmetric bond stretching vibrations.

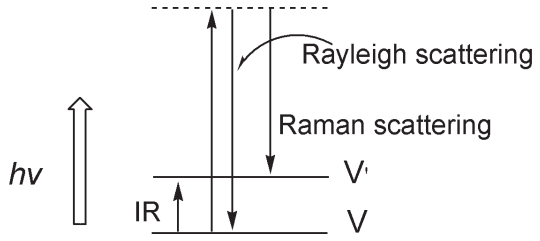

Figure 13. Infrared absorbance and Raman emission: absorption of an IR photon excites the molecule from the ground vibrational level *V* to an excited vibrational level *V'*, leading to a higher energetic state. In Raman spectroscopy, excitation leads to an energetically higher state. Relaxation will lead mostly to the population of *V* (Rayleigh scattering), a small population of *V'* will be accessed, which leads to the emission of a discrete vibrational mode. Adapted from ref 155

With the emergence of lasers, Raman spectroscopy has been revolutionized.[156] The first laser Raman spectra of proteins were recorded in 1968[157] and its application in biological sciences was expanded since. The intensity of Raman scattering strongly depends on the excitation wavelength. Tuning the laser into the vicinity of an allowed transition (resonance Raman, RR) can increase some of the Raman bands markedly (see below). Metalloporphyrins have been one of the most studied types of molecules in the modern era of RR spectroscopy due to their unique properties: i) the highly conjugated system of the porphyrin ring gives rise to two low-lying π-π* transitions, which can be easily excited with visible lasers; ii) configuration interaction and vibronic mixing between these transitions cause many interesting resonance effects, which can be studied selectively by tuning the excitation wavelength; iii) metalloporphyrins are available with a wide variety of peripheral substituents, metal ions, and axial ligands, which can be systematically investigated by Raman spectroscopy; iv) vibrational frequencies correlate with coordination environment, oxidation state, and spin state; v) metalloporphyrins are the prosthetic groups of various metalloproteins, which are important biological molecules.[158]

1.5.1.1. Electronic structure and resonance Raman enhancement

Porphyrins are heterocyclic macrocycles comprised of four pyrrole rings connected at their α carbons through methine bridges (=CH–) (Figure 14). They are highly conjugated systems (in the extreme case of ppIX, they are Hückel aromatic compounds), thus having very intense absorption bands in the visible region.

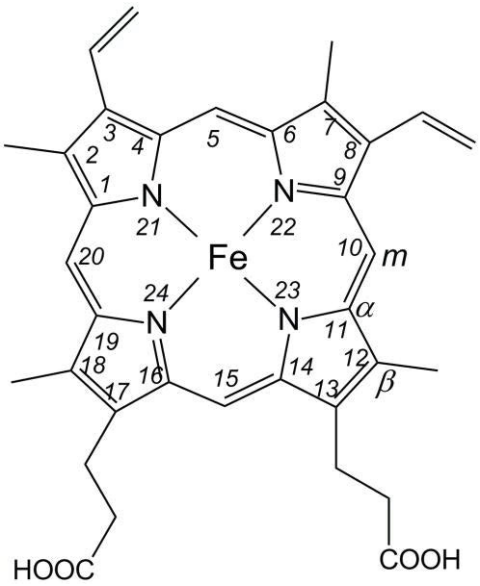

Figure 14. Iron–protoporphyrin IX (Heme *b*) is the porphyrin with the highest abundance in nature. The numbering of atoms follows those used to describe the ring vibrations.

Figure 15a presents the absorbance spectrum of NP7[Fe^{II}–OH^-] at pH 10.5 as an example. It shows a vey intense band, called the ***B*** or Soret band at 423 nm, and a pair of much weaker bands, called $\boldsymbol{Q_o}$ and $\boldsymbol{Q_v}$ or α and β, at 557 and 526 nm, respectively. According to the four-orbital model developed by Goutermann, in the idealized D_{4h} symmetry of the tetrapyrrole ring, the two LUMOs (π*) are degenerated having e_g symmetry, while the two HOMOs (π) have nearly the same energy and are of a_{1u} and a_{2u} symmetries.[159] The transition dipoles add up for the higher energy ***B*** transition, but nearly cancel for the lower energy $\boldsymbol{Q_o}$ transition. The latter $\boldsymbol{Q_o}$ transition regains about 10% of the intensity from the ***B*** transition *via* vibronic mixing, forming a side-band $\boldsymbol{Q_v}$ or β.[155,158]

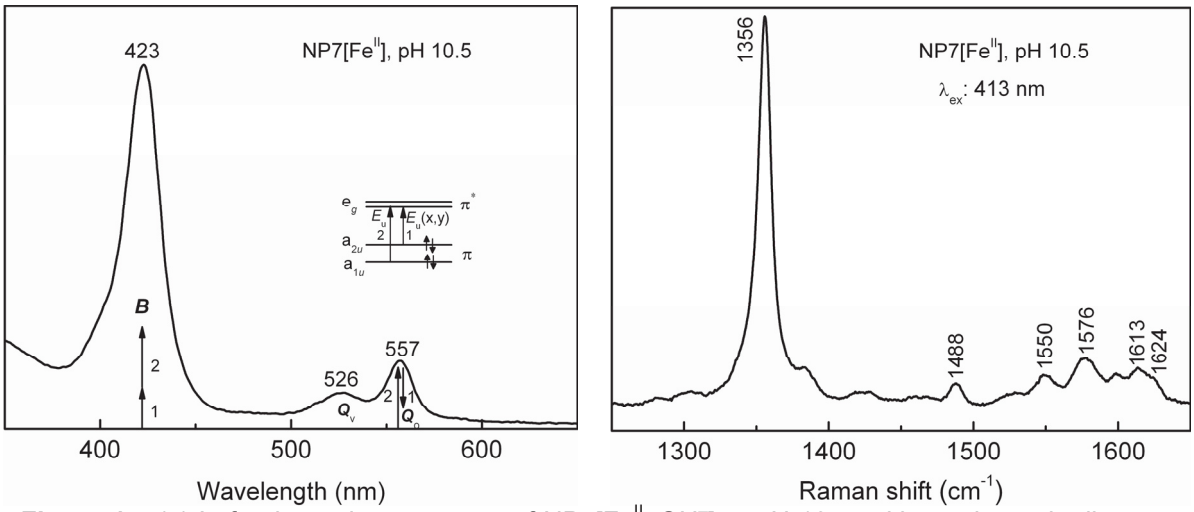

Figure 15. (a) Left, absorption spectrum of NP7[Fe^{II}–OH^-] at pH 10.5, with a schematic diagram of the four-orbital model for the visible bands. The two π-π* excitations, 1 and 2, experience strong configuration interaction, adding up for the higher energy ***B*** transition, and nearly cancelling in the lower energy $\boldsymbol{Q_o}$ transition. The $\boldsymbol{Q_v}$ band is the envelope of the 0 → 1 vibronic transitions induced by mixing of the ***Q*** and ***B*** electronic transitions.[158] (b) Right, high frequency region of the RR spectrum of NP7[Fe^{II}–OH^-] at pH 10.5, ambient temperature (λ_{ex} = 413 nm).

Different laser excitation wavelengths can selectively tune the RR spectra of metalloporphyrins. Excitation near the ***B*** absorption band results in the RR spectra dominated by polarized peaks arising from totally symmetric vibrations (Figure 15b).[155,158,160] The depolarization ratio $\rho = I_\perp / I_{||}$ is close to the expected value 1/8.[161] It is also possible to see Jahn-Teller-active modes (depolarized band ρ = 3/4) with moderate intensity arising from the degenerate excited state (a_{1u}, a_{2u}).[162] Excitation close to the ***Q*** absorption bands produces RR spectra dominated by depolarized peaks (dp) or anomalously polarized (ap ρ > 3/4) arising from non-totally symmetric modes. Since the $\boldsymbol{Q_o}$ band is much weaker compared to the ***B*** band, polarized peaks with moderate intensity can still be observed, however, the relative intensity is very different from that of ***B***-resonant spectra.

1.5.1.2. Porphyrin core vibrations

The structure-sensitive bands of porphyrin core vibrations in heme proteins were first reported in 1974.[163] Table 3 lists the four most important core-size marker bands from

selected heme proteins. The ν_4 is characteristic of the oxidation state, while ν_2, ν_3, and ν_{10} are sensitive to both oxidation and spin states. $\nu(C^{\alpha}–C^{m})$ and $\nu(C^{\alpha}–N)$ are the major contributors in the potential energy distribution in oxidation-state sensitive bands.[164] Back donation from *d*-electrons to the porphyrin π^* orbitals increases when the oxidation state is decreased. Thus, the porphyrin π-bonds are weakened, which leads to lower stretching frequencies. However, in the case of Fe^{II}, the oxidation state marker ν_4 strongly depends also on the nature of the axial ligands.[165] In the case of the strong π-donors Cys in cytochrome P450 (CYP_{450}),[166] ν_4 is much smaller compared to the His in the globins (1346 cm^{-1}, CYP_{450} vs. 1358 cm^{-1}, deoxyHb) (Table 3).

Table 3. Core-size marker bands of selected heme protein (cm^{-1})

Protein	Oxidation state	Spin state	Axial ligands	ν_4 (p)	ν_3 (p)	ν_2 (ap)	ν_{10} (dp)
Cyt *c*[a]	II	LS	His/Met	1362	1493	1584	1620
CYP_{450}[b]	II	HS	Cys	1346	1467	1562	1604
Cyt *c'*, pH 7.0[c]	II	HS	His	1352	1469	1577	
Cyt *c'*, pH 12.0[c]	II	LS	His/Lys	1358	1488	1592	
deoxyHb[a]	II	HS	His	1358	1473	1522	1607
oxyHb[a]	II	LS	His/O_2	1377	1506	1586	1640
Cyt *c*[a]	III	LS	His/Met	1374	1502	1582	1636
CN–metHb[a]	III	LS	His/CN^-	1374	1508	1588	1642
F–metHb[a]	III	HS	His/F^-	1374	1482	1555	1608

[a] from ref 163 .[b] from ref 166. [c] from ref 167.

Moreover, the ν_4 of 6c complexes is generally higher than that of 5c complexes. When π-acceptors (CO, NO, O_2, *etc.*) coordinate to the distal site, where π–back donation is significant, ν_4 increases to ~1374 cm^{-1}. Ligands like Met and Lys coordinate to the heme iron through a d_{z^2}(Fe)-lone pair σ-type interaction, leading to an increase of the ν_4 band by only a few wavenumbers.

The sensitivity of core size marker bands to the spin state has been attributed to the expansion of the out-of-plane deformation of the porphyrin core.[158,168] For both oxidation states, when the complex is low spin (LS), the six and/or five electron(s) occupy the d_{π} orbitals; when it becomes HS, the electrons occupy the antibonding d_{z^2} and $d_{x^2-y^2}$ orbitals

resulting in an elongation of the Fe–N bond (Figure 16) and, thus, to the expansion of the porphyrin-core plane or displacement of the Fe from the plane. This weakens the methane bridge force constants leading to the lower frequencies of the spin-state maker bands (ν_2, ν_3, and ν_{10}), since they all contain $\nu(C^{\alpha}–C^{m})$ as the major contribution in their normal mode.[168]

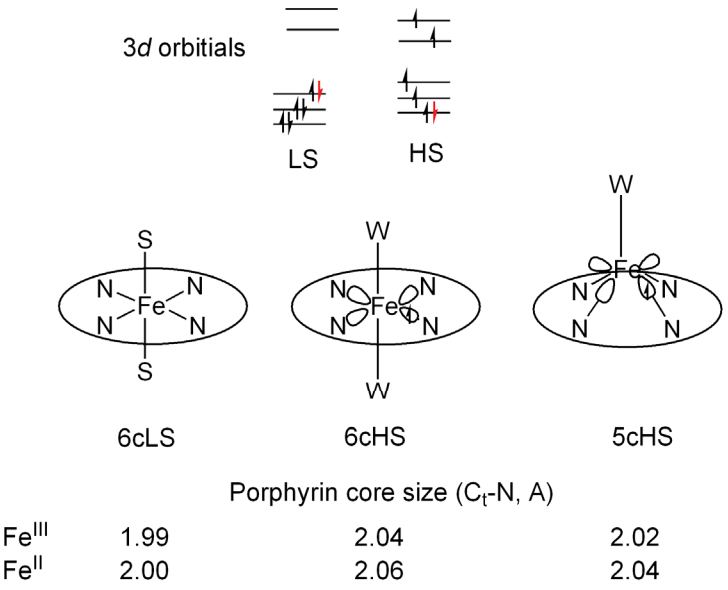

Figure 16. Schematic diagram for 6c/5c Fe prophyrin, with the typical core size indicated. S/W, strong- and weak field ligands. Occupancy of the *d* orbitals is shown for LS/HS complex (the extra electron of Fe^{II} is shown as red arrow). Adapted from ref 158.

1.5.2. Electron paramagnetic resonance spectroscopy

Electron paramagnetic resonance spectroscopy (EPR) is a powerful technique, which probes the paramagnetic centers of compounds with unpaired electron(s), including radicals, triplet states, and transition metal ions. For the S = 1/2 electron m_S is allowed to have two values, namely, ±1/2. Upon exposure to an external magnetic field, *B*, the electron can be either stabilized (-1/2) or destabilized (+1/2), and the magnitude of this effect varies linely with the intensity of *B* (Figure 17).[169]

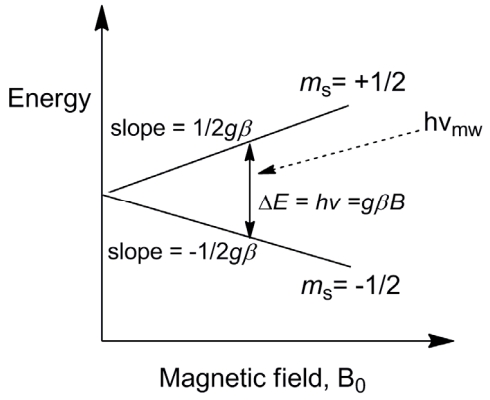

Figure 17. Dependence of the energies of the $m_S = \pm 1/2$ states of an electron on the magnetic field.

The resonance condition is also given in Eq. (10):

$$\Delta E = h\nu = g\beta B \qquad (10)$$

in which the energy of the microwave radiation produced by the source is equal to the energy difference ΔE between the two spin states generated by the external magnet. h is Planck's constant (6.62607 x 10^{-34} J s); β is the Bohr magneton (9.27401 x 10^{-24} J/T); ν is the microwave frequency of radiation; B is the external magnetic field, and g is the so-called the g factor or spectroscopic splitting factor (dimensionless).

In standard instrumentation, a fixed frequency source is used and the magnetic field is modulated. Such instrument is called a continuous wave (CW) EPR spectrometer. The most widely used frequency is ~9.4 GHz (X-band), while several other frequencies are also common in EPR, e.g., 1 GHz (L-band), 3 GHz (S-band), 35 GHz (Q-band), and 94 GHz (W-band). Low frequency spectra usually have high sensitivity and high resolution of otherwise unresolved hyperfine structures. High frequency is critical for a) increasing the resolution associated with g anisotropy and b) distinguishing spectral features due to

g anisotropy (field dependent) from those due to hyperfine or other interactions (field independent).[169,170]

1.5.2.1. EPR spectroscopy of heme complexes

Of great relevance to the present work is the EPR spectroscopy of heme complexes, thus it will be discussed in more detailed in the following. The electronic structures of heme complexes change according to the oxidation and coordination states of the iron, which can be addressed extensively by EPR spectroscopy. Figure 18 summarizes the spin delocalization patterns of the common oxidation and spin states of heme complexes.[171]

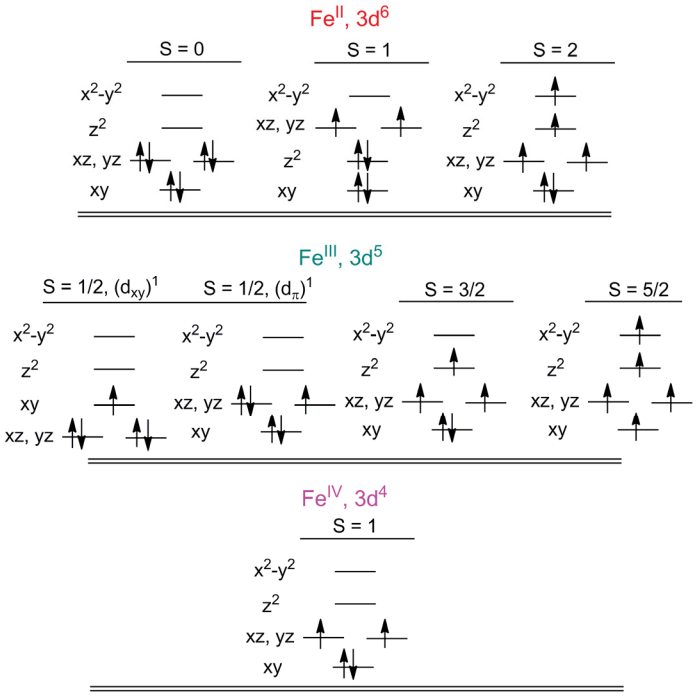

Figure 18. Common spin delocalization patterns for the physiologically relevant oxidation states of heme complexes. Adapted from ref 171.

Ferric heme complexes are half integer-spin systems (S = 1/2, 3/2, or 5/2). The LS ferric heme complexes (S = 1/2) have been investigated extensively because of the detailed information that can be obtained for the nature of the orbital of the unpaired electron. It is

also the most frequently encountered spin system in the presented work. There are two very distinct, limiting ground states for LS ferric heme complexes, the generally observed $(d_{xy})^2(d_{xz},d_{yz})^3$ state and the uncommon $(d_{xz},d_{yz})^4(d_{xy})^1$ state. For the $(d_{xy})^2(d_{xz},d_{yz})^3$ state, the EPR spectra may be either rhombic or appear as "large g_{max}" spectra (Figure 19). The "large g_{max}" EPR signal is indicative of near-degeneracy of d_{xz} and d_{yz}, for complexes with identical planar axial ligands, which correlates with the perpendicular alignment of these ligands.[172] However, in the case of non-identical axial ligads the origins of the "large g_{max}" EPR signal is rathe unclear. Previous studies shows that the presence of strong axial ligands (strong σ-donors and weak π-acceptors), a highly saddled heme plane, and/or electron-withdrawing substituents at the meso positions of the porphyrin might cause the "large g_{max}" EPR signal.[173]

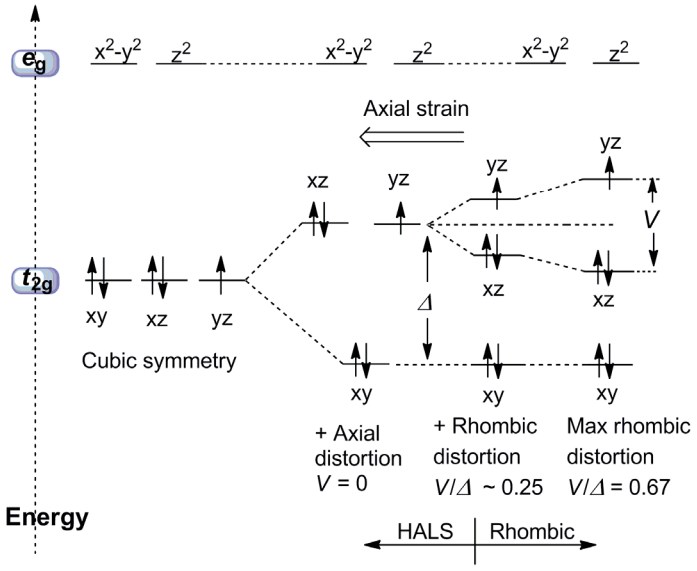

Figure 19. Energy diagram of the d-orbitals level for LS ferric ion with $(d_{xy})^2(d_{xz},d_{yz})^3$ orbital occupancy. Note that e_g orbitals are occupied when HS and intermediate spin (e.g., S = 3/2) states are present in the system.[173]

Their EPR spectra have a g_{max} value greater than 3.2, and the other two g-values are usually too broad and weak to be resolved. Therefore, this type of spectra is often referred to as highly anisotropic low-spin heme (HALS) (Figure 20a).[174,175] The other type

of the $(d_{xy})^2(d_{xz},d_{yz})^3$ state complexes have well-resolved rhombic EPR signals (Figure 20b), with parallel or non-perpendicular alignment of the planar axial liagnds and the energy is very different between d_{xz} and d_{yz} (Figure 19). In both cases, the three g-values follow the order $g_{zz} > g_{yy} > g_{xx}$. However, in the uncommon $(d_{xz},d_{yz})^4(d_{xy})^1$ ground state, the EPR spectra are nearly axial, and g_{zz} is the smallest (Figure 20c).[176] In this case, the d_{xz}, d_{yz} pair are degenerate, or nearly degenerate, and below the d_{xy} in energy (Figure 18). For symmetrical heme rings, this ground state leads to an axial EPR spectrum, with $2.6 \geq g_{\perp} > 2 > g_{II}$,[172] and g_{II} may not be resolved due to a large g-strain.

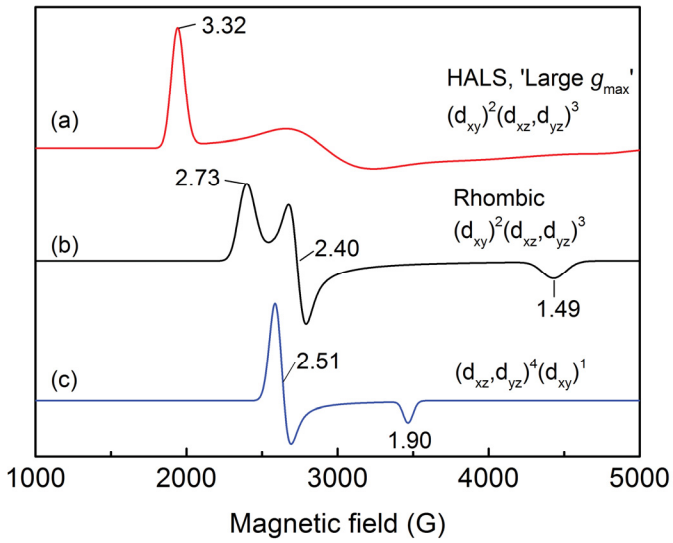

Figure 20. Simulated X-band EPR spectra of typical types of LS ferriheme complexes with their corresponding ground state indicated.

The relative energies of the d_{xy}, d_{xz}, and d_{yz} orbitals can be estimated from the g-values based on the Griffth's theory[177] and Taylor's formulation[176]. The energy separation of these orbitals can be approximated as:

$$\frac{V}{\lambda} = \frac{g_x}{g_z + g_y} + \frac{g_y}{g_z - g_x} \qquad (11)$$

$$\frac{\Delta}{\lambda} = \frac{g_x}{g_z + g_y} + \frac{g_z}{g_y - g_x} - \frac{V}{2\lambda} \qquad (12)$$

Where *V* is the energy difference between the d_{xy} and d_{yz} orbitals, Δ is the energy between the d_{xy} and the average of d_{xz} and d_{yz} orbitals, and λ is the spin-orbit coupling constant, which is, for example, 460 cm^{-1} for free ferric ions.

1.6. Aims and outline

As has been discussed above, heme complexes and proteins have very diverse reactivities with NO and NO_2^- and they are involved in all kinds of nitrogen chemistry. NO_2^- is present in blood and tissues with a concentration of 0.5 µM - 10 µM,[125] and can be physiologically recycled, forming NO and other nitrogen oxides (*Chapter 1.4*).[124,125,178-180] Prior to this study, NPs were mainly recognized as NO-transporters, their ability to store and transport NO being attributed to the much lower reduction potential of the heme cofactor and the different NO affinities at different pHs. The reactivity of NPs with other biological important compounds has almost not been addressed. Upon injection into the victim's blood, where NPs release the coordinated NO, the sixth binding site is open and ready to interact with blood components.

The present study focuses on the elucidation of the reactivity of NPs with nitrite. First of all, NPs and the related mutants have to be recombinantly expressed in *E. coli*. Then the interaction of NPs with nitrite is investigated by various spectroscopic techniques including UV/vis, RR, FT-IR, and EPR spectroscopy, and stopped-flow kinetics. The issues to be addressed include the stoichiometry of the reaction and the identification of the reaction mechanism as far as possible.

It is likely that the Fe^{II} state may present as intermediate upon incubation of NPs with nitrite, however, there is not very much known about the Fe^{II} state of unliganded NPs, except some crystallographic studies on the wild-type NP4.[19] Although NPs are ferri-heme proteins, the Fe^{II} state came recently into focus when the Fe^{II}–CO derivative was used as a model for the $\{FeNO\}^6$ compound as they are isoelectronic, in FT-IR and laser flash photolysis experiments.[109,181] The Fe^{II} state was also proposed as an intermediate in the reduction of the NP iron center with low molecular weight thiols.[182] $Na_2S_2O_4$ is the routinely used reducing agent for ferriheme proteins, however, in the case of disulfide-containing heme proteins it may also interact with the disulfide bond considering the much higher reduction potential of the disulfide bond (–120 to –270 mV vs. SHE pH 7.0, 25°C)[183,184] compared to $Na_2S_2O_4$ (-660 mV vs. SHE pH 7.0, 25°C).[185] In the case of NPs the two disulfide bonds are exposed to the solvent and it makes them even more liable to be attacked by $Na_2S_2O_4$. The presented thesis work focuses for the first time on the effect of $Na_2S_2O_4$ on the disulfide bond. After the proper way of making ferroheme NPs is established, these proteins will also be investigated in detail by UV/vis and RR.

1.7. References

1. Ribeiro, J. M. C., and Garcia, E. S. (1981) The role of the salivary glands in feeding in *Rhodnius prolixus*, *J. Exp. Biol. 94*, 219-230.
2. Ribeiro, J. M., Rossignol, P. A., and Spielman, A. (1984) Role of mosquito saliva in blood vessel location, *J. Exp. Biol. 108*, 1-7.
3. Ribeiro, J. M., Marinotti, O., and Gonzales, R. (1990) A salivary vasodilator in the blood-sucking bug, *Rhodnius prolixus*, *Br. J. Pharmacol. 101*, 932-936.
4. Ribeiro, J. M. C., Hazzard, J. M., Nussenzveig, R. H., Champagne, D. E., and Walker, F. A. (1993) Reversible binding of nitric oxide by a salivary heme protein from a bloodsucking insect, *Science 260*, 539-541.
5. Moncada, S., Martin, J., Beral, V., Bonita, R., and Beaglehole, R. (1993) Vasodilation: evolution of nitric oxide, *The Lancet 341*, 1511.
6. Champagne, D. E., Nussenzveig, R. H., and Ribeiro, J. M. C. (1995) Purification, partial characterization, and cloning of nitric oxide-carrying heme proteins (nitrophorins) from salivary glands of the blood-sucking insect *Rhodnius prolixus*, *J. Biol. Chem. 270*, 8691-8695.
7. Walker, F. A., and Montfort, W. R. (2001) The nitric oxide-releasing heme proteins from the saliva of the blood-sucking insect *Rhodnius prolixus*, in *Advances in Inorganic Chemistry*, pp 295-358, Academic Press, San Diego (USA).
8. Zeledón, R., and Rabinovich, J. E. (1981) Chagas' disease: An ecological appraisal with special emphasis on its insect vectors, *Annu. Rev. Entomol. 26*, 101-133.
9. Moreira, M. F., Coelho, H. S. L., Zingali, R. B., Oliveira, P. L., and Masuda, H. (2003) Changes in salivary nitrophorin profile during the life cycle of the blood-sucking bug *Rhodnius prolixus*, *Insect Biochem. Mol. Biol. 33*, 23-28.
10. Ribeiro, J. M. C., Andersen, J. F., Silva-Neto, M. A. C., Pham, V. M., Garfield, M. K., and Valenzuela, J. G. (2004) Exploring the sialome of the blood-sucking bug *Rhodnius prolixus*, *Insect Biochem. Mol. Biol. 34*, 61-79.
11. Andersen, J. F., Gudderra, N. P., Francischetti, I. M. B., Valenzuela, J. G., and Ribeiro, J. M. C. (2004) Recognition of anionic phospholipid membranes by an antihemostatic protein from a blood-feeding insect, *Biochemistry 43*, 6987-6994.
12. Walker, F. A. (2005) Nitric oxide interaction with insect nitrophorins and thoughts on the electron configuration of the $\{FeNO\}^6$ complex, *J. Inorg. Biochem. 99*, 216-236.
13. Knipp, M., Zhang, H., Berry, R. E., and Walker, F. A. (2007) Overexpression in *Escherichia coli* and functional reconstitution of the liposome binding ferriheme protein nitrophorin 7 from the blood sucking bug *Rhodnius prolixus Protein Expression and Purification 54*, 183-191.

14. Weichsel, A., Andersen, J. F., Champagne, D. E., Walker, F. A., and Montfort, W. R. (1998) Crystal structures of a nitric oxide transport protein from a blood-sucking insect, *Nat. Struc. Biol. 5*, 304-309.
15. Andersen, J. F., and Montfort, W. R. (2000) The crystal structure of nitrophorin 2. A trifunctional antihemostatic protein from the saliva of *Rhodnius prolixus*, *J. Biol. Chem. 275*, 30496-30503.
16. Andersen, J. F., Weichsel, A., Balfour, C. A., Champagne, D. E., and Montfort, W. R. (1998) The crystal structure of nitrophorin 4 at 1.5 Å resolution: Transport of nitric oxide by a lipocalin-based heme protein, *Structure 6*, 1315-1327.
17. Weichsel, A., Andersen, J. F., Roberts, S. A., and Montfort, W. R. (2000) Nitric oxide binding to nitrophorin 4 induces complete distal pocket burial, *Nat. Struc. Biol. 7*, 551-554.
18. Roberts, S. A., Weichsel, A., Qiu, Y., Shelnutt, J. A., Walker, F. A., and Montfort, W. R. (2001) Ligand-induced heme ruffling and bent NO geometry in ultra-high-resolution structures of nitrophorin 4, *Biochemistry 40*, 11327-11337.
19. Maes, E. M., Roberts, S. A., Weichsel, A., and Montfort, W. R. (2005) Ultrahigh resolution structures of nitrophorin 4: Heme distortion in ferrous CO and NO complexes, *Biochemistry 44*, 12690-12699.
20. Flower, D. R. (1996) The lipocalin protein family: Structure and function, *Biochem. J. 318*, 1-14.
21. Flower, D. R., North, A. C. T., and Sansom, C. E. (2000) The lipocalin protein family: Structural and sequence overview, *Biochim. Biophys. Acta 1482*, 9-24.
22. Knipp, M., Yang, F., Berry, R. E., Zhang, H., Shokhirev, M. N., and Walker, F. A. (2007) Spectroscopic and functional characterization of nitrophorin 7 from the blood-feeding insect *Rhodnius prolixus* reveals an important role of its isoform-specific N-terminus for proper protein function, *Biochemistry 46*, 13254-13268.
23. Hochepied, T., Berger, F. G., Baumann, H., and Libert, C. (2003) α_1-Acid glycoprotein: an acute phase protein with inflammatory and immunomodulating properties, *Cytokine Growth Factor Rev. 14*, 25-34.
24. Fournier, T., Medjoubi-N, N., and Porquet, D. (2000) Alpha-1-acid glycoprotein, *Biochimica et Biophysica Acta (BBA) - Protein Structure and Molecular Enzymology 1482*, 157-171.
25. Israili, Z. H., and Dayton, P. G. (2001) Human α-1-glycoprotein and its interactions with drugs, *Drug Metab. Rev. 33*, 161-235.
26. Rassart, E., Bedirian, A., Do Carmo, S., Guinard, O., Sirois, J., Terrisse, L., and Milne, R. (2000) Apolipoprotein D, *Biochimica et Biophysica Acta (BBA) - Protein Structure and Molecular Enzymology 1482*, 185-198.

27. Vogt, M., and Skerra, A. (2001) Bacterially produced apolipoprotein D binds progesterone and arachidonic acid, but not bilirubin or E-3M2H, *J. Mol. Recognit. 14*, 79-86.

28. Dilley, W. G., Haagensen, D. E., Cox, C. E., and Wells, S. A. (1990) Immunologic and steroid binding properties of the GCDFP-24 protein isolated from human breast gross cystic disease fluid, *Breast Cancer Res. Treat. 16*, 253-260.

29. Schreck, S. F., Parker, C., Plumb, M. E., and Sodetz, J. M. (2000) Human complement protein C8γ, *Biochimica et Biophysica Acta (BBA) - Protein Structure and Molecular Enzymology 1482*, 199-208.

30. Ortlund, E., Parker, C. L., Schreck, S. F., Ginell, S., Minor, W., Sodetz, J. M., and Lebioda, L. (2002) Crystal structure of human complement protein C8γ at 1.2 A resolution reveals a lipocalin fold and a distinct ligand binding site, *Biochemistry 41*, 7030-7037.

31. Halttunen, M., Kämäräinen, M., and Koistinen, H. (2000) Glycodelin: a reproduction-related lipocalin, *Biochimica et Biophysica Acta (BBA) - Protein Structure and Molecular Enzymology 1482*, 149-156.

32. Seppälä, M., Taylor, R. N., Koistinen, H., Koistinen, R., and Milgrom, E. (2002) Glycodelin: A major lipocalin protein of the reproductive axis with diverse actions in cell recognition and differentiation, *Endocr. Rev. 23*, 401-430.

33. Akerström, B., Lögdberg, L., Berggard, T., Osmark, P., and Lindqvist, A. (2000) α_1-Microglobulin: a yellow-brown lipocalin, *Biochimica et Biophysica Acta (BBA) - Protein Structure and Molecular Enzymology 1482*, 172-184.

34. Escribano, J., Grubb, A., and Mendez, E. (1988) Identification of retinol as one of the protein HC chromophores, *Biochem. Biophys. Res. Commun. 155*, 1424-1429.

35. Larsson, J., Allhorn, M., and Akerström, B. (2004) The lipocalin α_1-microglobulin binds heme in different species, *Arch. Biochem. Biophys. 432*, 196-204.

36. Kjeldsen, L., Cowland, J. B., and Borregaard, N. (2000) Human neutrophil gelatinase-associated lipocalin and homologous proteins in rat and mouse, *Biochimica et Biophysica Acta (BBA) - Protein Structure and Molecular Enzymology 1482*, 272-283.

37. Goetz, D. H., Holmes, M. A., Borregaard, N., Bluhm, M. E., Raymond, K. N., and Strong, R. K. (2002) The neutrophil lipocalin NGAL is a bacteriostatic agent that interferes with siderophore-mediated iron acquisition, *Mol. Cell 10*, 1033-1043.

38. Tegoni, M., Pelosi, P., Vincent, F., Spinelli, S., Campanacci, V. r., Grolli, S., Ramoni, R., and Cambillau, C. (2000) Mammalian odorant binding proteins, *Biochimica et Biophysica Acta (BBA) - Protein Structure and Molecular Enzymology 1482*, 229-240.

39. Briand, L., Eloit, C., Nespoulous, C., Bezirard, V., Huet, J.-C., Henry, C., Blon, F., Trotier, D., and Pernollet, J.-C. (2002) Evidence of an odorant-binding protein in the human olfactory mucus: Location, structural characterization, and odorant-binding properties, *Biochemistry 41*, 7241-7252.

40. Urade, Y., and Hayaishi, O. (2000) Biochemical, structural, genetic, physiological, and pathophysiological features of lipocalin-type prostaglandin D synthase, *Biochimica et Biophysica Acta (BBA) - Protein Structure and Molecular Enzymology 1482*, 259-271.
41. Newcomer, M. E., and Ong, D. E. (2000) Plasma retinol binding protein: structure and function of the prototypic lipocalin, *Biochimica et Biophysica Acta (BBA) - Protein Structure and Molecular Enzymology 1482*, 57-64.
42. Newcomer, M. E., Jones, T. A., Aqvist, J., Sundelin, J., Eriksson, U., Rask, L., and Peterson, P. A. (1984) The three-dimensional structure of retinol-binding protein, *EMBO J. 3*, 1451-1454.
43. Glasgow, B. J., Abduragintov, A. R., Farahbakhsh, T., Faull, K. F., and Hubbell, W. L. (1995) Tear lipocalins bind a broad array of lipid ligands, *Curr. Eye Res. 14*, 363-372.
44. Bernhard, R. (2000) Human tear lipocalin, *Biochimica et Biophysica Acta (BBA) - Protein Structure and Molecular Enzymology 1482*, 241-248.
45. Ribeiro, J. M. C., and Nussenzveig, R. H. (1993) Nitric oxide synthase activity from a hematophagous insect salivary gland, *FEBS Lett. 330*, 165-168.
46. Nussenzveig, R. H., Bentley, D. L., and Ribeiro, J. M. C. (1995) Nitric oxide loading of the salivary nitric-oxide-carrying hemoproteins (nitrophorins) in the blood-sucking bug *Rhodnius prolixus*, *J. Exp. Biol. 198*, 1093-1098.
47. Yuda, M., Hirai, M., Miura, K., Matsumura, H., Ando, K., and Chinzei, Y. (1996) cDNA cloning, expression and characterization of nitric-oxide synthase from the salivary glands of the blood-sucking insect *Rhodnius prolixus*, *Eur. J. Biochem. 242*, 807-812.
48. Enemark, J. H., and Feltham, R. D. (1974) Principles of structure, bonding, and reactivity for metal nitrosyl complexes, *Coord. Chem. Rev. 13*, 339-406.
49. Lehane, M. J. (2005) *The Biology of Blood-Sucking in Insects*, 2 ed., Cambridge University Press, Cambridge (United Kingdom).
50. Soares, A. C., Carvalho-Tavares, J., Gontijo, N. d. F., dos Santos, V. C., Teixeira, M. M., and Pereira, M. H. (2006) Salivation pattern of *Rhodnius prolixus* (Reduviidae; Triatominae) in mouse skin, *J. Insect Physiol. 52*, 468-472.
51. Andersen, J. F., Champagne, D. E., Weichsel, A., Ribeiro, J. M. C., Balfour, C. A., Dress, V., and Montfort, W. R. (1997) Nitric oxide binding and crystallization of recombinant nitrophorin I, a nitric oxide transport protein from the blood-sucking bug *Rhodnius prolixus*, *Biochemistry 36*, 4423-4428.
52. Ding, X. D., Weichsel, A., Andersen, J. F., Shokhireva, T. K., Balfour, C., Pierik, A. J., Averill, B. A., Montfort, W. R., and Walker, F. A. (1999) Nitric oxide binding to the ferri- and ferroheme states of nitrophorin 1, a reversible NO-binding heme protein from the saliva of the blood-sucking insect, *Rhodnius prolixus*, *J. Am. Chem. Soc. 121*, 128-138.

53. Taylor, J. F., and Morgan, V. E. (1942) Oxidation-reduction potentials of the metmyoglobin-myoglobin system, *J. Biol. Chem. 144*, 15-20.
54. Berry, R. E., Shokhirev, M. N., Ho, A. Y. W., Yang, F., Shokhireva, T. K., Zhang, H., Weichsel, A., Montfort, W. R., and Walker, F. A. (2009) Effect of mutation of carboxyl side-cahin amino acids near the heme on the midpoint potentials and ligand binding constants of nitrophorin 2 and its NO, histamine, and imidazole complexes, *J. Am. Chem. Soc. 131*, 2313-2327.
55. Shokhireva, T. K., Berry, R. E., Uno, E., Balfour, C. A., Zhang, H., and Walker, F. A. (2003) Electrochemical and NMR spectroscopic studies of distal pocket mutants of nitrophorin 2: Stability, structure, and dynamics of axial ligand complexes, *Proc. Natl. Acad. Sci. U.S.A. 100*, 3778-3783.
56. Traylor, T. G., and Sharma, V. S. (1992) Why NO?, *Biochemistry 31*, 2847-2849.
57. Weinberger, B., Laskin, D. L., Heck, D. E., and Laskin, J. D. (2001) The toxicology of inhaled nitric oxide, *Toxicol. Sci. 59*, 5-16.
58. Davidson, D., Barefield, E. S., Kattwinkel, J., Dudell, G., Damask, M., Straube, R., Rhines, J., Chang, C.-T., and Group, t. I.-N. P. S. (1998) Inhaled nitric oxide for the early treatment of persistent pulmonary hypertension of the term newborn: A randomized, double-masked, placebo-controlled, dose-response, multicenter study, *Pediatrics 101*, 325-334.
59. Snyder, S. (1992) Nitric oxide: first in a new class of neurotransmitters, *Science 257*, 494-496.
60. Moncada, S., Palmer, R. M., and Higgs, E. A. (1991) Nitric oxide: physiology, pathophysiology, and pharmacology, *Pharmacol. Rev. 43*, 109-142.
61. Butler, A. R., and Williams, D. L. H. (1993) The physiological role of nitric oxide, *Chem. Soc. Rev. 22*, 233-241.
62. Koshland, D. (1992) The molecule of the year, *Science 258*, 1861.
63. Ignarro, L. J., Bush, P. A., Buga, G. M., Wood, K. S., Fukuto, J. M., and Rajfer, J. (1990) Nitric oxide and cyclic GMP formation upon electrical field stimulation cause relaxation of corpus cavernosum smooth muscle, *Biochem. Biophys. Res. Commun. 170*, 843-850.
64. Schmidt, H., Warner, T., Ishii, K., Sheng, H., and Murad, F. (1992) Insulin secretion from pancreatic B cells caused by L-arginine-derived nitrogen oxides, *Science 255*, 721-723.
65. Furchgott, R. F., and Zawadzki, J. V. (1980) The obligatory role of endothelial cells in the relaxation of arterial smooth muscle by acetylcholine, *Nature 288*, 373-376.
66. Moncada, S., and Higgs, A. (1993) The L-arginine-nitric oxide pathway, *N. Eng. J. Med. 329*, 2002-2012.
67. Basu, S., Grubina, R., Huang, J., Conradie, J., Huang, Z., Jeffers, A., Jiang, A., He, X., Azarov, I., Seibert, R., Mehta, A., Patel, R., King, B. S., Hogg, N., Ghosh, A., Gladwin, M.

T., and Kim-Shapiro, D. B. (2007) Cataclytic generation of N_2O_3 by the concerted nitrite reductase and anhydrase activity of hemoglobin, *Nature Chem. Biol. 3*, 785-794.

68. Gladwin, M. T., Grubina, R., and Doyle, M. P. (2009) The new chemical biology of nitrite reactions with hemoglobin: R-state catalysis, oxidative denitrosylation, and nitrite reductase/anhydrase, *Acc. Chem. Res. 42*, 157-167.
69. Shiva, S., Huang, Z., Grubina, R., Sun, J., Ringwood, L. A., MacArthur, P. H., Xu, X., Murphy, E., Darley-Usmar, V. M., and Gladwin, M. T. (2007) Deoxymyoglobin is a nitrite reductase that generates nitric oxide and regulates mitochondrial respiration, *Circ. Res. 100*, 654-661.
70. Basu, S., Azarova, N. A., Font, M. D., King, S. B., Hogg, N., Gladwin, M. T., Shiva, S., and Kim-Shapiro, D. B. (2008) Nitrite reductase activity of cytochrome c, *J. Biol. Chem. 283*, 32590-32597.
71. Garbers, D. L., and Lowe, D. G. (1994) Guanylyl cyclase receptors, *J. Biol. Chem. 269*, 30741-30744.
72. Zhao, Y., Brandish, P. E., Ballou, D. P., and Marletta, M. A. (1999) A molecular basis for nitric oxide sensing by soluble guanylate cyclase, *Proc. Natl. Acad. Sci. U.S.A. 96*, 14753-14758.
73. Karow, D. S., Pan, D., Tran, R., Pellicena, P., Presley, A., Mathies, R. A., and Marletta, M. A. (2004) Spectroscopic characterization of the soluble guanylate cyclase-like heme domains from vibrio cholerae and *Thermoanaerobacter tengcongensis Biochemistry 43*, 10203-10211.
74. Rosselli, M., Keller, R., and Dubey, R. (1998) Role of nitric oxide in the biology, physiology and pathophysiology of reproduction, *Hum. Reprod. Upd. 4*, 3-24.
75. Murad, F. (1994) Regulation of cytosolic guanylyl cyclase by nitric oxide: The NO-cyclic GMP signal transduction system, in *Advances in Pharmacology*, pp 19-33, Academic Press.
76. Humbert, P., Niroomand, F., Fischer, G., Mayer, B., Koesling, D., Hinsch, K.-D., Gausepohl, H., Frank, R., Schultz, G., and Böhme, E. (1990) Purification of soluble guanylyl cyclase from bovine lung by a new immunoaffinity chromatographic method, *Euro. J. Biochem. 190*, 273-278.
77. Stone, J. R., and Marletta, M. A. (1995) Heme stoichiometry of heterodimeric soluble guanylate cyclase, *Biochemistry 34*, 14668-14674.
78. Deinum, G., Stone, J. R., Babcock, G. T., and Marletta, M. A. (1996) Binding of nitric oxide and carbon monoxide to soluble guanylate cyclase as observed with resonance Raman spectroscopy, *Biochemistry 35*, 1540-1547.

79. Stone, J. R., and Marletta, M. A. (1994) Soluble guanylate cyclase from bovine lung: Activation with nitric oxide and carbon monoxide and spectral characterization of the ferrous and ferric states, *Biochemistry 33*, 5636-5640.

80. Pellicena, P., Karow, D. S., Boon, E. M., Marletta, M. A., and Kuriyan, J. (2004) Crystal structure of an oxygen-binding heme domain related to soluble guanylate cyclases, *Proc. Natl. Acad. Sci. U.S.A. 101*, 12854-12859.

81. Suzuki, S., Yoshimura, T., Nakahara, A., Iwasaki, H., Shidara, S., and Matsubara, T. (1987) Electronic and magnetic circular dichroism spectra of pentacoordinate nitrosylhemes in cytochromes *c*' from nonphotosynthetic bacteria and their model complexes, *Inorg. Chem. 26*, 1006-1008.

82. Iwasaki, H., Yoshimura, T., Suzuki, S., and Shidara, S. (1991) Spectral properties of *Achromobacter xylosoxidans* cytochrome *c*' and their NO complexes, *Biochim. Biophys. Acta 1058*, 79-82.

83. Yoshimura, T., Fujii, S., Kamada, H., Yamaguchi, K., Suzuki, S., Shidara, S., and Takakuwa, S. (1996) Spectroscopic characterization of nitrosylheme in nitric oxide complexes of ferric and ferrous cytochrome *c*' from photosynthetic bacteria, *Biochim. Biophys. Acta 1292*, 39-46.

84. Lawson, D. M., Stevenson, C. E. M., Andrew, C. R., and Eady, R. R. (2000) Unprecedented proximal binding of nitric oxide to heme: Implications for guanylate cyclase, *EMBO J. 19*, 5661-5671.

85. Ma, X., Sayed, N., Beuve, A., and van den Akker, F. (2007) NO and CO differentially activate soluble guanylate cyclase via a heme pivot-bend mechanism, *EMBO J. 26*, 578-588.

86. Ford, P. C. (2010) Reactions of NO and nitrite with heme models and proteins, *Inorg. Chem. 49*, 6226-6239.

87. Praneeth, V. K. K., Paulat, F., Berto, T. C., George, S. D., Näther, C., Sulok, C. D., and Lehnert, N. (2008) Electronic structure of six-coordinate iron(III)-porphyrin NO adducts: The elusive Iron(III)-NO(radical) state and its influence on the properties of these complexes, *J. Am. Chem. Soc. 130*, 15288-15303.

88. Goodrich, L. E., Paulat, F., Praneeth, V. K. K., and Lehnert, N. (2010) Electronic structure of heme-nitrosyls and its significance for nitric oxide reactivity, sensing, transport, and toxicity in biological systems, *Inorg. Chem. 49*, 6293-6316.

89. Scheidt, W. R., Duval, H. F., Neal, T. J., and Ellison, M. K. (2000) Intrinsic structural distortions in five-coordinate (nitrosyl)iron(II) porphyrinate derivatives, *J. Am. Chem. Soc. 122*, 4651-4659.

90. Lehnert, N., Galinato, M. G. I., Paulat, F., Richter-Addo, G. B., Sturhahn, W., Xu, N., and Zhao, J. (2010) Nuclear resonance vibrational spectroscopy applied to [Fe(OEP)(NO)]:

The vibrational assignments of five-coordinate ferrous heme-nitrosyls and implications for electronic structure, *Inorg. Chem. 49*, 4133-4148.

91. Silvernail, N. J., Olmstead, M. M., Noll, B. C., and Scheidt, W. R. (2009) Tetragonal to triclinic-A phase change for [Fe(TPP)(NO)], *Inorg. Chem. 48*, 971-977.
92. Praneeth, V. K. K., Näther, C., Peters, G., and Lehnert, N. (2006) Spectroscopic properties and electronic structure of five- and six-coordinate iron(II) porphyrin NO complexes: Effect of the axial N-donor ligand, *Inorg. Chem. 45*, 2795-2811.
93. Deatherage, J. F., and Moffat, K. (1979) Structure of nitric oxide hemoglobin, *J. Mol. Biol. 134*, 401-417.
94. Andrew, C. R., George, S. J., Lawson, D. M., and Eady, R. R. (2002) Six- to five-coordinate heme-nitrosyl conversion in cytochrome c' and its releveance to guanylate cyclase., *Biochemistry 41*, 2353-2360.
95. Wyllie, G. R. A., Schulz, C. E., and Scheidt, W. R. (2003) Five- to six-coordination in (nitrosyl)iron(II) porphyrinates: Effects of binding the sixth ligand, *Inorg. Chem. 42*, 5722-5734.
96. Paulat, F., Berto, T. C., DeBeer George, S., Goodrich, L., Praneeth, V. K. K., Sulok, C. D., and Lehnert, N. (2008) Vibrational assignments of six-coordinate ferrous heme nitrosyls: New insight from nuclear resonance vibrational spectroscopy, *Inorg. Chem. 47*, 11449-11451.
97. Copeland, D. N., Soares, A. S., West, A. H., and Richter-Addo, G. B. (2006) Crystal structures of the nitrite and nitric oxide complexes of horse heart myoglobin, *J. Inorg. Biochem. 100*, 1413-1425.
98. Miller, L. M., Pedraza, A. J., and Chance, M. R. (1997) Identification of conformational substates involved in nitric oxide binding to ferric and ferrous myoglobin through difference fourier transform infrared spectroscopy (FTIR), *Biochemistry 36*, 12199-12207.
99. Tomita, T., Hirota, S., Ogura, T., Olson, J. S., and Kitagawa, T. (1999) Resonance raman investigation of Fe-N-O structure of nitrosylheme in myoglobin and its mutants., *J. Phys. Chem. B 103*, 7044-7054.
100. Stong, J. D., Burke, J. M., Daly, P., Wright, P., and Spiro, T. G. (1980) Resonance Raman spectra of nitrosyl heme proteins and of porphyrin analogs, *J. Am. Chem. Soc. 102*, 5815-5819.
101. Lad, L., Wang, J., Li, H., Friedman, J., Bhaskar, B., Ortiz de Montellano, P. R., and Poulos, T. L. (2003) Crystal structures of the ferric, ferrous, and ferrous-NO forms of the Asp140Ala mutant of human heme oxygenase-1: Catalytic implications, *J. Mol. Biol. 330*, 527-538.

102. Sun, J., Wilks, A., Ortiz de Montellano, P. R., and Loehr, T. M. (1993) Resonance Raman and EPR spectroscopic studies on heme-heme oxygenase complexes, *Biochemistry 32*, 14151-14157.

103. Gong, W., Hao, B., and Chan, M. K. (2000) New mechanistic insights from structural studies of the oxygen-sensing domain of *Bradyrhizobium japonicum* FixL, *Biochemistry 39*, 3955-3962.

104. Tomita, T., Gonzalez, G., Chang, A. L., Ikeda-Saito, M., and Gilles-Gonzalez, M. A. (2002) A comparative resonance Raman analysis of heme-binding PAS domains: Heme iron coordination structures of the *Bj*FixL, *Ax*PDEA1, *Ec*Dos, and *Mt*Dos proteins., *Biochemistry 41*, 4819-4826.

105. Ellison, M. K., Schulz, C. E., and Scheidt, W. R. (2000) Structural and electronic characterization of nitrosyl(octaethylporphinato)iron(III) perchlorate derivatives, *Inorg. Chem. 39*, 5102-5110.

106. Linder, D. P., Rodgers, K. R., Banister, J., Wyllie, G. R. A., Ellison, M. K., and Scheidt, W. R. (2004) Five-coordinate $Fe^{III}NO$ and $Fe^{II}CO$ porphyrinates: Where are the electrons and why does it matter?, *J. Am. Chem. Soc. 126*, 14136-14148.

107. Kondrashov, D. A., Roberts, S. A., Weichsel, A., and Montfort, W. R. (2004) Protein functional cycle viewed at atomic resolution: Conformational change and mobility in nitrophorin 4 as a function of pH and NO binding, *Biochemistry 43*, 13637-13647.

108. Zareba, A. A. (2006) Resonance Raman spectroscopic characterization of nitrophorins from *Rhodnius prolixus* and *Cimex lectularius*, in *Department of Chemistry*, University of Houston, Houston, Texas (USA).

109. Nienhaus, K., Maes, E. M., Weichsel, A., Montfort, W. R., and Nienhaus, G. U. (2004) Structural dynamics controls nitric oxide affinity in nitrophorin 4, *J. Biol. Chem. 279*, 39401-39407.

110. Benko, B., and Yu, N.-T. (1983) Resonance Raman studies of nitric oxide binding to ferric and ferrous hemoproteins: Detection of Fe(III)-NO stretching, Fe(III)-N-O bending, and Fe(II)-N-O bending vibrations, *Proc. Natl. Acad. Sci. U.S.A. 80*, 7042-7046.

111. Wang, J., Lu, S., Moenne-Loccoz, P., and Ortiz de Montellano, P. R. (2003) Interaction of nitric oxide with human heme oxygenase-1, *J. Biol. Chem. 278*, 2341-2347.

112. Spiro, T. G., Zgierski, M. Z., and Kozlowski, P. M. (2001) Stereoelectronic factors in CO, NO and O2 binding to heme from vibrational spectroscopy and DFT analysis, *Coord. Chem. Rev. 219-221*, 923-936.

113. Evangelista-Kirkup, R., Smulevich, G., and Spiro, T. G. (1986) Alternative carbon monoxide binding modes for horseradish peroxidase studied by resonance Raman spectroscopy, *Biochemistry 25*, 4420-4425.

114. Ray, G. B., Li, X. Y., Ibers, J. A., Sessler, J. L., and Spiro, T. G. (1994) How far can proteins bend the FeCO unit? Distal polar and steric effects in heme proteins and models, *J. Am. Chem. Soc. 116*, 162-176.

115. Ibrahim, M., Xu, C., and Spiro, T. G. (2006) Differential sensing of protein influences by NO and CO vibrations in heme addcuts, *J. Am. Chem. Soc. 128*, 16834-16845.

116. Spiro, T. G., and Wasbotten, I. H. (2005) CO as a vibrational probe of heme protein active sites., *J. Inorg. Biochem. 99*, 34-44.

117. Coyle, C. M., Vogel, K. M., Rush III., T. S., Kozlowski, P. M., Williams, R., Spiro, T. G., Dou, Y., Ikeda-Saito, M., Olson, J. S., and Zgierski, M. Z. (2003) FeNO structure in distal pocket mutants of myoglobin based on resonance Raman spectroscopy, *Biochemistry 42*, 4896-4903.

118. Eisenberg, R., and Meyer, C. D. (1975) Coordination chemistry of nitric oxide, *Acc. Chem. Res. 8*, 26-34.

119. Fernandez, B. O., and Ford, P. C. (2003) Nitrite catalyzes ferriheme protein reductive nitrosylation, *J. Am. Chem. Soc. 125*, 10510-10511.

120. Hoshino, M., Maeda, M., Konishi, R., Seki, H., and Ford, P. C. (1996) Studies on the reaction mechanism for reductive nitrosylation of ferrihemoproteins in buffer solutions, *J. Am. Chem. Soc. 118*, 5702-5707.

121. Jee, J.-E., and van Eldik, R. (2006) Mechanistic studies on the nitrite-catalyzed reductive nitrosylation of highly charged anionic and cationic Fe^{III} porphyrin complexes, *Inorg. Chem. 45*, 6523-6534.

122. Hoshino, M., Maeda, M., Konishi, R., Seki, H., and Ford, P. C. (1996) Studies on the reaction mechanism for reductive nitrosylation for ferrihemoproteins in buffer solutions, *J. Am. Chem. Soc. 118*, 5702-5707.

123. Mensinga, T. T., Speijers, G. J. A., and Meulenbelt, J. (2003) Health implications of exposure to environmental nitrogenous compounds, *Toxicol. Rev. 22*, 41-51.

124. Lundberg, J. O., Weitzberg, E., and Gladwin, M. T. (2008) The nitrate-nitrite-nitric oxide pathway in physiology and therapeutics, *Nat. Rev. Drug Discov. 7*, 156-167.

125. Cosby, K., Partovi, K. S., Crawford, J. H., Patel, R. P., Reiter, C. D., Martyr, S., Yang, B. K., Waclawiw, M. A., Zalos, G., Xu, X., Huang, K. T., Shields, H., Kim-Shapiro, D. B., Schechter, A. N., Cannon, R. O., and Gladwin, M. T. (2003) Nitrite reduction to nitric oxide by deoxyhemoglobin vasodilates the human circulation, *Nat Med 9*, 1498-1505.

126. Gladwin, M. T., Schechter, A. N., Kim-Shapiro, D. B., Patel, R. P., Hogg, N., Shiva, S., Cannon III., R. O., Kelm, M., Wink, D. A., Espey, M. G., Oldfield, E. H., Pluta, R. M., Freeman, B. A., Lancaster Jr., J. R., Feelisch, M., and Lundberg, J. O. (2005) The emerging biology of the nitrite anion, *Nature Chem. Biol. 1*, 308-314.

127. Averill, B. A. (1996) Dissimilatory nitrite and nitric oxide reductases, *Chem. Rev. 96*, 2951-2964.

128. Zumft, W. (1997) Cell biology and molecular basis of denitrification, *Microbiol. Mol. Biol. Rev. 61*, 533-616.

129. Moura, I., and Moura, J. J. G. (2001) Structural aspects of denitrifying enzymes, *Curr. Opin. Chem. Biol. 5*, 168-175.

130. Wasser, I. M., de Vries, S., Mönne-Loccoz, P., Schröder, I., and Karlin, K. D. (2002) Nitric oxide in biological denitrification: Fe/Cu metalloenzyme and metal complex NOx redox chemistry, *Chem. Rev. 102*, 1201-1234.

131. da Silva, G., Kennedy, E. M., and Dlugogorski, B. Z. (2006) Ab Initio procedure for aqueous-phase pKa calculation: The acidity of nitrous acid, *J. Phys. Chem. A 110*, 11371-11376.

132. Bard, A. J., Parsons, R., and Jordan, J. J. (1985) *Standard potentials in aqueous solutions, Marcel Dekker, New York.*

133. Samouilov, A., Kuppusamy, P., and Zweier, J. L. (1998) Evaluation of the magnitude and rate of nitric oxide production from nitrite in biological systems, *Arch. Biochem. Biophys. 375*, 1-7.

134. Wyllie, G. R. A., and Scheidt, W. R. (2002) Solid-state structures of metalloporphyrin NO_x compounds, *Chem. Rev. 102*, 1067-1089.

135. Nasri, H., Ellison, M. K., Chen, S., Huynh, B. H., and Scheidt, W. R. (1997) Sharing the π-bonding. An iron porphyrin derivative with trans, π-accepting axial ligands. Synthesis, EPR and Mössbauer spectra, and molecular structure of two forms of the complex nitronitrosyl(α,α,α,α-tetrakis(o-pivalamidophenyl)- porphinato)ferrate(II), *J. Am. Chem. Soc. 119*, 6274-6283.

136. Einsle, O., Messerschmidt, A., Huber, R., Kroneck, P. M. H., and Neese, F. (2002) Mechanism of the six-electron reduction of nitrite to ammonia by cytochrome *c* nitrite reductase, *J. Am. Chem. Soc. 124*, 11737-11745.

137. Williams, P. A., Fülöp, V., Garman, E. F., Saunders, N. F. W., Ferguson, S. J., and Hajdu, J. (1997) Haem-ligand switching during catalysis in crystals of a nitrogen-cycle enzyme, *Nature 389*, 406-412.

138. Crane, B. R., Siegel, L. M., and Getzoff, E. D. (1997) Probing the catalytic mechanism of sulfite reductase by X-ray crystallography: Structures of the *Escherichia coli* hemoprotein in complex with substrates, inhibitors, intermediates, and products, *Biochemistry 36*, 12120-12137.

139. Yi, J., Safo, M. K., and Richter-Addo, G. B. (2008) The nitrite anion binds to human hemoglobin via the uncommon *O*-nitrito mode, *Biochemistry 47*, 8247-8249.

140. Yi, J., Heinecke, J., Tan, H., Ford, P. C., and Richter-Addo, G. B. (2009) The distal pocket histidine residue in horse heart myoglobin directs the O-binding mode of nitrite to the heme iron, *J. Am. Chem. Soc. 131*, 18119-18128.

141. Goblirsch, B. R., Streit, B. R., DuBois, J. L., and Wilmot, C. M. (2010) Structural features promoting dioxygen production by *Dechloromonas aromatica* chlorite dismutase, *J. Biol. Inorg. Chem. 15*, 879-888.

142. Einsle, O., Messerschmidt, A., Stach, P., Bourenkov, G. P., Bartunik, H. D., Huber, R., and Kroneck, P. M. H. (1999) Structure of cytochrome c nitrite reductase, *Nature 400*, 476-480.

143. Einsle, O., Stach, P., Messerschmidt, A., Simon, J., Kröger, A., Huber, R., and Kroneck, P. M. H. (2000) Cytochrome c nitrite reductase from *Wolinella succinogenes*, *J. Biol. Chem. 275*, 39608-39616.

144. Doyle, M. P., and Hoekstra, J. W. (1981) Oxidation of nitrogen oxides by bound dioxygen in hemoproteins, *J. Inorg. Biochem. 14*, 351-358.

145. Huang, K. T., Keszler, A., Patel, N., Patel, R. P., Gladwin, M. T., Kim-Shapiro, D. B., and Hogg, N. (2005) The reaction between nitrite and deoxyhemoglobin, *J. Biol. Chem. 280*, 31126-31131.

146. Moore, E. G., and Gibson, Q. H. (1976) Cooperativity in the dissociation of nitric oxide from hemoglobin, *J. Biol. Chem. 251*, 2788-2794.

147. Heinecke, J., and Ford, P. C. (2010) Mechanistic studies of nitrite reactions with metalloproteins and models relevant to mammalian physiology, *Coord. Chem. Rev. 254*, 235-247.

148. Khin, C., Heinecke, J., and Ford, P. C. (2008) Oxygen atom transfer from nitrite mediated by Fe(III) porphyrins in aequous solution, *J. Am. Chem. Soc. 130*, 13820-13821.

149. Castro, C. E., and O'Shea, S. K. (1995) Activation of nitrite ion by iron(III) porphyrins. Stoichiometric oxygen transfer to carbon,. nitrogen, phosphorous, and sulfur, *J. Org. Chem. 60*, 1922-1923.

150. Conradie, J., and Ghosh, A. (2006) Iron(III)-nitro porphyrins: Theoretical exploration of a unique class of reactive molecules, *Inorg. Chem. 45*, 4902-4909.

151. O'Shea, S., Wall, T., and Lin, D. (2007) Activation of nitrite ion by biomimetic iron(III) complexes, *Trans. Met. Chem. 32*, 514-517.

152. Leonard, S. E., Reddie, K. G., and Carroll, K. S. (2009) Mining the thiol proteome for sulfenic acid modifications reveals new targets for oxidation in cells, *ACS Chem. Biol. 4*, 783-799.

153. Kettenhofen, N. J., and Wood, M. J. (2010) Formation, reactivity, and detection of protein sulfenic acids, *Chem. Res. Toxico. 23*, 1633-1646.

154. Raman, C. V., and Krishnan, K. S. (1928) A new type of secondary radiation, *Nature 121*, 501-502.

155. Spiro, T. G., and Czernuszewicz, R. S. (2000) Resonance Raman Spectroscopy, in *Physical Methods in Bioinorganic Chemistry - Spectroscopy and Magnetism* (Que Jr., L., Ed.) 1st ed., pp 59-119, University Science Books, Sausalito (CA).

156. Porto, S. P. S., and Wood, D. L. (1962) Ruby optical maser as a Raman source, *J. Opt. Soc. Am. 52*, 251-252.

157. Tobin, M. C. (1968) Raman Spectra of Crystalline Lysozyme, Pepsin, and Alpha Chymotrypsin, *Science 161*, 68-69.

158. Spiro, T. G., and Li, X.-Y. (1988) Resonance Raman spectroscopy of metalloporphyrins, in *Biological Application of Raman Spectroscopy, Vol. III, Resonance Raman spectroscopy of metalloporphyrins* (Spiro, T. G., Ed.) 1st ed., pp 1-38, John Wiley & Sons, New York (USA).

159. Gouterman, M. (1978) Optical spectra and electronic structure of porphyrins and related rings, in *The Porphyrins* (Dolphin, D., Ed.), pp 1-165, Academic Press, New York (United States).

160. Li, X. Y., Czernuszewicz, R. S., Kincaid, J. R., Stein, P., and Spiro, T. G. (1990) Consistent porphyrin force field. 2. Nickel octaethylporphyrin skeletal and substituent mode assignments from nitrogen-15, meso-d4, and methylene-d16 Raman and infrared isotope shifts, *J. Phys. Chem. 94*, 47-61.

161. Spiro, T. G., and Stein, P. (1977) Resonance effects in vibrational scattering from complex molecules, *Annu. Rev. Phys. Chem. 28*, 501-521.

162. Cheung, L. D., Yu, N.-T., and Felton, R. H. (1978) Resonance raman spectra and excitation profiles of soret-excited metalloporphyrins, *Chem. Phys. Lett. 55*, 527-530.

163. Spiro, T. G., and Strekas, T. C. (1974) Resonance Raman spectra of heme proteins. Effects of oxidation and spin state, *J. Am. Chem. Soc. 96*, 338-345.

164. Abe, M., Kitagawa, T., and Kyogoku, Y. (1978) Resnonce Raman spectra of octaethylporphyrinato-Ni(II) and *meso*-deuterated and ^{15}N substituted derivatives. II. A normal coordinate analysis, *J. Chem. Phys. 69*, 4526-4534.

165. Kitagawa, T., Kyogoku, Y., Iizuka, T., and Saito, M. I. (1976) Nature of the iron-ligand bond in ferrous low spin hemoproteins studied by resonance Raman scattering, *J. Am. Chem. Soc. 98*, 5169-5173.

166. Ozaki, Y., Kitagawa, T., Kyogoku, Y., Shimada, H., Iizuka, T., and Ishimura, Y. (1976) An anomaly in the resonance Raman spectra of cytochrome P-450cam in the ferrous high-spin state, *J. Biochem. 80*, 1447-1451.

167. Hobbs, J. D., Larsen, R. W., Meyer, T. E., Hazzard, J. H., Cusanovich, M. A., and Ondrias, M. R. (1990) Resonance Raman characterization of *Chromatium vinosum*

cytochrom *c*'. Effect of pH and comparison of equilibrium and photolyzed cabron monoxide species, *Biochemistry 29*, 4166-4174.

168. Nakamoto, K. (1997) Section V-1. Myoglobin and Hemoglobin, in *Infrared and Raman Spectra of Inorganic and Coordination Compounds, Part B: Application in Coordination, Organometallic, and Bioinorganic Chemistry* (Nakamoto, K., Ed.) 5th ed., pp 319-325, John Wiley & Sons, Inc., New York.
169. Palmer, G. (2000) Electron Paramagnetic Resonance of Metalloproteins, in *Physical Methods in Bioinroganic Chemistry* (Que, L., Ed.) 1st ed., pp 121-186, University Science Books, Sausalito, CA (USA).
170. Hagen, W. R. (2009) *Biomolecular EPR Spectroscopy*, 1st ed., CRC Press, Boca Raton, Florida (USA).
171. Rivera, M., and Caignan, G. A. (2004) Recent developments in the ^{13}C NMR spectroscopic analysis of paramagnetic hemes and heme proteins, *Anal. Bioanal. Chem. 378*, 1464-1483.
172. Walker, F. A. (1999) Magnetic spectroscopy (EPR, ESEEM, Mössbauer, MCD and NMR) studies of low-spin ferriheme centers and their corresponding heme proteins, *Coord. Chem. Rev. 185-186*, 471-534.
173. Zoppellaro, G., Harbitz, E., Kaur, R., Ensign, A. A., Bren, K. L., and Andersson, K. K. (2008) Modulation of the ligand-field anisotropy in a series of ferric low-spin cytochrome c mutants derived from *Pseudomonas aeruginosa* Cytochrome *c*-551 and *Nitrosomonas europaea* Cytochrome *c*-552: A nuclear magnetic resonance and electron paramagnetic resonance study, *J. Am. Chem. Soc. 130*, 15348-15360.
174. Migita, C. T., and Iwaizumi, M. (1981) Low-temperature EPR studies of highly anisotropic low-spin (protoporphyrinato)iron(III) complexes, *J. Am. Chem. Soc. 103*, 4378-4381.
175. Walker, F. A., Reis, D., and Balke, V. L. (1984) Models of the cytochromes *b*. 5. EPR studies of low-spin iron(III) tetraphenylporphyrins, *J. Am. Chem. Soc. 106*, 6888-6898.
176. Taylor, C. P. S. (1977) The EPR of low spin heme complexes. Relation of the t_{2g} hole model to the directional properties of the *g* tensor, and a new method for calculating the ligand field parameters, *Biochim. Biophys. Acta 491*, 137-149.
177. Griffith, J. S. (1957) Binding in haemoglobin azide as determined by electron resonance: Theory of electron resonance in ferrihaemoglobin azide, *Nature 180*, 30-31.
178. Benjamin, N., O'Driscoll, F., Dougall, H., Duncan, C., Smith, L., Golden, M., and McKenzie, H. (1994) Stomach NO synthesis, *Nature 368*, 502-502.
179. Lundberg, J. O., Weitzberg, E., Lundberg, J. M., and Alving, K. (1994) Intragastric nitric oxide production in humans: measurements in expelled air, *Gut 35*, 1543-1546.
180. Zweier, J. L., Wang, P., Samouilov, A., and Kuppusamy, P. (1995) Enzyme-independent formation of nitric oxide in biological tissues, *Nat Med 1*, 804-809.

181. Benabbas, A., Ye, X., Kubo, M., Zhang, Z., Maes, E. M., Montfort, W. R., and Champion, P. M. (2010) Ultrafast dynamics of diatomic ligand binding to nitrophorin 4, *J. Am. Chem. Soc. 132*, 2811-2820.

182. Ribeiro, J. M. C. (1996) Salivary thiol oxidase activity of *Rhodnius prolixus*, *Insect Biochem. Mol. Biol. 26*, 899-905.

183. Krause, G., Lundstrom, J., Barea, J. L., De la Cuesta, C. P., and Holmgren, A. (1991) Mimicking the active site of protein disulfide-isomerase by substitution of proline 34 in Escherichia coli thioredoxin, *J. Biol. Chem. 266*, 9494-9500.

184. Huber-Wunderlich, M., and Glockshuber, R. (1998) A single dipeptide sequence modulates the redox properties of a whole enzyme family, *Folding Des. 3*, 161-171.

185. Mayhew, S. G. (1978) The redox potential of dithionite and SO_2^- from equilibrium reactions with flavodoxins, methyl viologen and hydrogen plus hydrogenase, *Eur. J. Biochem. 85*, 535-547.

Chapter 2. Formation of nitric oxide from nitrite by the ferriheme *b* protein nitrophorin 7[‡‡]

(He, C.; Knipp, M. *J. Am. Chem. Soc.* **2009**, *131*, 12042-12403)

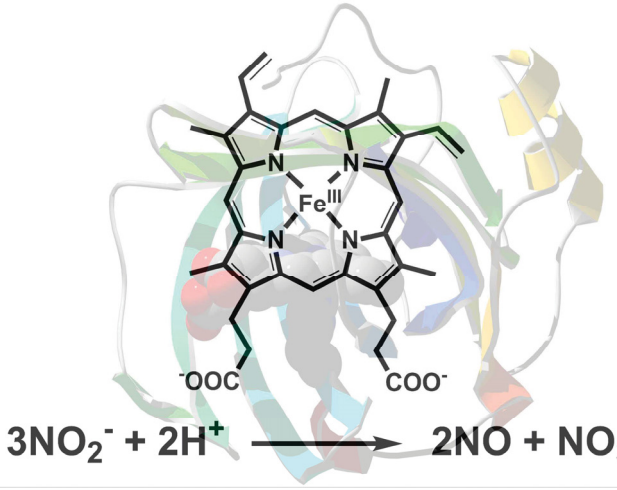

[‡‡]Reprinted with permission from He, C., Knipp, M. *J. Am. Chem. Soc.* **2009**, *113*, 12402-12403. Copyright 2009 American Chemical Society.

Abstract

Recently, the conversion of nitrite into NO by certain heme proteins, in particular hemoglobin, gained much interest as a physiologically important source of NO in human tissue. However, in an aqueous environment, nitrite reduction at an iron porphyrin occurs either through oxidation of ferroheme to ferriheme or with the assistance of a second substrate molecule. Here we report on the reduction of nitrite in the absence of a second substrate at the heme center of the ferriheme protein nitrophorin 7 (NP7) resulting in the formation of NO and restoration of the ferriheme center. The product was spectroscopically characterized, in particular by resonance Raman and FT-IR spectroscopy. Performing the reaction in the presence of the NO trap 2-(4-trimethylammonio)phenyl-4,4,5,5-tetramethylimidazoline-1-oxyl 3-oxide (TMA-PTIO) revealed that continuous NO production is possible, i.e., that NP7 is fully restored upon a single turnover. Thus, NP7 is the first case of a b-type heme that performs reduction of nitrite as a single substrate out of the iron(III) state.

J|A|C|S COMMUNICATIONS

Published on Web 08/05/2009

Formation of Nitric Oxide from Nitrite by the Ferriheme *b* Protein Nitrophorin 7

Chunmao He and Markus Knipp*

Max-Planck-Institut für Bioanorganische Chemie, Stiftstrasse 34-36, D-45470 Mülheim an der Ruhr, Germany

Received May 18, 2009; E-mail: mknipp@mpi-muelheim.mpg.de

The formation of the central signaling molecule NO[1] from NO_2^- occurring in the blood has recently been identified as an exceedingly important physiological reaction in the human organism.[2] The conversion is, at least in part, accomplished at the heme iron of hemoglobin (Hb). However, whereas deoxyHb exhibits nitrite reductase and anhydrase activities,[2c] reaction of NO_2^- with metHb and also met-myoglobin (metMb) is not observed.[3] Moreover, in the presence of certain base molecules functioning as oxygen atom acceptors, the conversion of NO_2^- into NO was described for the model heme Fe^{III}(TPPS) [TPPS = tetra(sulfonatophenyl)porphyrinato anion] in aqueous solution at pH 5.8 and 6.3.[4]

The nitrophorins (NPs) constitute a group of ferriheme proteins from the saliva of the blood-feeding insect *Rhodnius prolixus* that coordinate the heme via a His residue.[5] Their biological function is to transport NO as a vasodilator into the host's tissue (pH ~7.4). Contrary to metHb and metMb, recombinant nitrophorin 7 (NP7) shows a marked spectral change upon incubation with $NaNO_2$ as the sole substrate, as shown in Figure 1, even at pH 7.5.[6] The spectral change clearly exhibits isosbestic behavior and reaches saturation after some time, indicating the full conversion into a compound **1** that is EPR-silent. The absorption spectrum of **1** is similar to that of the {FeNO}^{6} species[7] of NP7,[8] but the resolution of UV−vis spectroscopy is not high enough for unambiguous identification.

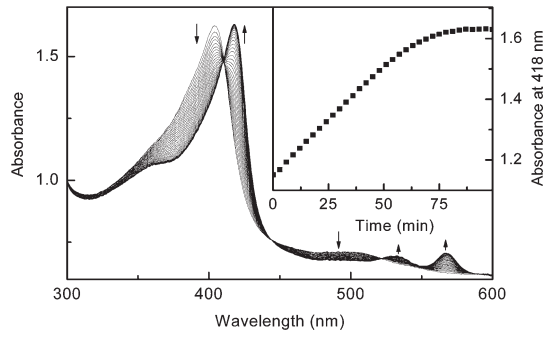

Figure 1. Spectral change observed for NP7 in 100 mM MOPS/NaOH, 50 mM NaCl (pH 7.5) at 37 °C in the presence of 1 mM $NaNO_2$.

For further characterization of **1**, resonance Raman (RR) spectroscopy of **1** in comparison to NP7[Fe^{III}] and NP7{FeNO}^{6} was performed. The high-frequency region of each of the resulting spectra is presented in Figure 2. In general, the spectra of NP7[Fe^{III}] and NP7{FeNO}^{6} compare well with the corresponding RR spectra reported for NP1 and NP4.[9] Moreover, the spectral traces of NP7{FeNO}^{6} and **1** are identical. As in the case of the NP1 and NP4 nitrosyls,[9] the so-called oxidation state marker $\nu_4 = 1376$ cm^{-1} for both NP7 complexes indicates significant ferriheme character. The ν_3 mode in case of NP7[Fe^{III}] (1484 cm^{-1}) exhibits the typical frequency of a six-coordinate high-spin (water on) heme, whereas the shift toward 1509 cm^{-1} upon NO binding is characteristic for six-coordinate low-spin hemes.[10]

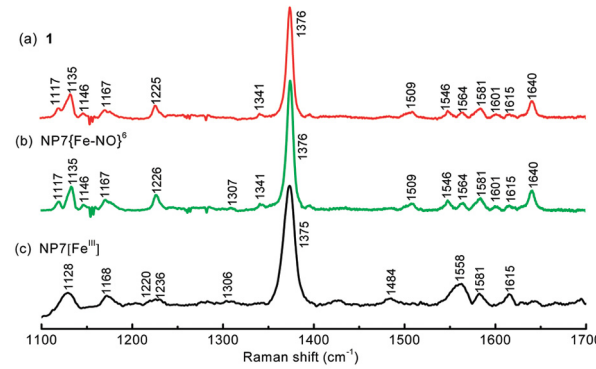

Figure 2. Resonance Raman spectra of (a) **1**, (b) NP7{FeNO}^{6}, and (c) NP7[Fe^{III}]. All samples were prepared in 100 mM MOPS/NaOH, 50 mM NaCl (pH 7.5). Spectra were recorded at 77 K with $\lambda_{ex} = 406.7$ nm.

The identification of **1** as an {FeNO}^{6} entity by RR spectroscopy is well-supported by FT-IR spectroscopy, which shows the vibrational mode of the Fe−N−O fragment at 1903 cm^{-1} and a shoulder at 1911 cm^{-1} (see Figure S1 in the Supporting Information). The comparison with other heme proteins in Table 1 shows that this mode is characteristic of ferriheme nitrosyl complexes.

Table 1. Frequency of the N−O Stretching Vibration of **1** in Comparison with Those in Nitrosyl Complexes of Some Representatives of Histidine-Coordinating Ferriheme Proteins

ferric heme protein	ν_{N-O} (cm^{-1})	reference
1 (this work)	1903, 1911 (shoulder)	this work
R. prolixus NP1	1904 (shoulder), 1917	11
R. prolixus NP4	1908, 1922 (weak)	12
human Hb	1925	13
horse Mb	1927	14
P. stutzeri cd_1 nitrite reductase	1910	13

2-(4-Trimethylammonio)phenyl-4,4,5,5-tetramethylimidazoline-1-oxyl 3-oxide (TMA-PTIO) was applied as a spin trap for NO quantification.[15] As Figure 3a shows, addition of TMA-PTIO to **1** leads to the loss of NO from the iron and concomitant formation of the initial high-spin NP7[Fe^{III}]. Upon completion of the reaction, the amount of NO was determined by EPR spectroscopy of TMA-PTIO (Figure S2 in the Supporting Information). An equimolar protein/NO ratio of 1:(1.1 ± 0.1) was determined. As a control, NO was not detected when TMA-PTIO was added to a solution void of NP7. Furthermore, initiation of the reaction in the presence of 15 μM TMA-PTIO did not change the Soret band absorption until TMA-PTIO was completely consumed (Figure 3b). This reflects the fact that the protein is fully recovered upon turnover and that it is generally capable of catalytically producing NO in the presence of an NO acceptor, as is the case in vivo. The integrity of the protein mass was confirmed by ESI-Q-TOF MS.

The only potential electron source is one or more other nitrite molecules. To test this hypothesis, the amounts of NO_2^- consumed

10.1021/ja9040362 CCC: $40.75

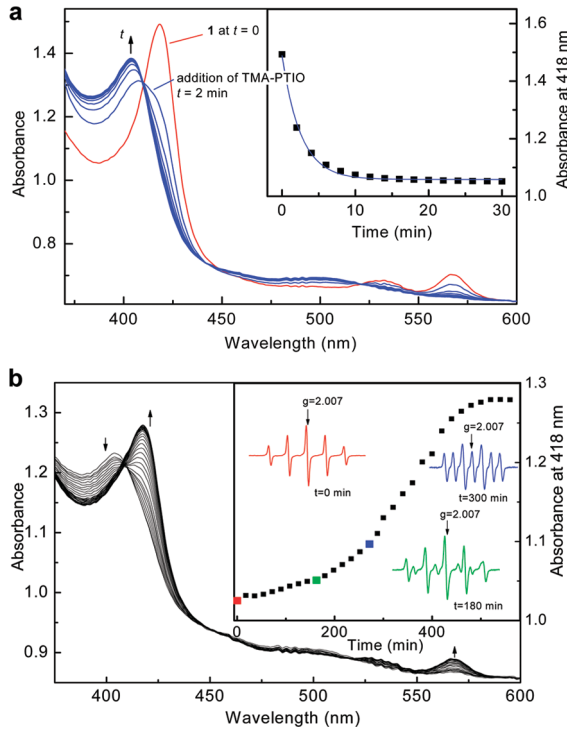

Figure 3. (a) Absorption spectrum of **1** in 100 mM MOPS/NaOH, 50 mM NaCl (pH 7.5) (red trace). The spectrum changes upon addition of TMA-PTIO (blue traces), leading to the initial species in a first-order process with $t_{1/2} = 1.7$ min ($R = 0.9981$) (inset). (b) Absorption spectra for the reaction of NP7 (10.6 μM) with 10 mM $NaNO_2$ in the presence of 15 μM TMA-PTIO at 37 °C. The inset shows the change of the Soret absorption vs time and the EPR spectra taken at room temperature at the indicated time points.

and NO_3^- produced were determined by an adapted Griess reaction.[16] In comparison with the amount of NP7, 1.41 ± 0.03 molar equiv of NO_2^- was consumed while 0.51 ± 0.01 molar equiv of NO_3^- was simultaneously produced.[17] Furthermore, the formation of **1** is strongly pH dependent: at pH 6.0, the conversion is rapidly accomplished (Figure S3 in the Supporting Information), in good agreement with the disproportionation

$$3NO_2^- + 2H^+ \rightarrow 2NO + NO_3^- + H_2O$$

By analogy to the nitrite anhydrase reaction catalyzed by metHb,[2c] N_2O_3, which homolyzes to NO and NO_2, is a considerable product. In water, NO_2 further decomposes, yielding NO_3^-. However, excess 5,5-dimethyl-1-pyrroline-*N*-oxide (DMPO)[18] in the NP7 reaction did not affect the yield of NO_3^- (Figure S4 in the Supporting Information). Furthermore, the expected nitroxide radical was not detected by EPR spectroscopy. Notably, NO is required as a trigger for metHb nitrite anhydrase reaction.[2] Altogether, the results suggest a significantly different reactivity of NP compared to metHb.

A reaction between the heme d_1 center of heme cd_1 nitrite reductase and NO_2^- was recently described with both hemes in Fe^{III}; however, the reductant is not clear.[19] The disproportionation of NO_2^- readily occurs in strongly acidic solution, but the rate is extremely low at pH ≥7.[20] Although the reaction is not promoted by heme proteins,[3] it was observed in a few model ferrihemes with exclusion of water.[21] Similarly, Fe^{III}salen promotes the NO_2^-disproportionation noncatalytically in dry CH_3CN, yielding $(Fe^{III}salen)_2O$, but water strongly decreases the yield.[22]

In conclusion, the catalytic NO_2^- disproportionation supported by the ferriheme of NP is an unprecedented case in an aqueous environment. This process suggests that in vivo NP may not only be a NO transporter but also can act as a NO producer.

Acknowledgment. The authors are grateful for the technical assistance of Johanna Taing, Fabian Kalveram, Maria Pandelia, and Jan Hanis. This work was financially supported by the Max Planck Society (MPG) and the Deutsche Forschungsgemeinschaft (DFG) (Grant KN 951/1-1 to M.K.).

Supporting Information Available: Complete refs 2b and 2c, experimental details, the FT-IR spectrum of **1**, NO quantification by EPR, UV-vis spectra for the reaction of NP7 with NO_2^- at pH 6.0 and the reaction in the presence of DMPO, and the stoichiometry of the reaction. This material is available free of charge via the Internet at http://pubs.acs.org.

References

(1) For reviews, see, for example: (a) Thomas, D. D.; Ridnour, L. A.; Isenberg, J. S.; Flores-Santana, W.; Switzer, C. H.; Donzelli, S.; Hussain, P.; Vacoli, C.; Paolocci, N.; Ambs, S.; Colton, C. A.; Harris, C. C.; Roberts, D. D.; Wink, D. A. *Free Radical Biol. Med.* **2008**, *45*, 18. (b) Knipp, M. *ChemBioChem* **2006**, *7*, 879. (c) Napoli, C.; Ignarro, L. J. *Annu. Rev. Pharmacol. Toxicol.* **2003**, *43*, 97.
(2) (a) Gladwin, M. T.; Grubina, R.; Doyle, M. P. *Acc. Chem. Res.* **2009**, *42*, 157. (b) Gladwin, M. T.; et al. *Nat. Chem. Biol.* **2005**, *1*, 308. (c) Basu, S.; et al. *Nat. Chem. Biol.* **2007**, *3*, 785.
(3) (a) Wanat, A.; Gdula-Argasińska, J.; Rutkowska-Żbik, D.; Witko, M.; Stochel, G.; van Eldik, R. *J. Biol. Inorg. Chem.* **2002**, *7*, 165. (b) Fernandez, B. O.; Ford, P. C. *J. Am. Chem. Soc.* **2003**, *125*, 10510. (c) Our own observations for horse-heart Mb under the same conditions as described here for NP7 (data not shown).
(4) Khin, C.; Heinecke, J.; Ford, P. C. *J. Am. Chem. Soc.* **2008**, *130*, 13830.
(5) (a) Lehane, M. J. *The Biology of Blood-Sucking in Insects*, 2nd ed.; Cambridge University Press: Cambridge, U.K., 2005. (b) Walker, F. A. *J. Inorg. Biochem.* **2005**, *99*, 216. (c) Ribeiro, J. M. C.; Hazzard, J. M.; Nussenzveig, R. H.; Champagne, D. E.; Walker, F. A. *Science* **1993**, *260*, 539.
(6) To avoid possible interference from atmospheric O_2, all of the reactions were carried out under strictly anaerobic conditions. The reaction with NO_2^- is also observed with other NPs when performed in phosphate buffer.
(7) According to the notation of Feltham and Enemark (see: Feltham, R. D.; Enemark, J. H. *Coord. Chem. Rev.* **1974**, *13*, 339).
(8) (a) Knipp, M.; Yang, F.; Berry, R. E.; Zhang, H.; Shokhirev, M. N.; Walker, F. A. *Biochemistry* **2007**, *46*, 13254. (b) Knipp, M.; Zhang, H.; Berry, R. E.; Walker, F. A. *Protein Expression Purif.* **2007**, *54*, 183.
(9) (a) Maes, E. M.; Walker, F. A.; Montfort, W. R.; Czernuszewicz, R. S. *J. Am. Chem. Soc.* **2001**, *123*, 1164. (b) Kubo, M.; Gruia, F.; Benabbas, A.; Barabanschikov, A.; Montfort, W. R.; Maes, E. M.; Champion, P. M. *J. Am. Chem. Soc.* **2008**, *130*, 9800.
(10) Spiro, T. G.; Stong, J. D.; Stein, P. *J. Am. Chem. Soc.* **1979**, *101*, 2648.
(11) Ding, X. D.; Weichsel, A.; Andersen, J. F.; Shokhireva, T. Kh.; Balfour, C.; Pierik, A. J.; Averill, B. A.; Montfort, W. R.; Walker, F. A. *J. Am. Chem. Soc.* **1999**, *121*, 128.
(12) Nienhaus, K.; Maes, E. M.; Weichsel, A.; Montfort, W. R.; Nienhaus, G. U. *J. Biol. Chem.* **2004**, *279*, 39401.
(13) Wang, Y.; Averill, B. A. *J. Am. Chem. Soc.* **1996**, *118*, 3972.
(14) Miller, L. M.; Pedraza, A. J.; Chance, M. R. *Biochemistry* **1997**, *36*, 12199.
(15) Osipov, A. N.; Gorbunov, N. V.; Day, B. W.; Elsayed, N. M.; Kagan, V. E. *Methods Enzymol.* **1996**, *268*, 193.
(16) Beda, N.; Nedospasov, A. *Nitric Oxide* **2005**, *13*, 93.
(17) Data for NP4 in phosphate buffer (pH 7.5): 1.48 ± 0.03 molar equiv of NO_2^- consumed; 0.50 ± 0.01 molar equiv of NO_3^- formed.
(18) DMPO is an effective NO_2 scavenger. See: (a) Astolfi, P.; Greci, L.; Panagiotaki, M. *Free Radical Res.* **2005**, *39*, 137. (b) Reszka, K. J.; McCormick, M. L.; Buettner, G. R.; Hart, C. M.; Britigan, B. E. *Nitric Oxide* **2006**, *15*, 133.
(19) (a) van Wonderen, J. H.; Knight, C.; Oganesyan, V. S.; George, S. J.; Zumpft, W. G.; Cheesman, M. R. *J. Biol. Chem.* **2007**, *282*, 28207. (b) Oganesyan, V. S.; Cheesman, M. R.; Thomson, A. J. *Inorg. Chem.* **2007**, *46*, 10950.
(20) Samouilov, A.; Kuppusamy, P.; Zweier, J. L. *Arch. Biochem. Biophys.* **1998**, *357*, 1.
(21) For example, see: Munro, O. Q.; Scheidt, W. R. *Inorg. Chem.* **1998**, *37*, 2308.
(22) Ankers, D. L.; Fanning, J. C. *Polyhedron* **2001**, *20*, 623.

JA9040362

Formation of Nitric Oxide from Nitrite by the Ferriheme *b* Protein Nitrophorin 7

Chunmao He and Markus Knipp*

Max-Planck-Institut für Bioanorganische Chemie, Stiftstrasse 34-36, D-45470 Mülheim an der Ruhr, Germany

* Supporting Information *

Content:

Complete References 2b and 2c

Experimental Details

Additional Figures:

- Figure S1
- Figure S2
- Figure S3
- Figure S4
- Figure S5

Additional Tables:

- Table S1

* Corresponding author; Phone: +49 (0)208 306 3581; Fax: +49 (0)208 306 3951; E-mail: mknipp@mpi-muelheim.mpg.de.

Complete References 2b and 2c

(2b) Gladwin, M. T.; Schechter, A. N.; Kim-Shapiro, D. B.; Patel, R. P.; Hogg, N.; Shiva, S.; Cannon III., R. O.; Kelm, M.; Wink, D. A.; Espey, M. G.; Oldfield, E. H.; Pluta, R. M.; Freeman, B. A.; Lancaster Jr.; J. R.; Feelish, M.; Lundberg, J. O. *Nature Chem. Biol.* **2005**, *1*, 308-314.

(2c) Basu, S.; Grubina, R.; Huang, J.; Conradie, J.; Huang, Z.; Jeffers, A.; Jiang, A.; He, X.; Azarov, I.; Seibert, R.; Mehta, A.; Patel, R.; King, S. B.; Hogg, N.; Ghosh, A.; Gladwin, M. T.; Kim-Shapiro, D. B. *Nature Chem. Biol.* **2007**, *3*, 785-794.

Experimental Details

Materials. Diethylammonium (*Z*)-1-(*N*,*N*-diethylamino)diazen-1-ium-1,2-diolate (DEA/NO),[†] 2-(4-trimethylammonio)phenyl-4,4,5,5-tetramethylimidazoline-1-oxyl 3-oxide · $CH_3SO_4^-$ (TMA-PTIO · $CH_3SO_4^-$), and 5,5-dimethyl-1-pyrroline-*N*-oxide (DMPO) were from Alexis Biochemicals. Stock solutions of DEA/NO (1 - 5 mM) were prepared freshly on a daily basis in 10 mM NaOH and kept on ice. Their concentrations were photometrically determined ($\epsilon_{250\ nm}$ = 6,500 M^{-1} cm^{-1}).[1] Stock solutions of $NaNO_2$ were prepared freshly every day in water and photometrically calibrated ($\epsilon_{210\ nm}$ = 5,380 M^{-1}

[†] **List of Abbreviations:** DEA/NO, diethylammonium (*Z*)-1-(*N*,*N*-diethylamino)diazen-1-ium-1,2-diolate; DMPO, 5,5-dimethyl-1-pyrroline-*N*-oxide; DTPA, diethylentriaminepentaacetic acid; MALDI, matrix-assisted laser desorption/ionization; TMA–PTIO, 2-(4-trimethylammonio)phenyl-4,4,5,5-tetramethylamidazoline-1-oxyl 3-oxide; TMA–PTI, 2-(4-trimethylammonio)phenyl-4,4,5,5-tetramethylamidazoline-1-oxyl; MES, 2-morpholino-ethanesulfonic acid; MOPS, 3-(*N*-morpholino)propanesulfonic acid; NP, nitrophorin; TOF, time-of-flight.

cm^{-1}).[2] Stock solutions of 5 mM TMA-PTIO were prepared in water using photometric calibration ($\epsilon_{255\ nm}$ = 10,965 M^{-1} cm^{-1}).[3] All other reagents were of the highest grade commercially available and used as received. The reactions were carried out in an anaerobic chamber containing 1 - 2% H_2 and Pd catalysts (Coy Laboratory Products Inc.; [O_2] < 1 ppm).

Protein Preparation. Prior to protein production, the plasmid for protein expression, pNP7^{Kan} [4,5] was transformed into *Escherichia coli* strain BL21(DE3) (Novagen). NP7 was expressed, then reconstituted by a step-wise heme insertion, and finally purified as was described previously.[4,6] Protein preparations were judged by SDS-PAGE to be ~90% pure. Protein was also subjected to MALDI-TOF MS to confirm the correct molecular masses including an initial Met-0 residue and accounting for two Cys–Cys disulfides (calculated for $[NP7 + H]^+$: 20,969 Da, observed: 20,966 Da). Proteins were stored at -20 ºC in 200 mM Na*OAc*/H*OAc*, 10% (v/v) glycerol (pH 5.0) until use.

Absorbance Spectroscopy. Proteins were thawed and the buffer was exchanged with 100 mM MOPS/NaOH, 50 mM NaCl (pH 7.5) or 100 mM MES/NaOH, 50 mM NaCl (pH 6.0) by dialysis (NMWL = 12 - 14 kDa) inside the anaerobic chamber. Reactions were carried out in a 1-cm quartz cuvette, which was located inside the anaerobic chamber. The cuvette temperature was adjusted to 37 ºC by a water bath. Solutions containing 7 - 15 μM of NP7 was incubated with 1 mM of $NaNO_2$ and the absorption spectra were recorded every 2 min on a Cary 50 spectrophotometer.

Resonance Raman (RR) Spectroscopy. Samples for RR spectroscopy were concentrated in Ultrafree ultrafiltration concentrators (NMWL = 10 kDa; Millipore). Upon

reaction, a degassed solution of $NaNO_2$ (10 mM) was added to the protein solution (~80 μM). NO-bound NP7 was prepared by the addition of excess DEA/NO (0.5 mM) to the protein. Samples were transferred to a 3 mm quartz tube and frozen in liquid nitrogen. RR spectra were recorded with a scanning double monochromator at 77 K. The excitation line (406.7 nm) was provided by a coherent K-2 Kr^+ ion laser.

FT-IR Spectroscopy. Samples for FT-IR spectroscopy were concentrated in Ultrafree ultrafiltration concentrators (NMWL = 10 kDa; Millipore). Upon reaction, an O_2-free solution of $NaNO_2$ (10 mM) was added to the protein solution (~120 μM). Samples were transferred to a 50-μL gas-tight transmission cell equipped with CaF_2 windows with 2 cm^{-1} resolution under anaerobic conditions. FT-IR spectra were recorded on a Bruker IFS 66v/S FTIR spectrometer equipped with an MCT photo-conductive detector and a KBr beam splitter. The temperature was set to 37 ℃ with a thermostat (RML, LAUDA).

Quantification of NO with TMA-PTIO by Room Temperature EPR Spectroscopy. To quantify the amount of NO, 25 μM of the highly specific spin-trap 2-(4-trimethylammonio)phenyl-4,4,5,5-tetramethylimidazoline-1-oxyl 3-oxide (TMA-PTIO) was added upon reaction of NP7 with $NaNO_2$ in 100 mM MOPS/NaOH, 50 mM NaCl (pH 7.5) according to the method of Osipov *et al.*[7] The experiment was carried out under anaerobic conditions at 37 ℃. The transfer of NO from NP7 to TMA-PTIO was followed photometrically. Afterwards, EPR spectra were obtained at room temperature on a Bruker ESP-300E spectrometer operating at X-band frequency with samples in quartz flat cells. The parameters of the spectrometer were set as follows: modulation frequency, 9.7 GHz; modulation amplitude, 0.5 G; field modulation, 100 kHz; time constant, 20 ms; sweep time, 2 s; microwave power, 1.25 mW; number of scans, 4.

Quantification of NO_2^- and NO_3^-. 0.92 mM of NP7 in 100 mM MOPS/NaOH (pH 7.5), 50 mM NaCl, 100 µM DTPA, 13.52 mM $NaNO_2$ was incubated at 35 ℃ overnight. Afterwards, a 10-µL aliqout was diluted into 240 µL of 100 mM MOPS/NaOH (pH 7.5), 50 mM NaCl and then the protein was removed using an Ultrafree (NMWL: 10 kDa) spin concentrator (Millipore). 150 and 20 µL of the filtrate were collected for the NO_3^- and the NO_2^- assay, respectively.

The quantification method was developed by Beda and Nedospaov to determine NO_3^- in the presence of excess NO_2^-.[8] This assay is based on the Griess reaction in combination with the reduction of NO_3^- by vanadium(III). For the NO_3^--calibration curve, solutions of 0, 5, 10, 15, 25, 50, and 100 µM of $NaNO_3$ in 100 mM MOPS/NaOH (pH 7.5), 50 mM NaCl, 1 mM $NaNO_2$ were prepared. Upon the Griess reaction, the absorbance at 540 nm was monitored and plotted *vs*. [NO_3^-] (Figure S5A). For the NO_2^--calibration curve, solutions of 0.2, 0.3, 0.5, 0.75, 1.0, and 2.0 mM of $NaNO_2$ were prepared in 100 mM MOPS/NaOH (pH 7.5), 50 mM NaCl. Upon the Griess reaction, the absorbance at 540 nm was monitored and plotted *vs*. [NO_2^-] (Figure S5B).

The experiment was repeated with 0.56 mM NP4 dissolved in 100 mM NaH_2PO_4/NaOH (pH 7.5), 100 µM DTPA. The reaction was started upon incubation with 11.4 mM $NaNO_2$.

Supplementary Figures

Figure S1: FT-IR spectrum of NP7 upon reaction with NO_2^- recorded in 100 mM MOPS/NaOH, 50 mM NaCl (pH 7.5) at 37 ℃.

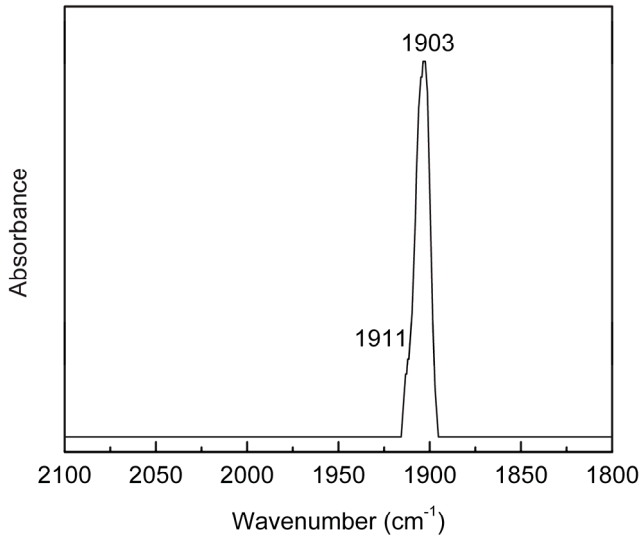

Figure S2: Quantification of NO by the NO specific spin trap TMA–PTIO using room temperature EPR spin quantification. The nitronyl nitroxide TMA-PTIO reacts with NO to form the nitroxide TMA-PTI; both radical species exhibit characteristic EPR spectra.[7] (A) EPR spectra of TMA-PTIO and TMA-PTI, respectively, in the absence (a) and presence (b - d) of different NO concentrations. The solution contained TMA-PTIO (25 µM) in 100 mM MOPS buffer, 50 mM NaCl (pH 7.5). 8 (b), 15 (c), and 25 µM (d) of NO were added, respectively. (B) Calibration curve for the detection of NO by TMA-PTIO. The EPR signal intensities of TMA-PTIO, *a*, and TMA-PTI, *b*, were read from the corresponding EPR spectra (compare arrows in A(c)). The calibration curve was plotted as (*b* / (*a* + *b*)) *versus* [NO] according to Osipov *et al.*[7]

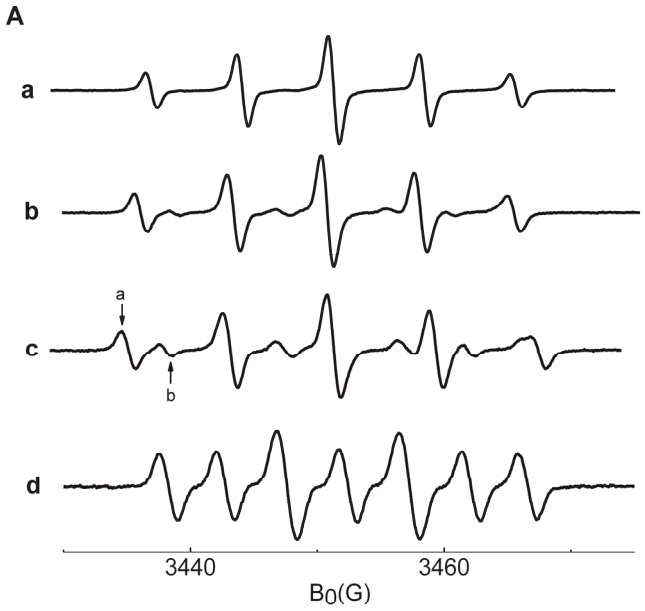

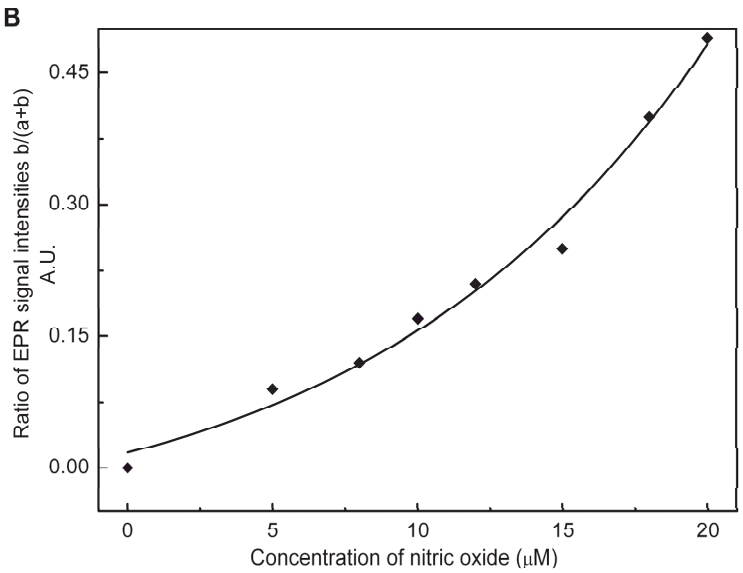

Figure S3: Reaction of NP7 with 1 mM $NaNO_2$ in 100 mM MES/NaOH, 50 mM NaCl (pH 6.0) at 37 ℃.

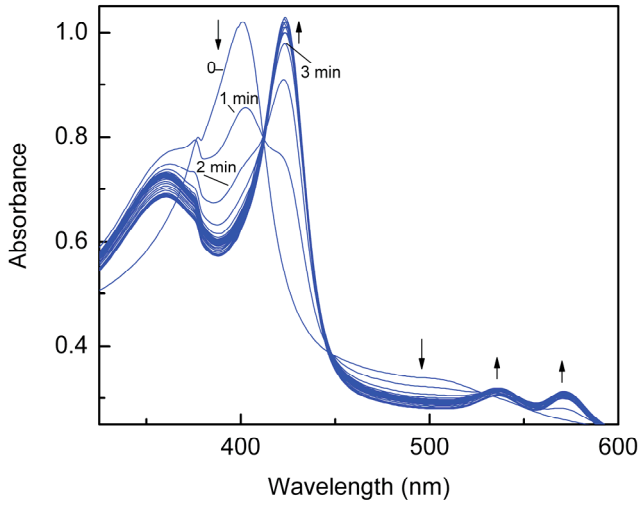

Figure S4: Reaction of 105 μM NP7 with 10 mM $NaNO_2$ in 100 mM MOPS/NaOH, 50 mM NaCl, 100 μM DTPA (pH 7.5) in the presence of 2 mM DMPO at 37 °C. The EPR measurement of the final reaction mixture was conducted as described elsewhere,[9] but no signal was detected. [NO_3^-] detected: 54 μM.

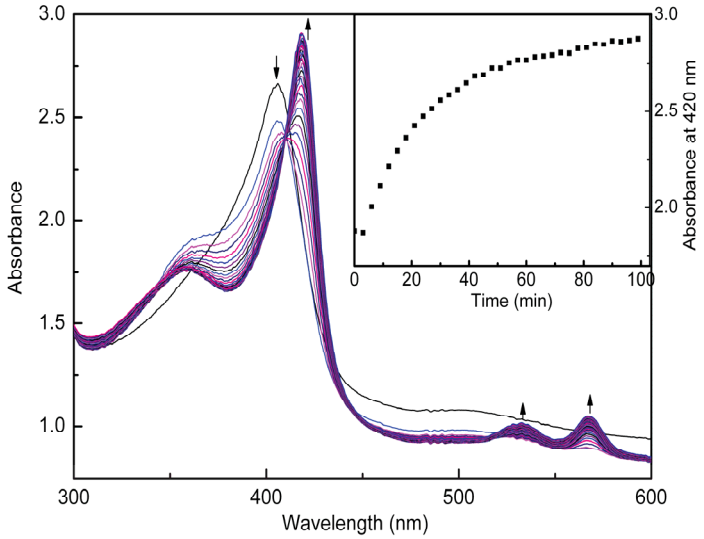

Figure S5: Calibration curve for the detection of (A) NO_3^- and (B) NO_2^-. Linear regression was performed, the slopes were 6.47 x 10^{-3} $(\mu M)^{-1}$ and 0.818 $(mM)^{-1}$ for A and B, respectively. The R-values were 0.99915 and 0.99903, respectively.

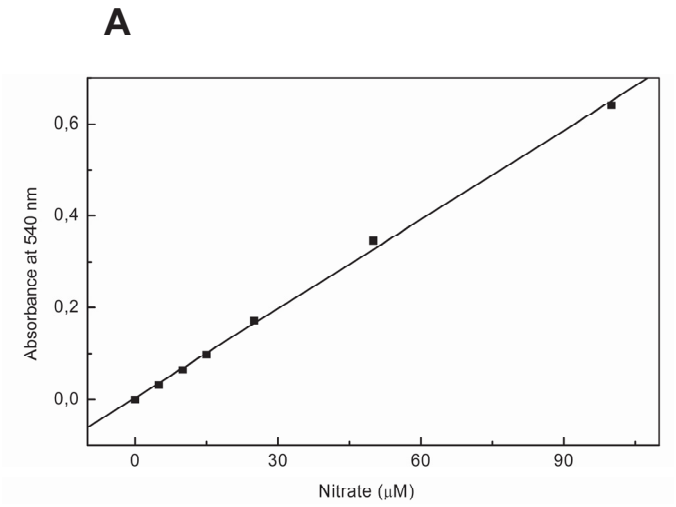

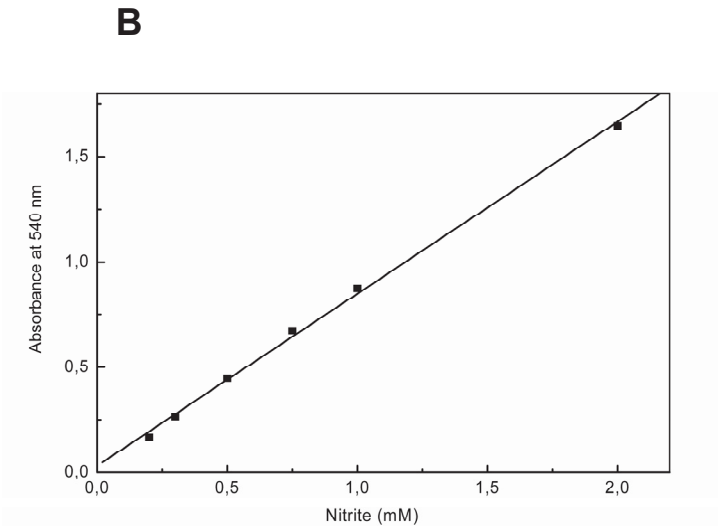

Supplementary Tables

Table S1: Ratio of the concentrations (in mM) of NO, NO_2^-, and NO_3^- at the end of the reaction of NP with NO_2^-.

Isoform	Start of reaction		End of reaction			Stoichiometry[a]
	$[NO_2^-]_0$[b] (mM)	[NP][b] (mM)	$[NO_2^-]$[c] (mM)	$\Delta[NO_2^-] = [NO_2^-]_0 - [NO_2^-]$ (mM)	$[NO_3^-]$[c] (mM)	NO_2^- (↓) / NO (↑) / NO_3^- (↑)
NP7[d]	13.52	0.92	12.22	1.30	0.47	1.41 : 1: 0.51
NP4[e]	11.4	0.56	10.57	0.83	0.28	1.48 : 1: 0.50

[a] Relative amount NO_2^- consumed compared to the amounts of NO (with [NO] = [NP]) and NO_3^- produced. NO was set to 1.
[b] Photometrically determined.
[c] Determined with adapted Griess assay.[8]
[d] Reaction performed in 100 mM MOPS/NaOH, 50 mM NaCl, 100 μM DTPA (pH 7.5).
[e] Reaction performed in 100 mM NaH_2PO_4/NaOH, 50 mM NaCl, 100 μM DTPA (pH 7.5).

References

(1) Maragos, C. M.; Morley, D.; Wink, D. A.; Dunams, T. M.; Saavedra, J. E.; Hoffman, A.; Bove, A. A.; Isaac, L.; Hrabie, J. A.; Keefer, L. K. *J. Med. Chem.* **1991,** *34*, 3242-3247.

(2) Strickler, S. J.; Kasha, M. *J. Am. Chem. Soc.* **1963,** *85*, 2899-2901.

(3) Woldman, Y. Y.; Khramtsov, V. V.; Grigor'ev, I. A.; Kiriljuk, I. A.; Utepbergenov, D. T. *Biochem. Biophys. Res. Commun.* **1994,** *202*, 195-203.

(4) Knipp, M.; Zhang, H.; Berry, R. E.; Walker, F. A. *Prot. Expr. Purif.* **2007,** *54*, 183-191.

(5) Yang, F.; Zhang, H.; Knipp, M. *Biochemistry* **2009,** *48*, 235-241.

(6) Knipp, M.; Yang, F.; Berry, R. E.; Zhang, H.; Shokhirev, M. N.; Walker, F. A. *Biochemistry* **2007,** *46*, 13254-13268.

(7) Osipov, A. N.; Gorbunov, N. V.; Day, B. W.; Elsayed, N. M.; Kagan, V. E. *Methods Enzymol.* **1996,** *268*, 193-203.

(8) Beda, N.; Nedospasov, A. *Nitric Oxide* **2005,** *13*, 93-97.

(9) Reszka, K. J.; McCormick, M. L.; Buettner, G. R.; Hart, C. M.; Britigan, B. E. *Nitric Oxide* **2006,** *15*, 133-141.

Chapter 3. Formation of the complex of nitrite with the ferriheme *b* *β*-barrel proteins nitrophorin 4 and nitrophorin 7[§§]

(He, C.; Ogata, H.; Knipp, M. *Biochemistry* **2010**, *49*, 5841-5851)

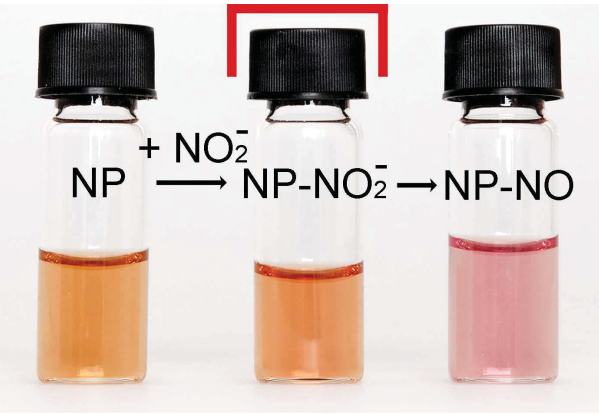

[§§] Reprinted with permission from He, C., Ogata, H., Knipp, M. *Biochemistry* **2010**, *49*, 5841-5851. Copyright 2010 American Chemical Society.

Abstract

The first spectroscopic characterization of the initial complexes of the two isoproteins NP4 and NP7 with nitrite is presented and compared to the data reported for metHb and met-myoglobin (metMb). Because upon nitrite binding, NPs, in contrast to metHb and metMb, continue to react with nitrite, resonance Raman spectroscopy and cw-EPR spectroscopy were applied to frozen samples. As a result, the existence of two 6-coordinate ferriheme low-spin complexes was established. Furthermore, X-ray crystallography of NP4 crystals soaked with nitrite revealed the formation of a η^1-N nitro complex, which is in contrast to the η^1-O bound nitrite in metMb and metHb. Stopped-flow kinetic experiments show that although the ligand dissociation constants of NP4 and NP7 (15 to 190 M^{-1}) are comparable to those of the metHb and metMb, the rates of ligand binding and release are significantly slower. Moreover, the reaction kinetics, but also EPR spectroscopy exhibits notable differences between the two isoproteins

BIOCHEMISTRY
including biophysical chemistry & molecular biology
Article

Biochemistry **2010,** *49,* 5841–5851 5841
DOI: 10.1021/bi100324z

Formation of the Complex of Nitrite with the Ferriheme *b* β-Barrel Proteins Nitrophorin 4 and Nitrophorin 7[†,‡]

Chunmao He, Hideaki Ogata, and Markus Knipp*

Max-Planck-Institut für Bioanorganische Chemie, Stiftstrasse 34-36, D-45470 Mülheim an der Ruhr, Germany

Received March 4, 2010; Revised Manuscript Received June 4, 2010

ABSTRACT: The interaction of ferriheme proteins with nitrite has recently attracted interest as a source for NO or other nitrogen oxides in mammalian physiology. However, met-hemoglobin (metHb), which was suggested as a key player in this process, does not convert nitrite unless small amounts of NO are added in parallel. We have recently reported that, in contrast, nitrophorins (NPs) convert nitrite as the sole substrate to form NO even at pH 7.5, which is an unprecedented case among ferrihemes [He, C., and Knipp, M. (2009) *J. Am. Chem. Soc. 131*, 12042−12043]. NPs, which comprise a class of unique heme *b* proteins from the saliva of the blood-sucking insect *Rhodnius prolixus*, appear in a number of concomitant isoproteins. Herein, the first spectroscopic characterization of the initial complexes of the two isoproteins NP4 and NP7 with nitrite is presented and compared to the data reported for metHb and met-myoglobin (metMb). Because upon nitrite binding, NPs, in contrast to metHb and metMb, continue to react with nitrite, resonance Raman spectroscopy and continuous wave electron paramagnetic resonance spectroscopy were applied to frozen samples. As a result, the existence of two six-coordinate ferriheme low-spin complexes was established. Furthermore, X-ray crystallography of NP4 crystals soaked with nitrite revealed the formation of an η^1-N nitro complex, which is in contrast to the η^1-O-bound nitrite in metMb and metHb. Stopped-flow kinetic experiments show that although the ligand dissociation constants of NP4 and NP7 (15−190 M^{-1}) are comparable to those of metHb and metMb, the rates of ligand binding and release are significantly slower. Moreover, not only the reaction kinetics but also electron paramagnetic resonance spectroscopy reveals notable differences between the two isoproteins

Nitrophorins (NPs)[1] comprise a unique class of ferriheme *b* proteins that are found in the saliva of the blood-sucking insect *Rhodnius prolixus* (*1*). From the saliva of these insects, four different NPs, designated NP1−4, have been isolated and characterized (*2*). Recently, a novel form, designated NP7, which is able to attach to negatively charged phospholipid membranes, was established by recombinant protein expression (*3*−*5*). The major biological function of these proteins is the delivery of NO to a host species during a blood meal.

Like many other heme proteins, NPs coordinate the heme iron by a His residue. The sixth coordination site of the iron is then ready to coordinate NO in the insect's saliva to be released upon administration to a host's tissue (*1*, *2*). In marked contrast to any other class of heme proteins, the protein fold consists mainly of β-strands, which form an eight-strand β-barrel that contains the cofactor; the fold is classified as a member of the lipocalin family (*6*). It was not until very recently that a heme *b* protein from *Arabidopsis thaliana* was described which consists of a 10-strand β-barrel (*7*). Previously, we have reported that NPs react with NO_2^- to form NO, where NO_2^- serves both as an electron donor and as an electron acceptor in a stoichiometry that is reflected by the total reaction depicted in Scheme 1 (*8*). This reaction is known as the nitrite disproportionation reaction that appears at low pH in aqueous solutions (*9*). However, NPs perform the reaction in a pH 7.5 buffered solution which has, to the best of our knowledge, not been reported for any other iron porphyrin.

Scheme 1

$$3NO_2^- + 2H^+ \xrightarrow{[NP^{III}]} 2NO + H_2O + NO_3^-$$

Another class of ferriheme *b* proteins that is currently being investigated for their interaction with NO_2^- consists of the globins, i.e., met-hemoglobin (metHb) (*10*) and met-myoglobin (metMb) (*11*). In the presence of small amounts of NO, a nitrite anhydrase/reductase reaction appears that may be of major importance for the physiological function of Hb via the production of N_2O_3 from blood NO_2^- (*12*−*15*). However, in the absence of NO, both metHb and metMb do not exhibit a reaction with NO_2^- other than NO_2^- binding (*16*).

Although some research has been conducted to elucidate the activation of NO_2^- by metMb, metHb, and several other ferriheme proteins, the exact mechanisms await adequate investigation. In case of the nitrophorins, this study is the first examination of the complex with NO_2^-, a prerequisite for understanding the mechanism of this unique reaction. For this purpose, UV−vis

[†]This work was financially supported by the Max Planck Society (MPG) and by the Deutsche Forschungsgemeinschaft (DFG), Grant KN 951/1-1 (to M.K.).

[‡]Coordinates and structure factor for the X-ray crystal structure of NP4 in a complex with nitrite reported here have been deposited in the Protein Data Bank (entry 3MVF).

*To whom correspondence should be addressed. Telephone: +49 (0)208 306 3581. Fax: +49 (0)208 306 3951. E-mail: mknipp@mpi-muelheim.mpg.de.

[1]Abbreviations: Hb, hemoglobin; HRP, horseradish peroxidase; HS, high-spin; ImH, imidazole; LS, low-spin; Mb, myoglobin; MALDI Q-TOF MS, matrix-assisted laser desorption ionization quadrupole time-of-flight mass spectrometry; metHb, ferriheme hemoglobin; metMb, ferriheme myoglobin; MOPS, 3-(*N*-morpholino)propanesulfonic acid; NiR, heme cd_1 nitrite reductase; NP, nitrophorin; py, pyridine; RR, resonance Raman; TpivPP, tetrakis(α,α,α,α-*o*-pivalamidophenyl)-porphyrinato dianion.

Published on Web 06/04/2010

absorption spectroscopy, electron paramagnetic resonance (EPR) spectroscopy, and resonance Raman (RR) spectroscopy were combined with stopped-flow kinetic measurements of both NP4 and NP7. Furthermore, X-ray crystallography of KNO_2-soaked NP4 crystals was performed. The data are discussed in comparison to those of other porphyrin[Fe^{III}—NO_2^-] complexes.

EXPERIMENTAL PROCEDURES

Materials. Stock solutions of $NaNO_2$ and KNO_2 were prepared freshly before use and the concentration was photometrically calibrated (ε_{210} = 5380 M^{-1} cm^{-1}) (*17*). All other reagents were of the highest grade commercially available and used as received.

NP4 and NP7 were recombinantly expressed in *Escherichia coli* strain BL21(DE3) (Novagen) and reconstituted as previously described (*4*, *18*). Protein preparations were routinely analyzed by SDS−PAGE to be >90% pure. The proteins were subjected to MALDI Q-TOF MS to confirm the correct molecular masses accounting for two Cys−Cys disulfides (calculated for $[NP4 + H]^+$ 20264 Da, observed 20279 Da; calculated for $[NP7 + H]^+$ 20969 Da, observed 20966 Da). Concentrations of NP4 and NP7 were determined photometrically using ε_{404} values of 141000 (*19*) and 81000 M^{-1} cm^{-1} (*4*), respectively. Human Hb was bought from Sigma. metHb was prepared by incubation with an excess of $K_3[Fe(CN)_6]$, followed by size-exclusion chromatography on Sephadex G-50. The concentration of metHb was determined photometrically using an ε_{405} of 180000 M^{-1} cm^{-1} (*16*).

Stopped-Flow Kinetic Measurements. The solvent of the protein was exchanged with 50 mM MOPS-NaOH (pH 7.0), and NP4 and NP7 were concentrated to 10 and 14 μM, respectively. Individually, reactant solutions of 200, 300, 400, 500, 600, and 800 mM $NaNO_2$ were prepared in 50 mM MOPS-NaOH (pH 7.0). To minimize mixing artifacts, NaCl was included in the protein solution at the same concentration as that of $NaNO_2$ in the respective reactant solution. The temperature of the solutions was equilibrated in the syringes of a water bath-thermostated UV−vis stopped-flow apparatus (RX.2000) equipped with a DA.1 pneumatic drive (Applied Photophysics Ltd.). The cuvette of the RX.2000 apparatus was inserted into the sample holder of a Cary 50 spectrophotometer (Varian Inc.). Upon temperature equilibration to 30 °C, the protein was mixed with the substrate while the absorption was followed at 404 nm. The absorbance was read every 0.1 s. The analysis of the kinetic data was performed using OriginPro version 7.5 (OriginLab Corp.).

Resonance Raman Spectroscopy. The solvent of the proteins was exchanged with 50 mM MOPS-NaOH (pH 7.0), and the concentration was adjusted to ~100 μM. For spectra of the NO_2^- complexes of metHb, NP4, and NP7, 200 mM $NaNO_2$ was added and the sample was incubated at room temperature for 5 min. The sample was quickly transferred to a 3 mm quartz tube and frozen in liquid N_2 where it was kept until measurement. RR spectra were recorded with a scanning double monochromator at 77 K. The excitation line at 413.1 nm was provided by a coherent K-2 Kr^+ ion laser.

EPR Spectroscopy. The solvent of the protein was exchanged with 50 mM MOPS-NaOH (pH 7.0), and the concentration was adjusted to ~100 μM. Upon being mixed with $NaNO_2$ at various concentrations, the sample was incubated at room temperature for a few minutes. The samples were quickly transferred into a 3 mm quartz tube and then rapidly frozen in liquid N_2 where they were kept until measurement. Continuous wave electron paramagnetic resonance (cw-EPR) spectra were recorded on a Bruker ESP-380E spectrometer at X-band equipped with a gas-flow cryogenic system with a liquid He cryostat from Oxford Inc. Spectra were recorded at 15 K with a microwave power of 2 mW, a field modulation of 100 kHz, and a modulation amplitude of 5 G. The obtained EPR spectra were simulated with the program GeeStrain5 version 1.0 (*20*).[2]

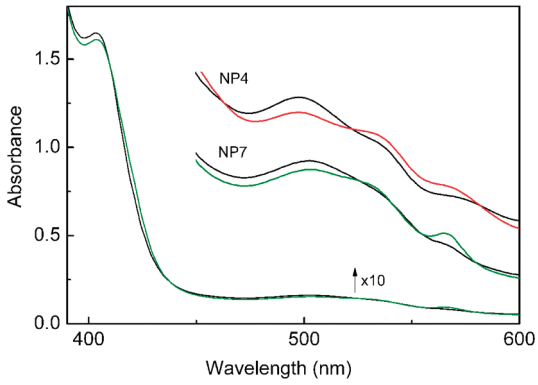

FIGURE 1: UV−vis absorption spectrum of 12 μM NP7 (green line) and 10 μM NP4 (red line) mixed with 50 mM $NaNO_2$ in 50 mM MOPS-NaOH (pH 7.0). For a comparison, the sums of the individual components are also displayed (black lines).

X-ray Crystallographic Analysis of the NP4−Nitrite Complex. Protein crystals were obtained using the vapor diffusion method with the conditions containing 3.2 M ammonium phosphate (pH 7.4). For the preparation of the nitrite complex, crystals were soaked in 3.2 M potassium phosphate (pH 7.4) with 15% glycerol and then in the same buffer supplemented with 0.2 M KNO_2 for 1 min. Afterward, the crystals were immediately frozen in liquid N_2 until the measurement. A diffraction data set was collected at 100 K using beamline BL14.2 at BESSYII (Berlin, Germany). The data sets were processed with XDS (*21*) and CCP4 (*22*). The molecular replacement method was applied to determine the phase using an initial model from NP4 [Protein Data Bank (PDB) entry 1X8Q]. Model building and refinement were conducted using Coot (*23*) and REFMAC5 (*22*), respectively. The stereochemical properties were checked by RamPage (*24*).

RESULTS

UV−Vis Absorption Spectroscopy of the Nitrite Complexes of NP4 and NP7. Unlike those of other heme proteins, the incubation of NPs with NO_2^- leads to the formation of NO in a pH 7.5 buffered solution according to Scheme 1 (*8*). This reaction is accompanied by the change in the Soret absorption maximum from 404 to 418 nm caused by the product, NO, which remains bound to the heme iron [$K_{eq}(NO) = 1.2 \times 10^{-7}$ M (NP4 at pH 8.0) (*25*), and $K_{eq}(NO) = 2.5 \times 10^{-7}$ M (NP7 at pH 7.5) (*5*)]. In the previous study, at 1 mM NO_2^-, the formation of the NP7[NO_2^-] complex was not observed in the absorption spectrum (*8*) because of the small $K_{eq}(NO_2^-)$ equilibrium constants (see below) in combination with the small absorption difference between NP and NP[NO_2^-]. As one can see in Figure 1, the addition of NO_2^- to a final concentration of 50 mM, which is significantly above $K_{eq}(NO_2^-)$ (see below), allows to record the UV−vis absorption spectra of NP4[NO_2^-] and NP7[NO_2^-] within 5 min upon incubation.

Besides the Soret band maximum at 404 nm, NP4 and NP7 show broad absorption maxima also at ~498 and ~503 nm,

[2]Available at http://www.bt.tudelft.nl/biomolecularEPRspectroscopy/.

respectively (*4*, *19*). A small band at ~530 nm originates from a fraction of the hydroxo complex.[3] As seen in Figure 1, the binding of excess NO_2^- to NP4 and NP7 leads to a slight red shift of the Soret band maximum to 406 nm with a relatively small decrease in the extinction coefficient [$\Delta\varepsilon_{404}(NO_2^-)$ = 3400 M^{-1} cm^{-1}]. The appearances of the α- and β-band are typical for the formation of low-spin complexes at 565 and 535 nm for NP4 and 567 and 533 nm for NP7, respectively. For metMb and metHb, the changes in the absorption spectrum upon NO_2^- binding were similar (*16*, *26*, *27*).

Determination of the Kinetic Parameters of the Nitrite Association Reaction of NP4 and NP7. Single-wavelength absorption detected (404 nm) stopped-flow kinetic measurements were performed with both NP4 and NP7, examples of which are shown in panels A and B of Figure 2. Experiments were performed in triplicate for a given NO_2^- concentration, and the results were averaged. However, it must be considered that the binding of NO_2^- to the NPs is only the initial step (see Scheme 2) of the total reaction represented by Scheme 1. For example, comparison of the rate constant for the formation of the NP[NO] complex at 30 °C with 300 mM NO_2^- versus that for the formation of the NP[NO_2^-] complex under the same conditions reveals that the formation of NO is significantly slower [$k_{obs}(NO) = 1.2 \times 10^{-3}$ s^{-1}, and $k_{obs}(NO_2^-) = 5 \times 10^{-2}$ s^{-1}] (see Figure S1 of the Supporting Information). On the other hand, the absorption change for the formation of NP[NO] is significantly larger than that for NP[NO_2^-] [$\Delta\varepsilon_{404}(NO) = 85800$ M^{-1} cm^{-1}]. Thus, the kinetic traces reflect the sum of NO_2^- binding and NO formation. Because NO formation during the recorded time is still in the linear initial phase, the last set of data points (3−5 min) were fit by linear regression analysis and the yielded function was subtracted from the kinetic trace before analysis with an exponential decay function (see Figure S2 of the Supporting Information).

The semilogarithmic plot of the data displayed in the insets of panels A and B of Figure 2 indicates that the data cannot be sufficiently approximated by a single exponential; however, a satisfying fit was obtained with a double exponential

$$A(t) = ae^{-tk} + be^{-tk'} + c \quad (1)$$

with A being the absorbance and t the time. In Figure 2C, the plot of k and k' for both NP4 and NP7 versus NO_2^- concentration is displayed, all of which reveal a linear behavior in agreement with a pseudo-first-order reaction. It should be mentioned that in case of the association reaction of NO with NP2 and NP3 a double exponential decay was applied (*25*, *28*) where the reaction among NP1, NP4, and NP7 was sufficiently described by a single-exponential fit (*5*, *25*). In the case of NP2 and NP3, a two-state model was used in which a NP2/3[NO] precomplex is expected to form in the first place (fast phase) followed by a monomolecular rearrangement toward the NP2/3[NO]* final complex (slow phase). The two-state model in this case is supported by the hyperbolic dependence of the slow phase on NO concentration (*28*). In contrast, the plots of k_{obs}^{slow} of NP4 and NP7 versus NO_2^- concentration show a linear dependence on NO_2^- concentration. Thus, the data were fit in accordance with Scheme 2 by the pseudo-first-order rate equation

$$k_{obs} = k_1[NO_2^-] + k_{-1} \quad (2)$$

[3]C. He and M. Knipp, work in progress.

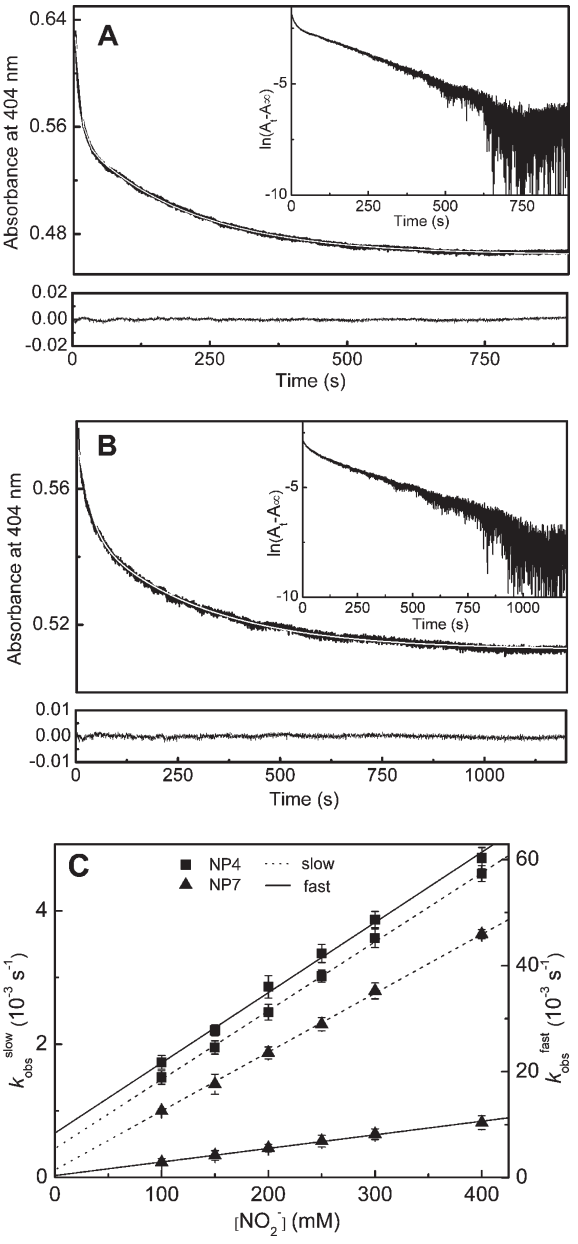

FIGURE 2: Representative examples of UV−vis absorption detected (404 nm) stopped-flow kinetics of the reaction between (A) NP4 (5 μM) or (B) NP7 (7 μM) and 300 mM $NaNO_2$ at pH 7.0 and 30 °C. The fit of the data by eq 1 is presented as a white line. The insets show a semilogarithmic representation of the data. (C) k_{obs} was plotted vs NO_2^- concentration, and data were fit with eq 2 [R^2 = 0.99862 (NP4, k_{obs}^{fast}), 0.99958 (NP4, k_{obs}^{slow}), 0.99899 (NP7, k_{obs}^{fast}), or 0.99992 (NP7, k_{obs}^{slow})].

Scheme 2

$$NP + NO_2^- \underset{k_{-1}}{\overset{k_1}{\rightleftharpoons}} NP[NO_2^-]$$

Such a behavior was previously described for metHb, and the data are interpreted as the appearance of a fast phase and a slow phase (see Discussion). The values are reported in Table 1 in comparison to reports for metHb and metMb. From these values, the equilibration constant

$$K_{eq} = \frac{k_1}{k_{-1}} \quad (3)$$

is estimated and reported in Table 1 as well.

Table 1: Rate Constants and Equilibrium Constants for the Binding of NO_2^- to NP4 and NP7 from *R. prolixus* in Comparison to metMb and metHb

	k_1^{fast} (M^{-1} s^{-1})	k_{-1}^{fast} (s^{-1})	k_1^{slow} (M^{-1} s^{-1})	k_{-1}^{slow} (s^{-1})	K_{eq} (M^{-1}) calculated fast[a]	K_{eq} (M^{-1}) calculated slow[b]	K_{eq} (M^{-1}) by titration	ref
NP4	0.13 ± 0.001[c]	0.0084 ± 0.0003[c]	0.01 ± 0.001[c]	0.00047 ± 0.00001[c]	15	21	178 ± 18[d]	tw[e]
NP7	0.076 ± 0.001[c]	0.00040 ± 0.00002[c]	0.0088 ± 0.0002[c]	0.00013 ± 0.00001[c]	190	68	400 ± 22[d]	tw[e]
metMb[f]	156 ± 3[g]	2.6 ± 0.1[g]	–	–	60	–	–	*16*
metHb[h]	260 ± 4[i]	1.70 ± 0.14[i]	28.1 ± 0.8[i]	0.20 ± 0.03[i]	153	141	–	*16*
metHb	–	–	–	–	–	–	556[j]	*30*
metHb[k]	–	–	–	–	–	–	901[l]	*26*
metHb[k]	–	–	–	–	–	–	333[l]	*27*
metHb[k]	140[m]	–	20[m]	–	–	–	–	*69*

[a] k_1^{fast}/k_{-1}^{fast}. [b] k_1^{slow}/k_{-1}^{slow}. [c] Performed at pH 7.0 and 30 °C. [d] Samples were prepared at ambient temperature and pH 7.0, and detection was performed by EPR spectroscopy at 15 K. [e] This work. [f] Horse Mb. [g] Performed at pH 7.4 and 20 °C. [h] Bovine Hb. [i] Performed at pH 7.4 and 30 °C. [j] Samples were prepared at ambient temperature and pH 7.4, and detection was performed by EPR spectroscopy at 77 K. [k] Human Hb. [l] Performed at pH 7.4 and 25 °C by optical titration. [m] Performed at pH 6.9 and 20 °C.

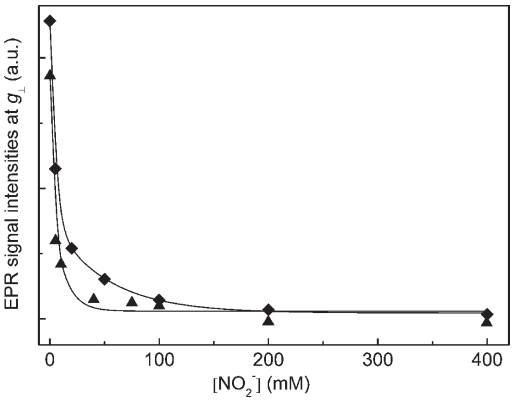

FIGURE 3: EPR signal intensities of (▲) NP7 and (◆) NP4 at $g_\perp$ (doubly integrated signal) vs NO_2^- concentration.

Determination of the Nitrite Association Constant of NP4 and NP7 by EPR Spectroscopy. According to the total reaction given in Scheme 1, the determination of $K_{eq}(NO_2^-)$ by simple titration experiments in solution under thermodynamic control, as is usually performed in studies of heme−ligand interactions (*29*), is not applicable. However, because cw-EPR spectroscopy allows the detection of the Fe^{III} high-spin species in frozen solutions, the signal intensity can be taken as a determinant of the degree of saturation with NO_2^-. For this purpose, samples of NP4 and NP7 were incubated with various concentrations of NO_2^- where equilibration was allowed for 5 min at ambient temperature. Afterward, the samples were rapidly frozen in liquid N_2 and kept frozen until the measurement. The optimum time for equilibration was estimated from a time-dependent experiment with both proteins in the presence of 200 mM NO_2^-. Samples were frozen after incubation for 2, 5, 10, and 20 min at room temperature (data not shown). Since the low-spin intensity for NP4 and NP7 slowly decreased after incubation for 5 min, i.e., the formation of NO reaches significant levels (compare Scheme 1), the system is equilibrated to the maximum possible extent.

For a comparison, the affinities of NO_2^- were also estimated by recording the EPR spectra of NP4 and NP7 incubated with various NO_2^- concentrations similar to what has been reported for metHb (*12*, *30*, *31*). The resulting plot of the EPR signal intensity at $g_\perp$ versus NO_2^- concentration [yielding $K_{eq(EPR)}^{NP4}(NO_2^-) = 178 \pm 18\ M^{-1}$ and $K_{eq(EPR)}^{NP7}(NO_2^-) = 400 \pm 20\ M^{-1}$] is displayed in Figure 3. As seen in Table 1, these values suggest

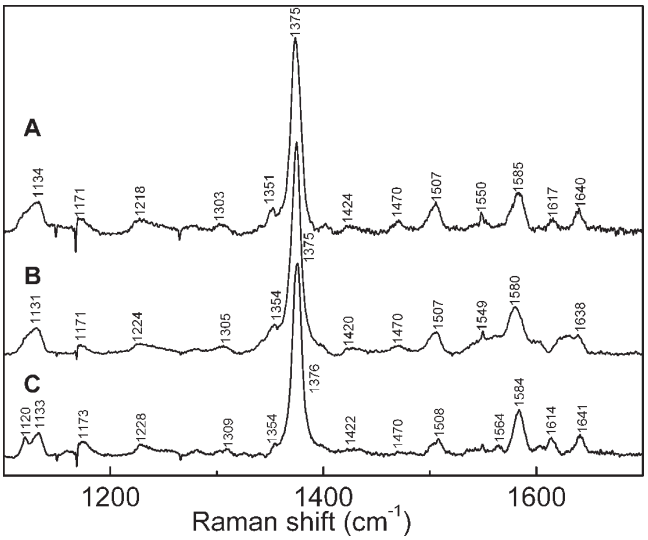

FIGURE 4: High-frequency RR spectra of (A) metHb[NO_2^-], (B) NP4[NO_2^-], and (C) NP7[NO_2^-] in 50 mM MOPS-NaOH (pH 7.0). Spectra were recorded at 77 K with a λ_{ex} of 413.1 nm.

a significantly higher NO_2^- affinity compared to the values obtained from the kinetic measurements, which is also true for metHb (*16*, *30*). However, unlike that for metHb (*27*), the thermodynamic equilibrium for the reaction displayed in Scheme 2 cannot be established because the reaction continues according to Scheme 1. Furthermore, it has to be considered that although the equilibration reaction can be performed at a defined temperature, the termination of the reaction and the sample preparation requires freezing; hence, before the sample reaches the frozen state, an undefined temperature decrease applies to the solution. Consequently, the obtained $K_{eq(EPR)}$ can only be considered as rough estimates for sample preparations in frozen solutions described in the following.

Resonance Raman Spectroscopy. RR spectra of NP4-[NO_2^-] and NP7[NO_2^-] together with a sample of metHb[NO_2^-] were recorded in frozen solution at 77 K, which allows the detection of the initial nitrite complex. To the best of our knowledge, this is the first published report of a RR study of ferriheme−nitrite adducts. All samples were excited into the Soret band absorption (see Figure 1) using a λ_{ex} of 413.1 nm. The resulting high-frequency spectra of NP4[NO_2^-], NP7[NO_2^-], and

Table 2: Comparison of the Raman Shifts (cm^{-1}) of the Aquo, NO, and NO_2^- Complexes of Ferriheme *b* Proteins NP1, NP4, and NP7 from *R. prolixus*, metMb from Horse Muscle, and metHb from Human Blood

protein	pH	temp (K)	ν_{10}	ν_2	ν_3	ν_4	ref
NP1	7.0	298	1611	1560	1481	1372	*32*
NP4	7.5	298	1610	1560	1481	1372	*35*
NP7	7.5	77	1615	1558	1484	1375	*8*
metMb	6.6	298	1611	1562	1482	1373	*34*
metHb	6.6	298	1610	1561	1481	1373	*34*
NP1[NO]	7.0	298	1636	1581	1504	1375	*32*
NP4[NO]	7.5	298	1640	1580	1505	1376	*35*
NP7[NO]	7.5	77	1640	1581	1509	1376	*8*
NP4[NO_2^-]	7.0	77	1638	1584	1507	1375	tw[a]
NP7[NO_2^-]	7.0	77	1641	1580	1506	1376	tw[a]
metHb[NO_2^-]	7.0	77	1640	1585	1507	1375	tw[a]

[a]This work.

metHb[NO_2^-] are depicted in Figure 4. The Raman shift frequencies of selected resonances with diagnostic potential for the assignment of the oxidation state and spin state are summarized in Table 2 in comparison to values of several ferric high-spin and nitrosyl ferric heme proteins from earlier reports.

For the nitrite complexes presented in Figure 4, the occurrence of the intense so-called oxidation state maker ν_4 = 1375 or 1376 cm^{-1} is typical for ferriheme proteins (*32*, *33*). This is also the case for the unliganded forms and NO complexes (Table 2). Another important feature seen in Figure 4 is the so-called spin state maker ν_3 that appears at 1507 or 1508 cm^{-1} which is diagnostic for six-coordinate low-spin (6cLS) hemes (1500−1510 cm^{-1}) (*34*). Where this also holds true for the nitrosyl complexes, the ν_3 resonance appears at 1480−1484 cm^{-1} in the case of the "unliganded" proteins, which is indicative of six-coordinate HS hemes (1475−1485 cm^{-1}) (*34*); i.e., the complexes have a water on them. Further, this spin state assignment is in good agreement with the Raman shifts of ν_{10} and ν_2 (*32*).

Overall, the RR spectra given in Figure 4 are highly similar. A significant difference can be seen in the region above 1600 cm^{-1}, where metHb[NO_2^-] and NP7[NO_2^-] exhibit clear bands at 1617 and 1614 cm^{-1}, respectively, whereas NP4[NO_2^-] exhibits an unresolved band in this region. The better resolution in the case of metHb and NP7 compared to NP4 holds true also for other ligand derivatives of these three proteins (*8*, *35*, *36*). For metMb, this resonance was assigned to the vinyl vibration $\nu_{(C=C)vinyl}$ (1621 cm^{-1}) (*36*) and hence indicates differences in the spatial environment of the heme substituents in NP4 compared to NP7.

In addition, in Figure 4, a well-separated band is seen at 1120 cm^{-1} for NP7[NO_2^-], which is not resolved in the case of metHb[NO_2^-] and NP4[NO_2^-]. On the basis of the previous attribution of this resonance in the case of deoxyMb (1117 cm^{-1}) and metMb[F^-] (1124 cm^{-1}), it can be assigned to the pyrrole C_b−vinyl stretch vibration (*36*). The lack of this band in Hb was previously noticed for metHb[F^-], although, and this is certainly also true for NP4[NO_2^-], the overlap with the neighboring band cannot be excluded (*36*). However, the band intensity is certainly weaker compared to those of NP7[NO_2^-] and metMb[F^-]. It was proposed that this resonance in Mb indicates an additional symmetry-lowering effect of the cofactor binding pocket, for example originating from charged groups, or dipoles, localized near the heme vinyls (*36*). In summary, besides the large spectral conformity depicted in Figure 4, subtle differences reflect the differences in the heme

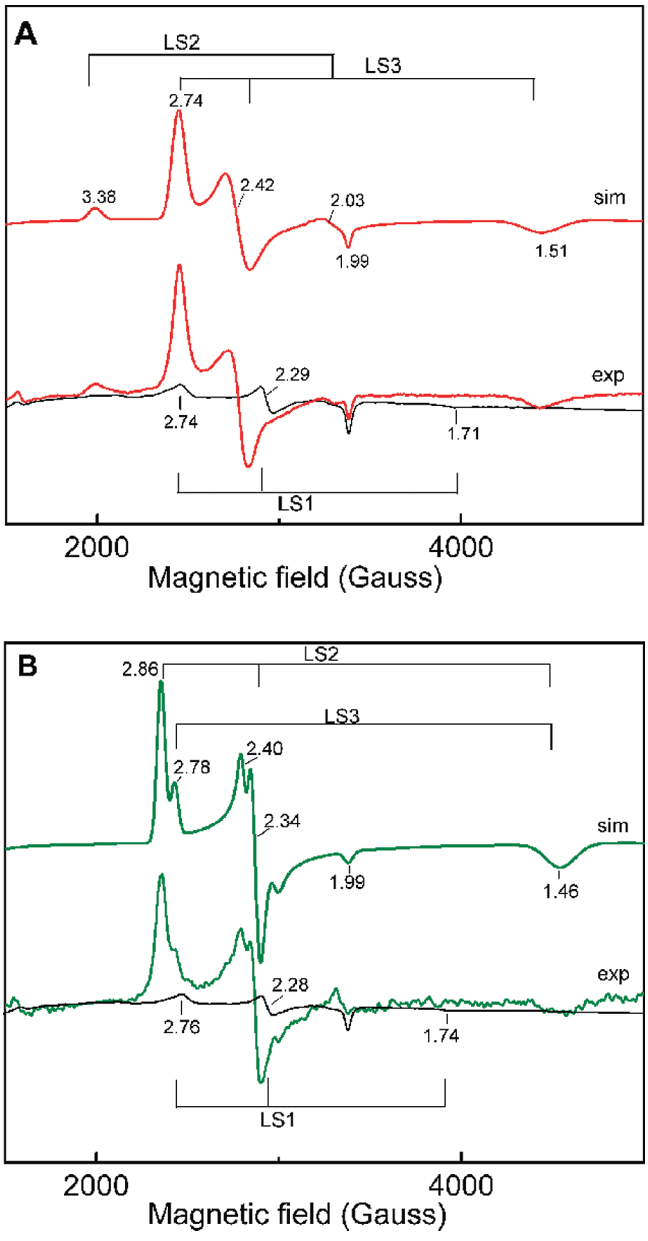

FIGURE 5: X-Band cw-EPR spectra of (A) NP4 and NP4[NO_2^-] and (B) NP7 and NP7[NO_2^-] recorded between 1500 and 5000 G. NP4 (200 μM) and NP7 (50 μM) were dissolved in 50 mM MOPS-NaOH (pH 7.0). For the spectra of the NP[NO_2^-] complexes, 200 mM $NaNO_2$ was added and samples were kept for 5 min at room temperature before being frozen. Spectra were recorded at 15 K. The corresponding *g* values are indicated in the spectra. Simulated spectra are designated "sim".

environment that may lead to variations in the ligand binding properties.

Characterization of the NP4 and NP7 Nitrite Complexes by cw-EPR Spectroscopy. The cw-EPR spectra of NP4 and NP7 frozen in a pH 7.0 buffered solution were recorded at 15 K and X-band frequency. An axial type of spectrum originating from the high-spin Fe^{III} form ($S = {}^5/_2$) of the proteins is detected with $g_\perp$ = 5.95 and $g_\parallel$ = 1.99 for NP4 and $g_\perp$ = 5.93 and $g_\parallel$ = 1.99 for NP7. These values are typical for most His-coordinated ferriheme *b* proteins with a water molecule bound to the iron, including metMb and metHb (*37*).

As one can see in Figure 5, a significant amount of a low-spin ($S = {}^1/_2$) rhombic type of spectrum (LS1) is also present in the

Table 3: Principle *g* Values of the Low-Spin Ferric Heme Complexes of NP4 and NP7 upon Binding of NO_2^- in Comparison to the EPR Parameters of Other Ferriheme[NO_2^-] Complexes

Fe^{III} porphyrin	reference or designation according to Figure 5	g_1	g_2	g_3	V/λ[a]	Δ/λ[b]	V/Δ	relative spin contribution[c] (%)
NP4[NO_2^-]	LS2	3.38	2.03	–	–	–	–	30
	LS3	2.74	2.42	1.51	2.26	2.17	1.04	70
NP7[NO_2^-]	LS2	2.86	2.34	1.46	1.95	2.55	0.76	80
	LS3	2.78	2.40	1.46	2.10	2.19	0.96	20
metHb[NO_2^-][d]	*g* values taken from ref *31*	3.03	2.33	1.47	1.77	2.91	0.61	nd[k]
		2.90	2.16	1.47	1.80	3.59	0.50	nd[k]
metHb[NO_2^-][e]	*g* values taken from ref *30*	2.98	2.12	1.41	1.63	3.66	0.44	nd[k]
		2.89	2.29	1.41	1.82	2.65	0.69	nd[k]
metMb[NO_2^-][f]	*g* values taken from ref *48*	3.11	2.30	1.00	1.27	1.94	0.66	40
		2.97	2.30	1.56	1.93	3.35	0.58	60
HRP[NO_2^-][g]	*g* values taken from ref *48*	2.99	2.24	1.31	1.58	2.67	0.59	–
NiR[NO_2^-][h]	*g* value taken from ref *48*	3.02	–	–	–	–	–	–
SiRHP[NO_2^-][i]	*g* values taken from ref *48*	2.93	–	–	–	–	–	50
		2.84	–	–	–	–	–	50
chlorite dismutase[NO_2^-][j]	*g* values taken from ref *70*	2.93	2.18	1.55	1.88	4.01	0.47	–
[Fe(TpivPP)(NO_2)(py)]	data taken from ref *42*	2.98	2.37	1.35	1.71	2.32	0.73	–
[Fe(TpivPP)(NO_2)(ImH)]	data taken from ref *42*	2.87	2.34	1.56	2.09	2.94	0.71	–

[a] $V/\lambda = g_x/(g_z + g_y) + g_y/(g_z - g_x)$. [b] $\Delta/\lambda = g_x/(g_z + g_y) + g_z/(g_y - g_x) - V/2\lambda$. [c] When obtained in the same EPR spectrum. [d] In a pH 6.5 buffered solution. [e] In a pH 7.4 buffered solution. [f] Sperm whale metMb at pH 7.7. [g] Horseradish peroxidase at pH 7.7. [h] *Thiobacillus denitrificans* heme cd_1 nitrite reductase at pH 7.7. [i] Heme protein subunit of the NADPH-sulfite oxidoreductase from *E. coli* at pH 7.7. [j] From the proteobacterium GR-1 at pH 7.0. [k] Not determined.

initial sample (for NP4, g = 2.74, 2.29, and 1.71; for NP7, g = 2.76, 2.28, and 1.74). These signals were assigned by pH titration experiments to originate from the hydroxide complexes.[3] Consequently, LS1 together with the high-spin signals disappears upon titration with NO_2^-.

Binding of NO_2^- to the iron center causes the appearance of two low-spin species, LS2 and LS3, in both NP4 and NP7. As one can see from the comparison with ferrihemes from literature in Table 3, the appearance of two low-spin species in ferriheme–NO_2^- complexes in proteins is a common phenomenon. The g values of $LS2^{NP7}$ and $LS3^{NP7}$ are very similar. They resemble a "normal" rhombic type of spectrum and, when compared to other ferriheme nitrite complexes, fit well in the range. Simulation of the spectra revealed $LS2^{NP7}$ to be the major species. The g values of $LS3^{NP4}$ are also very similar, in particular when compared to those of $LS3^{NP7}$, thus reflecting a comparable electronic situation. Remarkably, $LS2^{NP4}$ represents a "large g_{max}" spectrum with a g_{max} of 3.38 and is thus an exceptional case. However, spectral simulations reveal $LS3^{NP4}$ to be the major component (Table 3). From the resulting g values, the crystal field parameters Δ/λ (the tetragonality) and V/Δ (the rhombicity) were calculated according to the theory developed by Griffith and Taylor (*38*–*41*). For this purpose, the g values are assigned according to the "conventional" coordination system where $g_z = g_1$, $g_y = g_2$, and $g_z = g_3$. As a control, the orbital mixing parameters a, b, and c were calculated (*40*, *42*) to check how well the $a^2 + b^2 + c^2 \equiv 1$ relation is satisfied. Values between 0.99 and 1.02 were obtained in all cases, thus confirming the integrity of the g values.

X-ray Structure of the NP4–Nitrite Complex. Crystallization conditions for NP7 are not yet available. In contrast, crystallization conditions for NP4 are well established, and a number of ultra-high-resolution crystal structures were published (*43*). By analogy, crystals of NP4 were grown in ammonium phosphate (pH 7.4) (*44*), then soaked in potassium phosphate (pH 7.4) to remove the NH_3 ligand from the heme iron, and finally soaked in 200 mM KNO_2-containing buffer. The time for incubation with

Table 4: Data Collection and Refinement of the Data Sets of NP4 from *R. prolixus* Crystallized at pH 7.4 and Soaked with Nitrite[a]

	NP4[NO_2^-]
PDB entry	3MVF
Data Collection	
wavelength (Å)	0.91892
space group	*C*2
unit cell parameters	
a (Å)	70.31
b (Å)	42.91
c (Å)	52.46
β (deg)	94.05
resolution (Å)	30.53–1.40 (1.44–1.40)
no. of observed reflections	110960
no. of unique reflections	30694
R_{merge}	0.038 (0.193)
completeness (%)	97.7 (93.7)
$\langle I/\sigma(I)\rangle$	21.0 (6.8)
Refinement	
resolution range (Å)	15.0–1.4
R (%)	13.6
R_{free} (%)	18.7
no. of residues	184
no. of solvent molecules	223
no. of NO_2^- ions	2
rmsd[b] for bond lengths (Å)	0.025
rmsd[b] for bond angles (deg)	2.22
Ramachandran plot	
favored region (%)	99.5
allowed region (%)	0.5
outlier region (%)	0
average *B* factor (Å^2)	
protein	15.3
ligand (heme)	13.9
ligand (NO_2^-)	23.7
solvent	28.1

[a] Numbers in parentheses represent the values for the highest-resolution shell. [b] Root-mean-square deviation.

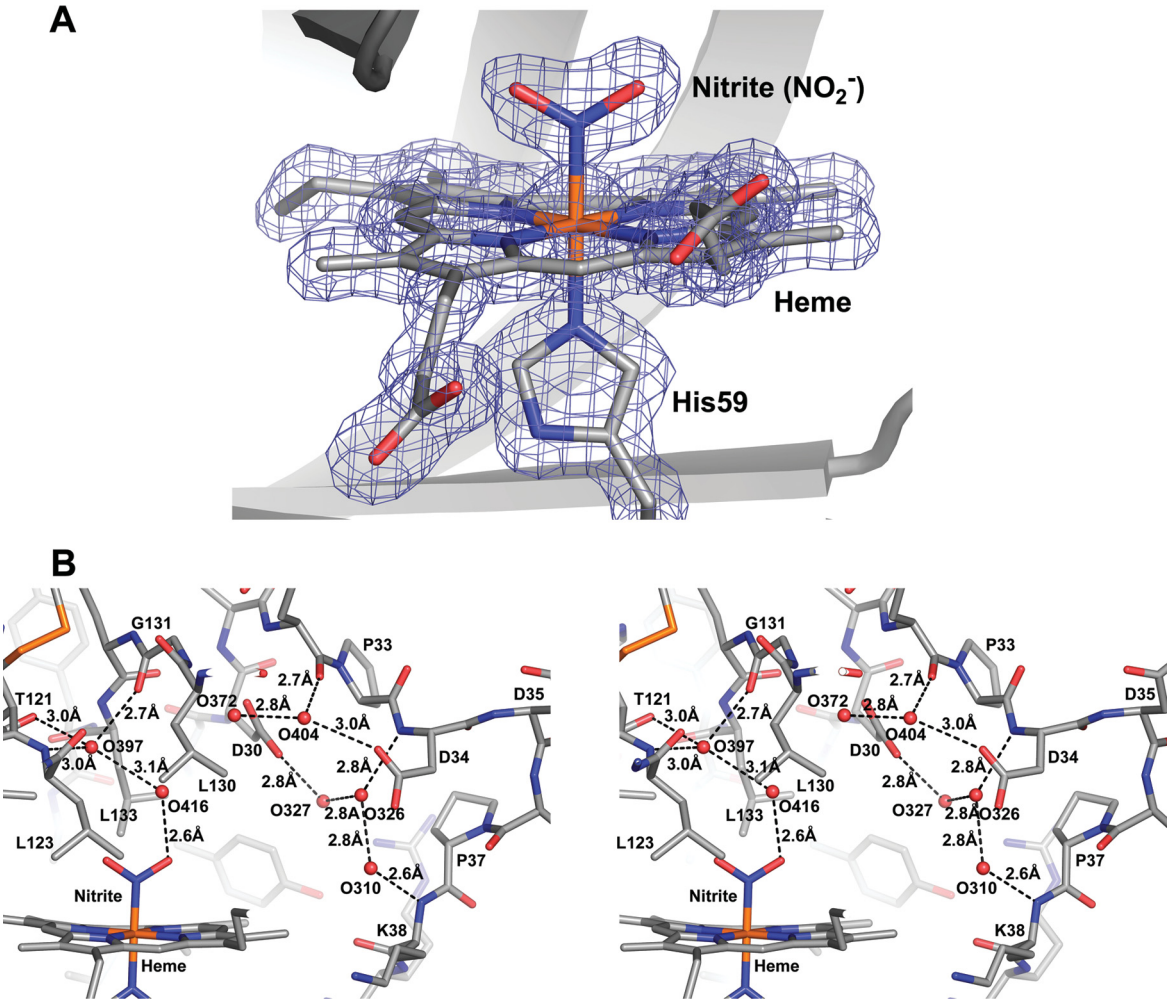

FIGURE 6: X-ray crystal structure of NP4 from *R. prolixus* soaked with NO_2^- at pH 7.4 at 1.4 Å resolution. (A) The $2F_o - F_c$ electron density map of the heme cofactor and its ligands is shown. On the upper heme plane, a nitrite molecule fits well into the electron density contour. (B) Stereoview of a stick representation of NP4 near the heme pocket and the A−B loop. The possible hydrogen bonds via water molecules (red spheres) are represented by the dashed lines.

KNO_2 was adjusted according to the EPR and RR studies to minimize the formation of NO before the crystals were frozen.

The crystals diffracted to 1.4 Å resolution (Table 4), and the structure was determined by the molecular replacement method based on the model of the already published NP4 structures. The overall fold (see Figure S3 of the Supporting Information) was very similar to the established NP4 structures with significant differences only in the A−B loop region (see below). Figure 6A displays the electron density map of the heme cofactor and the ligands. On the upper side of the cofactor, electron density is observed that can be modeled well by an η^1-N coordinated NO_2^-. The $Fe-N_{nitrite}$ and $Fe-N^{\tau}_{His59}$ distances are 1.96 and 2.01 Å, respectively. The $imidazole_{His59}$ plane and the NO_2^- plane are parallel (2° deviation) and oriented along the $C^{meso\text{-}\beta}$–$C^{meso\text{-}\delta}$ axis, i.e., 37° and 39°, respectively, oriented to the closest N_p-Fe-N_p axis. The angle between the ligand planes is nearly straight [$\angle(N_{nitrite}-Fe-N^{\tau}_{His59}) = 179°$]. A second NO_2^- is bound to Asp68 and Lys88, a location far from the cofactor and, therefore, probably simply a consequence of the high NO_2^- concentration under the crystallization conditions (Figure S4 of the Supporting Information).

The pH-dependent change in the flexibility of the two loops termed A−B and G−H in front of the heme cofactor is a major structural determinant of the NO delivery process of NP4 (*43*, *45*, *46*). Comparison with other NP4 structures revealed that NP4[NO_2^-] constitutes an open A−B loop conformation that is depicted in Figure 6B. Like with all NP4 structures, the A−B loop shows a high degree of flexibility (see Figure S3 of the Supporting Information) but is still well-defined as can be seen from the electron density map in Figure S5 of the Supporting Information. Furthermore, the crystal symmetry and the crystal packing did not deviate when the crystals were soaked with NO_2^- (Figure S3 of the Supporting Information) so that A−B loop rearrangement can be identifed as not being a crystallographic artifact.

The A−B loop in this case reveals a strong backbone rearrangement, i.e., between Pro33 and Tyr40; as a consequence of this rearrangement, the side chain of Asp35 moves out of the heme pocket where Asp34 moves toward the heme pocket, which further affects the positions of waters in the proximity of the heme (Figure 6B). Overall, where the A−B loop in the majority of the NP4 X-ray structures appears in a closed conformation, in some of the structures an open loop conformation was obtained. However, although the backbone of NP4[NO_2^-] compares better with the open A−B loop, this conformation is unique among all the NP4 structures (see Figure S6 of the Supporting Information). Superposition of the structures of NP4[NO_2^-] and NP4[NH_3] (PDB entry 1X8P) (*43*) shows that one of the NO_2^-

oxygens is oriented toward the methyl carbons of Val36 with an $O_{nitrite}-C_{Val36}$ distance of 3.8 Å. Thus, we can conclude that electrostatic repulsion may trigger the conformational change of the A−B loop upon NO_2^- binding (Figure S7 of the Supporting Information). At present, NO_2^- is the only structure of NP4 with a charged iron ligand. In contrast, the more hydrophobic ligands NO and imidazole cause the A−B loop to close, even at low pH (*43*, *47*). Thus, Val36 seems to play a major role in the sensing of the ligand and the response of the A−B loop conformation.

DISCUSSION

Spectral changes in UV−vis absorption spectroscopy upon binding of NO_2^- to NP4 and NP7 are small, although the eye detects a significant color change. Small absorption differences are also observed in the case of other ferriheme proteins, namely metMb, metHb (*16*, *48*), and ferriheme cd_1 nitrite reductase (NiR) (*49*). The increase in the magnitude of the α- and β-bands at ~570 and ~530 nm, respectively (Figure 1), is a strong indication for the formation of a Fe^{III} low-spin complex, which is confirmed by RR and EPR spectroscopy (Figures 4 and 5). The change in absorption was used to follow the binding of NO_2^- to the proteins (Figure 2). It is important to note that the formation of the initial complex is faster than the total reaction represented in Scheme 1 (*8*). However, UV−vis absorption spectroscopy is not unambiguous for the identification of the product because the decrease in the Soret absorption together with the increase in the magnitude of the α- and β-bands are also features of the formation of NP4/7[NO]. RR and EPR spectroscopy confirm that within the time of the kinetic measurements no significant amount of $\{FeNO\}^6$ is formed so that studies of the initial complex are possible.

In principle, the NO_2^- anion can coordinate in three different orientations to the metal center of a porphyrin, i.e., the η^1-N bound nitro form and in the η^1-O and η^2-O bound nitrito forms (*50*, *51*). In synthetic iron porphyrins, the N-bound form was found to be significantly more stable (*42*), although the five-coordinate complex of [Fe(*meso*-tetra-*p*-tolylporphyrinato)-(η^1-ONO)] was obtained (*52*). However, upon addition of a sixth coordinating ligand, the η^1-O liganded complex readily converted into the η^1-N species (*52*, *53*). An examination of the few X-ray structures of ferriheme proteins in complex with NO_2^- reveals that the η^1-N complex appears in most cases, i.e., *Thiosphera panthotropha* NiR (*54*), *Thioalkalivibria nitratireducens* NiR (*55*), *Wollinella succinogenes* NiR (*56*), and *E. coli* sulfite reductase hemoprotein (SiRHP) (*57*). Of these examples, only *T. panthotropha* NiR has a His *trans* to NO_2^-, but a hydroheme (heme d_1) is located in the active site (*54*). Where, in contrast, the two other NiR forms have a heme *c*, the iron in these cases is coordinated by Lys (*55*, *56*). Finally, SiHRP also contains a hydroheme (siroheme), but the iron coordination is performed by a very unusual Cys−$[Fe_4S_4]_{cluster}$ ligand (*57*). Thus, it appears that this is the first report of an η^1-N coordinated NO_2^- complex of a fully unsaturated heme inside a protein coordinated by a His residue.

Like NPs, Mb and Hb coordinate a heme *b* via a His residue. However, for both proteins it has been confirmed by X-ray crystallography that the proteins stabilize the $Fe^{III}-\eta^1$-ONO^- complex (*10*, *58*), which is currently the only example of a stable porphyrin (N-base−$Fe^{III}-\eta^1$-ONO^-). A recent examination of site-specific mutants in combination with X-ray crystallography experiments revealed that the NO_2^- orientation in metMb is dictated by the surrounding residues (*11*). The X-ray crystallographic analysis of NP4[NO_2^-] clearly shows the formation of an η^1-N bound NO_2^-. The fact that ferrihemes in general prefer the η^1-N coordination principally suggests the formation of NP[$Fe^{III}-\eta^1$-NO_2^-]. This is further supported by the recent finding that mutation of the distal pocket residue His64 to Val in Mb disrupts the formation of the nitrito complex where insertion of another H bonding residue, i.e., Mb(H64V,V67R), restored the formation of Mb[$Fe^{III}-\eta^1$-ONO^-]. It was concluded that the presence of an H bonding side chain in the heme pocket is crucial for this particular NO_2^- orientation (*11*). However, the heme pocket of NPs is characterized by the presence of numerous carboxylate residues concomitant with a lack of positively charged side chains (*29*), so that a stabilization of a nitrito ligand is not to be expected in NPs.

cw-EPR spectroscopy of NP4/7[NO_2^-] reveals the formation of a low-spin complex ($S = {}^1/_2$). RR spectra further indicate the presence of a six-coordinate complex, i.e., the His59/60 on. This cannot be established from the EPR spectra per se because five-coordinate nitro complexes usually also exhibit a low-spin complex (*59*, *60*). The EPR parameters of two well-characterized model hemes, [Fe(TpivPP)(η^1-NO_2)(py)] and [Fe(TpivPP)(η^1-NO_2)-(ImH)], are included in Table 3 (*42*). Like the proteins discussed here, these compounds exhibit π-donor base ligands *trans* to NO_2^-. Calculation of the rhombicity parameter V/Δ assuming the conventional coordination system, which suggests that the principle magnetic axis (assigned to *z*) is along the heme normal (i.e., $g_z = g_1$, $g_y = g_2$, and $g_x = g_3$), results in values exciding the $V/\Delta = {}^2/_3$ threshold (*40*, *42*). This might suggest a change in the direction of the principal magnetic axis where others ascribe this large rhombicity to the good π-acceptor and σ-donor abilities of the η^1-NO_2^- ligand (*59*). In agreement with the latter, complexes [Fe(TpivPP)(η^1-NO_2)$_2$]$^-$ and [Fe(TpivPP)(η^1-NO_2)(SC_6F_4H)]$^-$ exhibited V/Δ values of 1.34 (*61*) and 1.27 (*62*), respectively. Consequently, η^1-ONO^-, which is considered a good σ-donor but a much poorer π-acceptor (*63*) in the structurally well-defined compounds metMb[η^1-ONO^-] and metHb[η^1-ONO^-], exhibits a much smaller rhombicity (Table 3). The large rhombicity observed for NP4 and NP7 strongly supports the formation of a nitro complex.

Most of the proteins reveal two low-spin components in their EPR spectra (Figure 5 and Table 3). Where the two sets of *g* values of NP7 are rather similar, the divergence between the two sets of NP4 forms is very large; i.e., the spectrum of $LS2^{NP4}$ resembles a "large g_{max}" type of spectrum. It was speculated earlier that in the case of metHb[η^1-ONO^-] the two low-spin species may correspond to either (i) the presence of two different heme centers in Hb originating from the heterotetrameric $\alpha_2\beta_2$ tertiary structure or (ii) the concomitant appearance of a nitro and a nitrito complex (*31*). However, (i) two low-spin species are also observed for many monomeric proteins, and (ii) there is no support by the X-ray crystal structures of metHb[η^1-ONO^-] (*10*) and metMb[η^1-ONO^-] (*58*). Consequently, the origin of the two electronically different species requires an explanation.

Because EPR spectroscopy is primarily sensitive to the ligand orientation rather than the nature of the ligand, which was extensively shown for bis-imidazole-coordinated hemes (*41*, *64*), the two sets of low-spin signals likely reflect two distinct orientations of NO_2^- bound to the heme iron; thus, $LS2^{NP7}$, $LS3^{NP7}$, and $LS3^{NP4}$ reflect a close to parallel ligand plane orientation which is seen in the NP4[NO_2^-] structure. In

contrast, the structurally well-defined model complexes [Fe(TpivPP)(η^1-NO_2)(py)] and [Fe(TpivPP)(η^1-NO_2)(ImH)] exhibit a more perpendicular ligand orientation ($\Delta\phi$ = 77° and 69°, respectively) (*42*) which results in larger g_{max} values (*41*). Notably, the alignment of NO_2^- with respect to the heme plane is comparable, i.e., along those *meso* carbons that orient out of the normal heme plane toward NO_2^- of these nonplanar hemes, and the Fe−$N_{imidazole/py}$ and Fe−$N_{nitrite}$ distances are nearly identical. In contrast, the "large g_{max}" type of spectrum $LS2^{NP4}$ can be interpreted in terms of a perpendicular ligand plane orientation. Recently, the pH dependence of the **A**:**B**[4] ratio in NP2[ImH] was examined in detail by NMR spectroscopy (pH* 7.0 to 4.0)[5] (*65*, *66*). During this study, besides the well-established ^{1}H resonances originating from **A** and **B**, a novel set of resonances appeared with a decreasing pH, and the corresponding species was designated **B**′. **B**′, which is in slow chemical exchange with **B**, so that for **B**′ ⇄ **B**, k_1 = 8.0 s^{-1} and k_{-1} = 1.0 s^{-1} at pH* 5.5 and 30 °C, was further characterized to have the ImH plane ligand orientation nearly perpendicular to that of **B** (*66*). In accordance with these observations, the ImH experiments clearly indicate that the protein provides enough steric freedom for a three-atom V-shaped molecule to rotate in a fashion similar to that of ImH. Although **B**′ was not yet observed in X-ray crystallography, comparison of the crystal structures available for NP4[ImH] (pH 5.6) (*47*) and NP2[ImH] (pH 6.5) (*67*) reasonably explains the behavior (*66*). However, this is a very simple explanation that requires further careful analysis for a detailed understanding of the electronics of the system.

The kinetic parameters of the reaction depicted in Scheme 2 are summarized in Table 1 and are compared to the data obtained for metMb and metHb. It is obvious that the rate of binding (k_1) to NP4/7 is significantly lower compared to those of metMb and metHb. Interestingly, the rate of the release (k_{-1}) is also significantly slower, so that K_{eq} is similar to the globins. Sufficient fitting of the kinetic traces is achieved only if a double exponential is applied (Figure 2A,B). However, the linear behavior of the plot of k_{obs} versus NO_2^- concentration suggests the existence of independent fast and slow processes for both proteins. A similar model was used in the case of metHb + NO_2^- which can be explained with the heterotetrameric $\alpha_2\beta_2$ tertiary structure, and hence the appearance of two distinct heme centers (*16*). Where this interpretation does certainly not apply for NP4 and NP7, a possible explanation may be the presence of two NO_2^- binding modes, i.e., in linear and perpendicular orientation relative to His59/60. On the other hand, NO_2^- was obtained in the crystals only in the parallel orientation, which, on the basis of EPR spectroscopy, is favored in NP4 (Table 3), yet this may be due to the crystallization conditions. Currently, the origin of the two processes cannot be sufficiently explained, and further experimental work is required.

In summary, X-ray crystallography and spectroscopic data strongly reveal the formation of the common η^1-N bound nitro complexes in the case of the lipocalin type heme proteins NP4 and NP7 rather than the unusual η^1-O nitrito form obtained with the globin type metHb and metMb. This may, at least in part, account for the different reactivities observed between the two classes of proteins. Moreover, differences from the globins are also seen in the much slower association rates. On the other hand, the absence of the nitrite disproportionation reaction with other ferrihemes at neutral pH infers that this is a specific feature of nitrophorin structure. Moreover, the equilibration constants for NO_2^- ligand binding, although very small, are comparable to those of the globins. In the case of Mb and Hb, NO_2^- is widely accepted as a physiological relevant substrate (*14*, *68*). Because NPs in principle have the same "working environment", i.e., the blood, this strengthens the argument that NPs have the potential to use NO_2^- as a substrate in vivo as well.

[4]Because of the substituent arrangement of the protoporphyrin IX macrocycle, the heme *b* cofactor binds to the asymmetric environment of a protein's heme pocket in two different orientations, **A** and **B**. This phenomenon is often termed the "heme rotational disorder". For the determination of the orientation, the protoporphyrin IX ring is examined on top of the side opposite the coordinating His. If the pyrrole ring counting follows a clockwise order, then the orientation is termed **A**, otherwise **B**.

[5]The pH was not corrected for the D_2O used as the solvent.

ACKNOWLEDGMENT

We are grateful for the technical assistance of Johanna Taing, Jan Hanis, Marion Stapper, Gudrun Klihm, and Frank Reikowski at our institute. We further thank the staff of beamline BL14.2 at BESSYII for their assistance during the data collection. We thank Prof. F. Ann Walker (Department of Chemistry and Biochemistry, University of Arizona, Tucson, AZ) for the expression vectors.

SUPPORTING INFORMATION AVAILABLE

Kinetic traces of formation of the NP7[NO] complex (Figure S1), kinetic trace and correction of the NP7[NO_2^-] formation (Figure S2), overview of the total X-ray structure of NP4[NO_2^-] (Figure S3), binding site of the second NO_2^- (Figure S4), representation of the electron density of the A−B loop region in the X-ray structure of NP4[NO_2^-] (Figure S5), superposition of backbone structures of the A−B loop region of all NP4 structures available from Protein Data Bank (Figure S6), and superposition of the A−B loop region side chains of NP4[NO_2^-] with two other NP4 structures (Figure S7). This material is available free of charge via the Internet at http://pubs.acs.org.

REFERENCES

1. Walker, F. A., and Montfort, W. R. (2001) The nitric oxide-releasing heme proteins from the saliva of the blood-sucking insect *Rhodnius prolixus*. In Advances in Inorganic Chemistry, Vol. *51* pp 295−358, Academic Press, San Diego.
2. Walker, F. A. (2005) Nitric oxide interaction with insect nitrophorins and thoughts on the electron configuration of the {FeNO}^{6} complex. *J. Inorg. Biochem. 99*, 216–236.
3. Andersen, J. F., Gudderra, N. P., Francischetti, I. M. B., Valenzuela, J. G., and Ribeiro, J. M. C. (2004) Recognition of anionic phospholipid membranes by an antihemostatic protein from a blood-feeding insect. *Biochemistry 43*, 6987–6994.
4. Knipp, M., Zhang, H., Berry, R. E., and Walker, F. A. (2007) Overexpression in *Escherichia coli* and functional reconstitution of the liposome binding ferriheme protein nitrophorin 7 from the blood sucking bug *Rhodnius prolixus*. *Protein Expression Purif. 54*, 183–191.
5. Knipp, M., Yang, F., Berry, R. E., Zhang, H., Shokhirev, M. N., and Walker, F. A. (2007) Spectroscopic and functional characterization of nitrophorin 7 from the blood-feeding insect *Rhodnius prolixus* reveals an important role of its isoform-specific N-terminus for proper protein function. *Biochemistry 46*, 13254–13268.
6. Andersen, J. F., Weichsel, A., Balfour, C. A., Champagne, D. E., and Montfort, W. R. (1998) The crystal structure of nitrophorin 4 at 1.5 Å resolution: Transport of nitric oxide by a lipocalin-based heme protein. *Structure 6*, 1315–1327.
7. Bianchetti, C. M., Blouin, G. C., Bitto, E., Olson, J. S., and Phillips, G. N., Jr. (2010) The structure and NO binding properties of the nitrophorin-like heme-binding protein from *Arabidopsis thaliana* gene locus At1g79260.1. *Proteins 78*, 917–931.
8. He, C., and Knipp, M. (2009) Formation of nitric oxide from nitrite by the ferriheme *b* protein nitrophorin 7. *J. Am. Chem. Soc. 131*, 12042–12043.

9. Samouilov, A., Kuppusamy, P., and Zweier, J. L. (1998) Evaluation of the magnitude and rate of nitric oxide production from nitrite in biological systems. *Arch. Biochem. Biophys. 375*, 1–7.
10. Yi, J., Safo, M. K., and Richter-Addo, G. B. (2008) The nitrite anion binds to human hemoglobin via the uncommon *O*-nitrito mode. *Biochemistry 47*, 8247–8249.
11. Yi, J., Heinecke, J., Tan, H., Ford, P. C., and Richter-Addo, G. B. (2009) The distal pocket histidine residue in horse heart myoglobin directs the O-binding mode of nitrite to the heme iron. *J. Am. Chem. Soc. 131*, 18119–18128.
12. Basu, S., Grubina, R., Huang, J., Conradie, J., Huang, Z., Jeffers, A., Jiang, A., He, X., Azarov, I., Seibert, R., Mehta, A., Patel, R., King, B. S., Hogg, N., Ghosh, A., Gladwin, M. T., and Kim-Shapiro, D. B. (2007) Cataclytic generation of N_2O_3 by the concerted nitrite reductase and anhydrase activity of hemoglobin. *Nat. Chem. Biol. 3*, 785–794.
13. Gladwin, M. T., Schechter, A. N., Kim-Shapiro, D. B., Patel, R. P., Hogg, N., Shiva, S., Cannon, R. O., III, Kelm, M., Wink, D. A., Espey, M. G., Oldfield, E. H., Pluta, R. M., Freeman, B. A., Lancaster, J. R., Jr., Feelisch, M., and Lundberg, J. O. (2005) The emerging biology of the nitrite anion. *Nat. Chem. Biol. 1*, 308–314.
14. Gladwin, M. T., Grubina, R., and Doyle, M. P. (2009) The new chemical biology of nitrite reactions with hemoglobin: R-state catalysis, oxidative denitrosylation, and nitrite reductase/anhydrase. *Acc. Chem. Res. 42*, 157–167.
15. Perissinotti, L. L., Marti, M. A., Doctorovich, F., Luque, F. J., and Estrin, D. A. (2008) A microscopic study of the deoxyhemoglobin-catalyzed generation of nitric oxide from nitrite anion. *Biochemistry 47*, 9793–9802.
16. Wanat, A., Gdula-Argasińska, J., Rutkowska-Żbik, D., Witko, M., Stochel, G., and van Eldik, R. (2002) Nitrite binding to metmyoglobin and methemoglobin in comparison to nitric oxide binding. *J. Biol. Inorg. Chem. 7*, 165–176.
17. Strickler, S. J., and Kasha, M. (1963) Solvent effects on the electronic absorption spectrum of nitrite ion. *J. Am. Chem. Soc. 85*, 2899–2901.
18. Berry, R. E., Shokhireva, T. K., Filippov, I., Shokhirev, M. N., Zhang, H., and Walker, F. A. (2007) The effect of the N-terminus on heme cavity structure, ligand equilibrium and rate constants and reduction potentials of nitrophorin 2 from *Rhodnius prolixus. Biochemistry 46*, 6830–6843.
19. Maes, E. M., Roberts, S. A., Weichsel, A., and Montfort, W. R. (2005) Ultrahigh resolution structures of nitrophorin 4: Heme distortion in ferrous CO and NO complexes. *Biochemistry 44*, 12690–12699.
20. Hagen, W. R. (2009) Biomolecular EPR Spectroscopy, 1st ed., CRC Press, Boca Raton, FL.
21. Kabsch, W. (1993) Automatic processing of rotation diffraction data from crystals of initially unknown symmetry and cell constants. *J. Appl. Crystallogr. 26*, 795–800.
22. Collaborative Computational Project, Number 4 (1994) The *CCP*4 suite: Programs for protein crystallography. *Acta Crystallogr. D50*, 760–763.
23. Emsley, P., and Cowtan, K. (2004) Coot: Model-building tools for molecular graphics. *Acta Crystallogr. D60*, 2126–2132.
24. Lovell, S. C., Davis, I. W., Arendall, W. B., III, de Bakker, P. I. W., Word, J. M., Prisant, M. G., Richardson, J. S., and Richardson, D. C. (2003) Structure validation by Cα geometry: ϕ, ψ, and Cβ deviation. *Proteins: Struct., Funct., Genet. 50*, 437–450.
25. Andersen, J. F., Ding, X. D., Balfour, C., Shokhireva, T. K., Champagne, D. E., Walker, F. A., and Montfort, W. R. (2000) Kinetics and equilibria in ligand binding by nitrophorins 1−4: Evidence for stabilization of a nitric oxide-ferriheme complex through a ligand-induced conformational trap. *Biochemistry 39*, 10118–10131.
26. Rodkey, F. L. (1976) A mechanism for the conversion of oxyhemoglobin to methemoglobin by nitrite. *Clin. Chem. 22*, 1986–1990.
27. Smith, R. P. (1967) The nitrite methemoglobin complex: Its significance in methemoglobin analyses and its possible role in methemoglobinemia. *Biochem. Pharmacol. 16*, 1655–1664.
28. Kaneko, Y., Yuda, M., Iio, T., Murase, T., and Chinzei, Y. (1999) Kinetic analysis on nitric oxide binding of recombinant Prolixin-S, a nitric oxide transport protein from the bloodsucking bug. *Rhodnius prolixus. Biochim. Biophys. Acta 1431*, 492–499.
29. Berry, R. E., Shokhirev, M. N., Ho, A. Y. W., Yang, F., Shokhireva, T. K., Zhang, H., Weichsel, A., Montfort, W. R., and Walker, F. A. (2009) Effect of mutation of carboxyl side-cahin amino acids near the heme on the midpoint potentials and ligand binding constants of nitrophorin 2 and its NO, histamine, and imidazole complexes. *J. Am. Chem. Soc. 131*, 2313–2327.
30. Schwab, D. E., Stamler, J. S., and Singel, D. J. (2009) Nitrite-methemoglobin inadequate for hypoxic vasodilation. *Nat. Chem. Biol. 5*, 366.
31. Goetz, B. I., Shields, H. W., Basu, S., Wang, P., King, S. B., Hogg, N., Gladwin, M. T., and Kim-Shapiro, D. B. (2009) An electron paramagnetic resonance study of the affinity of nitrite for methemoglobin. *Nitric Oxide 22*, 149–154.
32. Maes, E. M., Walker, F. A., Montfort, W. R., and Czernuszewicz, R. S. (2001) Resonance Raman spectroscopic study of nitrophorin 1, a nitric oxide-binding heme protein from *Rhodnius prolixus*, and its nitrosyl and cyano adducts. *J. Am. Chem. Soc. 123*, 1164–1172.
33. Kincaid, J. R. (2000) Resonance Raman spectra of heme proteins and model compounds. In The Porphyrin Handbook (Kadish, K. M., Smith, K. M., and Guilard, R., Eds.) Vol. *7*, pp 225−291, Academic Press, San Diego.
34. Spiro, T. G., Stong, J. D., and Stein, P. (1979) Porphyrin core expansion and doming in heme proteins. New evidence from resonance Raman spectra of six-coordinate high-spin iron(III) hemes. *J. Am. Chem. Soc. 101*, 2648–2655.
35. Zareba, A. A. (2006) Resonance Raman spectroscopic characterization of nitrophorins from *Rhodnius prolixus* and *Cimex lectularius*. Ph.D. Thesis, Department of Chemistry, University of Houston, Houston.
36. Choi, S., Spiro, T. G., Langry, K. C., Smith, K. M., Budd, D. L., and La Mar, G. N. (1982) Structural correlations and vinyl influences in resonance Raman spectra of protoheme complexes and proteins. *J. Am. Chem. Soc. 104*, 4345–4351.
37. Ikeda-Saito, M., Hori, H., Andersson, L. A., Prince, R. C., Pickering, I. J., George, G. N., Sanders, C. R., II, Lutz, R. S., McKelvey, E. J., and Mattera, R. (1992) Coordination structure of the ferric heme iron in engineered distal histidine myoglobin mutants. *J. Biol. Chem. 267*, 22843–22852.
38. Taylor, C. P. S. (1977) The EPR of low spin heme complexes. Relation of the t_{2g} hole model to the directional properties of the *g* tensor, and a new method for calculating the ligand field parameters. *Biochim. Biophys. Acta 491*, 137–149.
39. Zoppellaro, G., Bren, K. L., Ensign, A. A., Herbitz, E., Kaur, R., Hersleth, H.-P., Ryde, U., Hederstedt, L., and Andersson, R. K. (2009) Studies of ferric heme proteins with highly anisotropic/highly axial low spin ($S = 1/2$) electron paramagnetic resonance signals with bis-histidine and histidine-methionine axial iron coordination. *Biopolymers 91*, 1064–1082.
40. Palmer, G. (2000) Electron Paramagnetic Resonance of Metalloproteins. In *Physical Methods in Bioinroganic Chemistry* (Que, L., Ed.) pp 121−186, University Science Books, Sausalito, CA.
41. Walker, F. A. (2004) Models of the bis-histidine-ligated electron-transferring cytochromes. Comparative geometric and electronic structure of low-spin ferro- and ferrihemes. *Chem. Rev. 104*, 589–615.
42. Nasri, H., Wang, Y., Huynh, B. H., Walker, F. A., and Scheidt, W. R. (1991) Reactions of bis(nitro)(α,α,α,α-tetrakis(*o*-pivalamidophenyl)-porphinato)ferrat(III) with pyridine and imidazole. EPR and Mössbauer spectra and molecular structures of the mixed-ligand species. *Inorg. Chem. 30*, 1483–1489.
43. Kondrashov, D. A., Roberts, S. A., Weichsel, A., and Montfort, W. R. (2004) Protein functional cycle viewed at atomic resolution: Conformational change and mobility in nitrophorin 4 as a function of pH and NO binding. *Biochemistry 43*, 13637–13647.
44. Schmidt, M., Achterhold, K., Prusakov, V., and Parak, F. G. (2009) Protein dynamics of a β-sheet protein. *Eur. Biophys. J. 38*, 687–700.
45. Maes, E. M., Weichsel, A., Andersen, J. F., Shepley, D., and Montfort, W. R. (2004) Role of binding site loops in controlling nitric oxide release: Structure and kinetics of mutant forms of nitrophorin 4. *Biochemistry 43*, 6679–6690.
46. Swails, J. M., Meng, Y., Walker, F. A., Martí, M. A., Estrin, D. A., and Roitberg, A. E. (2009) pH-dependent mechanism of nitric oxide release in nitrophorin 2 and 4. *J. Phys. Chem. B 113*, 1192–1201.
47. Roberts, S. A., Weichsel, A., Qiu, Y., Shelnutt, J. A., Walker, F. A., and Montfort, W. R. (2001) Ligand-induced heme ruffling and bent NO geometry in ultra-high-resolution structures of nitrophorin 4. *Biochemistry 40*, 11327–11337.
48. Young, L. J., and Siegel, L. M. (1988) On the reaction of ferric heme proteins with nitrite and sulfite. *Biochemistry 27*, 2790–2800.
49. van Wonderen, J. H., Knight, C., Oganesyan, V. S., George, S. J., Zumpft, W. G., and Cheesman, M. R. (2007) Activation of the cytochrome cd_1 nitrite reductase from *Paracoccus pantotrophus*: Reaction of oxidized enzyme with substrate drives a ligand switch at heme *c*. *J. Biol. Chem. 282*, 28207–28215.
50. Wyllie, G. R. A., and Scheidt, W. R. (2002) Solid-state structures of metalloporphyrin NO_x compounds. *Chem. Rev. 102*, 1067–1089.

51. Heinecke, J., and Ford, P. C. (2010) Mechanistic studies of nitrite reactions with metalloproteins and models relevant to mammalian physiology. *Coord. Chem. Rev. 254*, 235–247.
52. Kurtikyan, T. S., and Ford, P. C. (2006) Reactions of nitrogen oxides with heme models: Spectral charcterization of an elusive five-coordinate Fe^{III}(porphyrin) nitrtito intermediate. *Angew. Chem., Int. Ed. 45*, 492–496.
53. Kurtikyan, T. S., Hovhannisyan, A. A., Gulyan, G. M., and Ford, P. C. (2007) Interaction of nitrogen bases with iron-porphyrin nitrito complexes Fe(Por)(ONO) in sublimed solids. *Inorg. Chem. 46*, 7024–7031.
54. Williams, P. A., Fülöp, V., Garman, E. F., Saunders, N. F. W., Ferguson, S. J., and Hajdu, J. (1997) Haem-ligand switching during catalysis in crystals of a nitrogen-cycle enzyme. *Nature 389*, 406–412.
55. Polyakov, K. M., Boyko, K. M., Tikhonova, T. V., Slutsky, A., Antipov, A. N., Zvyagilskaya, R. A., Popov, A. N., Bourenkov, G. P., Lamzin, V. S., and Popov, V. O. (2009) High-resolution structural analysis of a novel octaheme cytochrome *c* nitrite reductase from the haloalkaliphilic bacterium *Thioalkalivibrio nitratireducens*. *J. Mol. Biol. 389*, 846–862.
56. Einsle, O., Messerschmidt, A., Huber, R., Kroneck, P. M. H., and Neese, F. (2002) Mechanism of the six-electron reduction of nitrite to ammonia by cytochrome *c* nitrite reductase. *J. Am. Chem. Soc. 124*, 11737–11745.
57. Crane, B. R., Siegel, L. M., and Getzoff, E. D. (1997) Probing the catalytic mechanism of sulfite reductase by X-ray crystallography: Structures of the *Escherichia coli* hemoprotein in complex with substrates, inhibitors, intermediates, and products. *Biochemistry 36*, 12120–12137.
58. Copeland, D. N., Soares, A. S., West, A. H., and Richter-Addo, G. B. (2006) Crystal structures of the nitrite and nitric oxide complexes of horse heart myoglobin. *J. Inorg. Biochem. 100*, 1413–1425.
59. Conradie, J., and Ghosh, A. (2006) Iron(III)-nitro porphyrins: Theoretical exploration of a unique class of reactive molecules. *Inorg. Chem. 45*, 4902–4909.
60. Nasri, H., Wang, Y., Huynh, B. H., and Scheidt, W. R. (1991) Nitrite-bound five-coordinate low-spin iron(II) model complex for the prosthetic group of nitrite reductase with an unusually large quadrupole splitting. Synthesis, Mössbauer properties, and molecular structure of the complex (nitro)(α,α,α,α-tetrakis(*o*-pivalamidophenyl)porphinato)-iron(II). *J. Am. Chem. Soc. 113*, 717–719.
61. Nasri, H., Goodwin, J. A., and Scheidt, W. R. (1990) Use of protected binding sites for nitrite binding in iron(III) porphyrinates. Crystal structure of the bis(nitro)(α,α,α,α-tetrakis(*o*-pivalamidophenyl)-porphinato)iron(III) anion. *Inorg. Chem. 29*, 185–191.
62. Nasri, H., Haller, K. J., Wang, Y., Huynh, B. H., and Scheidt, W. R. (1992) Reactions of bis(nitro)[α,α,α,α-*meso*-tetrakis(*o*-pivalamido-phenyl)porphinato]iron(III) with 2,3,5,6-tetraflurothiophenol and 2,3,5,6-tetrafluorothiophenolate. EPR and Mössbauer spectra and molecular structures. *Inorg. Chem. 31*, 3459–3467.
63. Hitchman, M. A., and Rowbottom, G. L. (1982) Transition metal nitrite complexes. *Coord. Chem. Rev. 42*, 55–132.
64. Walker, F. A. (1999) Magnetic spectroscopy (EPR, ESEEM, Mössbauer, MCD and NMR) studies of low-spin ferriheme centers and their corresponding heme proteins. *Coord. Chem. Rev. 185−186*, 471–534.
65. Yang, F., Zhang, H., and Knipp, M. (2009) A one-residue switch reverses the orientation of a heme *b* cofactor. Investigations on the ferriheme NO transporters nitrophorin 2 and 7 from the blood-feeding insect *Rhodnius prolixus*. *Biochemistry 48*, 235–241.
66. Yang, F., Knipp, M., Shokhireva, T. K., Berry, R. E., Zhang, H., and Walker, F. A. (2009) A ^{1}H and ^{13}C NMR spectroscopic study of the ferriheme resonances of three low-spin complexes of wild-type nitrophorin 2 and nitrophorin2(V24E) as a function of pH. *J. Biol. Inorg. Chem. 14*, 1077–1095.
67. Andersen, J. F., and Montfort, W. R. (2000) The crystal structure of nitrophorin 2. A trifunctional antihemostatic protein from the saliva of *Rhodnius prolixus*. *J. Biol. Chem. 275*, 30496–30503.
68. Shiva, S., Huang, Z., Grubina, R., Sun, J., Ringwood, L. A., MacArthur, P. H., Xu, X., Murphy, E., Darley-Usmar, V. M., and Gladwin, M. T. (2007) Deoxymyoglobin is a nitrite reductase that generates nitric oxide and regulates mitochondrial respiration. *Circ. Res. 100*, 654–661.
69. Gibson, Q. H., Parkhurst, L. J., and Geraci, G. (1969) The reaction of methemoglobin with some ligands. *J. Biol. Chem. 244*, 4668–4676.
70. Hagedoorn, P. L., de Geus, D. C., and Hagen, W. R. (2002) Spectroscopic characterization and ligand-binding properties of chlorite dismutase from the chlorate respiring bacterial strain GR-1. *Eur. J. Biochem. 269*, 4905–4911.

- Supporting Information –
-

Complex Formation of Nitrite with the Ferriheme *b* β-Barrel Proteins Nitrophorin 4 and Nitrophorin 7[†,‡]

Chunmao He, Hideaki Ogata, and Markus Knipp[*]

Max-Planck-Institut für Bioanorganische Chemie, Stiftstrasse 34-36, D-45470 Mülheim an der Ruhr, Germany

* Supporting Information *

[†] This work was financially supported by the Max Planck Society (MPG) and by the Deutsche Forschungsgemeinschaft (DFG), grant KN 951/1-1 (to M.K.).

[‡] Coordinates for the X-ray crystal structure reported herein have been deposited in the Protein Data Bank (PDB code 3MVF).

[*] To whom correspondence should be addressed: Telephone: +49 (0)208 306 3581. Fax: +49 (0)208 306 3951. E-mail: mknipp@mpi-muelheim.mpg.de.

- Supporting Information –

-

Supplementary Figures

FIGURE S1: Kinetic trace of the formation of NP4[NO] from 7 μM NP4 and 300 mM $NaNO_2$ in 50 mM MOPS/NaOH (pH 7.0) at 30 °C monitored at 418 nm.

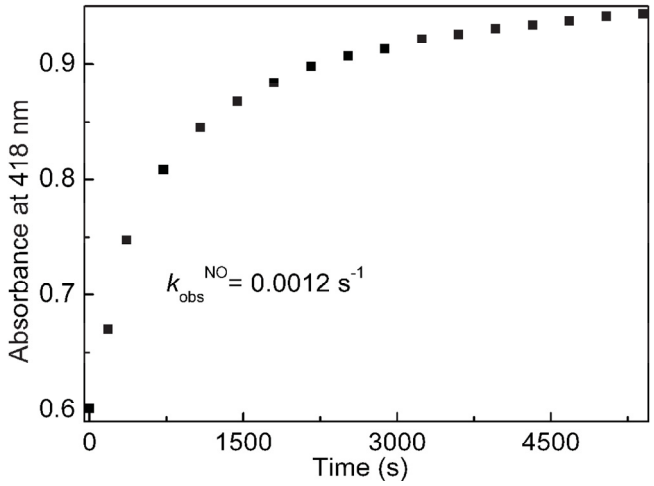

FIGURE S2: Example of the correction of the stopped-flow kinetics monitored at 404 nm for the formation of NP4[NO]. Kinetic trace of the absorbance change at 404 nm of the reaction of 5 μM NP4 with 300 mM $NaNO_2$ in 50 mM MOPS/NaOH, 300 mM NaCl (pH 7.0) at 30 °C (*black line*). The last 3 min were fit by linear regression analysis (*blue line*) and the resulting function subtracted from original data (*red line*).

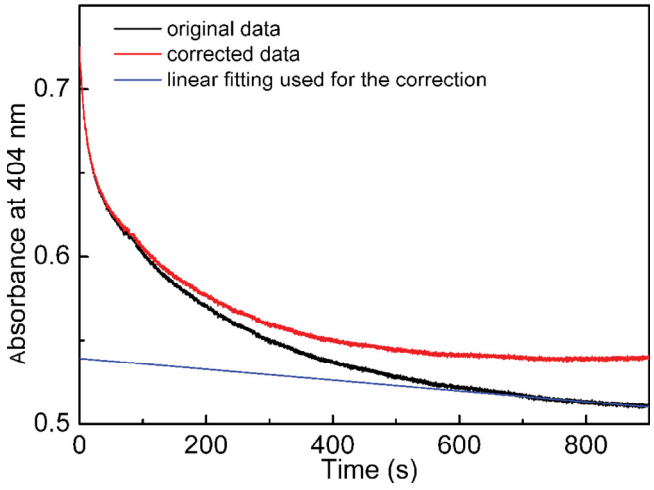

FIGURE S3: Stereo view of the ribbon representation of the total structure of recombinant NP4[NO_2^-] from *Rhodnius prolixus* crystallized at pH 7.4 in superposition with NP4[NH_3] (PDB code 1X8P) at pH 7.4 and NP4[OH_2] at pH 5.6 (PDB code 1X8Q). The colors gradually reflect the *B*-factor along the amino acid sequence with dark blue reflecting small *B*-factor, yellow reflecting a high *B*-factor.

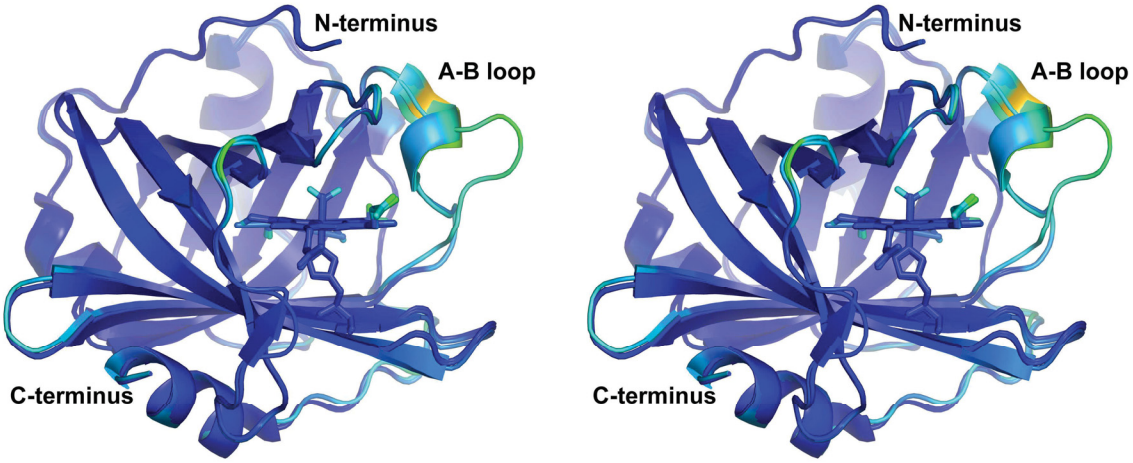

FIGURE S4: Binding site of the second NO_2^- molecule in NP4[NO_2^-] from *Rhodnius prolixus* at pH 7.4. Waters are displayed as red spheres.

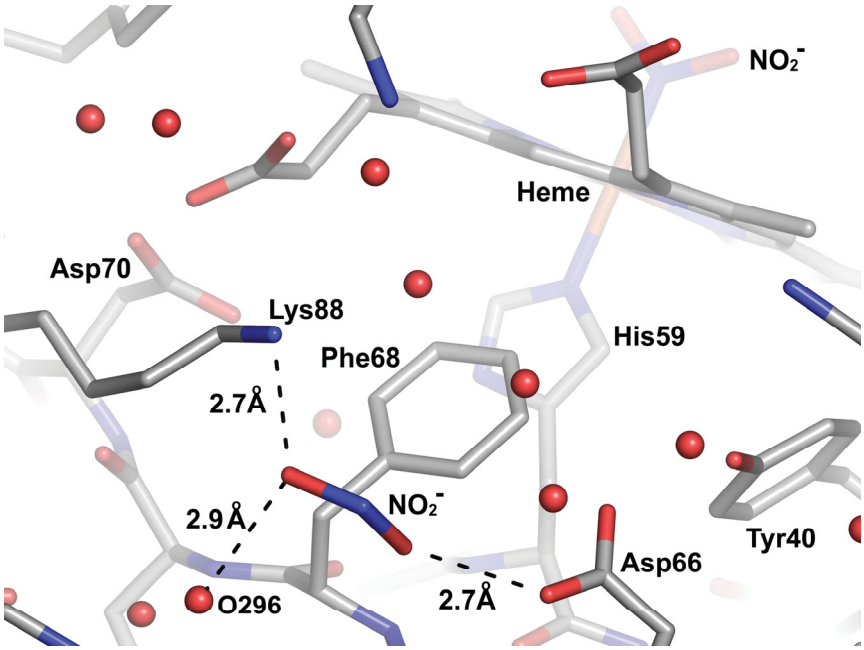

FIGURE S5: X-ray crystal structure of NP4 from *R. prolixus* soaked with NO_2^- at pH 7.4. Electron density from the $2F_0 - F_c$ map of the A–B loop is presented showing a good correlation of the model with the electron density.

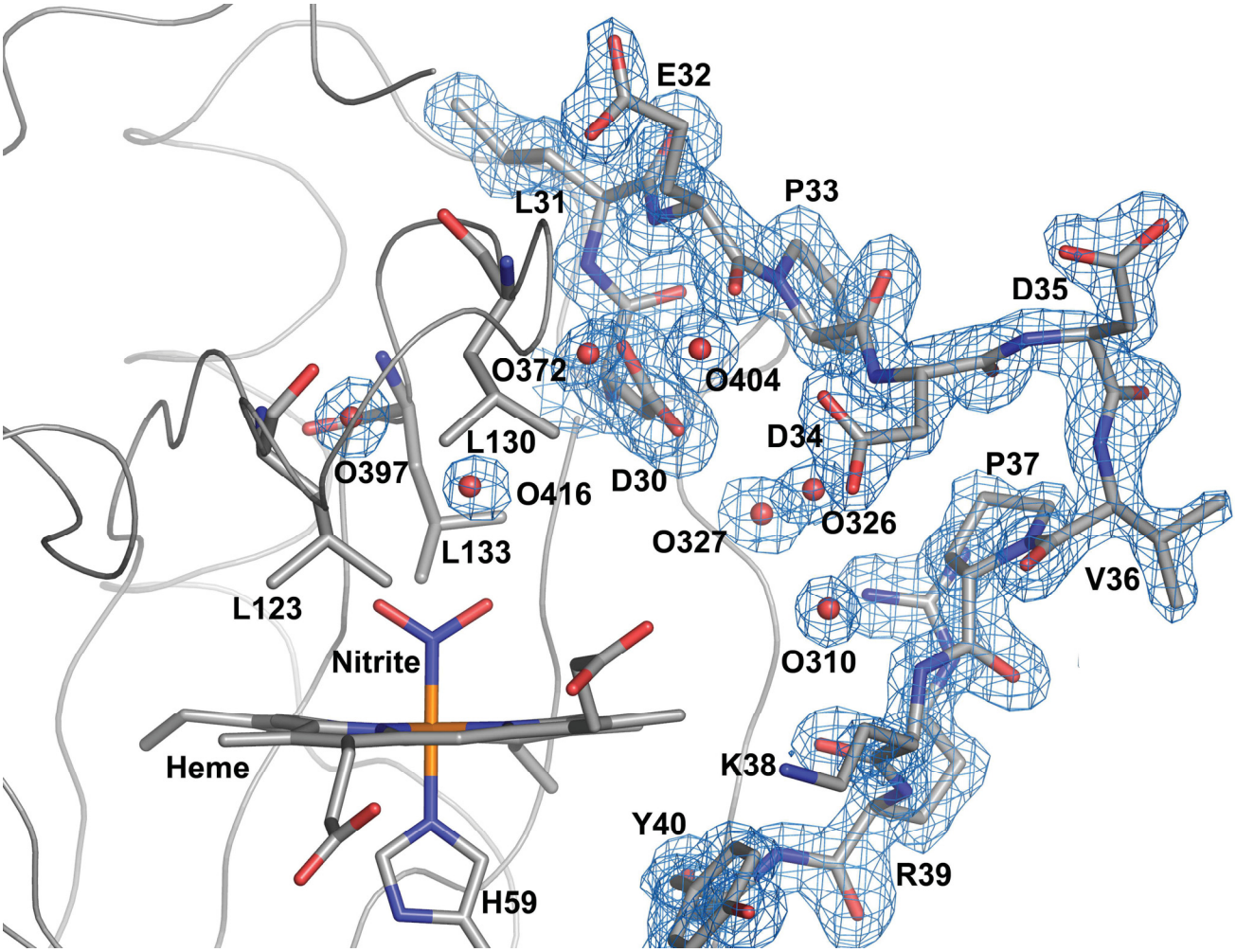

FIGURE S6: Superposition of the backbone of the X-ray structure of NP4[NO_2^-] (*red*) with the backbones of all other NP4 X-ray structures available from the PDB (*blue*). The A–B loop appears in two main conformations. Most structures appear in the closed conformation. However, the structures with the following PDB codes appear in an open conformation: 1D2U, 1D3S, 1IKE, 1NP4, 1YWD. The A–B loop conformation is unique among the NP4 structures.

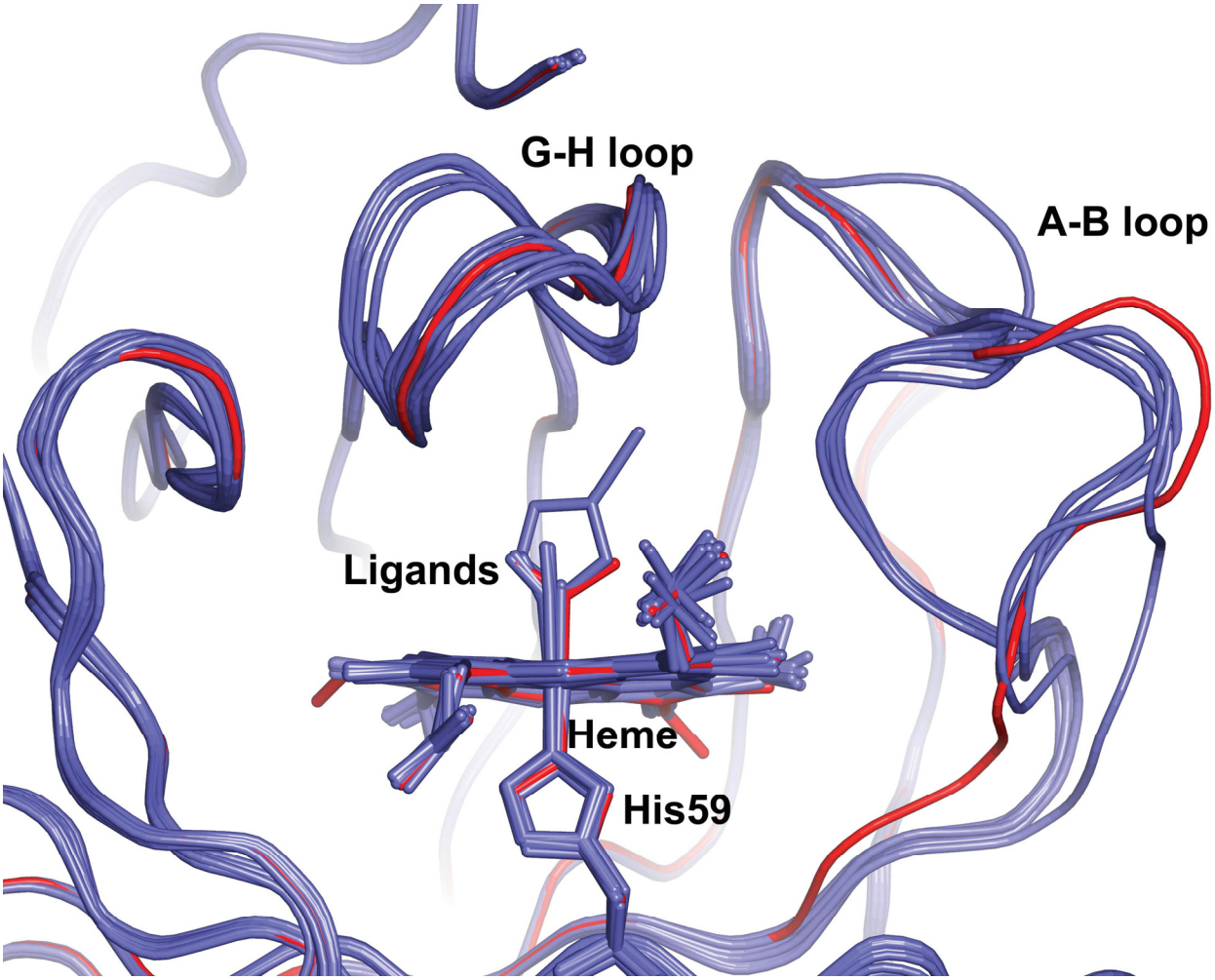

FIGURE S7: Superposition of the A-B loop region of the X-ray structure of NP4[NO_2^-] at pH 7.4 (*red*) with the structures of NP4[NH_3] at pH 7.4 (PDB code 1X8P, *green*) and NP4[OH_2] at pH 5.6 (PDB code 1X8Q, *yellow*). The distance between one of the nitrite oxygens of NP4[NO_2^-] and the Val36 methyl carbon of the two other structures is indicated.

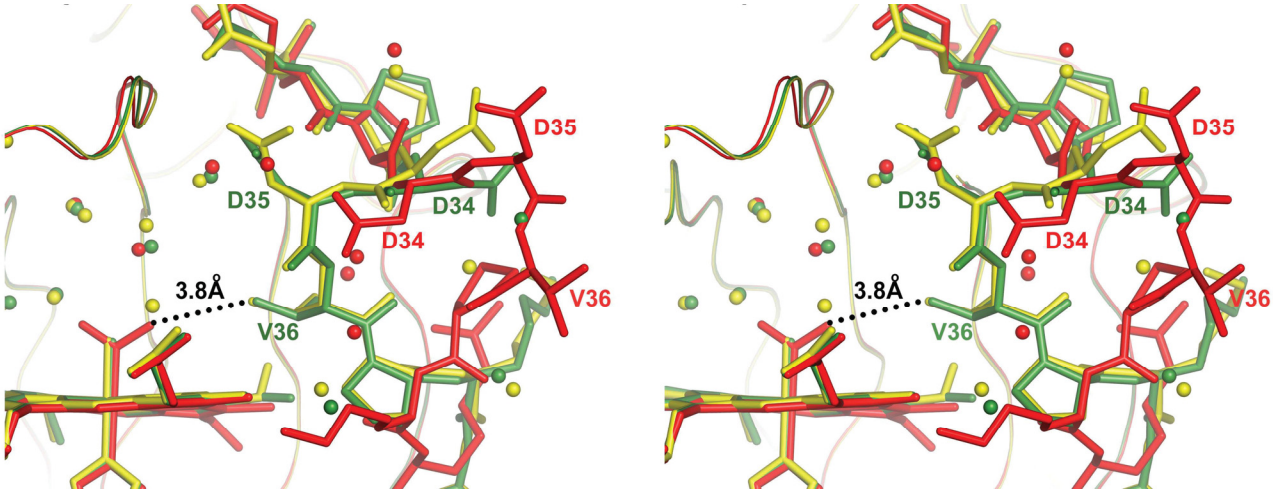

Chapter 4. Guanidine–iron coordination in a heme protein: Crystallographic and spectroscopic characterization of the L130R mutant of nitrophorin 4 from *Rhodnius prolixus*

(He, C.; Fuchs, M.; Ogata, H.; Knipp, M. Submitted)

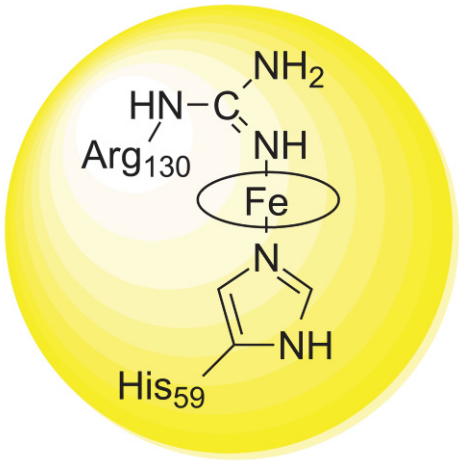

Abstract

The diversity of axial ligand coordination in heme proteins resembles a remarkable diversity of both coordination of protein resins and non-proteinous ligands. However, guanidine coordination has not yet been reported. Herein, we report on the coordination of an arginine guanidine nitrogen to the ferroheme cofactor of the nitrophorin 4 Leu130→Arg distal pocket mutant NP4(L130R).

Guanidine–Iron Coordination in a Heme Protein: Crystallographic and Spectroscopic Characterization of the L130R Mutant of Nitrophorin 4 from *Rhodnius prolixus*

Chunmao He[†], Martin R. Fuchs[‡], Hideaki Ogata[*,†], and Markus Knipp[*,†]

Max-Planck-Institut für Bioanorganische Chemie, Stiftstrasse 34-36, D-45470 Mülheim an der Ruhr, Germany

Swiss Light Source, Paul-Scherrer-Institut, CH-5232 Villigen, Switzerland

KEYWORDS: Arginine, Guanidine Coordination, Heme, Iron, Microspectrophotometer, Nitrophorin, Photoreduction.

Supporting Information available

ABSTRACT: Axial ligand coordination in heme proteins is accomplished by a remarkable diversity from both protein residues and non-proteinous ligands. However, guanidine coordination has not yet been reported, which is not surprising in view of the generally very limited number of reported guanidine–metal complexes. Herein, we report on the coordination of an arginine guanidine nitrogen to the ferroheme cofactor of the nitrophorin 4 Leu130→Arg distal pocket mutant NP4(L130R).

At low temperature, the novel L130R mutant of the heme protein nitrophorin 4 (NP4) coordinates the heme iron by the Arg130:N^{ω} atom. NP4 is a ferriheme protein that is found in the saliva of the blood-sucking insect *Rhodnius prolixus* and of which high-resolution X-ray structures were obtained.[1] Its architecture resembles the antiparallel 8-stranded β-barrel body structure of the lipocalins. The heme *b* cofactor is embedded in the barrel and concomitantly coordinated via His59:N^{τ}. The heme iron is typically in the ferriheme state and is ready to bind a number of ligands, including NO, histamine, CN^-, or ImH.[2] By analogy to the double mutant H64V,V67R of horse Mb, a potential H-bonding base residue was inserted into the distal heme pocket site of the NP4 structure.[3] The position of the distal pocket Leu130 was chosen for mutation because inspection of the X-ray structures suggests that the side-chain, which is part of the flexible G-H loop, should have ample space without disturbing the fold.[4,5]

The expression and purification of NP4(L130R) yields quantities of protein comparable to *wt* protein. The absorbance spectra (Figure S1) and resonance Raman (RR) spectra (Figure S2) are very similar to those of the *wt* protein indicating a 6-coordinate high-spin (HS) Fe^{III} complex ($S = {}^5/_2$), i.e., water-on. This is in good agreement with the obtained axial cw-EPR spectrum shown in Figure 1, which is typical for HS ferriheme proteins with a weak distal ligand, for example *wt* NP4[6] (Figure 1) or met-myoglobin.[7] However, in the case of *wt* NP4 a significant contribution of a low-spin (LS) species is obtained, which is attributed to the appearance of the hydroxo complex as a consequence of ligand water deprotonation,[8] which is virtually absent in case of NP4(L130R).

The large distal pocket of NPs allows the binding of rather bulky ligands, for example imidazole (ImH). Complexes with ImH are among the most intensely characterized LS species ($S = {}^1/_2$) of NPs. Furthermore, the bulkiness of ImH in combination with the sensitivity of the g tensor toward the rotational orientation relative to the heme macrocycle[9] makes it a good probe to study the influence of the mutation toward the heme pocket by EPR spectroscopy. The cw-EPR spectrum of NP4(L130R)[ImH] is displayed in Figure 1. The principle *g*-values are comparable to those reported for other NP[ImH] complexes as can be seen from Table 1. The significantly larger *g*-strain reflects minor inhomogeneity in the frozen solution with respect to the orientation of ImH on the heme plane.[9] Overall, NP4(L130R)[ImH] principally resembles the coordination of the *wt* structure.

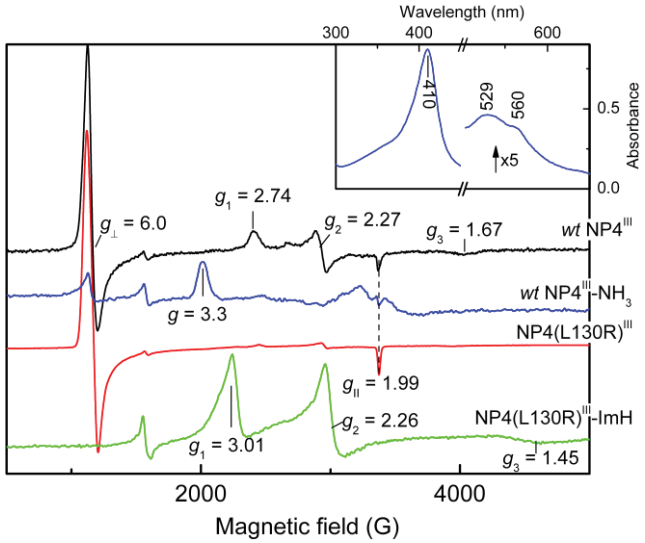

Figure 1. X-band EPR spectra of *wt* NP4 (*black*), *wt* NP4[NH_3] (*blue*), NP4(L130R) (*red*), and NP4(L130R)[ImH] (*green*). Spectra were recorded at 10 K. All samples were in 100 mM HEPES/NaOH, 25% glycerol (pH 7.2) except for *wt* NP4 [NH_3], which was in 2 M NH_4OAc, 100 mM MOPS/NaOH (pH 7.5). Inset: Absorbance spectrum of *wt* NP[NH_3] in 2 M NH_4OAc, 100 mM MOPS/NaOH (pH 7.5) at ambient temperature.

Crystals of NP4(L130R) appear after ~2 weeks using 3.2 M ammonium phosphate (pH 7.4) as precipitant, which is similar to the conditions previously reported for *wt* NP4.[1,4,10] Crystals of NP4(L130R)[ImH] were prepared by soaking in mother liquid containing 10 mM of ImH prior to freezing. Diffraction datasets were taken at 100 K over a period and the crystal structures of NP4(L130R) and NP4(L130R)[ImH] were solved by molecular replacement at a resolution of 1.3 and 1.4 Å, respectively.[11] The crystallographic refinement parameters are summarized in Table S1 and a comparison of the overall structures of NP4(L130R) and NP4(L130R)[ImH] with those of the respective *wt* protein structures is presented in Figures S3 and S4. Overall, the influence of the mutation toward the total structure is negligible as is indicated by the high degree of structural similarity between *wt* NP4 and NP4(L130R) (RMSD = 0.49 Å) and *wt* NP4[ImH] and NP4(L130R)[ImH] (RMSD = 0.69 Å).

Table 1. Comparison of the Principle *g*-Values of the ImH Complex of NP4(L130R) in Comparison with those of *wt* NP4, 2, and 7.

	g_1	g_2	g_3	Reference
NP4(L130R)	3.01	2.26	1.45	This work
wt NP4	3.02	2.25	1.46	[12]
wt NP2	3.02	2.26	1.37	[13]
wt NP7	3.07	2.19	1.36	[14]

A detailed representation of the heme pockets of NP4(L130R)[ImH] and NP4(L130R) is depicted in Figure 2. In case of NP4(L130R)[ImH] a single crystal form was obtained with very similar structural features compared to *wt* NP4[ImH].[15] Similar to Leu130 in the *wt*, the Arg130 side-chain is folded toward the front of the distal heme pocket and does not interfere with the ImH ligand. The similarity between the heme pockets is also reflected by only slightly affected heme distortion of the heme planarity (Figure S5).

In the heme pocket of NP4(L130R) the Arg130 appears in two conformations (Figure S4). Surprisingly, in the form with the higher occupancy (~60%), the iron is axially coordinated by Arg130:N$^{\omega}$ with an interatomic distance of 2.1 Å (Figure 2B). To the best of our knowledge, this is the first example of an Arg coordinated metalloporphyrin. The crystallographic results are surprising in view of the spectroscopic data that do not give evidence for a strong interaction of Arg130:N$^{\omega}$ with the iron, which is expected from the bond length. Examples of coordination complexes with guanine ligands are generally scarce, in biomolecules nearly not existing.[16] A big challenge for the formation of such complexes is the high pK_a value of guanidines, for example in the case of arginine ~12, so that in aqueous media deprotonation is hardly achieved.[16c] Metal complexes of guanidines have been reported for Co^{II}, Cu$^{I/II}$, Zn^{II}, Pd^{II}, Ni^{II}, Cr^{II}, Au^{I}, and Pt^{II} where in all cases the coordination was achieved via the imine nitrogen. Thus, although the resolution of the NP4(L130R) X-ray structure does not allow to distinguish between the –C–N$^{\omega}$H$_2$ and the –C=N$^{\omega}$H groups, by analogy –C=N$^{\omega}$(H)–Fe coordination can be expected via the N$^{\omega}$ lone pair. However, of the 150 guanidine–metal interactions deposited in the Cambridge Structural Database (CSD) most were found to be diguanidines and only 4 examples of individual guanidine–metal interactions were found.[16d] The few examples of protein structures containing Arg:N$^{\omega}$–metal bonds are the arginase of *Bacillus caldovelox* (Mn)[17] and a human carbonic anhydrase variant (Zn).[18] Most interestingly in this context, though, is the coordination of one of the iron in the [2Fe–2S] cluster of biotin synthase BioB.[16e,19] However, the rather low resolution of this structure of 3.4 Å (PDB code 1R30) does not provide reliable bond parameters. Recent QM/MM calculations on 4 conservable models of this site though support the –C=N$^{\omega}$(H)–Fe arrangement.[16e] Overall, the N$^{\omega}$–Fe distance is slightly longer compared to the mean N$_{guanidine}$–M^{n+} distance of 1.91 ± 0.06 Å found in the synthetic guanidine complexes[16d] but is very similar to the N$^{\omega}$–Fe distance calculated for the BioB [2Fe-2S] cluster models, which are between 2.05 and 2.18 Å.[16e] The ∠(C=N$^{\omega}$–Fe) of 141° is slightly wider compared to the mean ∠(C=N–M^{n+}) of 129° ± 2°. The dihedral ∠(N$^{\delta}$–C=N$^{\omega}$–Fe) of 0° is close to the mean angel in guanidine-metal compounds of (RNH–C=N–M^{n+}) = –1° ± 9°.[16d]

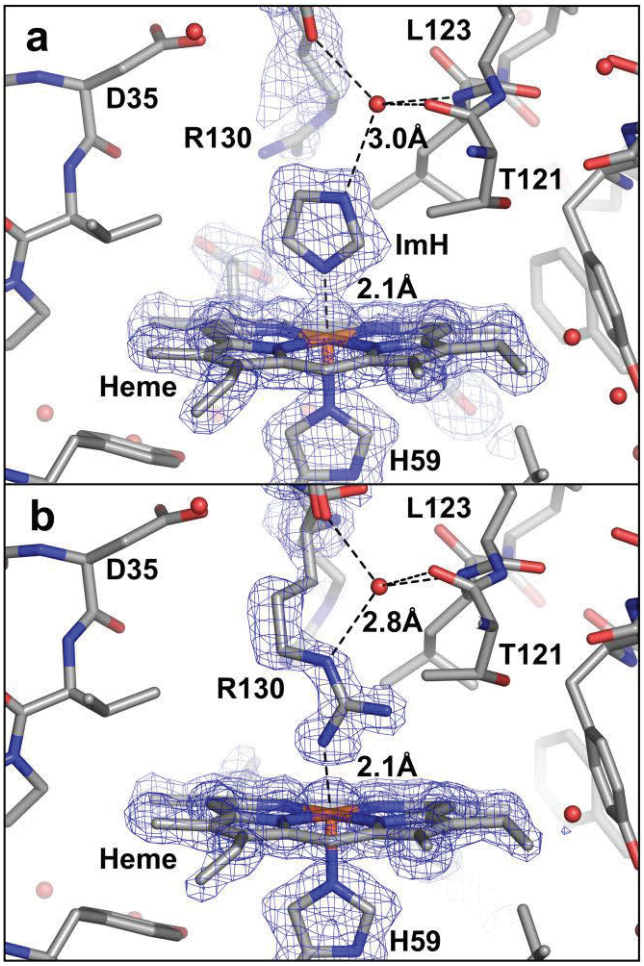

Figure 2. The $2F_o$–F_c electron density map of the heme-pocket of NP4, (a) NP4(L130R)[ImH] and (b) NP4(L130R). The electron density map represented the heme and the residues, His59 and Arg130.

Another aspect for the weakness of guanidine–metal ion complexes is the negligible Lewis basicity.[16c] Among the few metal complexes reported, only those with strong Lewis acidity form complexes, among which is Fe^{II} but not Fe^{III}.[16b] Therefore, to determine whether Fe^{II} might be the coordinating entity in

NP4(L130R) crystals, X-ray irradiation of NP4(L130R) crystals was performed under the inspection of UV/vis absorption using a microspectrophotometer attached to the beam line.[20] The initial absorbance spectrum of the crystal is depicted in Figure 3. It should be noted at this point that in NP crystals grown in ammonium phosphate NH_3 appears as a distal iron ligand. Although this has been previously proposed,[1,4,10,21] it was never shown experimentally. Here we show that the absorbance spectrum of the crystal resembles that of a LS complex which is indicated by the two intense Q-bands. For comparison, an absorbance spectrum in 2 M NH_4OAc was recorded and is presented in the inset in Figure 1. Also, the cw-EPR spectrum of this sample revealed a LS species indicated by a highly anisotropic low-spin (HALS) signal with g_{max} = 3.3 (Figure 1).

The crystals were then irradiated by a low intensity X-ray beam (12.4 keV, 3.5 × 10^{10} photons s^{-1}) and spectra were sampled continuously over a period of 5 min to a total dose of 0.45 MGy (Figure S6A). The kinetic trace in Figure S6B shows that the photon reduction of the crystal is accomplished to 50% within the first 0.2 MGy while apparently a novel LS species is formed as can be judged from the two sharp Q-bands in Figure 3. The total dose applied during the collection of the dataset that was used for the solution of the molecular structure of NP4(L130R) (Figure 2) was ~7-fold higher than the total dose for the spectral kinetic. Therefore, the structure represents the ferroheme state, i.e., NP4(L130R)[Fe^{II}–N^{ω}_{R130}].

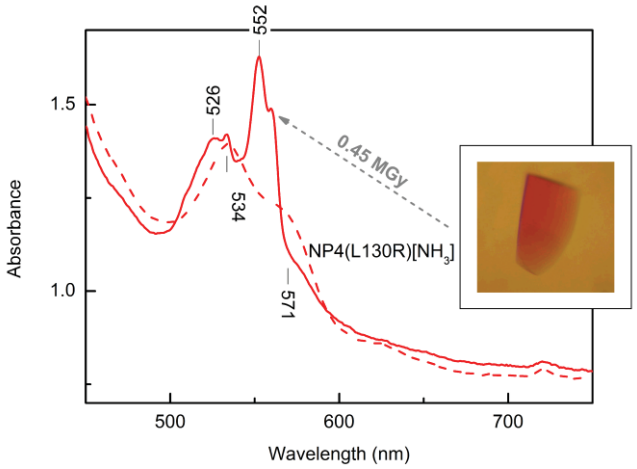

Figure 3. Absorbance spectrum of a crystal of NP4(L130R) grown in 3.2 M ammonium phosphate (pH 7.4) before (*dashed line*) and after (*continuous line*) X-ray irradiation.

However, at room temperature, the absorbance spectrum of ferroheme NP4(L130R) generated by the careful chemical reduction with $Na_2S_2O_4$, which is displayed in the inset in Figure 4, is not different from *wt* NP4[Fe^{II}].[1,22] The high-frequency region (1200 to 1700 cm^{-1}) of the Soret band excited RR spectrum has a high diagnostic potential toward the coordination and spin state of heme proteins.[23] The RR spectrum of NP4(L130R) recorded at room temperature is identical to those of *wt* NP4[Fe^{II}] (Figure 4). Thus, the so-called oxidation state marker band ν_4 is well in the range of ferrohemes (1350 to 1375 cm^{-1})[23-24] where the so-called coordination state marker band ν_3 is sensitive to the heme core size, which changes with the spin state of the iron in dependence of the oxidation state, i.e., 1460 to 1470 cm^{-1} for a 5cHS Fe^{II} and 1490 to 1510 cm^{-1} for a 5cLS or 6cLS Fe^{II}.[24-25] Thus, *wt* NP4 can be assigned to the expected 5cHS Fe^{II} complex as is also the case for NP4(L130R). However, repetition of the RR spectral recording in a frozen solution, i.e., at 77 K, reveals a significant change in case of NP4(L130R) with both ν_4 and ν_3 that indicates, in agreement with the absorbance spectrum of the frozen crystal, the presence of a LS species (Figure 4). Upon measurement of the RR spectrum at 77 K the sample was thawed and subjected to absorbance spectroscopy at room temperature, which revealed the HS spectrum. Thus, the process is fully reversible. As expected, the coordination and spin state in case of *wt* NP4[Fe^{II}] do not depend on temperature (Figure 4).

Scheme 1 summarizes the findings reported herein. The coordination of of Arg130:N^{ω} to the heme iron is highly dependent on the iron oxidation state, i.e., Fe^{II}, and on the temperature. Where the first effect can be explained with the higher Lewis acidity of Fe^{II} compared to Fe^{III}, the reason of the temperature dependence is less obvious. The concomitant appearance of Arg130:N^{ω} coordination in crystal state and in frozen solution rules out a crystallographic artifact due to structural deformation during crystal growth. Another option may be the change in the pK_a of Arg130 and/or the change of the pH of the solution both of which are temperature dependent parameters, where in principle the pH is not defined in the frozen solution. On the other hand, influence of temperature on the coordination and spin state is sometimes observed. For example, in case of NP1[FeNO][7] ($S = {}^1/_2$) a mixture of 5c and 6c complexed is observed in EPR spectroscopy at very low temperature (4.2 K) which is not observed at room temperature in absorbance spectroscopy.[26] Furthermore, RR spectroscopy of NP1[Fe^{III}] at 298 K suggests 6cHS, i.e., water-on, where at 77 K spectroscopic features indicating 6cLS are dominant.[27]

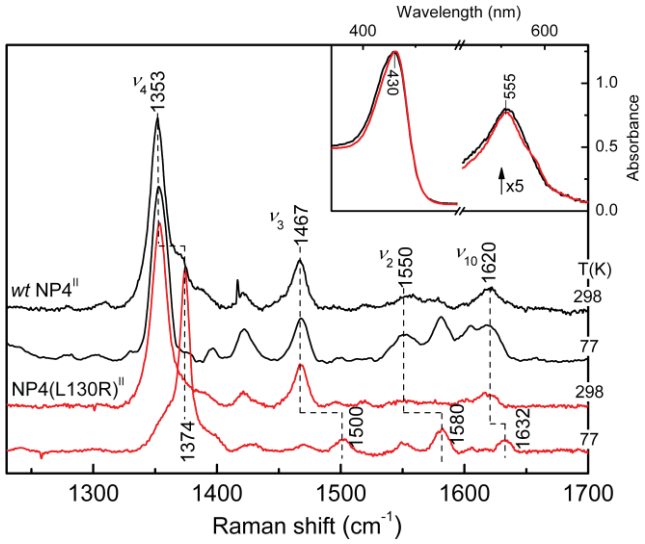

Figure 4. High-frequency resonance Raman spectra of *wt* NP4 (*black*) and NP4(L130R) (*red*) in 100 mM HEPES/NaOH (pH 7.2) at ambient temperature and at 77 K (λ_{ex} = 413.1 nm). Inset: absorbance spectra of *wt* NP4[Fe^{II}] and NP4(L130R)[Fe^{II}] in 100 mM HEPES/NaOH (pH 7.2) at ambient temperature.

A number of heme proteins, though, contain an Arg residue in the distal heme pocket site and a selection of those of which an X-ray structure is available and that have a meaningful Arg:N–Fe distance is presented in Table S2. However, NP4(L130R)

remains the only case in which formation of the Arg:N^{ω}–Fe bond occurs. Figure 2b shows that a water molecule is in H-bonding distance to Arg130:N^{δ}(H) and three other backbone atoms, thus, stabilizing the presented conformation of Arg. As can be seen form Figure 2a this water is also present in NP4(L130R)[ImH] coordinated to the N^{1}(H) of ImH. This water is generally stabilized since it is also found in the structures of *wt* NP4[ImH] (PDB code 1IKJ) and of *wt* NP4[histamine] (PDB code 1IKE).[15] The orientation of the guanidine plane toward the heme plane is very similar to the orientation of ImH and histamine in the NP4 structures and the bond distances and angels are comparable (see Table S3), which is another indicator for the imine N^{ω} coordination mode of Arg130 similar to the imine N^{3} coordination of the imidazoles.

Scheme 1. Tentative Reaction Scheme of the Binding of the Internal Arg130 Guanidine to the Ferroheme Iron in NP4(L130R).[a]

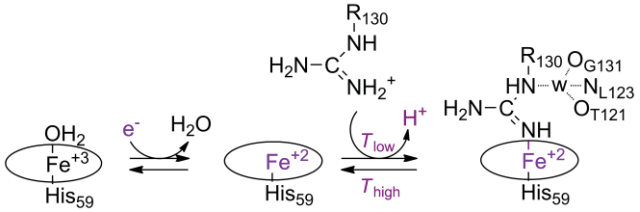

[a] w = water oxygen.

In conclusion, although NP4(L130R) is a non-native protein variant, this study shows that the rare case of an iron porphyrin–guanidine bond is principally possible. In NP4(L130R), the weak coordination is accomplished by the additional stabilization of Arg through a water molecule. However, stabilization was also achieved through low temperature conditions and by increase of Lewis acidity through reduction of the iron, which suggests that also in the case of, e.g., BioB crystal structure, X-ray photoreduction may have occurred.

ASSOCIATED CONTENT

Supporting Information. Material and methods; Table S1: crystallographic refinement parameters; Table S2: comparison of bond parameters; Table S3: summary of protein structures with Arg in the distal heme pocket; Figures S1: absorbance spectra of NP4(L130R) and NP4 with and without ImH; Figures S2: RR spectra of NP4, NP4(L130R), and NP4(L130R)[ImH]; Figure S3: comparison of the crystal structures of NP4(L130R) and NP4; Figure S4: comparison of the crystal structures of NP4(L130R)[ImH] and NP4[ImH]; Figure S5; analysis of heme plane distortions; Figure S6: kinetics of the absorbance detected photoreduction of an NP4(L130R) crystal. This material is available free of charge via the Internet at http://pubs.acs.org/.

AUTHOR INFORMATION

Corresponding Authors

mknipp@mpi-muelheim.mpg.de
ogata@mpi-muelheim.mpg.de

ACKNOWLEDGMENT

We are grateful for the technical assistance of Yvonne Brandenburger, Jan Hanis, Robyn L. Kosinsky, Alina Steinbach, and Johanna J. Taing at our institute. We thank Koji Nikishikawa (MPI Mülheim) and the staff of beamline BL14.2 at BESSYII (Berlin) as well as Florian Dworkowski and Guillaume Pompidor of the Spectrolab facility at beamline X10SA of the Swiss Light Source at the Paul Scherrer Institute, Villigen (Switzerland) for their assistance during the data collection. Further, we thank F. Ann Walker (Department of Chemistry and Biochemistry, University of Arizona, Tucson, AZ) for the gift of the NP4 expression plasmid. This work was financially supported by the Max Planck Society (MPG) and by the Deutsche Forschungsgemeinschaft (DFG), Grant KN 951-1/1 and 2 (to M.K.).

REFERENCES

(1) Maes, E. M.; Roberts, S. A.; Weichsel, A.; Montfort, W. R. *Biochemistry* **2005**, *44*, 12690-12699.

(2) (a) Walker, F. A. *J. Inorg. Biochem.* **2005**, *99*, 216-236; (b) Knipp, M.; He, C. *IUBMB Life* **2011**, *63*, 304-312.

(3) The purpose for this experiment is described in the subsequent paper.

(4) Maes, E. M.; Weichsel, A.; Andersen, J. F.; Shepley, D.; Montfort, W. R. *Biochemistry* **2004**, *43*, 6679-6690.

(5) In contrast, two other spatially close distal pocket Leu residues, Leu123 and Leu133, were demonstrated to have a major impact on the heme ruffling and, thus, reduction potential. Shokhireva et al PNAS.

(6) He, C.; Ogata, H.; Knipp, M. *Biochemistry* **2010**, *49*, 5841-5851.

(7) Fittipaldi, M.; Carcía-Rubio, I.; Trandafir, F.; Gromov, I.; Schweiger, A.; Bouwen, A.; Van Doorslaer, S. *J. Phys. Chem. B* **2008**, *112*, 3859-3870.

(8) This was determined by pH titration experiments and is in preparation for publication (C. He and M. Knipp). It was already shown for NP2 and NP3 that the pKa values of the liagnd-water is relatively low, i.e., ~10.1 and ~9.2, respectively. Shokhireva, T. Kh.; Berry, R. E.; Zhang, H.; Shokhirev, N. V.; Walker, F. A. Inorg. Chim. Acta 2008, 361, 925-940.

(9) (a) Walker, F. A. *Chem. Rev.* **2004**, *104*, 589-615; (b) Walker, F. A. *Coord. Chem. Rev.* **1999**, *185-186*, 471-534.

(10) Schmidt, M.; Achterhold, K.; Prusakov, V.; Parak, F. G. *Eur. Biophys. J.* **2009**, *38*, 687-700.

(11) The structural coordinates were deposited in the Brookhaven Protein Database with the designations 3TGA for NP4(L130R) and 3TGB for NP4(L130R)[ImH], respectively.

(12) Berry, R. E.; Ding, X. D.; Shokhireva, T. K.; Weichsel, A.; Montfort, W. R.; Walker, F. A. *J. Biol. Inorg. Chem.* **2004**, *9*, 135-144.

(13) Shokhireva, T. K.; Shokhirev, N. V.; Walker, F. A. *Biochemistry* **2003**, *42*, 679-693.

(14) Knipp, M.; Yang, F.; Berry, R. E.; Zhang, H.; Shokhirev, M. N.; Walker, F. A. *Biochemistry* **2007**, *46*, 13254-13268.

(15) Roberts, S. A.; Weichsel, A.; Qiu, Y.; Shelnutt, J. A.; Walker, F. A.; Montfort, W. R. *Biochemistry* **2001**, *40*, 11327-11337.

(16) (a) Ratilla, E. M. A.; Kostić, N. M. *J. Am. Chem. Soc.* **1988**, *110*, 4427-4428; (b) Wittmann, H.; Raab, V.; Schorm, A.; Planckmeyer, J.; Sundermeyer, J. *Eur. J. Inorg. Chem.* **2001**, 1937-1948; (c) Bailey, P. J.; Pace, S. *Coord. Chem. Rev.* **2001**, *214*; (d) Di Costanzo, L.; Flores Jr., L. V.; Christianson, D. W. *PROTEINS: Struct. Func. Gen.* **2006**, *65*, 637-642; (e) Fuchs, M. G. G.; Meyer, F.; Ryde, U. *J. Biol. Inorg. Chem.* **2010**, *15*, 203-212.

(17) Bewley, M. C.; Jaffrey, P. D.; Patchett, M. L.; Kanyo, Z. F.; Baker, E. N. *Structure* **1999**, *7*, 435-448.

(18) Ferraroni, M.; Tilli, S.; Briganti, F.; Chegwidden, W. R.; Supuran, C. T.; Wiebauer, K. E.; Tashian, R. E.; Scozzafava, A. *Biochemistry* **2002**, *41*, 6237-6244.

(19) (a) Broach, R. B.; Jarrett, J. T. *Biochemistry* **2006**, *45*, 14166-14174; (b) Berkovitch, F.; Nicolet, Y.; Wan, J. T.; Jarrett, J. T.; Drennan, C. L. *Science* **2004**, *303*, 76-79.

(20) Owen, R. L.; Pearson, A. R.; Meents, A.; Boehler, P.; Thominet, V.; Schulze-Briese, C. *J. Synchrotron Rad.* **2009**, *16*, 173-182.

(21) Kondrashov, D. A.; Roberts, S. A.; Weichsel, A.; Montfort, W. R. *Biochemistry* **2004**, *43*, 13637-13647.

(22) Knipp, M.; Taing, J. J.; He, C. *J. Inorg. Biochem.* **2011**, *doi: 10.1016/j.jinorgbio.2011.07.009*.

(23) (a) Spiro, T. G.; Czernuszewicz, R. S. In *Physical Methods in Bioinorganic Chemistry - Spectroscopy and Magnetism*; 1st ed.; Que Jr., L., Ed.; University Science Books: Sausalito (CA), 2000, p 59-119; (b) Kincaid, J. R.

In *The Porphyrin Handbook*; 1st ed.; Kadish, K. M., Smith, K. M., Guilard, R., Eds.; Academic Press (CA): San Diego, 2000; Vol. 7, p 225-291; (c) Spiro, T. G.; Li, X.-Y. In *Resonance Raman Spectra of Heme and Metalloproteins*; 1st ed.; Spiro, T. G., Ed.; John Wiley & Sons: New York (USA), 1988, p 1-38.

(24) (a) Andersson, L. A.; Mylrajan, M.; Sullivan, E. P., Jr.; Strauss, S. H. *J. Biol. Chem.* **1989**, *264*, 19099-19102; (b) Kitagawa, T.; Kyogoku, Y.; Iizuka, T.; Saito, M. I. *J. Am. Chem. Soc.* **1976**, *98*, 5169-5173.

(25) Spiro, T. G.; Stong, J. D.; Stein, P. *J. Am. Chem. Soc.* **1979**, *101*, 2648-2655.

(26) Ding, X. D.; Weichsel, A.; Andersen, J. F.; Shokhireva, T. K.; Balfour, C.; Pierik, A. J.; Averill, B. A.; Montfort, W. R.; Walker, F. A. *J. Am. Chem. Soc.* **1999**, *121*, 128-138.

(27) Maes, E. M.; Walker, F. A.; Montfort, W. R.; Czernuszewicz, R. S. *J. Am. Chem. Soc.* **2001**, *123*, 1164-1172.

Guanidine–Iron Coordination in a Heme Protein: Crystallographic and Spectroscopic Characterization of the L130R Mutant of Nitrophorin 4 from Rhodnius prolixus

Chunmao He[†], Martin R. Fuchs[‡], Hideaki Ogata[*,†], and Markus Knipp[*,†]

[†] Max-Planck-Institut für Bioanorganische Chemie, Stiftstrasse 34-36, D-45470 Mülheim an der Ruhr, Germany.

[‡] *Swiss Light Source, Paul-Scherrer-Institut, CH-5232 Villigen, Switzerland.*

– Supporting Information –

[*] Address correspondence to:
Dr. Hideaki Ogata
Max-Planck-Institut für Bioanorganische Chemie
Stiftstrasse 34-36
D-45470 Mülheim an der Ruhr
Germany
Tel.: +49 (0)208-306-3508
Fax: + 49 (0)208-306-3951
ogata@mpi-muelheim.mpg.de

Dr. Markus Knipp
Max-Planck-Institut für Bioanorganische Chemie
Stiftstrasse 34-36
D-45470 Mülheim an der Ruhr
Germany
Tel.: +49 (0)208-306-3671
Fax: + 49 (0)208-306-3951
mknipp@mpi-muelheim.mpg.de

Abbreviations Used:

BioB, biotine synthase; Cld, chlorite dismutase; HALS, highly anisotropic low-spin; HEPES, 2-(4-(2-hydroxyethyl)-1-piperazinyl)-ethanesulfonic acid; HS, high-spin; ImH, imidazole; LS, low-spin; Mb, myoglobin; metMb, ferriheme myoglobin; MOPS, 3-(*N*-mopholino)-propanesulfonic acid; NP, nitrophorin; PDB, Brookhaven Protein Data Bank; RMSD, root mean square deviation; RR, resonance Raman; SHE, standard hydrogen electrode; *wt*, wild-type.

Materials and Methods

Protein expression and Purification

For the expression of the mutant protein NP4(L130R), a plasmid pNP4(L130R)^{Kan} was generated by the quick change mutagenesis method[1] using the *wt* NP4 expression plasmid as a template[2] with *Pfu* DNA polymerase (Stratagene). The following pair of primers was used: 5'-TTG CAT AAA GGA AAC AAG GAC CGT GGA GAT CTC TAC GCT GTA TTA-3' and 5'-TAA TAC AGC GTA GAG ATC TCC ACG GTC CTT GTT TCC TTT ATG CAA-3' (the sites of mutation are underlined). The correctness of the coding regions of the expression plasmid was confirmed through commercial DNA sequencing.

NP4(L130R) was recombinantly expressed in *Escherichia coli* strain BL21(DE3) (Novagen) and reconstituted as was previously described for *wt* NP4.[3] Protein preparations were routinely analyzed by SDS-PAGE to be >90% pure. The proteins were subjected to MALDI-TOF MS to confirm the correct molecular masses accounting for two Cys–Cys disulfides (calculated for $[NP4(L130R) + H]^+$: 20,307 Da, observed: 20,310 Da. Protein concentrations were determined photometrically using $\epsilon_{404\ nm}$ = 141,000 M^{-1} cm^{-1}.[4] Proteins were kept frozen until using.

Crystallization and Data Collection

Protein crystals were obtained by the vapor-diffusion method with 3.2 M ammonium phosphate (pH 7.4) as precipitant.[4-5] The crystals were soaked in 3.2 M potassium phosphate (pH 7.4) with 15 % glycerol as a cryo protectant. Afterwards, the crystals were immediately frozen in liquid N_2 until the measurement. For the preparation of the imidazole (ImH) complex, crystals were soaked in 3.2 M potassium phosphate (pH 7.4) containing 10 mM ImH prior to incubation in the cryo protectant. The diffraction data sets was collected at 100 K using the beamline BL14.2 at BESSYII (Berlin, Germany). Combined diffraction and UV/vis absorption measurements with an on-axis *in situ*-microspectrophotometer[6] were performed at beamline X10SA of the Swiss Light Source at the Paul Scherrer Institute (PSI Villigen, Switzerland). Dose calculation was performed with the program RADDOSE.[7]

Structure Determination and Refinement

The data sets were processed with XDS[8] and CCP4.[9] The molecular-replacement method was using MOLREP[9] applied to determine the phases using an initial model from NP4 (PDB code 3MVF).[10] The model building and the refinement were carried out using WINCOOT[11] and PHENIX,[12] respectively. Data collection and refinement statistics were summarized in Table S1. The stereochemical properties were checked by RAMPAGE.[13]

cw-EPR Spectroscopy

The solvent of the protein was exchanged to 100 mM HEPES/NaOH (pH 7.2), 25% glycerol and the protein concentration was adjusted to ~100 µM. The samples were transferred into a 3 mm quartz tube and then frozen in liquid N_2 where they were kept until measurement. cw-EPR spectra were recorded on a Bruker ESP-380E X-band spec-

trometer equipped with a gas-flow cryogenic system with a liquid He cryostat from Oxford Inc. Spectra were recorded at 10 K with a microwave power of 2 mW, a field modulation of 100 kHz, and a modulation amplitude of 5 G.

Resonance Raman Spectroscopy

The solvent of the proteins was exchanged to 100 mM HEPES/NaOH (pH 7.2) and the concentration was adjusted to ~10 µM. The samples were transferred to a 3 mL-circular quartz cuvette. Resonance Raman (RR) spectra were recorded with a scanning double monochromatic. The excitation line at 413.1 nm was provided by a coherent K-2 Kr^+ ion laser with a light power of ~30 mW. During the measurement, the sample was rotated with a frequency of ~10 Hz. For measurements in frozen solution, samples of ~50 µM were filled into 3 mm quartz tubes and kept in a quartz Dewar filled with liquid N_2 during the measurement.

Supplementary Tables

Table S1. Data Collection and Refinement Statistics of the Native Data Sets. Numbers in Parenthesis Represent the Values for the Highest Resolution Shell.

	NP4(L130R)	NP4(L130R)[ImH]	NP4(L130R)
PDB	3TGA	3TGB	
Data collection			
Beamline	BESSYII BL14.2	BESSYII BL14.2	SLS PXII
Wavelength (Å)	0.91841	0.91841	1.00000
Space group	*C*2	*C*2	*C*2
Unit-cell parameters			
a (Å)	69.89	69.72	69.46
b (Å)	43.06	43.06	42.84
c (Å)	52.59	52.47	52.27
β (°)	94.36	94.43	94.07
Resolution (Å)	30.61-1.30 (1.33-1.30)	21.72-1.35 (1.39-1.35)	36.44- 1.57 (1.61 – 1.57)
No. of observed reflections	141289	126176	138816
No. of unique reflections	38430	34144	21348
R_{merge}	0.035 (0.312)	0.038 (0.351)	0.033 (0.267)
Completeness (%)	99.8 (99.9)	99.8 (99.9)	99.6 (95.6)
$\langle I/\sigma(I) \rangle$	21.1 (4.2)	19.6 (3.8)	30.8 (5.5)
Refinement			
Resolution range (Å)	30.6-1.3	21.7-1.35	36.44-1.57
R (%)	14.5	14.3	16.9
R_{free} (%)	17.2	18.6	19.6
No. of the residues	184	184	184
No. of solvent molecules	177	189	165
No. of imidazole	-	1	-
Rmsd bond lengths (Å)	0.007	0.007	0.007
Rmsd angles (°)	1.12	1.10	1.20
Ramachandran plot			
favoured region (%)	98.48	98.55	98.48
allowed region (%)	1.52	1.45	1.52
outlier region (%)	0	0	0
Average B-factors (Å^2)			
protein	14.6	15.5	20.2
ligand (Heme)	15.2	15.9	23.4
ligand (imidazole)	-	12.5	-
solvent	26.6	29.6	26.5

Table S2. Comparison of the bond parameters in crystal structures of *wt* NP4 and NP4(L130R)

NP complex	$Fe \leftrightarrow N_L$ (Å)[a]	$Fe \leftrightarrow N_{His}$ (Å)	φ_1[b]	φ_2[c]	$\Delta\varphi$[d]	Reference
wt NP4[ImH]	2.02	1.95	6°	-26°	32°	[14]
wt NP4[Hm]	2.04	2.00	2°	-33°	35°	[14]
NP4(L130R)	2.12	2.02	7°	-17°	24°	tw
NP4(L130R)[ImH]	2.05	2.05	5°	-25°	30°	tw

[a] Distance between Fe and the axial ligand.
[b] Dihedral angle between the $C^{meso\text{-}\beta}$-$C^{meso\text{-}\delta}$ axis and the proximal His plane normal.
[c] Dihedral angle between the $C^{meso\text{-}\beta}$-$C^{meso\text{-}\delta}$ axis and the nitrite plane normal.
[d] dihedral angle between nitrite plane normal and His plane normal

Table S3. Summary of Unliganded His Coordinated Heme Protein Structures with Arg in the Distal Heme Pocket.

Protein	PDB code	closest $N_{Arg} \leftrightarrow Fe_{heme}$ distance (Å)
NP4(L130R)	3TGA	2.1 (Arg130:N^{ω})
metMB(H64V,V67R)	3HEN[15]	9.5 (Arg67:N^{ω})
Cld(R183L)	3NN4[16]	5.2 (Lys183:N^{6})[a]
HRP	1H5A[17]	4.6 (Arg38:N^{ω})
HTHP	2OYY[18]	3.9 (Arg26:N^{ω})

[a] An unliganded structure of the *wt* is not available. The quoted structure corresponds to the R183L mutant and the distance refers to the Lys side-chain nitrogen.

Supplementary Figures

Figure S1. Absorbance spectra of *wt* NP4 (*black*), *wt* NP4[ImH] (*green*), NP4(L130R) (*red*), and NP4(L130R)[ImH] (*magenta*) at ambient temperature. Proteins were dissolved in 100 mM HEPES/NaOH (pH 7.2)

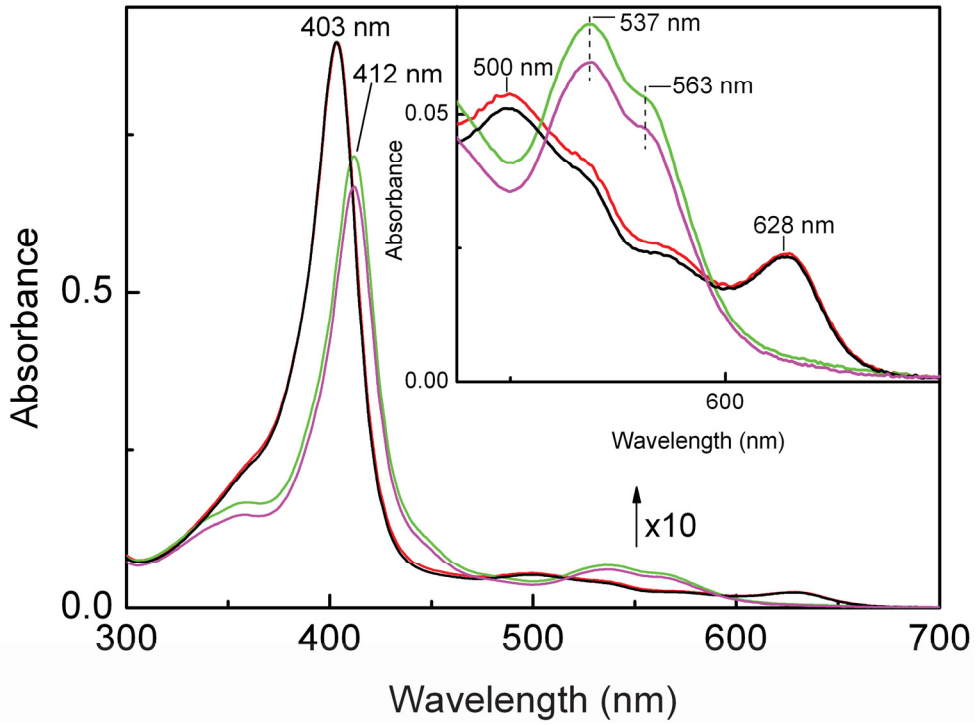

Figure S2. High-frequency resonance Raman spectra of *wt* NP4 (*black*), NP4(L130R) (*red*), and NP4(L130R)[ImH] (*green*) recorded at ambient temperature in 100 mM HEPES/NaOH (pH 7.2). (λ_{ex} = 413.1 nm) As a result, the oxidation state marker bands ν_4 of all forms NP4(L130R)[ImH] are in agreement with Fe^{III} complexes.[19] In contrast, the so-called spin-state marker band ν_3 increases by 31 cm^{-1} upon binding of ImH to NP4(L130R) which reflects the conversion from a HS (1475 to 1485 cm^{-1}) to a LS complex (1500 to 1510 cm^{-1}).[20] Also ν_2 and ν_{10} appear at the respectively typical values for HS (NP4(L130R)) and LS complexes (NP4(L130R)[ImH]).[19a]

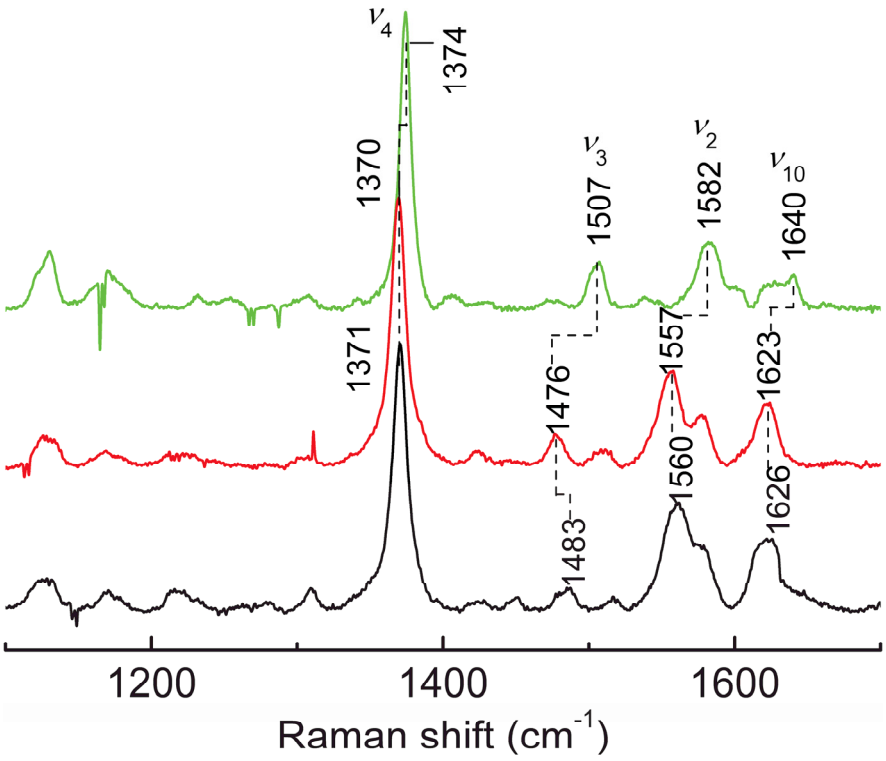

Figure S3. Comparison of the X-ray structures of *wt* NP4 (PDB code 1X8P)[21] and NP4(L130R) (PDB 3TGA; this work). (a) The cartoon representation of *wt* NP4 (*yellow*) and NP4(L130R) (*red*). The two different conformations in the G-H loop of NP4(L130R) are depicted in *red* (R130-Heme bound form) and *blue* (unbound conformation). RMSD of the *wt* NP4 and NP4(L130R) was calculated with the value of 0.49. (b) The enlarged view of the G-H loop region. The heme, His59 and the residues, Leu130 (*wt*) and Arg130 (L130R mutant), are represented by in stick model.

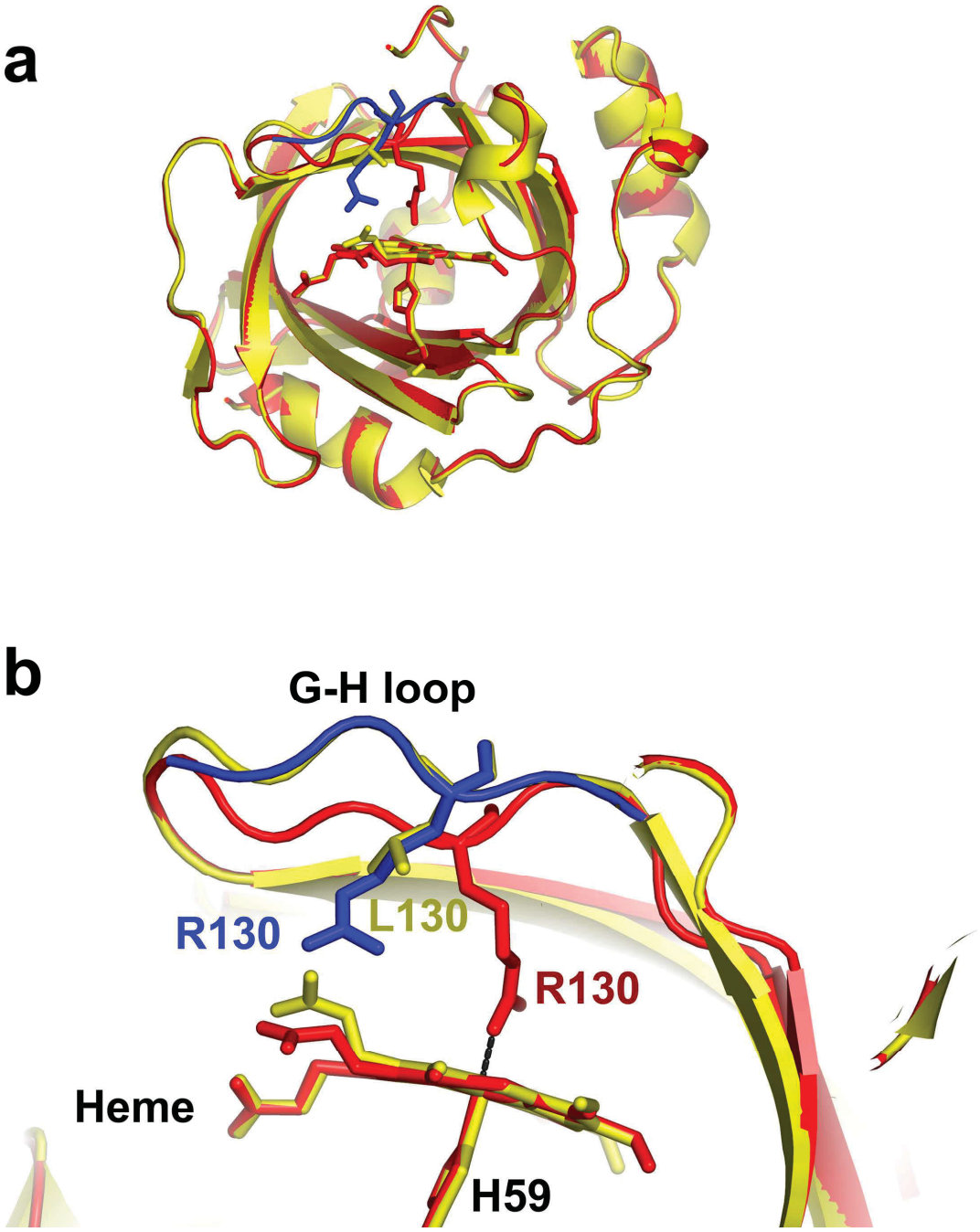

Figure S4. Comparison of the X-ray structures of *wt* NP4[ImH] (PDB code 1IKJ)[14] and NP4(L130R)[ImH] (PDB code 3TGB; this work). (a) The cartoon representation of *wt* NP4[imH] (*yellow*) and NP4(L130R)[ImH] (*red*). The two different conformations in the G-H loop region of the *wt* NP4[ImH] are depicted in *yellow* and *light brown*. RMDS of the *wt* NP4[ImH] and NP4(L130R)[ImH] was calculated with the value of 0.69. (b) The enlarged view of the G-H loop region. The heme, His59 and the residues, Leu130 (*wt*) and Arg130 (L130R mutant), are represented by the stick.

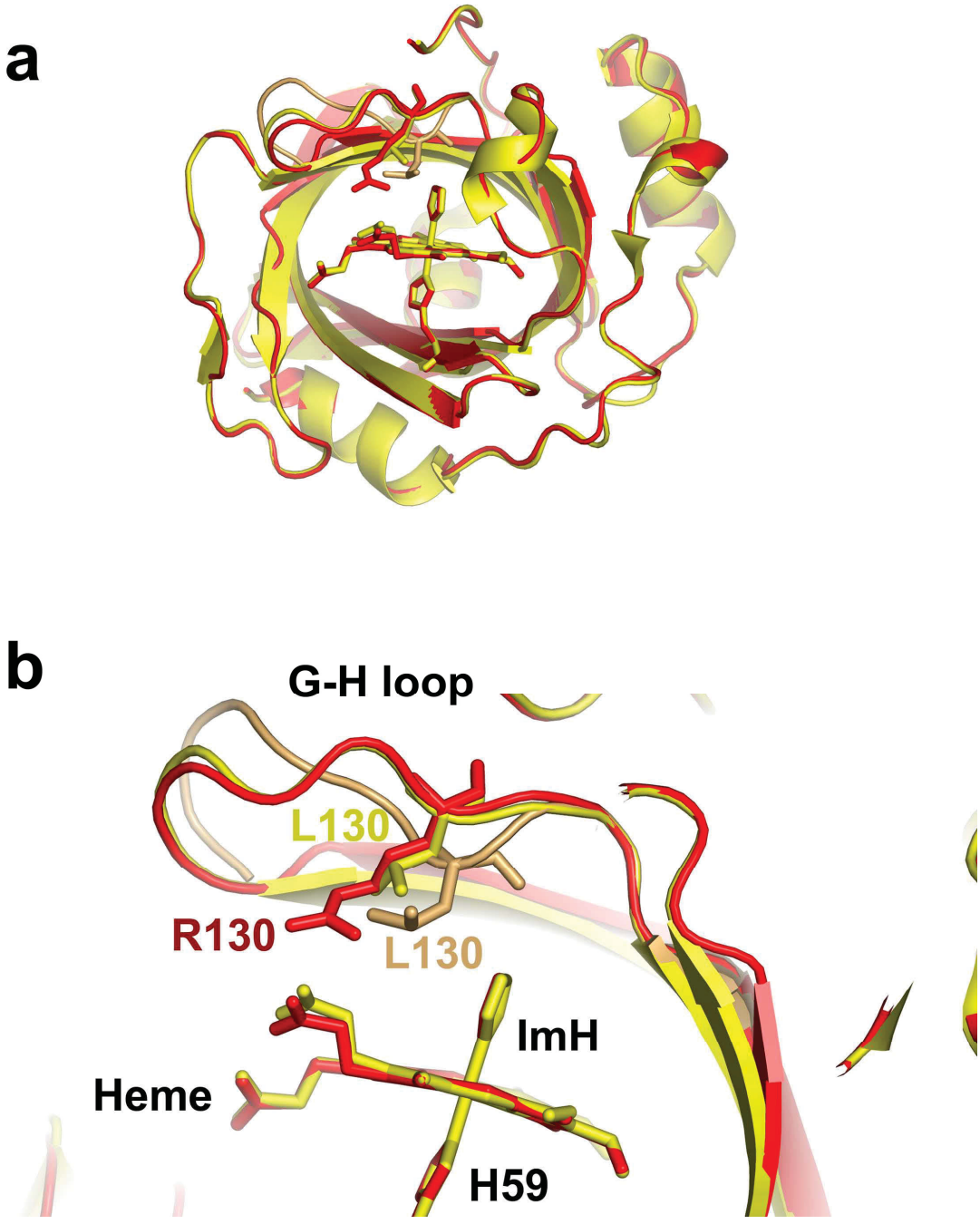

Figure S5. Heme plane distortions were calculated with the program PDBTRANSFORM v3.2 (http://www.shokhirev.com/nikolai/programs/prgsciedu.html). The contour maps demonstrate the degree of distortion with respect to the heme normal plane. The porphyrin is oriented such that the $C^{meso\text{-}\alpha}$ is located at the bottom and the His59 is below the plane. (a) NP4(L130R), (b) *wt* NP4 (PDB code 1X8P), (c) NP4(L130R)[ImH] (d) wt NP4[ImH] (PDB code 1IKJ).

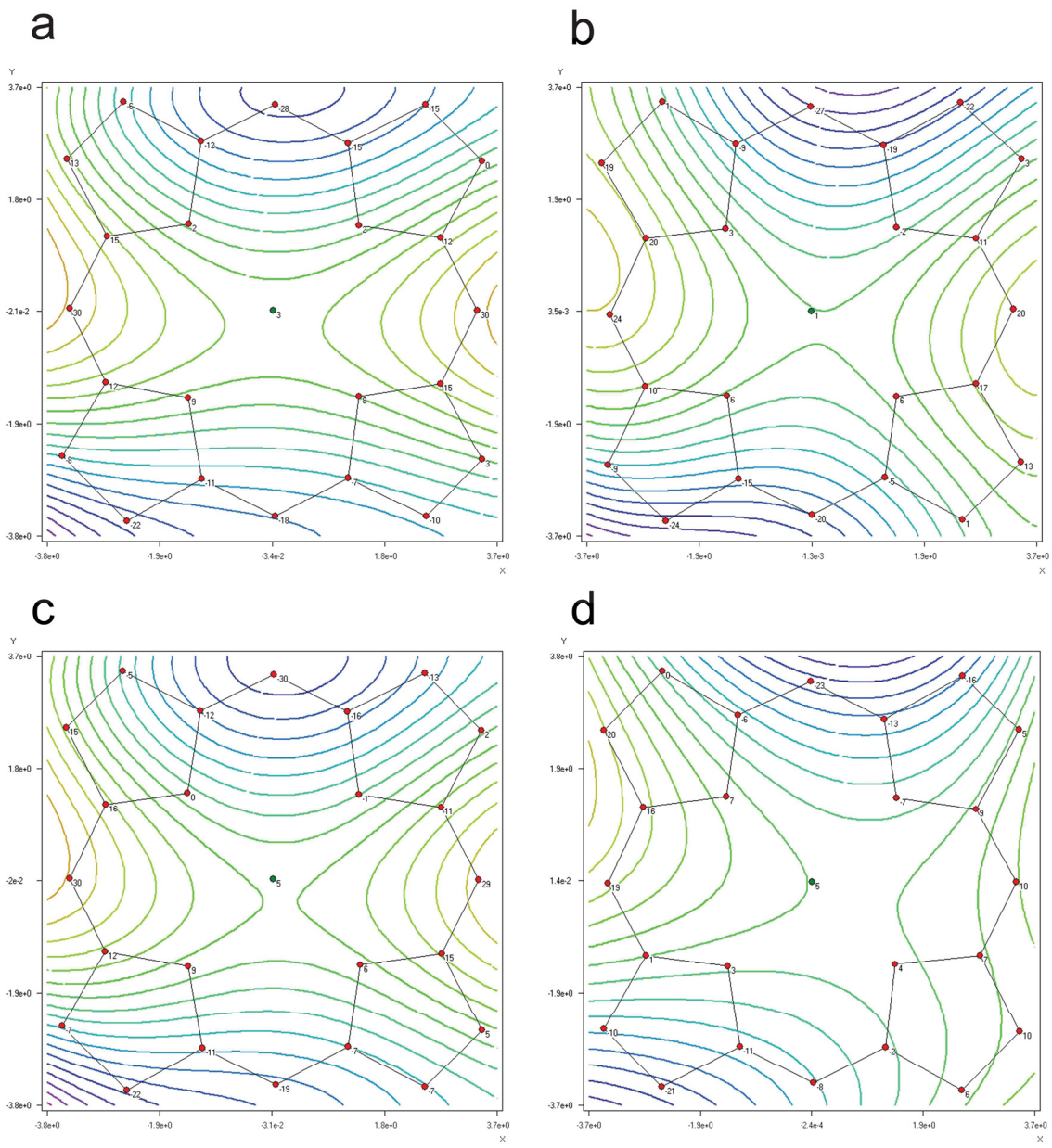

Figure S6. Kinetic of the photo reduction of a NP4(L130R) crystal mounted at beamline X10SA at the PSI. (A) Absorbance spectra were recorded with a microspectrophotometer every 1 s using a diode array detector. A X-ray beam of 12.8 keV was applied to the crystal. (B) The wavelength at 555 nm was plotted *vs.* time.

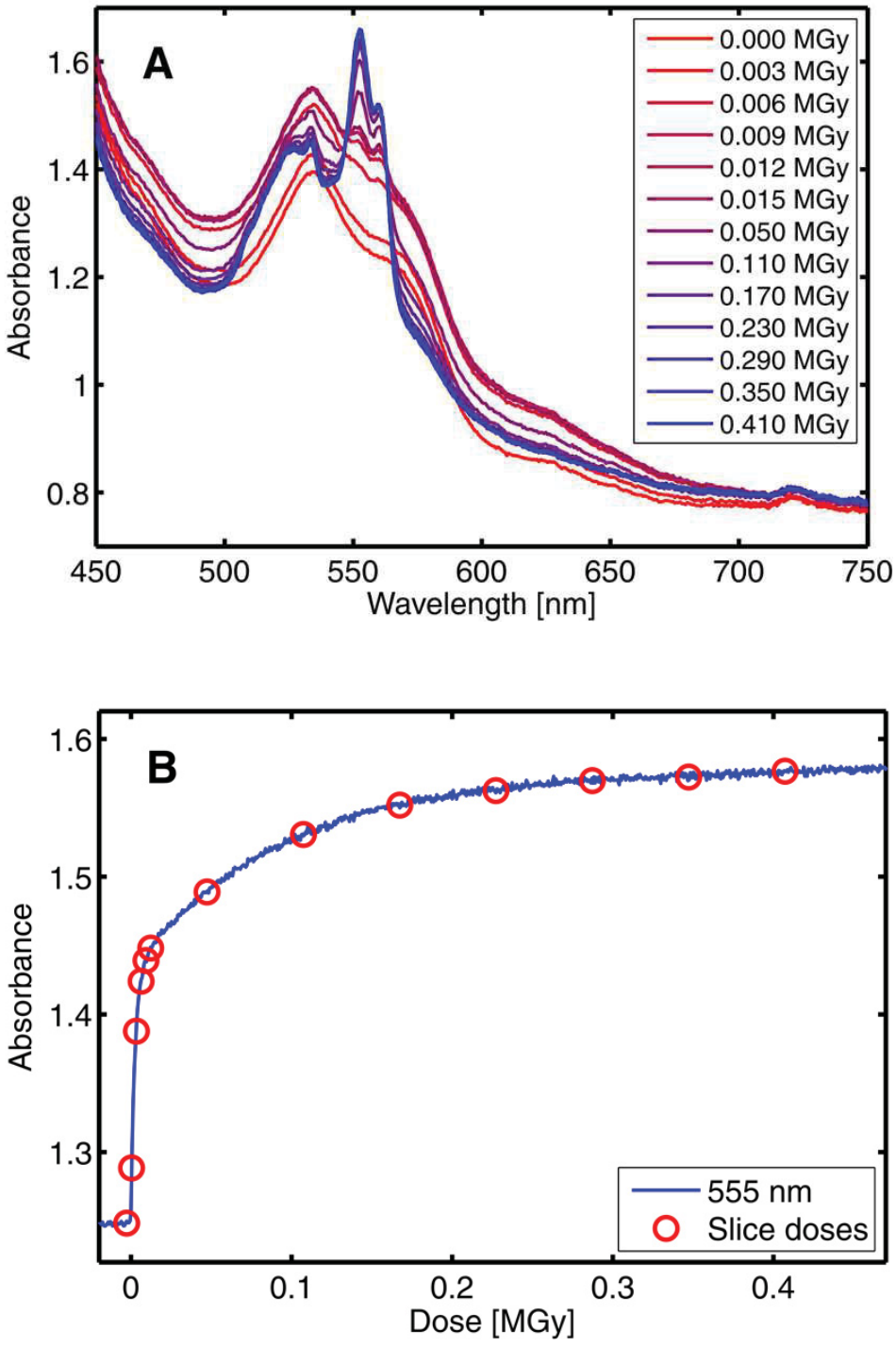

References

(1) Wang, W.; Malcolm, B. A. *BioTechniques* **1999**, *26*, 680-682.
(2) Berry, R. E.; Ding, X. D.; Shokhireva, T. K.; Weichsel, A.; Montfort, W. R.; Walker, F. A. *J. Biol. Inorg. Chem.* **2004**, *9*, 135-144.
(3) Andersen, J. F.; Weichsel, A.; Balfour, C. A.; Champagne, D. E.; Montfort, W. R. *Structure* **1998**, *6*, 1315-1327.
(4) Maes, E. M.; Roberts, S. A.; Weichsel, A.; Montfort, W. R. *Biochemistry* **2005**, *44*, 12690-12699.
(5) (a) Schmidt, M.; Achterhold, K.; Prusakov, V.; Parak, F. G. *Eur. Biophys. J.* **2009**, *38*, 687-700; (b) Maes, E. M.; Weichsel, A.; Andersen, J. F.; Shepley, D.; Montfort, W. R. *Biochemistry* **2004**, *43*, 6679-6690.
(6) Owen, R. L.; Pearson, A. R.; Meents, A.; Boehler, P.; Thominet, V.; Schulze-Briese, C. *J. Synchrotron Rad.* **2009**, *16*, 173-182.
(7) Paithankar, K. S.; Owen, R. L.; Garman, E. F. *J. Synchrotron Rad.* **2009**, *16*, 152-162.
(8) Kabsch, W. *J. Appl. Cryst.* **1993**, *26*, 795-800.
(9) Collaborative Computational Project, N. *Acta Cryst.* **1994**, *D50*, 760-763.
(10) He, C.; Ogata, H.; Knipp, M. *Biochemistry* **2010**, *49*, 5841-5851.
(11) Emsley, P.; Cowtan, K. *Acta Cryst.* **2004**, *D60*, 2126-2132.
(12) Afonine, P. V.; Grosse-Kunstleve, R. W.; Adams, P. D. *CCP4 Newsletter 42* **2005**, *Contribution 8*.
(13) Lovell, S. C.; Davis, I. W.; Arendall III, W. B.; de Bakker, P. I. W.; Word, J. M.; Prisant, M. G.; Richardson, J. S.; Richardson, D. C. *PROTEINS: Struct. Func. Gen.* **2003**, *50*, 437-450.
(14) Roberts, S. A.; Weichsel, A.; Qiu, Y.; Shelnutt, J. A.; Walker, F. A.; Montfort, W. R. *Biochemistry* **2001**, *40*, 11327-11337.
(15) Yi, J.; Heinecke, J.; Tan, H.; Ford, P. C.; Richter-Addo, G. B. *J. Am. Chem. Soc.* **2009**, *131*, 18119-18128.
(16) Kostan, J.; Sjöblom, B.; Maixner, F.; Mlynek, G.; Furtmüller, P. G.; Obinger, C.; Wagner, M.; Daims, H.; Djinović-Carugo, K. *J. Struc. Biol.* **2010**, *172*, 331-342.
(17) Berglund, G. I.; Carlsson, G. H.; Smith, A. T.; Szoke, H.; Henrikson, A.; Hadju, J. *Nature* **2002**, *417*, 463.
(18) Jeoung, J.-H.; Pipping, D. A.; Martins, B. M.; Wagener, N.; Dobbek, H. *J. Mol. Biol.* **2007**, *368*, 1122-1131.
(19) (a) Maes, E. M.; Walker, F. A.; Montfort, W. R.; Czernuszewicz, R. S. *J. Am. Chem. Soc.* **2001**, *123*, 1164-1172; (b) Kincaid, J. R. In *The Porphyrin Handbook*; 1st ed.; Kadish, K. M., Smith, K. M., Guilard, R., Eds.; Academic Press (CA): San Diego, 2000; Vol. 7, p 225-291.
(20) Spiro, T. G.; Stong, J. D.; Stein, P. *J. Am. Chem. Soc.* **1979**, *101*, 2648-2655.
(21) Kondrashov, D. A.; Roberts, S. A.; Weichsel, A.; Montfort, W. R. *Biochemistry* **2004**, *43*, 13637-13647.

Chapter 5. Insertion of an H-bonding residue into the distal pocket of the ferriheme protein nitrophorin 4: Effect on the nitrite-iron coordination and nitrite disproportionation

(He, C.; Ogata, H.; Knipp, M. Submitted)

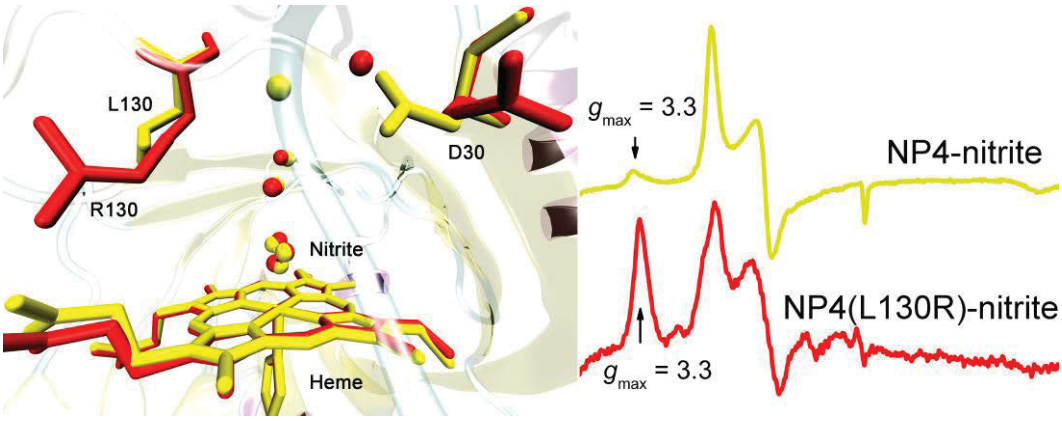

Characterization of the nitrite complex of NP4(L130R)

Abstract

We report on the L130R mutant of the NP isoprotein NP4 that provides the Arg130 residue as a potential H-bonding residue. Importantly, it was previously demonstrated that the structural and electronic properties of this mutant are widely preserved compared to wild-type NP4. This study demonstrates that, in contrast to metMb, the Arg130 residue does not lead to an *O*-bonded nitrite complex as was seen in the X-ray structure. However, spectroscopic investigations show that in solution a second ligand rotational orientation exists, which is in fast exchange equilibrium with the normal, parallel ligand orientation. Moreover, the nitrite disproportionation is inhibited in NP4(L130R). Thus, this study demonstrates that the nitrite binding mode, although dependent on the presence of an H-bonding residue in metMb, is not dictated by such a residue alone. Furthermore, for the nitrite disproportionation to function, a more apolar distal heme site is required.

Insertion of an H-bonding residue into the distal pocket of the ferriheme protein nitrophorin 4: Effect on nitrite–iron coordination and nitrite disproportionation†

Chunmao He, Hideaki Ogata, and Markus Knipp*

Max-Planck-Institut für Bioanorganische Chemie, Stiftstrasse 34-36, D-45470 Mülheim an der Ruhr, Germany

Funding

†This study was financially supported by the Max Planck Society (MPG) and the Deutsche Forschungsgemeinschaft (DFG), Grants KN 951/1-1 and 2 (to M.K.).

***Corresponding Author**

Phone: +49 (0)208 306 3671; Fax: +40 (0)208 306 3951; E-mail: mknipp@mpi-muelheim.mpg.de.

Abbreviations

*cc*NiR, cytochrome *c* nitrite reductase; cd_1NiR, heme cd_1 nitrite reductase; Cld, chlorite dismutase; cw, continuous wave; HALS, highly anisotropic low-spin; Hb, hemoglobin; HEPES, 2-(4-(2-hydroxyethyl)-1-piperazinyl)-ethanesulfonic acid; HS, high-spin; ImH, imidazole; LS, low-spin; MALDI, matrix assisted laser desorption/ionization; Mb, myoglobin; metHb, ferriheme hemoglobin; metMb, ferriheme myoglobin; MOPS, 3-(*N*-mopholino)-propanesulfonic acid; NP, nitrophorin; PDB, Brookhaven Protein Data Bank; pH*, pH was adjusted in proton solution and later not corrected for the deuterium effect; RMSD, root mean square deviation; SHE, standard hydrogen electrode; SiHRP, sulfite reductase; TOF, time-of-flight; TpivPP, tetrakis($\alpha,\alpha,\alpha,\alpha$-*o*-pivalamidophenyl)-porphyrinato dianion; *wt*, wild-type.

ABSTRACT: Heme proteins are important entities for the metabolism of nitrite. At least two different types of reactions occur at ferriheme centers. In the case of met-myoglobin (metMb), which catalyzes the nitrite anhydrase reaction, the presence of an H-bonding base residue in the distal pocket was found to be essential for the unusual *O*-binding interaction of nitrite at the heme center. In nitrophorins (NPs), which in contrast bind nitrite in the *N*-binding mode and catalyze the nitrite disproportionation reaction, such residue is missing. Here we report on the L130R mutant of the NP isoprotein NP4 that provides the Arg130 residue as a potential H-bonding residue. Importantly, it was previously demonstrated that the structural and electronic properties of this mutant are widely preserved compared to wild-type NP4. This study demonstrates that, in contrast to metMb, the Arg130 residue does not lead to an *O*-bonded nitrite complex as was seen in the X-ray structure. However, spectroscopic investigations show that in solution a second ligand rotational orientation exists, which is in fast exchange equilibrium with the normal, parallel ligand orientation. Moreover, the nitrite disproportionation is inhibited in NP4(L130R). Thus, this study demonstrates that the nitrite binding mode, although dependent on the presence of an H-bonding residue in metMb, is not dictated by such a residue alone. Furthermore, for the nitrite disproportionation to function, a more apolar distal heme site is required.

Characterization of the nitrite complex of NP4(L130R)

The reduction of NO_2^- by the heme proteins nitrite reductases (heme NiR) is an important step in bacterial metabolism, in which NO_2^- reduction to NO (*cd*$_1$NiR) or NH_3 (multiheme NiR or *cc*NiR) occurs at a catalytic heme center from the Fe^{II} state, where (an) electron(s) are/is provided from (a) secondary heme center(s).[1] Recently, NO_2^- reduction was also considered an important source for NO in mammals,[2] where Mb and Hb are suggested important catalysts of this process. However, the simple reduction from the globins' ferroheme state[3] raises concerns about the feasibility *in vivo*. Therefore, a novel nitrite anhydrase reaction from metHb/Mb was proposed for which the presence of substoichiometric amounts of NO are required.[3, 4] Independently, we have recently reported about a novel type of "only nitrite" reaction at the ferriheme center of nitrophorins (NPs), i.e., the nitrite disproportionation reaction represented in Scheme 1.[5-7]

At present, it is not clear which features of a heme pocket determine the type of reaction. To understand the mechanism of the reaction of ferrihemes with NO_2^-, studies of the initial complexes were conducted with proteins and model hemes. It appeared that in the majority of cases that were structurally characterized the η^1-N bonding "nitro" mode is formed (see Chart 1).[8, 9] (The examples that we are aware of are: *cc*NiR from *W. succinogenes*;[10] *cd*$_1$NiR from *T. pantotropha*;[11] SiHRP from *Escherichia coli*;[12] the model compounds [Fe(TpivPP)(NO_2)(ImH)] and [Fe(TpivPP)(NO_2)(py)].[13]) It was, therefore, surprising that in the crystal structures of the NO_2^- adducts of human metHb and horse metMb both the η^1-O bonding "nitrito" mode appeared (see Chart 1).[14, 15] Recently, it was demonstrated that the distal H-bonding His64 in metMb dictates the O-bonding mode.[16] Consequently, the mutation His64→Val led to an N-oriented interaction with the Fe^{III}. (The long Fe–N distance of 2.6 Å indicates the absence of a bond.) Conversely, the reinsertion of another H-bonding residue into the double mutant metMb(H64V,V67R) restores the O-bonding nitrito mode. A recent X-ray structure of the

NO_2^- adduct of chlorite dismutase (Cld) from *D. aromatica* also revealed a η^1-O-bonding mode. Remarkably, this protein exhibits a native Arg183 residue in the distal heme pocket in H-bonding distance to the NO_2^- ligand.[17]

In the case of NP4 and NP7, it was demonstrated that NO_2^- coordinates the Fe^{III} center in the η^1-N-bonding nitro mode.[6] In contrast to the above mentioned examples, NPs do not contain H-bonding residues in the distal pocket. In the present study, we used a mutant protein NP4(L130R), which provides a flexible H-bonding residue in the distal heme pocket[18] to address the questions (*i*) if the residue would be capable to reverse the NO_2^- binding mode and (*ii*) how the NO_2^- reactivity may be affected.

The characterization of the X-ray structure and spectroscopy of unliganded NP4(L130R) (PDB code 3TGA) and in complex with imidazole (ImH) (PDB code 3TGB) are described elsewhere.[18] The X-ray data indicate that the overall structural properties in comparison to *wt* NP4 are preserved. In the NP4(L130R)[ImH], the position of the Arg130 side-chain is poorly defined, indicating a high degree of flexibility inside the distal heme pocket. Moreover, cw-EPR spectroscopy demonstrates that the effect of the mutation on the electronic structure of the ferriheme centers is negligible. This is particularly remarkable in the case of the complex with ImH, of which the orientation of the ImH plane is principally not affected by the presence of Arg130, which indicates that the structural flexibility of this side-chain must be high enough to arrange in various orientations.

Based on this information, we wanted to know to which extend the cationic Arg130 would be able to interact with the anionic NO_2^- ligand. Both the mode of binding of NO_2^- to the ferriheme and on the effect on the nitrite disproportionation reactivity were addressed. The study included the determination of the X-ray structure, and spectroscopic investigations of the UV-vis, EPR, and NMR spectroscopy. The reactivity was determined in comparison to the *wt* protein and the mutant protein NP4(D30N).

EXPERIMENTAL PROCEDURES

Protein Expression and Purification. For the expression of the mutant proteins NP4(L130R) and NP4(D30N), plasmids pNP4(L130R)^{Amp} and pNP4(D30N)^{Amp} and were generated by the QuickChange mutagenesis method[19] (*Pfu* DNA polymerase (Stratagene)) using the *wt* NP4 expression plasmid[20] as a template. The following pairs of primers were used: pNP4(L130R)^{Amp}: 5'-TTG CAT AAA GGA AAC AAG GAC CGT GGA GAT CTC TAC GCT GTA TTA-3' and 5'-TAA TAC AGC GTA GAG ATC TCC ACG GTC CTT GTT TCC TTT ATG CAA-3'; pNP4(D30N)^{Amp}: 5'- TGG TAC GTG ACA GAT TAC CTA AAC TTG GAA CCT GAC GAC GTT CCA-3' and 5'-TGG AAC GTC GTC AGG TTC CAA GTT TAG GTA ATC TGT CAC GTA CCA-3' (the sites of mutation is underlined). The correctness of the coding regions of the expression plasmid was confirmed through DNA sequencing.

NP4(L130R) and NP4(D30N) were recombinantly expressed in *Escherichia coli* strain BL21(DE3) (Novagen) and reconstituted as was previously described for *wt* NP4.[21] Protein preparations were routinely analyzed by SDS-PAGE to be >90% pure. The proteins were subjected to MALDI-TOF MS to confirm the correct molecular masses accounting for two Cys–Cys disulfides (calculated for $[NP4(L130R) + H]^+$: 20,307 Da, observed: 20,310 ± 20 Da $[NP4(D30N) + H]^+$: 20,264 Da, observed: 20,272 ± 20 Da). Protein concentrations were determined photometrically using $\epsilon_{404\ nm}$ = 141,000 M^{-1} cm^{-1}.[22] Proteins were kept frozen in 200 mM NaO*Ac*/HO*Ac* (pH 5.5), 5% glycerol until use.

Crystallization and Data Collection. Protein crystals were obtained using the vapor-diffusion method with the conditions containing the 3.2 M ammonium phosphate (pH 7.4). The crystals were soaked for 10 min on ice in 3.2 M potassium phosphate (pH 7.4) containing 200 mM KNO_2 and afterwards in 3.2 M potassium phosphate (pH 7.4), 15% glycerol as a cryo protectant. Afterwards, the crystals were immediately frozen in liquid

N_2 and kept there until the measurement. A diffraction data set was collected at 100 K using the beamline BL14.2 at BESSYII (Berlin, Germany).

Structure Solution and Refinement. The data sets were processed with XDS[23] and CCP4.[24] The molecular-replacement method was using MOLREP[24] applied to determine the phases using an initial model from NP4 (PDB code 3MVF).[6] The model building and the refinement were carried out using WINCOOT[25] and PHENIX,[26] respectively. Data collection and refinement statistics were summarized in Table S1. The stereochemical properties were checked by RAMPAGE.[27]

cw-EPR Spectroscopy. The solvent of the protein was exchanged to 100 mM HEPES/NaOH (pH 7.2) and the concentration was adjusted to ~100 µM. The samples were transferred into a 3 mm quartz tube and then frozen in liquid N_2 where they were kept until measurement. cw-EPR spectra were recorded on a Bruker ESP-380E spectrometer at X-band equipped with a gas-flow cryogenic system with a liquid He cryostat from Oxford Inc. Spectra were recorded at 10 K with a microwave power of 2 mW, a field modulation of 100 kHz, and a modulation amplitude of 5 G. The obtained EPR spectra were simulated with the program GEESTRAIN5 V 1.0.[28]

NMR Spectroscopy. For the buffered NMR solution exchangeable protons in stock solutions of 30 mM K_2HPO_4/NaOH (pH 7.8), 3 M KNO_2, and 100 mM ImH/HCl (pH 7.8) were exchanged against deuterons by three solvation/freeze-dry cycles with D_2O. The obtained pH values are not corrected for the deuterium isotope effect and are, therefore, designated pH*. Protein samples were concentrated using Biomax ultrafiltration concentrators (NMWL: 10 kDa) (Millipore). Buffer was exchanged through extensive washing (5 times) with 30 mM Na_2DPO_4/NaOD in D_2O (pH* 7.8) in the same ultrafiltration devices.

Characterization of the nitrite complex of NP4(L130R)

NMR samples finally consisted of 1 - 2 mM of protein solutions. NMR data were collected over the temperature range 10 – 40°C with the chemical shift referenced to residual water on Bruker DRX-400 spectrometer operating at 400.13-MHz proton Larmor frequency, respectively. Upon recording of the high-spin species, 100 mM KNO_2 in D_2O was added and the spectrum recorded at various temperatures. Afterwards 10 mM of ImH/HCl in D_2O (pH 7.8) was added and a spectrum was recorded again at 30°C.

RESULTS AND DISCUSSION

The Crystal Structure of NP4(L130R)[NO_2^-]. By analogy to *wt* NP4,[6] crystals of NP4(L130R) were soaked in crystallization buffer containing KNO_2 before freezing. The resulting crystals diffracted to 1.4 Å resolution and the structure was solved by molecular replacement. The refinement statistics are given in Table 1.

Upon refinement, the structure was deposited n the PDB (PDB code 3TGC). Overall, the structure is very similar to those of NP4{NO_2^-}[6] (Figure S1). The heme pocket is depicted in Figure 1a, where the NO_2^- was best modeled in an N-bonded conformation. The Fe—N bond distance of 2.1 Å is slightly extended compared to *wt* NP4[NO_2^-] with 2.0 Å. The electron density of the side chain of Arg130 is poorly defined, indicating a high degree of flexibility and dynamic. Thus, unlike in any other of the crystallized protein-nitrite complexes (compare Chart S1), the orientation of NO_2^- is not stabilized through electrostatic interaction with this an H-bonding donor. This is also reflected by the only slightly decreased dissociation constant of NO_2^- to NP4(L130R) ($K_d^{NP4(L130R)}$ = 59 mM (Figure S2)) compared to NP4 ($K_d^{wt\ NP4}$ = 66 mM).[6]

Spectroscopic Investigation of NP4(L130R)[NO_2^-] in Solution. However, although the coordination in the crystal of NP4(L130R)[NO_2^-] is identical to *wt* NP4[NO_2^-], solutions of NP4(L130R) undergo a remarkable eye detectable color change (from brown to red)

upon incubation with NO_2^- in contrast to wt NP4 and metMb, which remains nearly the same color. In absorbance spectroscopy, like for metMb,[29] the change in the absorbance spectrum of *wt* NP4 upon NO_2^- binding is very small ($\Delta\varepsilon_{404nm}^{wt\ NP4}$ = 3,400 M^{-1} cm^{-1}).[6] However, in the case of NP4(L130R) the spectral change is much more pronounced, as can be seen in Figure 2, i.e., the Soret band maximum shifts to 408 nm ($\Delta\varepsilon_{404nm}^{NP4(L130R)}$ = 12,500 M^{-1} cm^{-1}). In the Q-band region, the bands at 628 and 500 nm decrease where two new, stronger absorbance maxima appear at 553 and 567 nm. When compared to *wt* NP4[NO_2^-], it can be seen that the two new Q-bands also appear, just to a much lesser extend.

To get deeper insight into the electronic situation, X-band cw-EPR spectra at 10 K reveal a mixture of two low-spin (LS) Fe^{III} hemes (S = $^1/_2$), *i.e.*, a normal rhombic species (g = 2.70, 2.42, 1.49) and a so-called "highly anisotropic low-spin" (HALS) compound[30, 31] with g_{max} = 3.3 (Figure 3). However, although the g-values of all EPR transitions are very similar to those of the *wt*, the intensity of the HALS species dramatically increased from 30% of the total LS signal (NP4[NO_2^-])[6] to 75% (NP4(L130R)[NO_2^-]). Notably, like in the case of NP4(L130R)[ImH],[18] the spectrum of the NO_2^- complex has a larger g-strain indicating the presence of a number of subspecies, which cannot be sufficiently simulated.

Because EPR spectroscopy is primarily sensitive to the ligand orientation rather than the nature of the ligand, which was extensively demonstrated for bis-imidazole-coordinated hemes,[32-34] the two sets of LS signals reflect two distinct orientations of NO_2^- bound to the heme Fe^{III}; thus, the normal rhombic species can be interpreted as the close to parallel ligand plane orientation seen in the crystal structures of NP4[NO_2^-] ($\Delta\varphi$ = 6°) and NP4(L130R)[NO_2^-] ($\Delta\varphi$ = 18°) (Table 2). In contrast, the model porphyrins [Fe(TpivPP)(η^1-NO_2)(py)] and [Fe(TpivPP)(η^1-NO_2)(ImH)] exhibit a more perpendicular

ligand orientation ($\Delta\varphi$ = 77° and 69°, respectively) [13] which typically results in larger g_{max} values as a consequence of increased axial strain.[32, 33] Notably, in these models the alignment of NO_2^- with respect to the heme plane is comparable to NP4[NO_2^-]. and NP4(L130R)[NO_2^-] as are the Fe—$N_{nitrite}$ bond distances (see Table 2). The HALS type of spectrum can thus be interpreted by a rotational isomer NP4(L130R)[NO_2^-]$_\perp$.[32-34]

The turn-over rate of NO_2^- by NP4 does not allow the prolonged study of the NO_2^- complex in solution, for example by ^{1}H NMR spectroscopy; however, in the case of NP4(L130R) the NO_2^- reactivity is dramatically decreased (see below). Thus, to gain insight about the dynamic in NP4(L130R)[NO_2^-] in solution, the paramagnetically shifted ^{1}H NMR signals of the heme cofactor were used as probes (Figure 4). The spectral resolution of NP4 in NMR spectroscopy is rather low,[35, 36] partly because of the heme rotational disorder, i.e., the appearance of two orientation isomers **A** and **B** as a result of the specific pattern of substituents in protoporphyrin IX;[37, 38] in NP4 **A** and **B** appear in a ratio of ~1.1:1.[35, 36] As can be seen from Figure 4, in agreement with the high structural similarity,[18] the paramagnetically shifted heme ^{1}H resonances of NP4(L130R), which are very sensitive to changes in the chemical environment and to the heme ligand orientation, compare well with those of NP4 (for the partial assignment, see Table S1).[35] Upon addition of NO_2^-, the heme ^{1}H resonance signals disappear (determined over the range of 10-40℃), indicating a chemical exchange faster than NMR time scale. As a control, ImH was added which substitutes the NO_2^-. The ^{1}H chemical shifts indicate a LS heme of very similar values compared to *wt* NP4[ImH],[36] indicating that the protein fold and iron oxidation state were not affected by the incubation with NO_2^-. Thus, the disappearance of the heme resonances suggest a fast equilibrium between the two ligand orientation isomers detected in EPR spectroscopy.

$$\text{NP4(L130R)}[NO_2^-]_{\parallel} \leftrightarrows \text{NP4(L130R)}[NO_2^-]_{\perp}$$

in solution. The second form NP4(L130R)[NO_2^-]$_\perp$ is not represented in the electron density map, which may be a consequence of the crystal packing that does not allow the free rotation of NO_2^- upon crystal soaking. Unfortunately, attempts to crystallize NP4(L130R) in the presence of NO_2^- failed.

Ligand rotation was observed in the case of NP2[ImH]. NMR spectroscopy reveals a major heme **B** orientation in NP2[ImH];[36] however, lowering the pH results in a species **B**' that is in chemical exchange with **B** and is related to a second ImH orientation.[37, 38] In the crystal structure of NP2[ImH] (PDB code 1PEE, solved at pH 7.0) a water molecule is H-bonded between ImH and Asp29 (Asp30 in NP4; for the different residue numbering in the NP isoproteins see for example ref [39]). The appearance of **B'** is attributed to protonation of Asp29, thus disrupting the Asp29···water···ImH network, so that ImH can rotate on the heme plane. Similar, in NP4(L130R) Asp30, which is part of the flexible A-B loop,[40] moves out of the heme pocket and loses contact to w^C and w^D (Figure 5 and Scheme 2), thus providing NO_2^- the freedom for rotation. This rearrangement of the A-B loop (Figure S1) is a consequence of the interaction of Arg130:N^ω with Asp35, which moves into the heme pocket (Figure 5).

Influence of the Mutation on the Nitrite Disproportionation Reaction. How then does this change in the water arrangement of the heme pocket influence the nitrite disproportionation? Figure 6 shows the determination of the nitrite disproportionation activity of NP4(L130R) in comparison to *wt* NP4 and another mutant NP4(D30N) where NP4(L130R) is practically inactive. The two water molecules w^A and w^B are H-bonded to one of the $O_{nitrite}$, which is preserved in NP4(L130R)[NO_2^-] (Scheme 2). As a major difference to the *wt*, w^C and w^D are lost where Asp35:O^δ takes the place of w^C. The nitrite disproportionation is strongly dependent on [H^+]. Previous calculations and ultrahigh resolution structures an unusually high pK_a for Asp30.[41-43] Similar, in the lipocalin β-

lipocalin β-lactoglobulin a pH-dependent structural transition like in the NPs has been observed, the so-called “Tanford transition.” In this case, for Glu89, which has a similar structural position in the E-F loop of β-lactoglobulin, a pK_a ≈ 7.3 was estimated.[44] Therefore, it can be proposed that Asp30 or the local arrangement Asp30···w^C···w^D···Asp35 can serve as an H^+ donating entity. This is further supported by the decreased activity in the case of NP4(D30N).

CONCLUSIONS

In summary, unlike with metMb, the insertion of the H-bonding residue Arg130 into the distal pocket of NP4 does not change the NO_2^- binding mode to O-binding. Moreover, in the crystal structure of NP4(L130R)[NO_2^-] even in the N-bound mode Arg130 does not form a salt bridge to NO_2^- although the flexibility of the side-chain and the required space are available. Thus, the mode of NO_2^- coordination in a protein’s heme pocket is determined by multiple factors. However, in solution a second orientation of liganded NO_2^- is present, termed NP4(L130R)[NO_2^-]$_\perp$, which is in fast equilibrium exchange with the orientation seen in X-ray crystallography, termed (L130R)[NO_2^-]$_\parallel$. Thus, NP4(L130R)[NO_2^-]$_\perp$, which is to a lesser extend also present in *wt* NP4[NO_2^-], is stabilized by Arg130, which supports a Arg130$^+$···$^-$ONO interaction. On the other hand, insertion of Arg130 leads to the complete loss of nitrite disproportionation reactivity. Although the structure in NP4(L130R) compared to the *wt* protein is largely preserved, Arg130 leads to a movement of Asp30 in the A-B loop region that results in the loss of two water molecules in the distal pocket which are H-bonded to Asp30. Due to its unusual high pK_a, Asp30 can probably serve as an H^+ donor for the reaction (compare Scheme 1) so that displacement of the Asp30 side-chain results in the loss of activity. In summary, the study of the interaction of NP4(L130R) with NO_2^- provides important

insight into the nitrite-ferriheme interaction and in the structural requirements for a heme pocket to enable the nitrite disproportiontion reaction.

ACKNOWLEDGMENT

The authors are grateful for the technical assistance of Yvonne Brandenburger, Robyn L. Kosinsky, Dagmar Merkel, Alina Steinbach, and Johanna J. Taing. We also thank Koji Nishikawa, Max Planck Institute for Bioinorganic Chemistry, for support during the X-ray data collection and F. Ann Walker, Department of Chemistry and Biochemistry, University of Tucson, Arizona (USA) for the gift of the NP4 expression plasmid. The X-ray diffraction was conducted at the beamline BL 14.2 at BESSY II (Berlin, Germany).

Supporting Information. Table S1, comparison of ^{1}H NMR chemical shifts; Figure S1, comparison of the X-ray structures of NP4[NO_2^-] and NP4(L130R)[NO_2^-]; Figure S2, titration of NP4(L130R) with $NaNO_2$. This material is available free of charge via the Internet at http://pubs.acs.org/.

REFERENCES

1. Averill, B. A. (2007) Nitrogen Metabolism: Denitrification, in *Biological Inorganic Chemistry: Structure and Reactivity* (Bertini, I., Gray, H. B., Stiefel, E. I., and Valentine, J. S., Eds.) 1st ed., pp 494-507, University Science Books, Sausalito (California).
2. Lundberg, J. O., Weitzberg, E., and Gladwin, M. T. (2008) The nitrate-nitrite-nitric oxide pathway in physiology and therapeutics, *Nat. Rev. Drug Discov. 7*, 156-167.
3. Ford, P. C. (2010) Reactions of NO and nitrite with heme models and proteins, *Inorg. Chem. 49*, 6226-6239.
4. Basu, S., Grubina, R., Huang, J., Conradie, J., Huang, Z., Jeffers, A., Jiang, A., He, X., Azarov, I., Seibert, R., Mehta, A., Patel, R., King, B. S., Hogg, N., Ghosh, A., Gladwin, M. T., and Kim-Shapiro, D. B. (2007) Cataclytic generation of N_2O_3 by the concerted nitrite reductase and anhydrase activity of hemoglobin, *Nature Chem. Biol. 3*, 785-794.
5. He, C., and Knipp, M. (2009) Formation of nitric oxide from nitrite by the ferriheme *b* protein nitrophorin 7, *J. Am. Chem. Soc. 131*, 12042-12043.
6. He, C., Ogata, H., and Knipp, M. (2010) Formation of the complex of nitrite with the ferriheme *b* β-barrel proteins nitrophorin 4 and nitrophorin 7, *Biochemistry 49*, 5841-5851.
7. Knipp, M., and He, C. (2011) Nitrophorins: Nitrite disproportionation reaction and other novel functionalities of insect heme-based nitric oxide transport proteins, *IUBMB Life 63*, 304-312.
8. Nasri, H., Ellison, M. K., Shang, M., Schulz, C. E., and Scheidt, W. R. (2004) Variable π-Bonding in Iron(II) Porphyrinates with Nitrite, CO, and tert-Butyl Isocyanide: Characterization of [Fe(TpivPP)(NO2)(CO)], *Inorg. Chem. 43*, 2932-2942.
9. Wyllie, G. R. A., and Scheidt, W. R. (2002) Solid-state structures of metalloporphyrin NO_x compounds, *Chem. Rev. 102*, 1067-1089.
10. Einsle, O., Messerschmidt, A., Huber, R., Kroneck, P. M. H., and Neese, F. (2002) Mechanism of the six-electron reduction of nitrite to ammonia by cytochrome *c* nitrite reductase, *J. Am. Chem. Soc. 124*, 11737-11745.
11. Williams, P. A., Fülöp, V., Garman, E. F., Saunders, N. F. W., Ferguson, S. J., and Hajdu, J. (1997) Haem-ligand switching during catalysis in crystals of a nitrogen-cycle enzyme, *Nature 389*, 406-412.
12. Crane, B. R., Siegel, L. M., and Getzoff, E. D. (1997) Probing the catalytic mechanism of sulfite reductase by X-ray crystallography: Structures of the *Escherichia coli* hemoprotein in complex with substrates, inhibitors, intermediates, and products, *Biochemistry 36*, 12120-12137.
13. Nasri, H., Wang, Y., Huynh, B. H., Walker, F. A., and Scheidt, W. R. (1991) Reactions of bis(nitro)(α,α,α,α-tetrakis(*o*-pivalamidophenyl)porphinato)ferrat(III) with pyridine and imidazole. EPR and Mössbauer spectra and molecular structures of the mixed-ligand species, *Inorg. Chem. 30*, 1483-1489.

14. Copeland, D. N., Soares, A. S., West, A. H., and Richter-Addo, G. B. (2006) Crystal structures of the nitrite and nitric oxide complexes of horse heart myoglobin, *J. Inorg. Biochem. 100*, 1413-1425.

15. Yi, J., Safo, M. K., and Richter-Addo, G. B. (2008) The nitrite anion binds to human hemoglobin *via* the uncommon *O*-nitrito mode, *Biochemistry 47*, 8247-8249.

16. Yi, J., Heinecke, J., Tan, H., Ford, P. C., and Richter-Addo, G. B. (2009) The distal pocket histidine residue in horse heart myoglobin directs the O-binding mode of nitrite to the heme iron, *J. Am. Chem. Soc. 131*, 18119-18128.

17. Goblirsch, B. R., Streit, B. R., DuBois, J. L., and Wilmot, C. M. (2010) Structural features promoting dioxygen production by *Dechloromonas aromatica* chlorite dismutase, *J. Biol. Inorg. Chem. 15*, 879-888.

18. He, C., Fuchs, M., Ogata, H., and Knipp, M. Guanidine-iron coordination in a heme protein: Crystallographic and spectroscopic characterization of the L130R mutant of nitrophorin 4 from *Rhodnius prolixus*, *under revision*.

19. Wang, W., and Malcolm, B. A. (1999) Two-stage PCR protocol allowing introduction of multiple mutations, deletions and insertions using QuikChange Site-Directed Mutagenesis, *BioTechniques 26*, 680-682.

20. Berry, R. E., Ding, X. D., Shokhireva, T. K., Weichsel, A., Montfort, W. R., and Walker, F. A. (2004) Axial ligand complexes of the *Rhodnius* nitrophorins: Reduction potentials, binding constants, EPR spectra, and structures of the 4-iodopyrazole and imidazole complexes of NP4, *J. Biol. Inorg. Chem. 9*, 135-144.

21. Andersen, J. F., Weichsel, A., Balfour, C. A., Champagne, D. E., and Montfort, W. R. (1998) The crystal structure of nitrophorin 4 at 1.5 Å resolution: Transport of nitric oxide by a lipocalin-based heme protein, *Structure 6*, 1315-1327.

22. Maes, E. M., Roberts, S. A., Weichsel, A., and Montfort, W. R. (2005) Ultrahigh resolution structures of nitrophorin 4: Heme distortion in ferrous CO and NO complexes, *Biochemistry 44*, 12690-12699.

23. Kabsch, W. (1993) Automatic processing of rotation diffraction data from crystals of initially unknown symmetry and cell constants, *J. Appl. Cryst. 26*, 795-800.

24. Collaborative Computational Project, N. (1994) The CCP4 suite: Programs for protein crystallography, *Acta Cryst. D50*, 760-763.

25. Emsley, P., and Cowtan, K. (2004) COOT: Model-building tools for molecular graphics, *Acta Cryst. D60*, 2126-2132.

26. Afonine, P. V., Grosse-Kunstleve, R. W., and Adams, P. D. (2005) The PHENIX refinement framework, *CCP4 Newsletter 42 Contribution 8*.

27. Lovell, S. C., Davis, I. W., Arendall III, W. B., de Bakker, P. I. W., Word, J. M., Prisant, M. G., Richardson, J. S., and Richardson, D. C. (2003) Structure validation by Cα geometry: ϕ,ψ, and Cβ deviation, *PROTEINS: Struct. Func. Gen. 50*, 437-450.

28. Hagen, W. R. (2009) *Biomolecular EPR Spectroscopy*, 1st ed., CRC Press, Boca Raton, Florida (USA).

29. Wanat, A., Gdula-Argasińska, J., Rutkowska-Żbik, D., Witko, M., Stochel, G., and van Eldik, R. (2002) Nitrite binding to metmyoglobin and methemoglobin in comparison to nitric oxide binding, *J. Biol. Inorg. Chem. 7*, 165-176.

30. Walker, F. A., Reis, D., and Balke, V. L. (1984) Models of the cytochromes *b*. 5. EPR studies of low-spin iron(III) tetraphenylporphyrins, *J. Am. Chem. Soc. 106*, 6888-6898.

31. Migita, C. T., and Iwaizumi, M. (1981) Low-temperature EPR studies of highly anisotropic low-spin (protoporphyrinato)iron(III) complexes, *J. Am. Chem. Soc. 103*, 4378-4381.

32. Walker, F. A. (2004) Models of the bis-histidine-ligated electron-transferring cytochromes. Comparative geometric and electronic structure of low-spin ferro- and ferrihemes, *Chem. Rev. 104*, 589-615.

33. Walker, F. A. (1999) Magnetic spectroscopy (EPR, ESEEM, Mössbauer, MCD and NMR) studies of low-spin ferriheme centers and their corresponding heme proteins, *Coord. Chem. Rev. 185-186*, 471-534.

34. Zoppellaro, G., Harbitz, E., Kaur, R., Ensign, A. A., Bren, K. L., and Andersson, K. K. (2008) Modulation of the Ligand-Field Anisotropy in a Series of Ferric Low-Spin Cytochrome c Mutants derived from Pseudomonas aeruginosa Cytochrome c-551 and Nitrosomonas europaea Cytochrome c-552: A Nuclear Magnetic Resonance and Electron Paramagnetic Resonance Study, *J. Am. Chem. Soc. 130*, 15348-15360.

35. Shokhireva, T. K., Smith, K. M., Berry, R. E., Shokhirev, N. V., Balfour, C. A., Zhang, H., and Walker, F. A. (2007) Assignment of the ferriheme resonances of the high-spin forms of nitrophorins 1 and 4 by ^{1}H NMR spectroscopy: Comparison to structural data obtained from X-ray crystallography, *Inorg. Chem. 46*, 170-178.

36. Shokhireva, T. K., Weichsel, A., Smith, K. M., Berry, R. E., Shokhirev, N. V., Balfour, C. A., Zhang, H., Montfort, W. R., and Walker, F. A. (2007) Assignment of the ferriheme resonances of the low-spin complexes of nitrophorins 1 and 4 by ^{1}H and ^{13}C NMR spectroscopy: Comparison to structural data obtained from X-ray crystallography, *Inorg. Chem. 46*, 2041-2056.

37. Yang, F., Zhang, H., and Knipp, M. (2009) A one-residue switch reverses the orientation of a heme *b* cofactor. Investigations on the ferriheme NO transporters nitrophorin 2 and 7 from the blood-feeding insect *Rhodnius prolixus*, *Biochemistry 48*, 235-241.

38. Yang, F., Knipp, M., Shokhireva, T. K., Berry, R. E., Zhang, H., and Walker, F. A. (2009) A ^{1}H and ^{13}C NMR spectroscopic study of the ferriheme resonances of three low-spin complexes

of wild-type nitrophorin 2 and nitrophorin2(V24E) as a function of pH, *J. Biol. Inorg. Chem. 14*, 1077-1095.

39. Knipp, M., Yang, F., Berry, R. E., Zhang, H., Shokhirev, M. N., and Walker, F. A. (2007) Spectroscopic and functional characterization of nitrophorin 7 from the blood-feeding insect *Rhodnius prolixus* reveals an important role of its isoform-specific N-terminus for proper protein function, *Biochemistry 46*, 13254-13268.

40. Maes, E. M., Weichsel, A., Andersen, J. F., Shepley, D., and Montfort, W. R. (2004) Role of binding site loops in controlling nitric oxide release: Structure and kinetics of mutant forms of nitrophorin 4, *Biochemistry 43*, 6679-6690.

41. Menyhárd, D. K., and Keserü, G. M. (2005) Proteonation state of Asp30 exerts crucial influence over surface loop rearrangements responsible for NO release in nitrophorin 4, *FEBS Lett. 579*, 5392-5398.

42. Weichsel, A., Andersen, J. F., Roberts, S. A., and Montfort, W. R. (2000) Nitric oxide binding to nitrophorin 4 induces complete distal pocket burial, *Nat. Struc. Biol. 7*, 551-554.

43. Swails, J. M., Meng, Y., Walker, F. A., Martí, M. A., Estrin, D. A., and Roitberg, A. E. (2009) pH-dependent mechanism of nitric oxide release in nitrophorin 2 and 4, *J. Phys. Chem. B 113*, 1192-1201.

44. Qin, B. Y., Bewley, M. C., Creamer, L. K., Baker, H. M., Baker, E. N., and Jameson, G. B. (1998) Structural basis of the Tanford transition of bovine β-lactoglobulin, *Biochemistry 37*, 14014-14023.

TABLES

Table 1. Data Collection and Refinement Statistics of the Native Data Sets. Numbers in Parenthesis Represent the Values for the Highest Resolution Shell.

	NP4(L130R)[NO_2^-]
PDB entry	3TGC
Data collection	
Beamline	BESSYII BL14.2
Wavelength (Å)	0.91841
Space group	*C*2
Unit-cell parameters	
a (Å)	69.76
b (Å)	43.11
c (Å)	52.43
β (°)	94.40
Resolution (Å)	30.59-1.40 (1.44-1.40)
No. of observed reflections	111125
No. of unique reflections	30602
R_{merge}	0.038 (0.285)
Completeness (%)	99.6 (99.6)
$<I/\sigma(I)>$	20.7 (4.7)
Refinement	
Resolution range (Å)	30.59-1.40
R (%)	15.0
R_{free} (%)	18.7
No. of the residues	184
No. of solvent molecules	158
No. of nitrite	1
Rmsd bond lengths (Å)	0.006
Rmsd angles (°)	1.05
Ramachandran plot	
favoured region (%)	98.13
allowed region (%)	1.88
outlier region (%)	0
Average B-factors (Å^2)	
protein	15.1
ligand (heme)	16.3
NO_2^-	23.7
solvent	26.7

Table 2. Comparison of the Bond Parameters from the Crystallographic Data of Nitrite complexes of Ferric Hemes with Imidazole or Pyridine *trans*-Ligands.

Nitrite complex	**Fe-N_{NO2} (Å)**	**Fe-N_{His} (Å)**	**φ_1**[a]	**φ_2**[b]	**$\Delta\varphi$**[c]	**Reference**
wt NP4[NO_2^-]	1.96	2.01	1°	-5°	6°	[6]
NP4(L130R)[NO_2^-]	2.06	2.07	3°	-15°	18°	tw[d]
cd_1NiR[NO_2^-]	2.00	1.96	-61°	7°	68°	[11]
[Fe(NO_2)(py)(TpivPP)]	1.960	2.093			77°	[13]
[Fe(NO_2)(ImH)(TpivPP)]	1.949	2.037			69°	[13]

[a] Dihedral angle between the $C^{meso-\beta}$-$C^{meso-\delta}$ axis and the proximal His plane normal. [b] Dihedral angle between the $C^{meso-\alpha}$-$C^{meso-\gamma}$ axis and the nitrite plane normal. [c] Dihedral angle between the nitrite plane normal and the His plane normal. [d] tw, this work.

SCHEMES

Scheme 1.

$$3NO_2^- + 2H^+ \xrightarrow{[NP^{III}]} 2NO + H_2O + NO_3^-$$

Scheme 2. Schematic representation of water molecules (w) and significant side-chains in (a) NP4[NO_2^-] and (b) NP4(L130R)[NO_2^-].

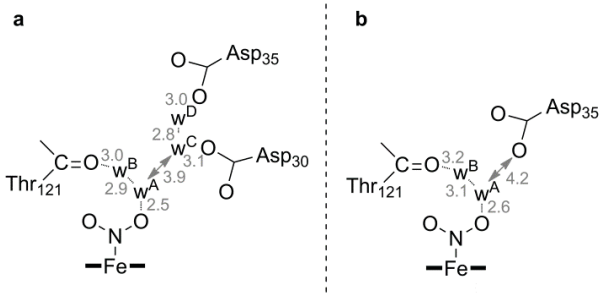

CHARTS

Chart 1.

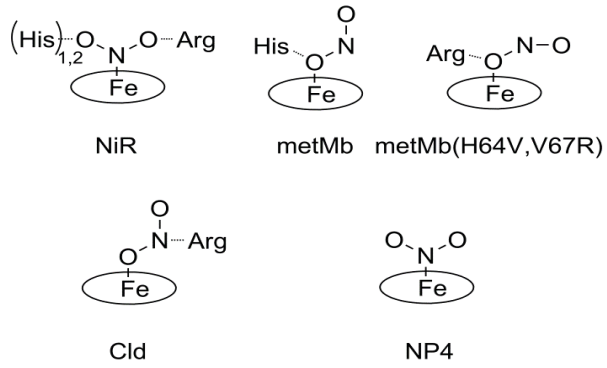

[a] Cld, chlorite dismutase; *cd*$_1$NiR, heme *cd*$_1$ nitrite reductase; *cc*NiR, cytochrome *c* nitrite reductase; SiHRP, sulfite reductase.

FIGURES

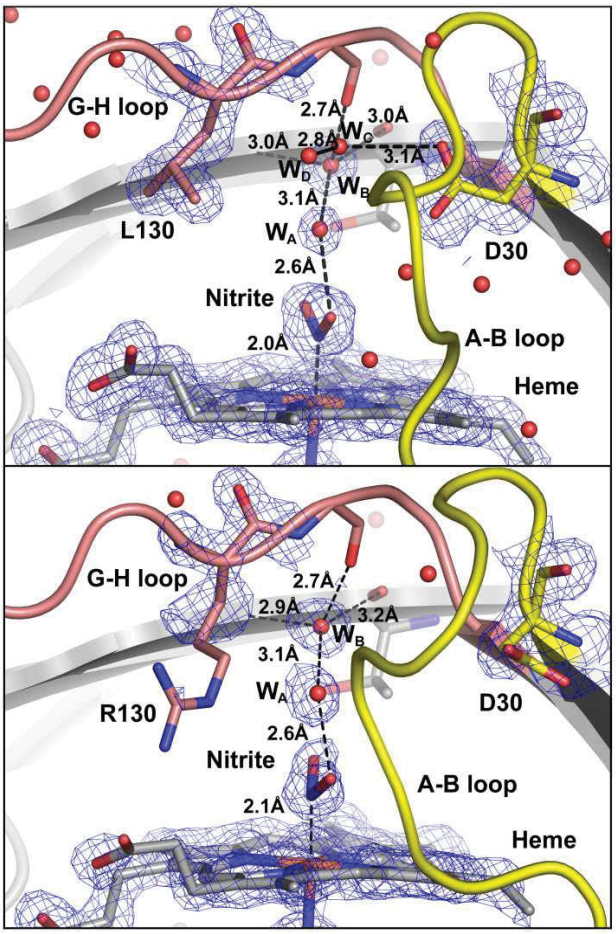

Figure 1. The $2F_o - F_c$ electron density map of the heme environment in the crystal structures of (a) *wt* NP4[NO_2^-] (PDB code 3MVF)[6] and (b) NP4(L130R)[NO_2^-] (PDB code 3TGC). The position of the Arg130 side chain, which is poorly defined in the electron density map, was modeled during the refinement process into the structure.

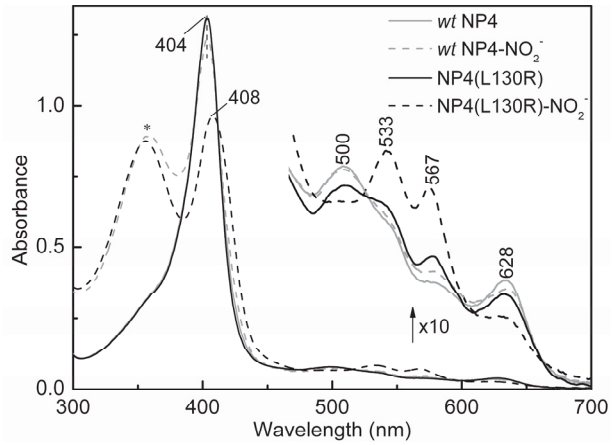

Figure 2. Change in the absorbance spectra of 10 μM NP4(L130R) and *wt* NP4 upon incubation with 25 mM $NaNO_2$ in 100 mM MOPS/NaOH (pH 7.2) at 37℃. The band at 3 52 nm (*) originates from the addition of NO_2^-.

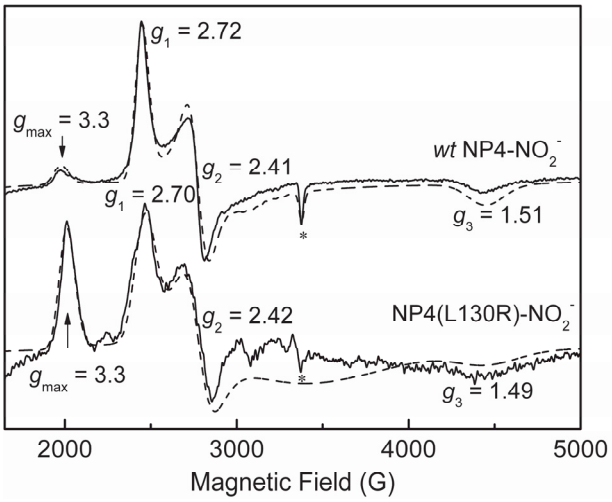

Figure 3. X-band cw-EPR spectra of NP4[NO_2^-] and NP4(L130R)[NO_2^-] in 100 mM HEPES/NaOH (pH 7.2), 25% glycerol at 10 K. The asterisk indicates the $g_{||}$ of the residual HS species. Spectral simulations are presented as dashed lines.

Characterization of the nitrite complex of NP4(L130R)

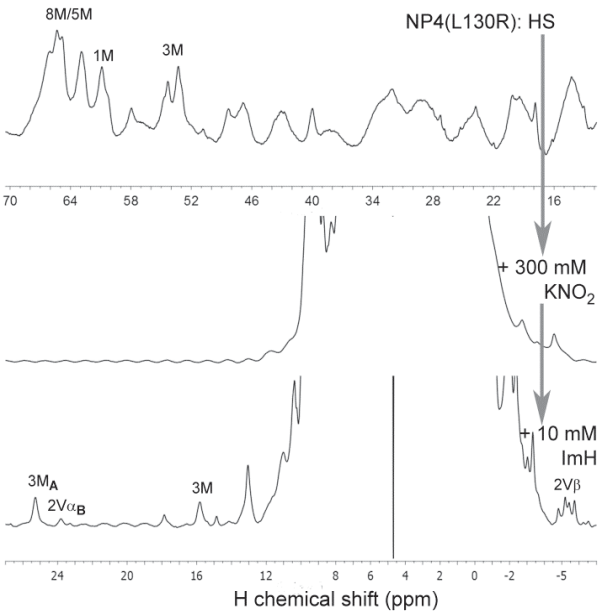

Figure 4. ^{1}H NMR spectra of 2 mM NP4(L130R) at in 30 mM K-phosphate buffer in D_2O (pH* 7.8) at 35℃. *Top*: unliganded HS form; *center*: upon addition of 300 mM of KNO_2; *bottom*: upon addition of 1 mM ImH. (For details of the assignments, refer to Table S2.)

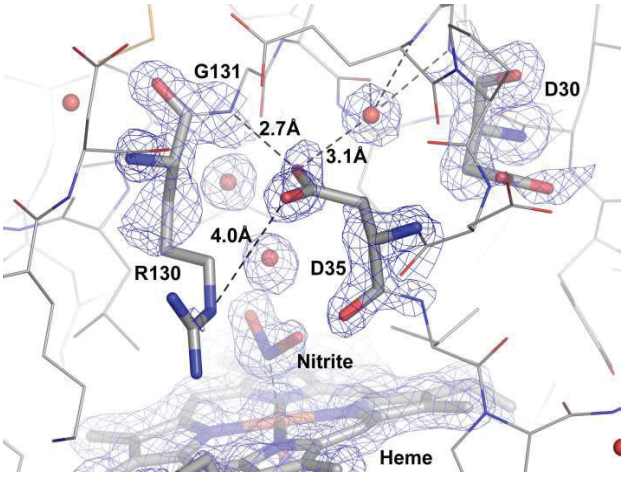

Figure 5. Detailed representation of the spatial surrounding of Asp35 in the crystal structure of NP4(L130R)[NO_2^-]. The $2F_o–F_c$ electron density map of the critical residues is presented in superposition with the model. For the side-chain of Arg130 little electron density is observed, wherefore the side-chain was modeled into the structure by energy minimization.

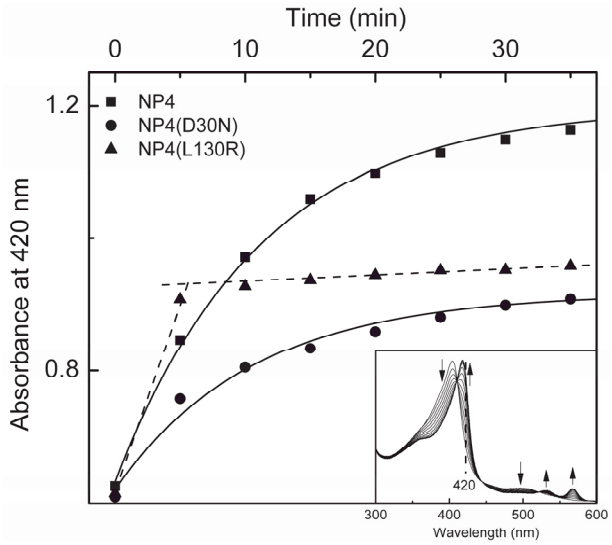

Figure 6. Absorbance detected nitrite disproportionation by NP4(L130R) in comparison to NP4 and NP4(D30N) in 100 mM MOPS/NaOH (pH 7.0) at 37℃ according to Scheme 1. The large initial change in the case of NP4(L130R) is a matter of the strong change in absorbance upon NO_2^- coordination (Figure 1). *Inset*: Time dependent spectral change of NP4 incubated with NO_2^-.

Characterization of the nitrite complex of NP4(L130R)

Insertion of an H-Bonding Residue into the Distal Pocket of the Ferriheme Protein Nitrophorin 4: Effect on Nitrite–Iron Coordination and Nitrite Disproportionation

Chunmao He, Hideaki Ogata, and Markus Knipp*

Max-Planck-Institut für Bioanorganische Chemie, Stiftstrasse 34-36, D-45470 Mülheim an der Ruhr, Germany.

– Supporting Information –

* Address correspondence to:
Dr. Markus Knipp
Max-Planck-Institut für Bioanorganische Chemie
Stiftstrasse 34-36
D-45470 Mülheim an der Ruhr
Germany
Tel.: +49 (0)208-306-3671
Fax: + 49 (0)208-306-3951
mknipp@mpi-muelheim.mpg.de

Supplementary Tables

Table S1. ^{1}H Chemical shifts (in ppm) of NP4(L130R) and NP4(L130R)[ImH] in somparison to *wt* NP4 and *wt* NP4[ImH]. Chemical Shifts for NP4(L130R) and NP4(L130R)[ImH] were assigned based on the comparison with the respective data for *wt* protein.

	NP4[a]		NP4(L130R)[b]	
	A	**B**	**A**	**B**
1M	62.4?	61.5?	60.9, ~60.3	
3M	55.5	~57.2	54.3, 53.3	
5M	66.1	64.7	66.0, 65.3, 64.8, 62.9	
8M	67.4	64.0		
average	62.8	61.9		
spread, D	11.9	7.5		

	NP4[ImH][c]		NP4(L130R)[ImH][b]	
	A	**B**	**A**	**B**
1M	1.7	9.4		
3M	25.7	16.4	25.3	15.8
5M	5	10.3		
8M	10.9	0.2		
2Vα	13.0	23.5	13.1	23.8
2Vβ	-5.5-5.9	-5.3, -4.9	-4.8, -5.2, -5.4, -5.7	
4Vα	9.4			
6Pα	11.1, 4.4	15.7, 8.6		
6Pβ	-2.7, -3.7	-2.0, 0.1		
7Pα	15.1, 8.2	10.9, 5.1		
7Pβ		-2.6, -3.7		
meso-α	-3.5	-3.0		
meso-γ		-2.6		
meso-γ	5.1			

[a] At 25℃, pH* 7.0. From Shokhireva, T. K.; Smith, K. M.; Berry, R. E.; Shokhirev, N. V.; Balfour, C. A.; Zhang, H.; Walker, F. A. *Inorg. Chem.* **2007**, *46*, 170-178. [b] At 35℃, pH* 7.8. [c] At 30℃, pH* 7.0. From Shokhireva, T. K.; Weichsel, A.; Smith, K. M.; Berry, R. E.; Shokhirev, N. V.; Balfour, C. A.; Zhang, H.; Montfort, W. R.; Walker, F. A. *Inorg. Chem.* **2007**, *46*, 2041-2056.

Supplementary Figures

Figure S1. Comparison of the X-ray structures of *wt* NP4[NO_2^-] (PDB code 3MVF) and NP4(L130R) [NO_2^-] (PDB code 3TGC; this work). (a) The cartoon representation of *wt* NP4[NO_2^-] (*yellow*) and NP4(L130R) [NO_2^-] (*red*). RMDS of the *wt* NP4[NO_2^-] and NP4(L130R) [NO_2^-] was calculated with the value of 0.41 (except A-B loop). (b) The enlarged view of the heme pocket. The heme, His59 and the residues, Asp30, Leu130 (*wt*) and Arg130 (L130R mutant), are represented by the stick model.

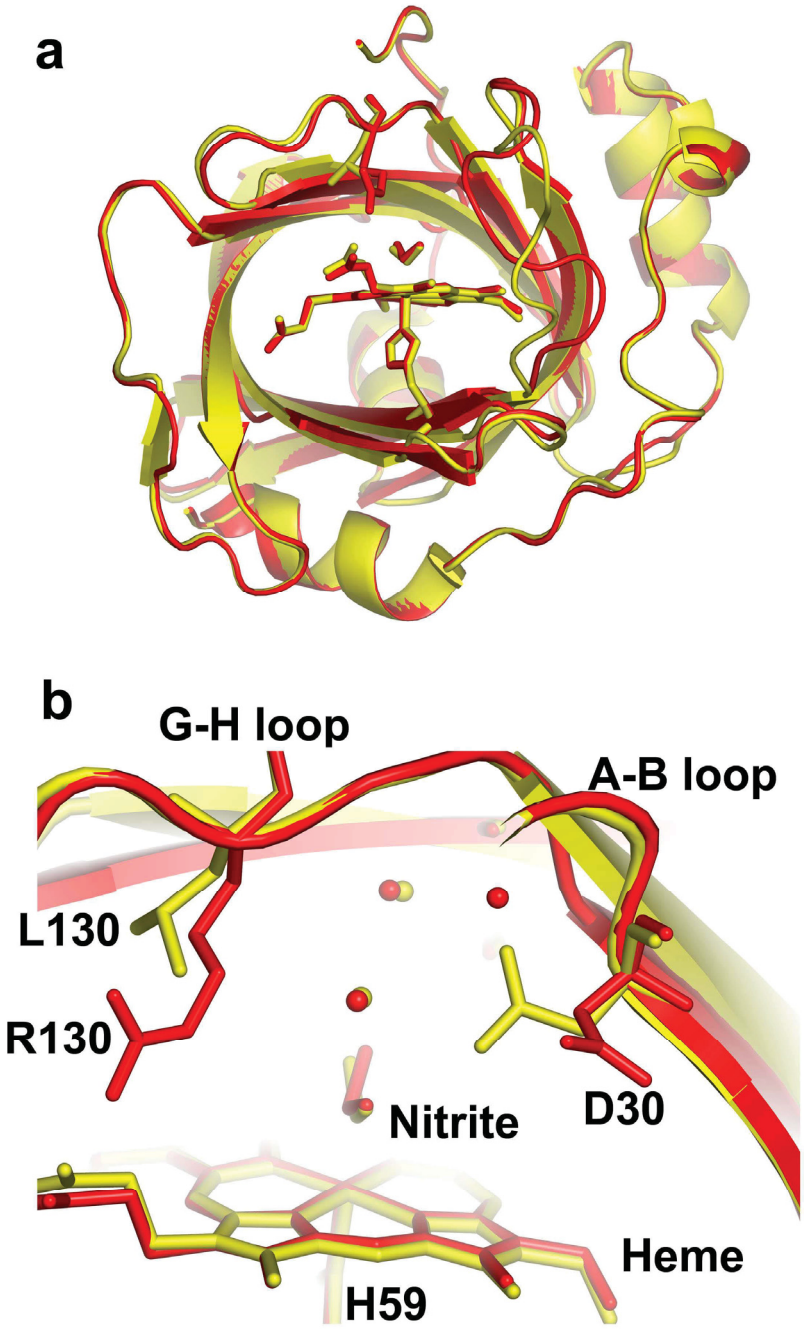

Characterization of the nitrite complex of NP4(L130R)

Figure S2. Equilibrium titration of NP4(L130R) with $NaNO_2$ in 100 mM MOPS/NaOH, pH 7.2. The absorbance change at 404 nm was monitored and plotted *vs.* $[NO_2^-]$.

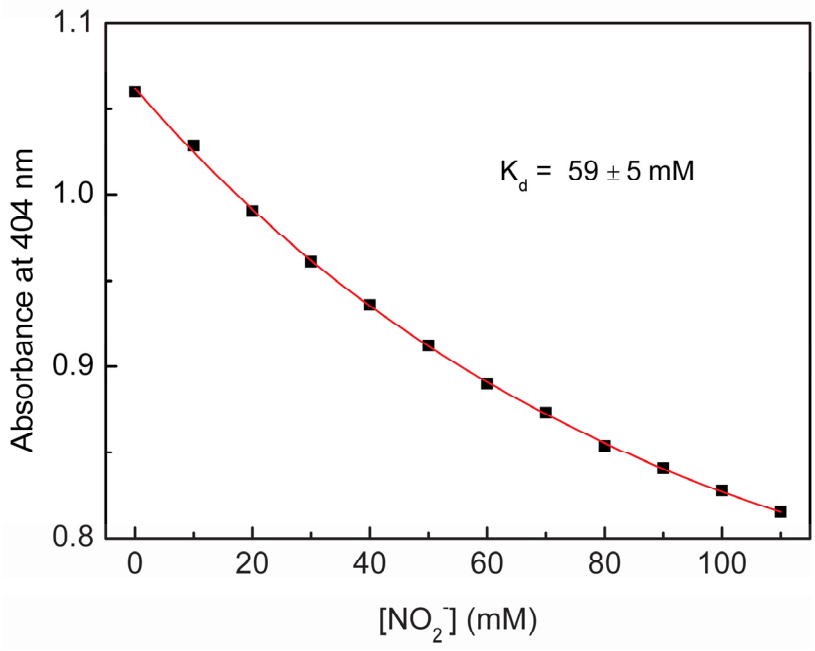

Chapter 6. Reduction of the lipocalin type heme containing protein nitrophorin – Sensitivity of the fold-stabilizing cysteine disulfides toward routine heme-iron reduction[***]

(Knipp, M.; Taing, J. J.; He, C. *J. Inorg. Biochem.* **2011**, *105*, 1405-1412)

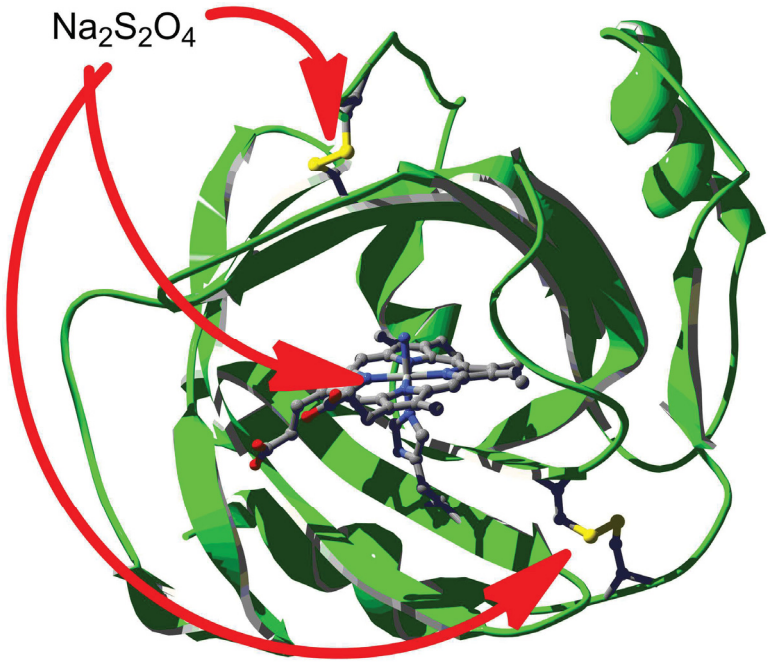

[***] Reprinted from *J. Inorg. Biochem.* Vol105, M. Knipp, J. Taing, C. He, 1405-1412, Copyright (2011), with permission from Elsevier.

Abstract

For the preparation of the ferroheme oxidation state of heme proteins, the most widely used reductant is probably sodium dithionite. Using nitrophorin 4, nitrophorin 7, and oxidized glutathione, we show that dithionite not only reduces the heme iron but also disulfide bonds when used in excess. Therefore, care must be taken when disulfide containing ferroheme proteins are prepared *via* dithionite reduction.

Journal of Inorganic Biochemistry 105 (2011) 1405–1412

Contents lists available at SciVerse ScienceDirect

Journal of Inorganic Biochemistry

journal homepage: www.elsevier.com/locate/jinorgbio

Reduction of the lipocalin type heme containing protein nitrophorin — Sensitivity of the fold-stabilizing cysteine disulfides toward routine heme-iron reduction

Markus Knipp *, Johanna J. Taing, Chunmao He

Max-Planck-Institut für Bioanorganische Chemie, Stiftstrasse 34-36, D-45470 Mülheim an der Ruhr, Germany

ARTICLE INFO

Article history:
Received 20 October 2010
Received in revised form 19 July 2011
Accepted 20 July 2011
Available online 11 August 2011

Keywords:
Disulfide
Dithionite
Mercury
Ferroheme
S-alkyl thiosulfate
Glutathione

ABSTRACT

The determination of the redox properties of the cofactor in heme proteins provides fundamental insight into the chemical characteristics of this wide-spread class of metalloproteins. For the preparation of the ferroheme state, probably the most widely applied reductant is sodium dithionite, which at neutral pH has a reduction potential well below the reduction potential of most heme centers. In addition to the heme iron, some heme proteins, including the nitrophorins (NPs), contain cysteine – cysteine disulfide bonds. In the present study, the effect of dithionite on the disulfides of NP4 and NP7 is addressed. To gain deeper understanding of the disulfide/dithionite reaction, oxidized glutathione (GSSG), as a model system, was incubated with dithionite and the products were characterized by ^{13}C NMR spectroscopy and reverse phase chromatography in combination with mass spectrometry. This revealed the formation of one equivalent each of thiol (GSH) and glutathione-*S*-thiosulfate ($GS-SO_3^-$). With this background information, the effect of dithionite on the cystines of NP4 and NP7 was studied after trapping of the thiols with *para*-cloromercurybenzyl sulfonate (*p*-CMBS) and subsequent matrix assisted laser desorption/ionization time-of-flight mass spectrometry (MALDI-TOF MS) where the heterolytic cleavage of the S – S bond appears with only 2 molar equivalents of the reductant. Furthermore, prolonged electrochemical reduction of NP4 and NP7 in the presence of electrochemical mediators also leads to disulfide breakage. However, due to sterical shielding of the disulfide bridges in NP4 and NP7, the cystine reduction can be largely prevented by the use of stoichiometric amounts of reductant or limited electrochemical reduction. The described disulfide breakage during routine iron reduction is of importance for other heme proteins containing cystine(s).

1. Introduction

Nitrophorins (NPs) comprise a unique class of ferriheme proteins originating from the blood feeding insect *Rhodnius prolixus* [1]. Four nitrophorins, designated NP1–4, were isolated from the insect saliva [2,3] and later recombinantly expressed [4,5]. Another nitrophorin, NP7, was recently established from a cDNA library and then recombinantly expressed [6,7]. The major biological function of these proteins is the transport and delivery of nitric oxide (NO) from the insect saliva to the host tissue where it acts as a vasodilator and blood-coagulation inhibitor [8]. The NO transport is accomplished through the binding of NO to the heme iron. The protein experiences a significant pH change when subjected from the acidic pH of the saliva (5–6) [9] to those of the blood plasma (~7.4) which decreases the affinity for NO, for example for NP7 from $>10^9\,M^{-1}$ (pH 5.5) to $4\times10^6\,M^{-1}$ (pH 7.5) [10]. Recently, it was established that ferriheme NPs, at least *in vitro*, are able to produce NO from NO_2^-, which is a unique feature among ferriheme proteins [11,12].

In NPs, the heme cofactor is located inside an 8-standed β-barrel which is an unusual case for a heme protein [13]. The heme iron is coordinated by a His residue where the 6th coordination site is open for the binding of various ligands including the native ligands NO and histamine [14]. The protein fold, an example of which is depicted in Fig. 1, has been classified as a lipocalin type of fold [13], which is a very common fold among the proteome, typically found in proteins that bind lipophilic molecules [15]. A special feature of the lipocalins is the presence of at least one Cys–Cys disulfide; in case of the nitrophorins two Cys–Cys disulfides are present, which are formed in a crossed fashion, *i.e.*, Cys_A–Cys_C and Cys_B–Cys_D, in a given order $\cdots Cys_A \cdots Cys_B \cdots Cys_C \cdots Cys_D \cdots$ along the peptide sequence (see Fig. 1).

In contrast to other ferriheme proteins, *e.g.*, myoglobin (Mb), of which the ferriheme state is easily reduced by excess NO [16], NPs stabilize the Fe^{III} state through a number of carboxylate residues near the heme pocket [17], and a ruffled heme geometry, which is induced mainly by several side chains that point toward the distal side of the macrocycle [18]. This way, the reduction potential is established at, for example, −303 mV *vs.* SHE at pH 7.5 for NP1 compared to

* Corresponding author. Tel.: +49 208 306 3671; fax: +49 208 306 3951.
E-mail address: mknipp@mpi-muelheim.mpg.de (M. Knipp).

0162-0134/$ – see front matter © 2011 Elsevier Inc. All rights reserved.
doi:10.1016/j.jinorgbio.2011.07.009

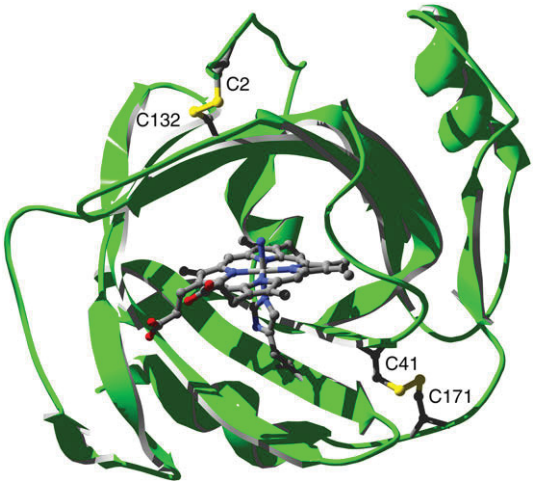

Fig. 1. Ribbon representation of the crystal structure of NP4 from the blood-feeding insect *Rhodnius prolixus* at pH 7.4 (PDB #1X8P [65]). The heme cofactor and the two Cys–Cys disulfide bridges are displayed in a ball-and-stick model. The figure was created with SWISS PDB VIEWER V. 3.75 (http://www.expasy.org/pdbviewer/) [66] and rendered with POVRAY V. 3.6 (http://www.povray.org).

~0 mV *vs.* SHE for Mb [19]. The resulting stabilization of the $\{FeNO\}^6$ complex is important for NP function because ferroheme–NO, *i.e.*, $\{FeNO\}^7$, association constants are too large ($K_{eq} = 10^{13}$–$10^{14}\ M^{-1}$) [10,17] to allow effective NO release *in vivo* [20].

Although, nitrophorins are ferriheme proteins, the Fe^{II} state came recently into focus when the Fe^{II}–CO derivative was used as a model for the $\{FeNO\}^6$ compound, for example in FT-IR and laser flash photolysis experiments [21,22]. Furthermore, the crystal structures of NP4[Fe^{II}], NP4[Fe^{II}–CO], and NP4[Fe^{II}–NO] were previously reported [23]. Moreover, the determination of $Fe^{II \rightleftharpoons III}$ reduction potentials by spectroelectrochemistry was extensively used for the characterization of NP function [10,17–19,24,25]. Finally, the Fe^{II} state was proposed as an intermediate in the reduction of the NP iron center with low molecular weight thiols [26]. However, although the heme iron is typically investigated as the redox active center, the presence of the Cys–Cys moieties in the protein fold represent two other redox active centers, which have not yet been considered. In this study, we focus for the first time on the stability of the Cys–Cys moieties in NP4 and NP7 toward reducing agents.

2. Materials and methods

2.1. Materials

Stock solutions of $Na_2S_2O_4$ were always prepared freshly before use. The effective concentration of $Na_2S_2O_4$ was determined through reduction of $[Fe(CN)_6]^{3-}$ in deaerated water ($\epsilon_{420\ nm} = 1{,}026\ M^{-1}\ cm^{-1}$) [27]. Sodium 4-(chloromercury)benzyl sulfonate (*p*-CMBS)[1] was from Santa Cruz Biotechnology, Inc. 2,7-Dibromo-4-(hydroxymercuri)-fluorescein (merbromin)[1] was from Sigma-Aldrich. *a*-Cyano-4-hydroxy-cinnamic acid (CHCA; >99%) and 2,5-dihydroxobenzoic acid (DHB; >99%) were from Fluka, 3-(4-hydroxy-3,5-dimethoxyphenyl)prop-2-enoic acid (sinapinic acid, SA; >97%) was from Acros. Solutions of *p*-CMBS, merbromin, CHCA, DHB, and SA were always prepared freshly and then kept in the dark. All reagents were of the highest grade commercially available and used as received.

NP4 and NP7 were recombinantly expressed in *Escherichia coli* strain BL21(DE3) (Novagen) and purified and reconstituted as was previously described [7,10,25]. Protein preparations were routinely analyzed by SDS-PAGE to be >90% pure. The proteins were subjected to MALDI-TOF MS to confirm the correct molecular masses accounting for two Cys–Cys disulfides (calculated for $[NP4+H]^+$: 20,264 Da, observed: 20,279 Da; calculated for $[NP7+H]^+$: 20,969 Da, observed: 20,966 Da). Concentrations of NP4 and NP7 were determined photometrically using $\epsilon_{404\ nm} = 141{,}000\ M^{-1}\ cm^{-1}$ [23] and $81{,}000\ M^{-1}\ cm^{-1}$ [7], respectively.

Experiments under strictly anaerobic conditions were carried out inside an anaerobic chamber (Coy, Inc.) with an atmosphere comprised of 98% N_2/2% H_2 in the presence of Pd catalysts. All solutions were rendered essentially O_2 free by three freeze–pump–thaw cycles performed on a vacuum line.

2.2. Absorption spectroscopy

Absorption spectra were recorded using a Cary-50 absorption spectrophotometer equipped with a fiber optic coupler (Varian, Inc.). Flexible fiber optics (Ocean Optics, Inc.) were used to connect the spectrophotometer with a cuvette holder (Ocean Optics, Inc.) inside the anaerobic chamber which allows to record absorption spectra under strict anaerobic conditions.

2.3. ^{13}C NMR spectroscopy

Two samples of 10 mM of GSSG were prepared in 50 mM KH_2PO_4/KOH in D_2O (pH* 7.0).[2] One of the samples was mixed with 20 mM *p*-CMBS or merbromin. To each sample 20 mM of $Na_2S_2O_4$ was added and then incubated for 1 h at ambient temperature. Afterwards, ^{13}C {^1H} and ^{13}C DEPT-135 NMR spectra were recorded at 30 °C on a Bruker 400 MHz NMR spectrometer. For comparison, GSH, GSSG, and GS–*p*-MBS or GS–merbromin, respectively, *i.e.*, a mixture of equal concentrations of GSH and *p*-CMBS, were recorded under the same conditions.

2.4. Detection of GSH upon GSSG reduction by MALDI-TOF MS

1 mM of GSSG in 100 mM NaH_2PO_4/NaOH, 100 μM DTPA (pH 7.5) was incubated with 1 mM merbromin and analyzed as such or incubated with either 2 mM of $Na_2S_2O_4$ or 2 mM of TCEP. All samples were kept at ambient temperature for 1 h in the dark before mixing with CHCA dissolved in 0.1% TFA in H_2O/CH_3CN (2:1). Upon drying, samples were subjected to MALDI-TOF MS. MADLI-TOF MS experiments were performed on a Voyager DE Pro (Applied Biosystems) equipped with a nitrogen laser (337 nm; pulse energy at 10 Hz, 324 μJ). The instrument is routinely calibrated, so that the standard error at ~20 kDa amounts to 0.2%.

At <1 kDa, the accuracy is estimated to at least 0.05%.

2.5. Chromatographic and mass spectrometric identification of GSX

10 mM of GSSG in 25 mM NaH_2PO_4/NaOH, 25 μM DTPA (pH 7.5) was incubated with 0, 2, 5, 10, or 20 mM of $Na_2S_2O_4$ for 1 h at room temperature. The sample was analyzed by C_{18}-RPC using isochratic elution with 2% CH_3CN, 0.05% TFA and absorption detection at 215 nm. The fractions at 4.8 min were collected and pooled. Afterwards, the sample was dried in a SpeedVac (colorless solid). Repeated chromatographic analysis confirmed that the sample was largely stable over the time of preparation (2 to 3 days). Part of the sample was dissolved in CH_3OH and injected to an ESI MS Bruker ESQ 3000 equipped with an Agilent ESI source in negative mode.

[1] Mercury compounds are highly toxic and should be handled with care.

[2] The pH was adjusted using a standard pH electrode in H_2O; the buffers used for NMR spectroscopy are not corrected for the deuterium effect and are, therefore, designated as pH*.

2.6. Detection of reduced Cys in NP4 and NP7 by MALDI-TOF MS

Two aliquots of 100 μM of NP4 or NP7, respectively, were dissolved in 100 mM MOPS/NaOH, 50 mM NaCl, 100 μM DTPA, and 8 mM *p*-CMPS (pH 8.0) under anaerobic conditions. 200 μM of $Na_2S_2O_4$ was added to one aliquot and then incubated at ambient temperature for 1 h in the dark. 1 μL of each solution was mixed with 15 μL of SA dissolved in H_2O/CH_3CN (2:1) and subjected to MALDI-TOF MS upon drying.

2.7. Electrochemistry

Protein samples (500 μL) of 50 μM in 100 mM MOPS/NaOH, 50 mM NaCl, and 1 mM imidazole (ImH) (pH 8.0) were used in a SEC-C optical transparent thin layer electrochemical (OTTLE) quartz cell equipped with a Pt-grid working electrode and a Pt counter electrode (ALS Co., Ltd). An Ag/AgCl electrode (BASi Co., Ltd.) was used as reference. $[Ru(NH_3)_6]Cl_3$, anthraquinone-2-sulfonic acid, and methyl viologen were added as electrochemical mediators into the protein solution [10,17,24,25]. A potential of −545 mV *vs.* SHE was applied for 1 h at ambient temperature using a potentiostat (ϵpsilon, Bioanalytical Systems, Inc.). Determination of the absorption spectrum revealed a fully reduced cofactor. Afterwards, 10 μL was collected from the area of the working electrode using a Hamilton syringe and immediately mixed with 2 μL of 40 mM *p*-CMBS. After 1 h at ambient temperature in the dark, 1 μL of the sample was mixed with 15 μL of SA in H_2O/CH_3CN (2:1), spotted on a MALDI target plate, and subjected to MALDI-TOF MS.

3. Results and discussion

3.1. Reduction of NP4 and NP7 with $Na_2S_2O_4$ under aerobic conditions

The reduction of heme proteins with $Na_2S_2O_4$ for the preparation of the ferroheme state is routine praxis in research laboratories around the world and was also applied in the past to the nitrophorins for various experimental attempts [21–23,28]. Often ferroheme proteins are prepared by the addition of excess of $Na_2S_2O_4$ which takes care both of the O_2 present in solution and of the heme reduction. Absorption spectra of the titration of ferriheme NP7 with $Na_2S_2O_4$ under aerobic conditions are displayed in Fig. 2. Ferriheme NP7 exhibits a Soret band absorption maximum at 404 nm (Fig. 2a) [7]. Upon the first administration of $Na_2S_2O_4$ (4-fold excess over NP7), the Soret band absorption did not change (Fig. 2b), which is likely due to the consumption of $Na_2S_2O_4$ by atmospheric O_2 dissolved in the solution. Further administration of $Na_2S_2O_4$ aliquots resulted in a step-wise decrease of the Soret band absorption up to a 42-fold molar excess over NP7 (Fig. 2c–g). CO blown over the solution surface did not cause a change of the absorption spectrum (data not shown). Because CO is selective for ferroheme (see below), this confirms that the absorption change is not due to the iron reduction, but reflects bleaching of the heme. Heavy excess of $Na_2S_2O_4$ (200- to 2000-fold molar excess) resulted in a shift of the Soret band maximum to 418 nm (Fig. 2h–i), but supplementation with CO did not generate a change in the absorption spectrum (data not shown). Repetition of the experiments with ferriheme NP4 yielded similar results (data not shown).

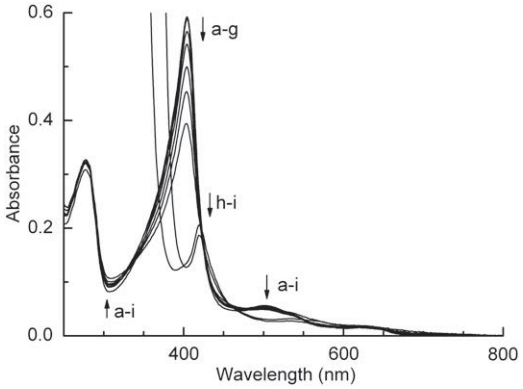

Fig. 2. Reduction of NP7 with $Na_2S_2O_4$ under aerobic conditions. Titration of 7.2 μM NP7 with $Na_2S_2O_4$ was performed in 100 mM MOPS/NaOH, 50 mM NaCl (pH 7.5) in an open quartz cuvette and monitored by UV–vis spectroscopy; a, original spectrum; b–i, addition of 4, 8, 12, 22, 31, 42, 200, and 2000-fold molar excess of $Na_2S_2O_4$.

Similarly, a bleaching of heme in NP2 was described upon administration of 0.5 mM L-cysteine, which was inhibited by the addition of catalase, *i.e.*, suggesting that H_2O_2 may be transiently formed [29]. Thus, the "bleaching" is likely a consequence of fast re-oxidation of the Fe^{II} to Fe^{III} in the presence of O_2 yielding $O_2^{\bullet-}$, which is, for instance, found to be part of the catalytic cycle of nitric oxide synthase (NOS) [30]. Rapid mixing kinetic investigations indeed reveal a very fast reaction of ferroheme NPs with O_2 [31]. To see whether atmospheric O_2 is involved in this process, the titration with $Na_2S_2O_4$ was repeated under anaerobic conditions.

3.2. Reduction of NP4 and NP7 with $Na_2S_2O_4$ under anaerobic conditions

In contrast to the aerobic titration of NP4, titration with equimolar amounts of $Na_2S_2O_4$ under anaerobic conditions yielded spectral conversion with decent isosbestic behavior. The ferroheme species is indicated by the appearance of a new Soret band absorption maximum at 427 nm and a broad Q band at ~557 nm (data not shown). This is in good agreement with the previously reported results [23]. NP7, in contrast, converts to a sample with two different Soret band maxima at 423 nm and 391 nm and a broad Q band with the maximum at ~591 nm. In this case, isosbestic behavior is not obtained. If NP4[Fe^{II}] or NP7[Fe^{II}] is generated under anaerobic conditions, the addition of CO results, similar to the previous report [23], in the formation of a single Soret band maximum at 419 nm, indicating the overall integrity of the sample in contrast to the degradation observed in the presence of O_2 (see above).

Nevertheless, a certain instability of the ferroheme NPs was already mentioned [23,28] and is also experienced in our laboratory. At this point, it was considered that the nitrophorins comprise not only the heme iron as a redox active center, but also the two disulfide bridges (Fig. 1). Therefore, a closer examination of the redox properties of the cystines was initiated.

3.3. The reduction of GSSG with dithionite — analysis by MALDI-TOF MS

Not only the complexity of proteins, but also the frequently occurring limitations in solubility and availability, makes it hard or even impossible to spectroscopically investigate the status of the Cys residues by simple NMR spectroscopic experiments like the one reported in Section 3.4. Furthermore, the Cys–Cys reduction in NPs leads to protein precipitation as a consequence of fold destabilization. Moreover, the presence of multiple Cys–Cys bonds and/or the asymmetry of the protein disulfide bonds, *i.e.*, Cys–Cys′, further complicate the analysis. Thus, a method was sought that would be applicable to distinguish cystines from cysteines in heme proteins upon reduction, in particular with the reagent $S_2O_4^{2-}$.

An analytical technique that overcomes many of the disadvantages mentioned above and that is widely available is mass spectrometry upon modification of CysH/Cys^- residues. Among the many reagents that are in use for the detection of thiols/thiolates, the class of mercury mono-organyls RHg(Cl/HO) (R = aryl) was considered in this study because the large mass of the Hg atom allows to distinguish the

modified species in MS when bound to a protein while R can be small to avoid sterical hindrance that could keep the reagent from reacting with the target CysH. Furthermore, the specificity and selectivity of mercury compounds reacting with sulfhydryl groups are very high; for example, the dissociation constant of cysteine and CH_3Hg^+ is $10^{-20.3}$ [32]. The principal applicability of RHg(Cl/HO) (R = aryl) as a probe for free thiols in proteins by MALDI-TOF MS was previously described [33–36].

To test for the principle applicability of these reagents in the presence of $Na_2S_2O_4$ as the reducing agent, the method was established on GSSG. Apparently, the detection of GSH and GSSG by MALDI MS is very limited, not only because of the appearance of the matrix signals in the mass range of the analytes but also because of their well documented poor ionization efficiency [37]. This was overcome, for example, by the application of dye coated gold nanoparticles [38]. Another approach is the application of thiol reactive agents that, upon reaction, shift the mass out of the matrix signal area (>500 Da). For this purpose, GSSG was incubated at pH 7.5 with $Na_2S_2O_4$ in the presence of merbromin. Upon incubation for 1 h at ambient temperature, the sample was analyzed by MALDI-TOF MS. This was compared to a sample without $Na_2S_2O_4$ and a sample that was fully reduced with TCEP. The resulting spectra are displayed in Fig. 3. As expected [37,38], peaks that correspond to GSH or GSSG were not detected; however, two novel species that reflect the mass of GSH in adduct with merbromin were identified (Fig. 3B and C). Careful analysis involving the calculation of the isotopic distribution revealed that one species is $[GS–merbromin + H]^+$ (calculated for the main isotopic species: 999 Da; observed: 999 Da) and that the second product reflects a species where one Br is abstracted, *i.e.*, $[GS–merbromin' + H]^+$ (calculated for the main isotopic species: 919 Da; observed: 919 Da). The calculation of the isotopic distribution is presented in the inset in Fig. 4C. The results demonstrate that $Na_2S_2O_4$ is able to reduce Cys – Cys similar to TCEP, which is well established as a highly efficient and specific Cys – Cys reductant. Moreover, the results also indicate that mercury mono-organyls can be used to detect the formation of CysH/Cys^- by $S_2O_4^{2-}$ in MALDI-TOF MS, *i.e.*, also for the analysis of the sensitivity of Cys – Cys in proteins toward $S_2O_4^{2-}$ reduction.

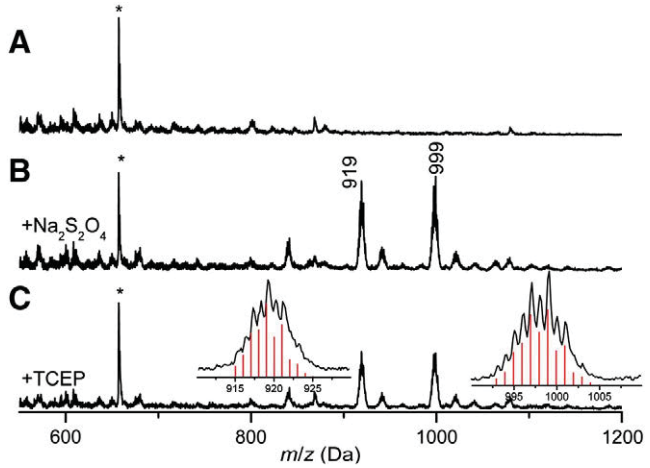

Fig. 3. Mass spectrometric analysis of GSSG reduction by $S_2O_4^{2-}$. Samples of 1 mM GSSG in 100 mM NaH_2PO_4/NaOH and 100 μM DTPA (pH 7.5) were mixed with 1 mM of merbromin. The mixture was either (A) applied as such or (B) incubated with 2 mM of $Na_2S_2O_4$ or (C) 2 mM of TCEP for 1 h at ambient temperature in the dark. Afterwards, the samples were mixed 1:15 with α-cyano-4-hydroxycinnamic acid in H_2O/CH_3CN (2:1) and analyzed by MALDI-TOF MS. The peak indicated by * is obtained from the buffered solution. *Insets*: The isotopic distribution of the two species with the main fraction at 919 Da and 999 Da, respectively, was analyzed by ISOTOPIDENT (available at http://education.expasy.org/student_projects/isotopident/htdocs/) using the following chemical formulas: 919 Da, $C_{30}H_{28}O_{11}N_3S_1Br_1Hg_1$; and 999 Da, $C_{30}H_{27}O_{11}N_3S_1Br_2Hg_1$.

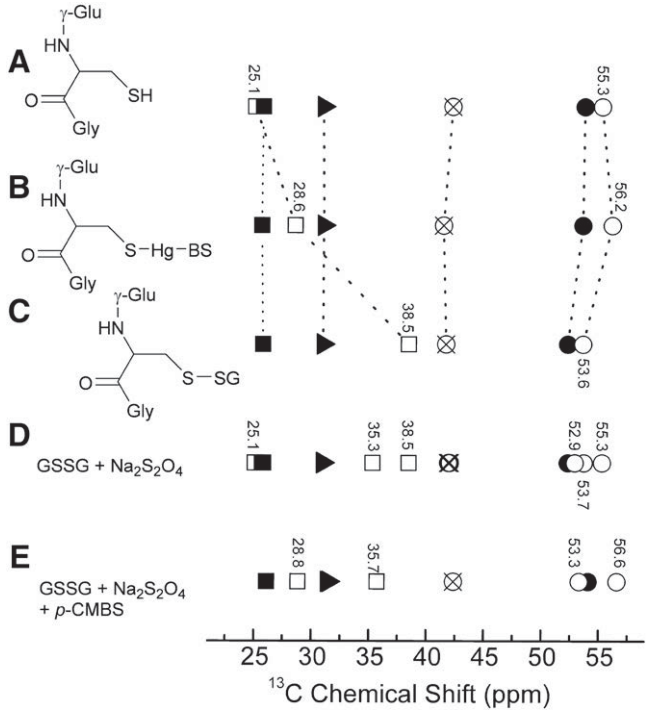

Fig. 4. Analysis of the reduction of GSSG with $S_2O_4^{2-}$ by ^{13}C NMR spectroscopy. On display is a schematic representation of the chemical shifts of the Cα (*circles*), Cβ (*squares*), and Cγ nuclei (*triangles*) of glutathione. Chemical shift positions of the Glu residue are displayed in filled symbols (●, ■, and ▶), of the Cys residue in open symbols (○ and □), and of the Gly residue in crossed symbols (⊗). The chemical shifts of the Cys:Cα and Cys:Cβ are indicated next to the corresponding symbol. Spectra were recorded of (A) GSH, (B) GS–*p*-MBS, (C) GSSG, (D) GSSG incubated with $Na_2S_2O_4$, and (E) GSSG incubated with $Na_2S_2O_4$ in the presence of *p*-CMBS. All samples were prepared in 50 mM KH_2PO_4/KOH (pH* 7.0) in D_2O.

3.4. ^{13}C NMR spectroscopy of the dithionite reduction of oxidized glutathione

The reduction potentials of disulfides at neutral pH are significantly higher compared to the reduction potential of $Na_2S_2O_4$; for example, the reduction potential of glutathione

$$2GSH \leftrightarrows GSSG + 2H^+ + 2e^-$$

was reported to −240 mV *vs.* SHE in pH 7.0 at room temperature [39]. Similarly, disulfide bonds in proteins exhibit reduction potentials between −122 mV (DsbA) [40] and −270 mV (thioredoxin) [41]. In contrast, the reduction potential of $2SO_2^{\bullet-}$, which is the reactive radical anion occurring from homolytic decomposition

$$S_2O_4^{2-} \leftrightarrows 2SO_2^{\bullet-}$$

[42] was estimated −660 mV *vs.* SHE for the couple $SO_2^{\bullet-}/HSO_3^-$ in pH 7.0 at 25 °C [43]. This was further supported by several reports about the application of $Na_2S_2O_4$ as a disulfide cleaving agent for synthetic preparations in aqueous media [44–46]. However, reports about the reduction of disulfides in biomolecules by $S_2O_4^{2-}/SO_2^{\bullet-}$ are scarce. We found one report where the reduction of GSSG with $S_2O_4^{2-}$ was applied in the context of the simultaneous quantification of GSSG and GSH by HPLC [47]. Interestingly, in this report one thiol equivalent was detected per GSSG and it was speculated that the thiosulfinate $GS–SO_2^-$ may be the second product GSX [47]; however, this compound is expected to be very labile in aqueous solutions. Further insights were gained by ^{13}C NMR spectroscopy.

^{13}C NMR resonances are very sensitive to changes in the molecular composition so that the chemical shift of Cys:Cβ (and to a lesser

extend Cys:Cα) of glutathione is sensitive to substitution on Cys:Sγ and is, therefore, used as a probe. The $^{13}C\{^1H\}$ and ^{13}C DEPT-135 NMR spectra of GSSG were recorded in the presence of $Na_2S_2O_4$ and the obtained chemical shift positions are compared to the spectra of GSH ($\delta_{Cys:C\beta}=25.1$ ppm) and GSSG ($\delta_{Cys:C\beta}=38.5$ ppm) in Fig. 4. Resonances of GSH and GSSG were assigned according to a previous report [48]. Comparison of the chemical shifts reveals the presence of GSH ($\delta_{Cys:C\beta}=25.1$ ppm) and a novel compound GSX ($\delta_{Cys:C\beta}=35.4$ ppm). Repetition of the experiment in the presence of *p*-CMBS and comparison with synthetically prepared GS–*p*-MBS ($\delta_{Cys:C\beta}=28.6$ ppm) confirmed the presence of GSX ($\delta_{Cys:C\beta}=35.7$ ppm) and GS–*p*-MBS ($\delta_{Cys:C\beta}=28.8$ ppm). Thus, the asymmetric breaking of the Cys – Cys bond yielding a CysH and another product CysX, which is indifferent to *p*-CMBS modification, is confirmed.

3.5. Identification of GSX

For the identification of GSX, aliquots of 10 mM GSSG were incubated with 0, 2, 5, 10, and 20 mM of $Na_2S_2O_4$ at pH 7.5 and incubated for 1 h at room temperature. Afterwards, the solutions were analyzed by C_{18}-RPC with absorbance detection at 215 nm. In comparison to the retention times of GSSG (20.8 min), GSH (9.0 min), and residual $Na_2S_2O_4$ (4.1 min), a novel compound appeared at 4.8 min (Fig. 5A).

For the mass spectrometric identification of the novel compound, a larger fraction of the reaction product was collected from C_{18}-RPC. The sample was subjected to ESI-MS spectroscopy in negative mode and revealed a species with $m/z=386$ Da. This corresponds well with the mass of glutathione-*S*-thiosulfate, *i.e.*, $[GS–SO_3H–H]^-$ (see Fig. S1 in the Supporting Information). To the best of our knowledge, this is the first time that this compound was reported.

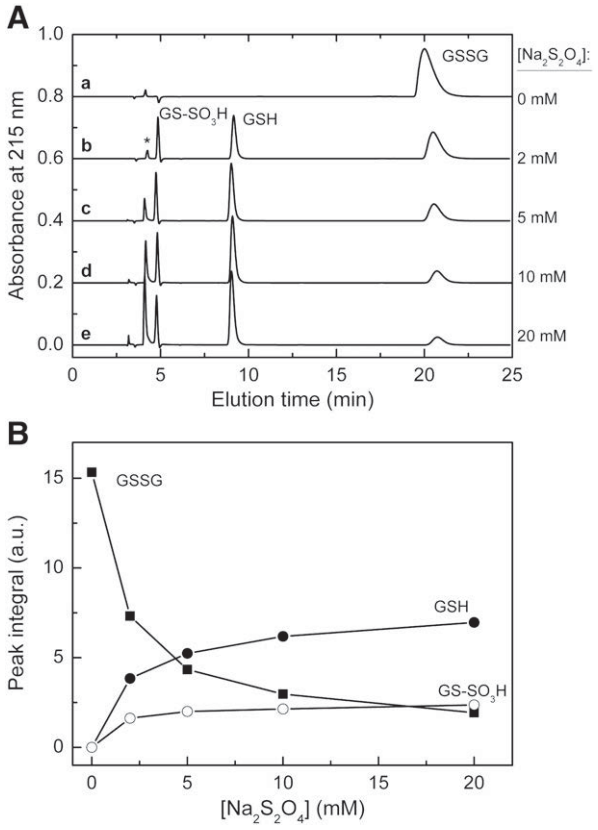

Fig. 5. Chromatographic analysis of the reaction of GSSG with $Na_2S_2O_4$. (A) 10 mM of GSSG in 25 mM NaH_2PO_4/NaOH, 25 μM DTPA (pH 7.5) was incubated with (a) 0, (b) 2, (c) 5, (d) 10, or (e) 20 mM $Na_2S_2O_4$ and incubated for 1 h at room temperature. Subsequently, the mixture was subjected to C_{18}-RPC using isocratic elution with 2% CH_3CN, 0.05% TFA. The elution times of GSSG, GSH, buffer components, and residual $Na_2S_2O_4$ (*) were identified by analysis of the individual components (data not shown). (B) The integrals of the peaks identified by the C_{18}-RPC were plot *vs.* $[Na_2S_2O_4]$.

In Fig. 5B, the integrals of the peaks of the chromatograms presented in Fig. 5A were plotted *vs.* $[Na_2S_2O_4]$, demonstrating the decay of [GSSG] and the simultaneous raising of [GSH] and $[GS–SO_3^-]$ with increasing supplementation of $[Na_2S_2O_4]$. Because the absorbance at 215 nm in all three compounds is mainly determined by the $n\rightarrow\pi^*$ transitions of the peptide bonds, the molar extinction coefficient of GSH can be estimated ~1/2 that of GSSG, which allows an approximate quantitative comparison between the substrate and the products based on the peak integrals of the chromatography. As expected, Fig. 5B demonstrates that ~1 mol equiv of GSH is formed per GSSG. Apparently, however, the amount of $GS–SO_3^-$ seems to be smaller. However, it cannot be excluded that $GS–SO_3^-$ is unstable and decaying with time. Moreover, $GS–SO_2^-$ may be the initial product and $GS–SO_3^-$ may be formed through air oxidation during the time of sample preparation.

Although for the biological functionality of the NPs tissue pH (~7.4) is the most interesting, the fact that the proteins are prepared and kept under the acidic pH of the insect saliva usually requires the investigation of NPs at pH 5–6. The reduction potential of the couple $SO_2^{\bullet-}/HSO_3^-$ depends on the pH; however, at pH 5 the midpoint potential is still at −520 mV [43] so that reduction of the NP heme iron is still readily possible considering the reduction potentials of NPs (at pH 5.5, NP3 has the lowest reduction potential at −321 mV *vs.* SHE [28]). The reduction potential for the thiol/disulfide couple is even rising to approx. −80 mV *vs.* SHE at pH 5.0 (determined for GSH/GSSG [49]). Therefore, care has to be taken also for the prevention of the protein cystines at low-pH conditions.

3.6. The reduction of NP4 and NP7 with $S_2O_4^{2-}$ — detection by MALDI-TOF MS

After the methodology for the expected cystine reduction through $S_2O_4^{2-}$ was successfully established with GSSG, it was applied to NP4 and NP7. For this purpose, merbromin was substituted with *p*-CMBS because it shows no degradation during MALDI-TOF MS, which reduces the complexity of the mass spectra. In addition, a higher ionizability compared to other mercury organyls, *i.e.*, highest signal intensity, was obtained for *p*-CMBS in studies that compared the applicability of various RHg(Cl/HO) [33,34]. Furthermore, in contrast to merbromin, the much smaller *p*-CMBS molecule is expected to provide a higher trapping efficiency when applied to buried CysH/Cys^- in a protein fold, like NP4 and NP7 (see Fig. S2 in the Supporting Information). The resulting spectra are displayed in Fig. 6 for both NP4 and NP7. Control samples without $Na_2S_2O_4$ supplement are presented in Fig. 6A and C, indicating the purity and integrity of the starting material, *i.e.*, no adduct was formed without a free thiol group. In contrast, the addition of only a 2-fold molar excess of $Na_2S_2O_4$ over NP4 or NP7, respectively, lead to several modifications as can be seen from the spectra depicted in Fig. 6B and D. Details of the $[M+H]^+$ regions of Fig. 6B and D are displayed in Fig. S3. The observed masses were analyzed by comparison with theoretical masses calculated on the basis of the reaction seen with GSSG and the results are summarized in Table 1. In summary, the peaks match well with insertion of one or two *p*-MBS modifications where the presence of SO_3H and/or Hg^{2+} was also confirmed. The insertion of Hg^{2+} was not observed in the case of GSSG reduction, which may be a matter of the chelate effect provided by two Cys residues in the protein structure, which may then lead to the stripping of the organic ligand as a side reaction. That the SO_3H modification is not seen in all cases and may be explained with its lability under the conditions of MALDI MS. In summary, the results confirm that, like in the case of GSSG, the disulfide bonds of NP4/7 are cleaved by relatively small amounts of $Na_2S_2O_4$. Furthermore, the appearance of the SO_3H modification reflects the heterolytic reduction mechanism observed with GSSG

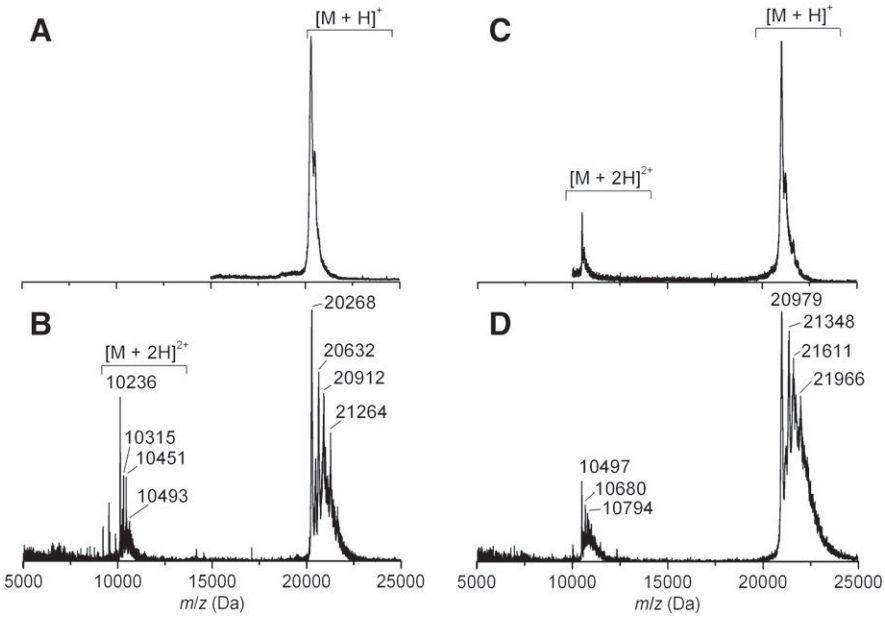

Fig. 6. Mass spectrometric detection of NP disulfide reduction by $S_2O_4^{2-}$. Samples of 100 μM of NP4 (A and B) and NP7 (C and D) were incubated with 0 (A and C) and 200 μM (B and D) of $Na_2S_2O_4$ in the presence of 4 mM *p*-CMPS and incubated for 1 h at ambient temperature in the dark. Afterwards, the samples were mixed 1:15 with SA in H_2O/CH_3CN (2:1) and analyzed by MALDI-TOF MS. Details of the $[M+H]^+$ regions of spectra B and D are displayed in Fig. S3.

although the observed partly modification with Hg^{2+} suggests that the chemistry may be more complex.

3.7. Electrochemical reduction of Cys–Cys disulfides of NP4[ImH] and NP7[ImH]

The reduction potential of NP iron centers is routinely determined by spectroelectrochemistry in an OTTLE cell [10,17–19,24,25]. However, information about the condition of the Cys–Cys sites cannot be obtained from UV–vis electronic spectra and, therefore, the measurements were performed so far under the assumption of the integrity of the disulfides, despite of the fact that reduction potentials were applied, which are much lower than the expected reduction potential for $Cys-Cys + 2e^- + 2H^+ \leftrightarrows 2CysH$ (compare Section 3.4). Among the various ligand complexes of NPs that have been probed by spectroelectrochemistry, the ImH and histamine (Hm) complexes show the lowest reduction potentials ranging from −339 mV *vs.* SHE (NP1[Hm] at pH 5.5) [28] to −474 mV *vs.* SHE (NP2[Hm] at pH 7.5) [24].

In this study, NP4[ImH] and NP7[ImH] were electrochemically reduced in an OTTLE cell equipped with two Pt electrodes and a Ag/AgCl reference electrode. The samples contained small amounts of $[Ru(NH_3)_6]Cl_3$, anthraquinone-2-sulfonate, and methyl viologen as electrochemical mediators [10,17,24]. A potential of −545 mV *vs.* SHE was applied for 1 h and spectra were recorded to confirm that the equilibrium $Fe^{III} + e^- \leftrightarrows Fe^{II}$ was established at the given potential. Aliquots were taken at various time points and immediately mixed with 8 mM *p*-CMBS. After 1 h of incubation, samples were subjected to MALDI-TOF MS and the results are presented in Fig. 7. Although the spectroscopic evaluation of both compounds shows the presence of a large fraction of unaffected NP4 (20,272 Da) and NP7 (20,988 Da), it also indicates that at least one of the Cys–Cys disulfides in NP4 and NP7 is sensitive to electrochemical reduction under conditions that are routinely applied for nitrophorin characterization. In contrast to the reduction with $S_2O_4^{2-}/SO_2^{\bullet-}$, electrochemical reduction of NP4 leads to a much cleaner mass spectrum (Fig. 7A) where, besides unmodified NP4, only NP4(−*p*-MBS)$_2$ (20,907 Da) is a major component, which suggests the preferential reduction of one of the Cys–Cys under the applied conditions.

The mass spectrum of NP7 is, similar to the reduction with $S_2O_4^{2-}$, less homogeneous (Fig. 7B). Besides the unmodified protein (20,988 Da), a species corresponding to NP7–*p*-MBS is identified (21,346 Da). At higher *m/z*, a number of other species appear. The most prominent peak, however, occurs at 21,171 Da. Besides the protein, three electrochemical mediators are contained in the solution, two of which are organic compounds. It is expected that the first step of the reduction involves the 1-electron process

$$Cys-Cys + e^- \rightarrow Cys^- + Cys^{\bullet},$$

which was previously experimentally and theoretically investigated in the case of small molecule disulfides [50,51]. As a result, where the resulting thiol/thiolate is indeed capable to react with *p*-CMBS, the reduced form of the organic mediators $R^{\bullet+}$ may, at least in part, be able to combine with $Cys^{\bullet}$. In any case, the mass spectra show that

Table 1
Comparison of the masses found in samples of NP4 and NP7, respectively, after incubation with $Na_2S_2O_4$ in the presence of *p*-CMBS.

	Observed[a] *m/z* (Da)	Calculated[b] *m/z* (Da)	Modification
NP4	20,268	20,263	–
	20,466	20,464	Hg^{2+}
	20,632	20,621	*p*-MBS
	20,902	20,903	*p*-MBS, Hg^{2+}, SO_3H
	20,988	20,979	2 *p*-MBS
	21,264	21,262	2 *p*-MBS, Hg^{2+}, SO_3H
NP7	20,979	20,969	–
	21,176	21269	Hg^{2+}
	21,348	21,327	*p*-MBS
	21,536	21,527	*p*-MBS, Hg^{2+}
	21,611	21,608	*p*-MBS, Hg^{2+}, SO_3H
	21,684	21,684	2 *p*-MBS
	21,726	21,765	2 *p*-MBS, SO_3H
	21,966	21,966	2 *p*-MBS, Hg^{2+}, SO_3H

Cys residues were calculated without the proton because they are assumed to occur either as cystines or as being in adduct with *p*-MBS. For the calculation of the modified proteins, adducts with 1, 2, or 3 *p*-MBS were considered as indicated.

[a] Data derived from the measurements depicted in Fig. 6B and D (accuracy: ±25 Da).

[b] Masses of $[NP+H]^+$ were based on the amino acid sequences (NP4: Swiss-Prot #Q94734; NP7: Swiss-Prot #Q6PQK2).

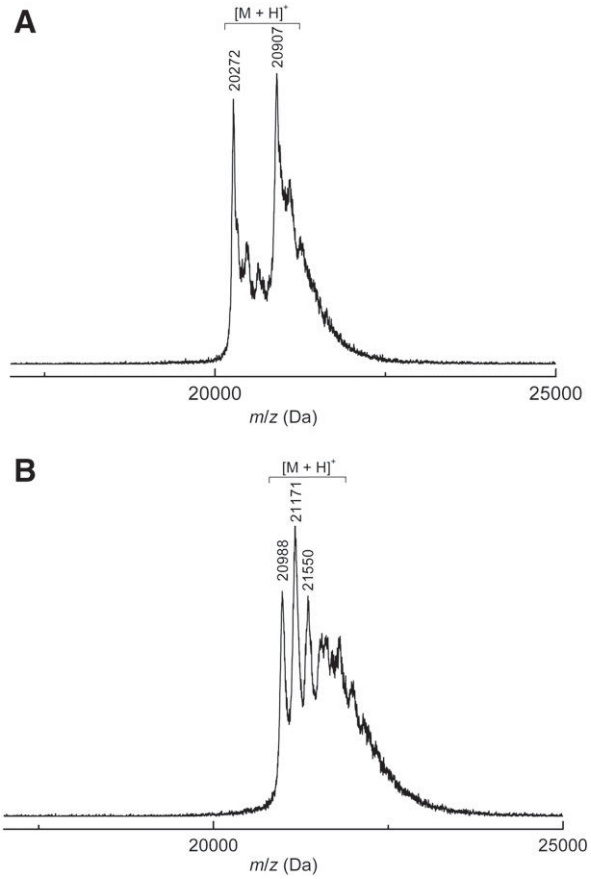

Fig. 7. MALDI-TOF MS analysis of electrochemically reduced nitrophorins. A potential of −545 mV *vs.* SHE was applied for 60 min at ambient temperature to (A) NP4 and (B) NP7 in 100 mM MOPS/NaOH, 50 mM NaCl, and 1 mM imidazole (ImH) (pH 8.0) supplemented with $[Ru(NH_3)_6]Cl_3$, anthraquinone-2-sulfonate, and methyl viologen. Afterwards, an aliquot of 10 μL was collected from the area close to the Pt-grid working electrode and mixed with 2 μL 8 mM *p*-CMBS. After 1 h incubation at ambient temperature in the dark, the sample was subjected to MALDI-TOF MS.

extended electrochemical treatment of NPs leads to degradation of the sample.

It was previously reported that NP7 has some unique structural features among the NPs [6,7,10,52,53] and it is interesting to note that different electrochemical reduction efficiencies are obtained for the two proteins. The most important difference between NP4 and NP7 is the surface charge that allows NP7 to bind to negatively charged phospholipid membranes, which NP1-4 cannot do [6,7]. This difference could account for different interaction with the electrochemical mediators as well as with $S_2O_4^{2-}/SO_2^{\bullet-}$ and, thus, to influence the interaction with Cys – Cys.

3.8. Alternative reductants

Other biocompatible reductants with reduction potentials that are low enough to assess the Fe^{II} oxidation state of NPs may be considered which are capable to effectively reduce the NP heme iron, but less effectively the Cys – Cys. The following compounds were examined: [Methyl viologen]$^{\bullet+}$ (−447 mV) [54],[3] Ti^{III}–citrate (<−800 mV) [55],[4] and $NaBH_4$ (<−1,000 mV). The potential of these compounds to reduce disulfides was examined with GSSG as described in Section 3.3 where TCEP or $Na_2S_2O_4$ were simply substituted by the same concentrations of the alternative compounds (see Fig. 3). The results are presented in Fig. S4 in the Supporting Information section. In conclusion, only in the case of methyl viologen breaking of the disulfide bond was obtained.

All three compounds were also tested for their ability to reduce the NP7 heme iron (data not shown). In summary, where [methyl viologen]$^{\bullet+}$ and Ti^{III}–citrate are very effective in the reduction of the iron (stoichiometric amounts), in the case of $NaBH_4$ large quantities are required, though it was sometimes sufficiently used for the reduction of heme proteins [56]. Where [methyl viologen]$^{\bullet+}$ does not represent a better alternative for $Na_2S_2O_4$, because of the Cys – Cys reduction and the necessary pre-preparation of the cation radical, Ti^{III}–citrate does in principle host the potential to be an effective reducing agent for NP heme. However, because of the high sensitivity of Ti^{III} salts toward O_2, the handling and preparation of Ti^{III}–citrate is a lot more elaboratous and it was found that the careful titration of NPs with $Na_2S_2O_4$ under the control of UV–vis spectroscopy is a much more convenient for routine work.

4. Conclusions

For the preparation of ferrous NP4 and NP7 anaerobic conditions are required. Dithionite and electrochemical reduction break the disulfide bonds in both NP4 and NP7 in an unspecific manner. The products from Cys – Cys disulfide breakage by $Na_2S_2O_4$ are one thiol/thiolate CysH/Cys^- and the cysteine-*S*-thiosulfate (Cys – SO_3^-), where it is not clear if (an) intermediate compound(s) may appear and to what extend other side reactions may occur.

The products from electrochemical reduction of NP4 are much more uniform resulting in two CysH where NP7 yields an unknown mixture of products similar to the treatment with $Na_2S_2O_4$. However, it is important to note that the electrochemical reduction is a slow process, so that in case of limited treatment only a small fraction of NP4 or NP7 will be affected. This can be explained by the limited accessibility of the cystines in the protein structure, which can be estimated from Fig. S2 in the Supporting Information. Moreover, although electrochemical reduction of the protein cystines in NPs does occur during spectroelectrochemical titrations, the conditions usually applied are less intense, *i.e.*, shorter reaction times are typically used. This together with the limited reduction because of sterical shielding allows the conclusion that the reported reduction potentials are reliable.

For the preparation of ferroheme NPs it is important that the corruption of cystines by $Na_2S_2O_4$ can be prevented by titration with the reductant under control of absorption spectroscopy. Furthermore, the reduction of cystines by $S_2O_4^{2-}$ is important not only for the handling of NPs, but also for other heme proteins and proteins that bind redox active metals. For example, both the human heme proteins cytoglobin (Cygb) and neuroglobin (Ngb) contain a pair of Cys that is able to form a disulfide bond, which has impact on the proteins' functionality [57,58]. In contrast to the extracellular NPs, the oxidation/reduction of the disulfide bonds of these cytosolic proteins may have important physiological consequences. Other examples of disulfide containing heme proteins are horseradish peroxidase (HRP) [59], lactoperoxidase (LPO) [60], FixL from *Sinorhizobium meliloti* [61], human heme oxygenase-2 (HO-2) [62,63], or the human BK channel [64].

Abbreviations

CHCA	α-cyano-4-hydroxy-cinnamic acid
Cygb	cytoglobin
DHB	2,5-dihydroxobenzoic acid
DTPA	diethylenetriamine-pentaacetic acid
GSH	reduced glutathione
GSSG	oxidized glutathione
Hm	histamine

[3] Prior to use, the cation radical of methyl viologen was freshly prepared in an anaerobic environment by reduction with $Na_2S_2O_4$.

[4] Ti^{III}–citrate was freshly prepared by dissolving of $TiCl_3$ crystals in anaerobic Na_3citrate solution with a stoichiometry of 1:2 (Ti^{III}/citrate).

IAM 2-iodoacetamide
ImH imidazole
MALDI-TOF MS matrix assisted laser desorption/ionization time-of-flight mass spectrometry
merbromin 2,7-dibrom-4-(hydroxymercuri)-fluorescein
Mb myoglobin
Ngb neuroglobin
NP nitrophorin
NOS nitric oxide synthase
OTTLE optical transparent thin-layer electrochemical
p-CMBS 4-(chloromercury)bezyl sulfonate
p-MBS 4-mercuryphenyl sulfonate
RPC reverse phase chromatography
SA 3-(4-hydroxy-3,5-dimethoxyphenyl)prop-2-enoic acid
SHE standard hydrogen electrode
TCEP tris-(carboxyethyl)phosphine

Acknowledgments

The authors are thankful for the technical assistance of Jörg Bitter, Norbert Dickmann, Heinz-Werner Klein (MPI für Kohleforschung), Dagmar Merkl, Gabriele Schmitz, and Manuela Trinoga. This work was financially supported by the Max Planck Society (MPG) and by the Deutsche Forschungsgemeinschaft (DFG), grant KN 951/1-1 (to M.K.).

Appendix A. Supplementary data

Supplementary data to this article can be found online at doi:10.1016/j.jinorgbio.2011.07.009.

References

[1] M.J. Lehane, The Biology of Blood-Sucking in Insects, 2 ed. Cambridge University Press, Cambridge (United Kingdom), 2005.
[2] J.M.C. Ribeiro, J.M. Hazzard, R.H. Nussenzveig, D.E. Champagne, F.A. Walker, Science 260 (1993) 539–541.
[3] J.F. Andersen, N.P. Gudderra, I.M.B. Francischetti, J.M.C. Ribeiro, Arch. Insect Biochem. Physiol. 58 (2005) 97–105.
[4] J.F. Andersen, D.E. Champagne, A. Weichsel, J.M.C. Ribeiro, C.A. Balfour, V. Dress, W.R. Montfort, Biochemistry 36 (1997) 4423–4428.
[5] J.F. Andersen, W.R. Montfort, J. Biol. Chem. 275 (2000) 30496–30503.
[6] J.F. Andersen, N.P. Gudderra, I.M.B. Francischetti, J.G. Valenzuela, J.M.C. Ribeiro, Biochemistry 43 (2004) 6987–6994.
[7] M. Knipp, H. Zhang, R.E. Berry, F.A. Walker, Protein Expr. Purif. 54 (2007) 183–191.
[8] J.M.C. Ribeiro, I.M.B. Francischetti, Annu. Rev. Entomol. 48 (2003) 73–88.
[9] A.C. Soares, J. Carvalho-Tavares, N.d.F. Gontijo, V.C. dos Santos, M.M. Teixeira, M.H. Pereira, J. Insect Physiol. 52 (2006) 468–472.
[10] M. Knipp, F. Yang, R.E. Berry, H. Zhang, M.N. Shokhirev, F.A. Walker, Biochemistry 46 (2007) 13254–13268.
[11] C. He, M. Knipp, J. Am. Chem. Soc. 131 (2009) 12042–12043.
[12] C. He, H. Ogata, M. Knipp, Biochemistry 49 (2010) 5841–5851.
[13] A. Weichsel, J.F. Andersen, D.E. Champagne, F.A. Walker, W.R. Montfort, Nat. Struct. Biol. 5 (1998) 304–309.
[14] F.A. Walker, J. Inorg. Biochem. 99 (2005) 216–236.
[15] D.R. Flower, A.C.T. North, C.E. Sansom, Biochim. Biophys. Acta 1482 (2000) 9–24.
[16] M. Hoshino, M. Maeda, R. Konishi, H. Seki, P.C. Ford, J. Am. Chem. Soc. 118 (1996) 5702–5707.
[17] R.E. Berry, M.N. Shokhirev, A.Y.W. Ho, F. Yang, T.K. Shokhireva, H. Zhang, A. Weichsel, W.R. Montfort, F.A. Walker, J. Am. Chem. Soc. 131 (2009) 2313–2327.
[18] T.K. Shokhireva, R.E. Berry, E. Uno, C.A. Balfour, H. Zhang, F.A. Walker, Proc. Natl. Acad. Sci. U.S.A. 100 (2003) 3778–3783.
[19] X.D. Ding, A. Weichsel, J.F. Andersen, T.K. Shokhireva, C. Balfour, A.J. Pierik, B.A. Averill, W.R. Montfort, F.A. Walker, J. Am. Chem. Soc. 121 (1999) 128–138.
[20] T.G. Traylor, V.S. Sharma, Biochemistry 31 (1992) 2847–2849.
[21] K. Nienhaus, E.M. Maes, A. Weichsel, W.R. Montfort, G.U. Nienhaus, J. Biol. Chem. 279 (2004) 39401–39407.
[22] A. Benabbas, X. Ye, M. Kubo, Z. Zhang, E.M. Maes, W.R. Montfort, P.M. Champion, J. Am. Chem. Soc. 132 (2010) 2811–2820.
[23] E.M. Maes, S.A. Roberts, A. Weichsel, W.R. Montfort, Biochemistry 44 (2005) 12690–12699.
[24] R.E. Berry, X.D. Ding, T.K. Shokhireva, A. Weichsel, W.R. Montfort, F.A. Walker, J. Biol. Inorg. Chem. 9 (2004) 135–144.
[25] R.E. Berry, T.K. Shokhireva, I. Filippov, M.N. Shokhirev, H. Zhang, F.A. Walker, Biochemistry 46 (2007) 6830–6843.
[26] J.M.C. Ribeiro, Insect Biochem. Mol. Biol. 26 (1996) 899–905.
[27] C. Creutz, N. Sutin, Proc. Natl. Acad. Sci. U.S.A. 70 (1973) 1701–1703.
[28] J.F. Andersen, X.D. Ding, C. Balfour, T.K. Shokhireva, D.E. Champagne, F.A. Walker, W.R. Montfort, Biochemistry 39 (2000) 10118–10131.
[29] J.M.C. Ribeiro, Insect Biochem. Mol. Biol. 28 (1998) 1051–1057.
[30] O.W. Griffith, D.J. Stuehr, Annu. Rev. Physiol. 57 (1995) 707–736.
[31] M. Knipp, C. He, IUBMB Life 63 (2011) 304–312.
[32] R.B. Simpson, J. Am. Chem. Soc. 83 (1961) 4711–4717.
[33] E.J. Zaluzec, D.A. Gage, J.T. Watson, J. Am. Soc. Mass Spectrom. 5 (1994) 359–366.
[34] S.L. Cohen, J.C. Padovan, B.T. Chait, Anal. Chem. 72 (2000) 574–579.
[35] D.J. Kutscher, M.E. del Castillo Busto, N. Zinn, A. Sanz-Medel, J. Bettmer, J. Anal. At. Spectrom. 23 (2008) 1359–1364.
[36] M. Xu, X. Yan, Q. Xie, L. Yang, Q. Wang, Anal. Chem. 82 (2010) 1616–1620.
[37] M. Borissova, R. Mahlapuu, M. Vaher, Talanta 83 (2010) 274–280.
[38] Y.-F. Huang, H.-T. Chang, Anal. Chem. 78 (2006) 1485–1493.
[39] F. Åslund, K.D. Berndt, A. Holmgren, J. Biol. Chem. 272 (1997) 30780–30786.
[40] M. Huber-Wunderlich, R. Glockshuber, Folding Des. 3 (1998) 161–171.
[41] G. Krause, J. Lundström, J.L. Barea, C. Pueyo de la Cuesta, A. Holmgren, J. Biol. Chem. 266 (1991) 9494–9500.
[42] S.V. Makarov, Russ. Chem. Rev. 70 (2001) 885–895.
[43] S.G. Mayhew, Eur. J. Biochem. 85 (1978) 535–547.
[44] R.-Y. Tang, P. Zhong, Q.-I. Lin, J. Fluorine Chem. 127 (2006) 948–953.
[45] R.-y. Tang, P. Zhong, Q.-l. Lin, Synthesis (2007) 85–91.
[46] R.-Y. Tang, P. Zhong, Q.-l. Lin, Phosphorous, Sulfur, and Silicon 182 (2007) 167–174.
[47] A.P. Senft, T.P. Dalton, H.G. Shertzer, Anal. Biochem. 280 (2000) 80–86.
[48] G. Jung, E. Breitmaier, W. Voelter, Eur. J. Biochem. 24 (1972) 438–445.
[49] D.E. Green, Biochem. J. 27 (1933) 678–689.
[50] S. Antonello, K. Daasbjerg, H. Jensen, F. Taddei, F. Maran, J. Am. Chem. Soc. 125 (2003) 14905–14919.
[51] S. Antonello, R. Benassi, G. Gavioli, F. Taddei, F. Maran, J. Am. Chem. Soc. 124 (2002) 7529–7538.
[52] F. Yang, H. Zhang, M. Knipp, Biochemistry 48 (2009) 235–241.
[53] F. Yang, M. Knipp, T.K. Shokhireva, R.E. Berry, H. Zhang, F.A. Walker, J. Biol. Inorg. Chem. 14 (2009) 1077–1095.
[54] F.M. Hawkridge, T. Kuwana, Anal. Chem. 46 (1973) 1021–1026.
[55] M. Guo, F. Sulc, M.W. Ribbe, P.J. PFarmer, B.K. Burgess, J. Am. Chem. Soc. 124 (2002) 12100–12101.
[56] M.R. Kumar, J.M. Fukuto, K.M. Miranda, P.J. Farmer, Inorg. Chem. 49 (2010) 6283–6292.
[57] D. Hamdane, L. Kiger, S. Dewilde, B.N. Green, A. Pesce, J. Uzan, T. Burmester, T. Hankeln, M. Bolognesi, L. Moens, M.C. Marden, J. Biol. Chem. 278 (2003) 51713–51721.
[58] C. Lechauve, C. Chauvierre, S. Dewilde, L. Moens, B.N. Green, M.C. Marden, C. Célier, L. Kiger, FEBS J. (2010) 1–9.
[59] L. Smeller, F. Meersman, J. Fidy, K. Heremans, Biochemistry 42 (2003) 553–561.
[60] A.K. Singh, R.P. Kumar, N. Pandey, N. Singh, M. Sinha, A. Bhushan, P. Kaur, S. Sharma, T.P. Singh, J. Biol. Chem. 285 (2010) 1569–1576.
[61] S. Akimoto, A. Tanaka, K. Nakamura, Y. Shiro, H. Nakamura, Biochem. Biophys. Res. Commun. 304 (2003) 136–142.
[62] L. Yi, S.W. Ragsdale, J. Biol. Chem. 282 (2007) 21056–21067.
[63] L. Yi, P.M. Jenkins, L.I. Leichert, U. Jakob, J.R. Martens, S.W. Ragsdale, J. Biol. Chem. 284 (2009) 20556–20561.
[64] L. Yi, J.T. Morgan, S.W. Ragsdale, J. Biol. Chem. 285 (2010) 20117–20127.
[65] D.A. Kondrashov, S.A. Roberts, A. Weichsel, W.R. Montfort, Biochemistry 43 (2004) 13637–13647.
[66] N. Guex, M.C. Peitsch, Electrophoresis 18 (1997) 2714–2723.

Reduction of the heme containing protein nitrophorin – Sensitivity of the fold-stabilizing cysteine disulfides toward routine heme-upon reduction

Markus Knipp[†††], Johanna J. Taing, Chunmao He

Max-Planck-Institut für Bioanorganische Chemie, Stiftstrasse 34-36, D-45470 Mülheim an der Ruhr, Germany

* Supporting Information *

[†††] Submit correspondence to: Dr. Markus Knipp, Max-Planck-Institut für Bioanorganische Chemie, Stifstrasse 34-36, D-45470 Mülheim an der Ruhr, Germany. Tel.: +49-(0)208-306-3581. Fax: +49-(0)208-306-3951. E-mail: mknipp@mpi-muelheim.mpg.de.

Table S1. Summary of thiol modifying reagents used throughout this study.

	Name	Molecular mass (Da)
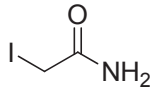	iodoacetamide, IAM	184.97
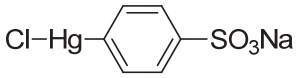	sodium *para*-chloromercurybenzylsulfonate, *p*-CMBS	415.19
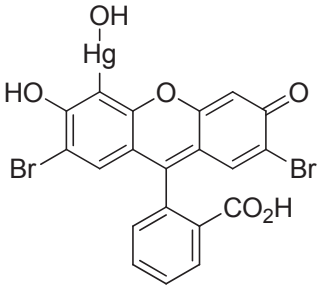	merbromin, 2,7-dibromo-4-(hydroxymercury)-fluorescein	706.69

Scheme S1. Chemical Structures of (*top*) reduced glutathione (GSH, 307.36 Da) and (*bottom*) oxidized glutathione (GSSG, 612.70 Da).

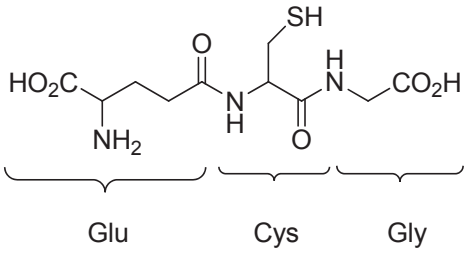

GSH

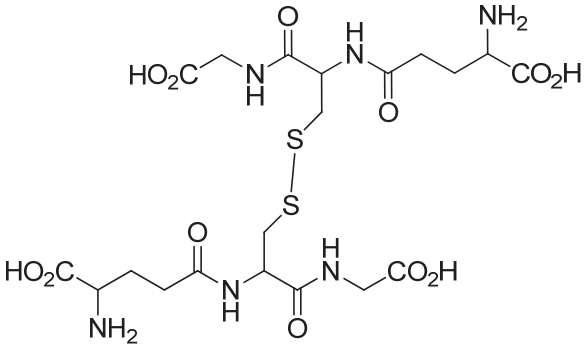

GSSG

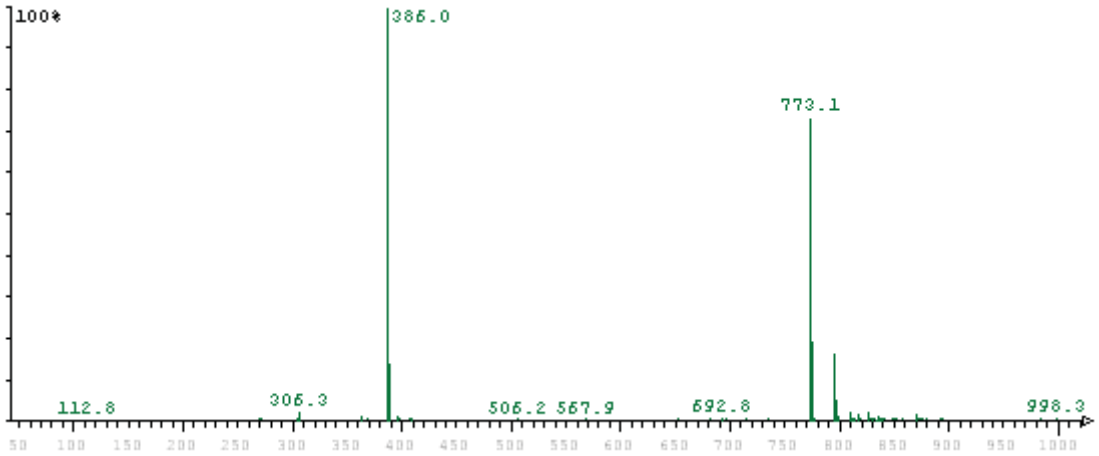

Figure S1. ESI MS (negative mode) of the product of the reduction of GSSG with $Na_2S_2O_4$, termed GSX, upon purification by C_{18}-RPC (see Fig. 5). The sample was injected as a solution in CH_3OH. The following masses were identified and assigned as follows:
386 Da: $[GS–SO_3H – H]^-$
773 Da: $[2GS–SO_3H – H]^-$
795 Da: $[2GS–SO_3H + Na – H]^-$

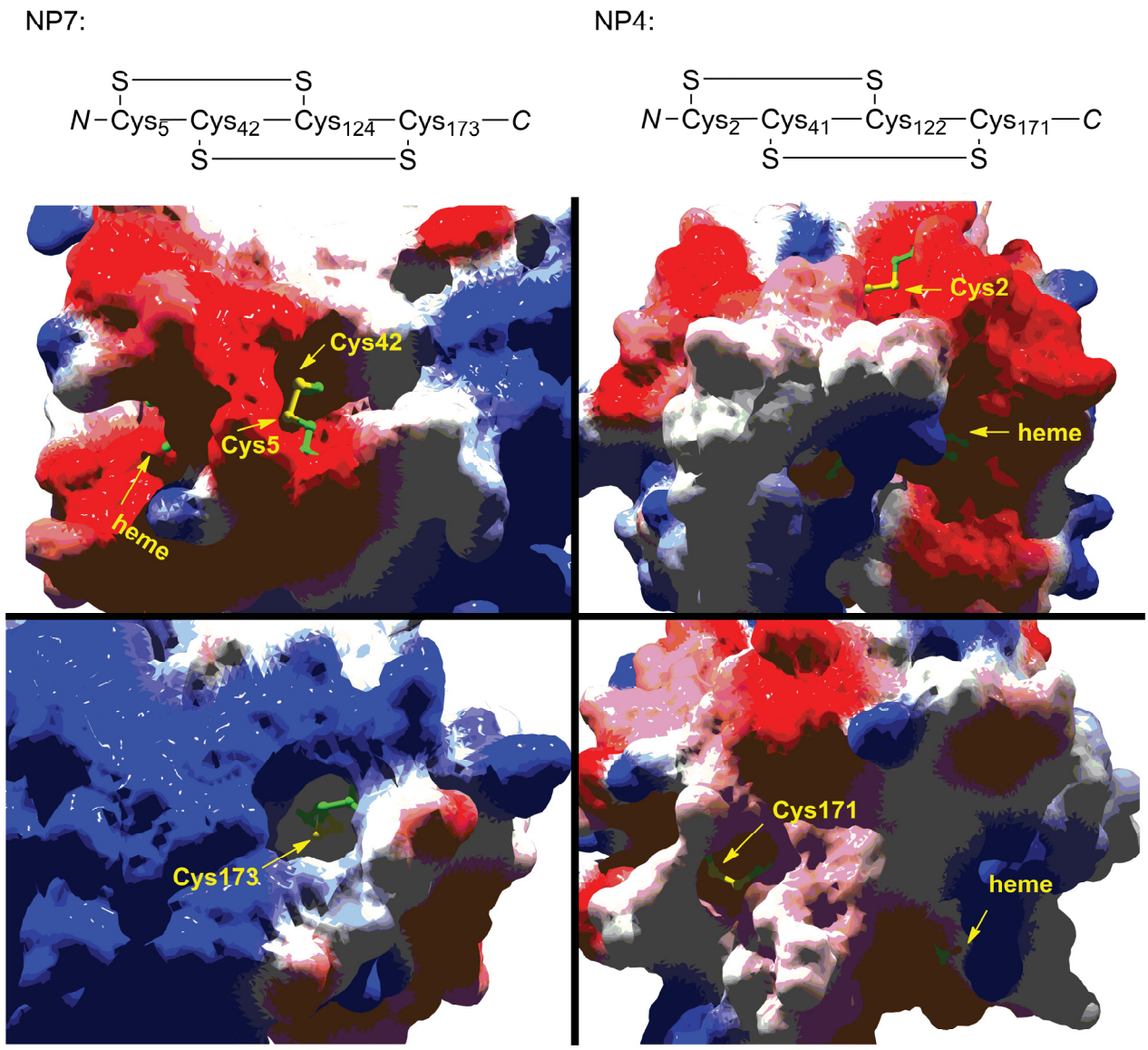

Figure S2. Position of the two Cys–Cys disulfide bonds in the NP7 and NP4 structure. A surface representation of the calculated electrostatic potential of the homology model of NP7 [1] and the X-ray structure of NP4 (PDB #1X8P) [2] was created with SWISS PDB VIEWER V 4.01 (http://www.expasy.org/PDBviewer/) [3]. The structures were rendered with POVRAY V. 3.6 (http://www.povray.org/). The cystines and the heme cofactor are depicted in a ball-and-stick model as indicated.

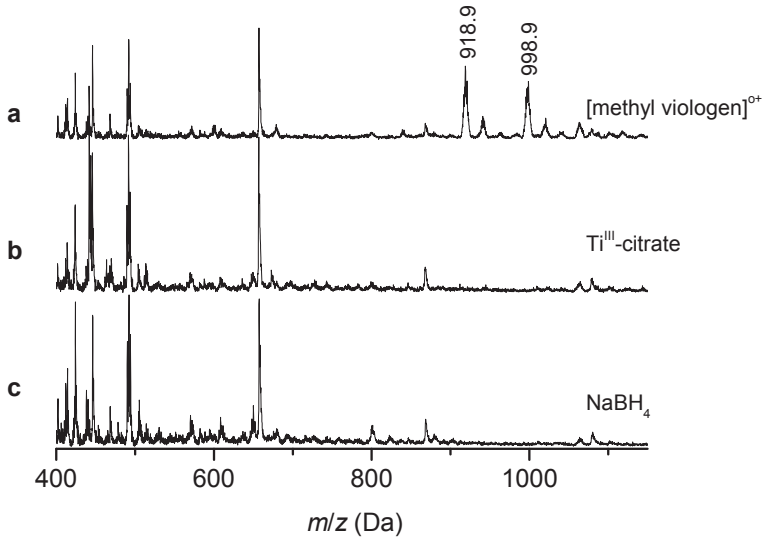

Figure S3. MALDI-TOF MS analysis of the reduction of GSSG with [methyl viologen]$^{\bullet+}$, Ti^{III}-citrate, and $NaBH_4$. 1 mM of GSSG in 100 mM NaH_2PO_4/NaOH, 100 µM DTPA (pH 7.5) was incubated for 1 h at room temperature with 1 mM of (a) [methyl viologen]$^{\bullet+}$, (b) Ti^{III}-citrate, and (c) $NaBH_4$ under anaerobic conditions Afterwards, 2 mM of merbromin was added and incubated for 1 h at room temperature. The samples were then analyzed by MALDI-TOF MS using a CHCA matrix. The two peaks at 919 Da and 999 Da can be attributed to [GS–merbromin + H]$^+$ and [GS–merbromin' + H]$^+$ (merbromin' = merbromin upon abstraction of one Br).

References

[1] M. Knipp, F. Yang, R.E. Berry, H. Zhang, M.N. Shokhirev, F.A. Walker, Biochemistry 46 (2007) 13254-13268.

[2] D.A. Kondrashov, S.A. Roberts, A. Weichsel, W.R. Montfort, Biochemistry 43 (2004) 13637-13647.

[3] N. Guex, M.C. Peitsch, Electrophoresis 18 (1997) 2714-2723.

Chapter 7. Breaking the proximal Fe^{II}–N_{His} bond in heme proteins through local structural tension: Lessons from the heme *b* proteins nitrophorin 4, nitrophorin 7, and related site-directed mutant proteins[‡‡‡]

(He, C.; Neya, S.; Knipp, M. *Biochemistry* **2011**, *50*, 8559-8575)

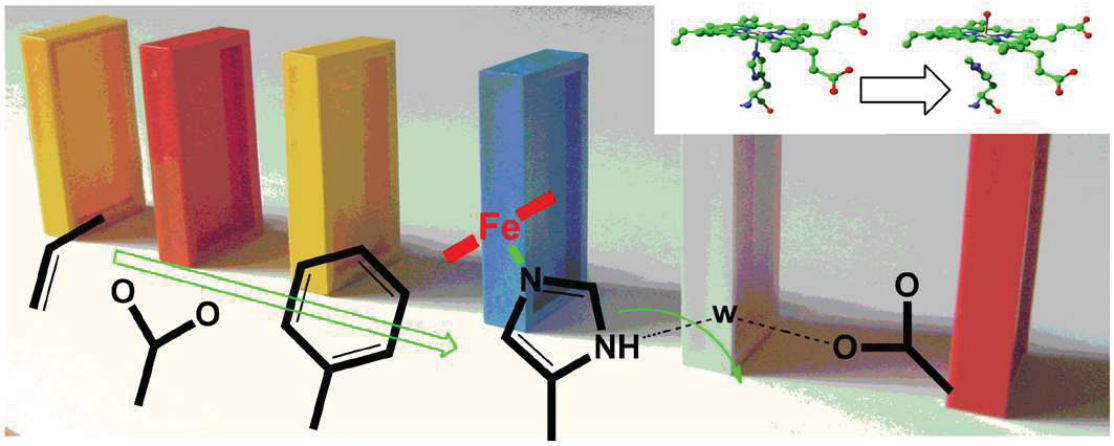

[‡‡‡]Reprinted with permission from He, C., Neya, S., Knipp, M. *Biochemistry* **2011**, *50*, 8559-8575. Copyright 2011 American Chemical Society.

Abstract

The factors leading to the breakage of the proximal iron-histidine bond in the ferroheme protein soluble guanylate cyclase (sGC) are still a matter of debate. This event is a key mechanism in the sensing of NO which leads to the production of the second messenger molecule cGMP. Surprisingly, in the heme protein nitrophorin 7 (NP7), it was noticed by UV-vis absorbance spectroscopy and resonance Raman spectroscopy that heme reduction leads to a loss of the proximal histidine coordination, which is not observed for the other isoproteins NP1-4. Structural considerations led to the generation and spectroscopic investigation of the site directed mutants NP7(E27V), NP7(E27Q), NP4(D70A), and NP2(V24E). Spectroscopic investigation of these proteins shows that the spatial arrangement of the residues Glu27, Phe43, and His60 in the proximal heme pocket of NP7 is the reason for the weakened Fe^{II}–His60 bond through steric demand. Spectroscopic investigation of the sample of NP7 reconstituted with 2,4-dimethyldeuterohemin ("symmetric heme") demonstrated that the heme vinyl substituents are also responsible factors. Where the breaking of the iron-histidine bond is rarely seen among unliganded ferroheme proteins, the breakage of the Fe^{II}–His bond upon binding of NO to the sixth coordination site is sometimes observed due to the negative *trans* effect of NO. However, it is still a rare case among the heme proteins which is in contrast to *trans* liganded nitrosyl model hemes. Thus, the question arises which factors determine the Fe^{II}–His bond labilization in proteins. Surprisingly, the mutant NP2(V24E) turned out to be particularly behaving similar to sGC, i.e., the Fe^{II}–His bond is sensitive to breakage upon NO binding where the unliganded form binds the proximal His at neutral pH. To the best of our knowledge, NP2(V24E) is the first example where the ability for the His-on↔His-off switch was engineered into a heme protein by site-directed mutagenesis other than the proximal His itself. Steric tension is, therefore, introduced as a potential structural determinant for the proximal Fe^{II}–His bond breakage in heme proteins.

BIOCHEMISTRY
including biophysical chemistry & molecular biology

Article

pubs.acs.org/biochemistry

Breaking the Proximal Fe^{II}–N_{His} Bond in Heme Proteins through Local Structural Tension: Lessons from the Heme *b* Proteins Nitrophorin 4, Nitrophorin 7, and Related Site-Directed Mutant Proteins

Chunmao He,[†] Saburo Neya,[‡] and Markus Knipp*[,†]

[†]Max-Planck-Institut für Bioanorganische Chemie, Stiftstrasse 34-36, D-45470 Mülheim an der Ruhr, Germany

[‡]Department of Physical Chemistry, Graduate School of Pharmaceutical Sciences, Chiba University, Image-Yayoi, Chiba 263-8522, Japan

Supporting Information

ABSTRACT: The factors leading to the breakage of the proximal iron–histidine bond in the ferroheme protein soluble guanylate cyclase (sGC) are still a matter of debate. This event is a key mechanism in the sensing of NO that leads to the production of the second-messenger molecule cGMP. Surprisingly, in the heme protein nitrophorin 7 (NP7), we noticed by UV–vis absorbance spectroscopy and resonance Raman spectroscopy that heme reduction leads to a loss of the proximal histidine coordination, which is not observed for the other isoproteins (NP1–4). Structural considerations led to the generation and spectroscopic investigation of site-directed mutants NP7(E27V), NP7(E27Q), NP4(D70A), and NP2(V24E). Spectroscopic investigation of these proteins shows that the spatial arrangement of residues Glu27, Phe43, and His60 in the proximal heme pocket of NP7 is the reason for the weakened Fe^{II}–His60 bond through steric demand. Spectroscopic investigation of the sample of NP7 reconstituted with 2,4-dimethyldeuterohemin ("symmetric heme") demonstrated that the heme vinyl substituents are also responsible. Whereas the breaking of the iron–histidine bond is rarely seen among unliganded ferroheme proteins, the breakage of the Fe^{II}–His bond upon binding of NO to the sixth coordination site is sometimes observed because of the negative *trans* effect of NO. However, it is still rare among the heme proteins, which is in contrast to the case for *trans* liganded nitrosyl model hemes. Thus, the question of which factors determine the Fe^{II}–His bond labilization in proteins arises. Surprisingly, mutant NP2(V24E) turned out to be particularly similar in behavior to sGC; i.e., the Fe^{II}–His bond is sensitive to breakage upon NO binding, whereas the unliganded form binds the proximal His at neutral pH. To the best of our knowledge, NP2(V24E) is the first example in which the ability to use the His-on ↔ His-off switch was engineered into a heme protein by site-directed mutagenesis other than the proximal His itself. Steric tension is, therefore, introduced as a potential structural determinant for proximal Fe^{II}–His bond breakage in heme proteins.

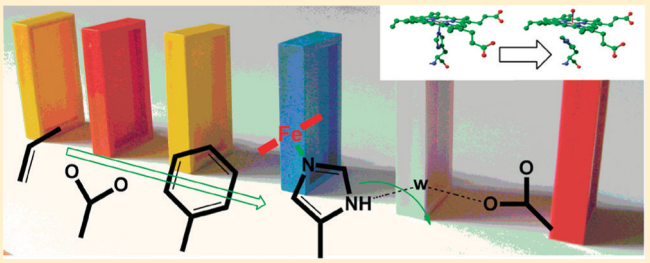

Nitrophorins (NPs) comprise a unique class of ferriheme proteins originating from the blood-feeding insect *Rhodnius prolixus*. The biological function of the NPs is the storage, transport, and delivery of NO from the insect to the host tissue, where NO acts as a vasodilator and blood-coagulation inhibitor.[2] The reactive molecule NO (in vivo, $t_{1/2} \approx 100$ ms)[3] is preserved through coordination to the heme iron inside the insect saliva. The protein experiences a significant pH change when subjected to the acidic pH of the saliva (between pH 5 and 6)[4] versus that of the blood plasma (~7.4); consequently, the affinity for NO is decreased, so that NO release occurs in the host tissue.

In NPs, the heme cofactor is located inside an eight-stranded β-barrel, which is an unusual case for a heme protein.[5] The protein fold has been classified as a lipocalin type of fold, which is a very common fold in the proteome. It is typically found in proteins that bind lipophilic molecules. The heme iron is coordinated by a His residue where the sixth coordination site is open for coordination of various small ligands.[6]

In contrast to other ferriheme proteins, i.e., met-myoglobin (metMb), which are reduced by excess NO (the so-called "autoreduction"),[7] in NPs the Fe^{III} state is stabilized by a number of carboxylate residues near the heme pocket[8] in combination with a ruffled heme geometry,[9] so that the reduction potential is established at, for example, −303 mV versus the SHE at pH 7.5 for NP1 compared to ~0 mV versus the SHE at pH 7.5 for Mb.[10] This is important for NP function because ferroheme–NO, i.e., $\{FeNO\}^7$ in the notation of Enemark and Feltham,[11] association constants are too large ($K_{eq} = 10^{13}$–10^{14} M^{-1})[8−10,12−14] to allow sufficient NO release under in vivo conditions.[15] In contrast, the NO association constants of ferriheme NPs, i.e., $\{FeNO\}^6$, are significantly smaller, for example, 4.0×10^6 M^{-1} for NP7 at pH 7.5.[14]

Received: July 12, 2011
Revised: August 24, 2011
Published: August 25, 2011

Although nitrophorins are ferriheme proteins, the Fe^{II} state came recently into focus when the Fe^{II}−CO derivative was used as a model for the $\{FeNO\}^6$ complex, for example, in FT-IR and laser flash photolysis experiments.[16,17] Previously, the crystal structures of several NP4[Fe^{II}] derivatives were reported.[18] Furthermore, the determination of $Fe^{III} \rightarrow Fe^{II}$ reduction potentials by spectroelectrochemistry was extensively used for the characterization of NP structure−function relationships.[8−10,12−14] Moreover, the Fe^{II} state was proposed as an intermediate in the reduction of the NP iron center with several low-molecular weight thiols.[19] Therefore, deeper investigation of the properties of ferroheme nitrophorins is required.

In a broader context, the production, handling, and sensing of NO in vertebrates are eminently associated with heme proteins. Thus, the NO production is performed at the heme-containing active site of nitric oxide synthases (NOSs).[20] This cytochrome P450 type of enzyme acts in the higher oxidation states of iron, so that the product NO is bound to the ferriheme protein. In contrast, the sensing of NO by soluble guanylate cyclase (sGC) is performed in the Fe^{II} oxidation state.[21] Recently, the involvement of other heme proteins, in particular the globins, with respect to NO signaling and the associated handling of this radical was brought to attention.[22,23] The members of this class of heme proteins are typically in the Fe^{II} oxidation state, which then forms very stable complexes with NO. However, recently, the partial existence of met-globins, in particular met-hemoglobin (metHb), in conjunction with the NO metabolism is discussed. Altogether, comparison of the properties of heme proteins improves our understanding of the structure−function relationships. At present, a systematic investigation of the ferroheme NPs is missing. Therefore, this study was initiated with the aim of investigating the properties of ferroheme nitrophorins NP4 and NP7.

EXPERIMETAL PROCEDURES

Materials. Stock solutions of $Na_2S_2O_4$ were prepared freshly before use. The effective concentration of $Na_2S_2O_4$ was determined through reduction of $[Fe(CN)_6]^{3-}$ in deaerated water (ε_{420} = 1026 M^{-1} cm^{-1}).[24] All reagents were of the highest grade commercially available and used as received. Catalase and glucose oxidase (both from *Aspergillus niger*) were bought from Serva. *S*-[^{15}N]Nitrosoglutathione ($GS^{15}NO$) was prepared as previously described.[25,26] Iron 2,4-dimethyldeuteroporphyrin ("symmetric heme") was prepared as previously described.[27]

Most experiments were performed under strictly anaerobic conditions inside an anaerobic tent (Coy Ltd.) with an atmosphere consisting of 98% N_2 and 2% H_2 in the presence of Pd catalysts. All solutions were rendered essentially O_2 free by three freeze−pump−thaw cycles performed on a vacuum line ($p < 0.5 \times 10^{-4}$ mbar). In addition, after the solutions were brought to the anaerobic environment, they were supplemented with 100 mM D-glucose, 0.1 mg/mL glucose oxidase, and 300 units/mL catalase.[28]

Molecular Biology. For the expression of the mutant protein NP4(D70A), plasmid pNP4(D70A)^{Kan} was generated by the QuikChange mutagenesis method[29] from the *wt* NP4 expression plasmid[12] using *Pfu* DNA polymerase (Stratagene). The following primers were used: 5′-TGG TAC GTG ACA GAT TAC CTA AAC TTG GAA CCT GAC GAC GTT CCA-3′ and 5′-TGG AAC GTC GTC AGG TTC CAA GTT TAG GTA ATC TGT CAC GTA CCA-3′ (the sites of mutation are underlined). The correctness of the coding regions of all expression plasmids was confirmed via DNA sequencing.

Production of Recombinant Proteins. Prior to expression, plasmids were transformed into *Escherichia coli* strain BL21(DE3) (Novagen). NP4 and NP4(D70A) were expressed, reconstituted, and purified as described previously for NP4.[13] The other proteins were reconstituted by a stepwise heme insertion described for the preparation of NP7.[30,31] The protein preparations were judged by sodium dodecyl sulfate−polyacrylamide gel electrophoresis to be >90% pure. Proteins were also subjected to MALDI MS to confirm the correct molecular masses, including two Cys−Cys disulfide bonds: calcd for $[NP4 + H]^+$ 20264 Da, observed 20,296 Da; calcd for $[NP4(D70A) + H]^+$ 20220 Da, observed 20225 Da; calcd for $[NP7 + H]^+$ 20969 Da, observed 21002 Da; calcd for $[NP7(E27Q) + H]^+$ 20969 Da, observed 20975 Da; calcd for $[NP7(E27V) + H]^+$ 20939 Da, observed 20939 Da; calcd for $[NP2(V24E) + H]^+$ 20080 Da, observed 20070 Da. Proteins were kept at −20 °C in 200 mM NaOAc/HOAc and 10% (v/v) glycerol (pH 5.0) until use.

Absorption Spectroscopy. A Cary-50 spectrophotometer (Varian, Inc.) equipped with an opto coupler (Varian, Inc.) was placed outside the glovebox. The light beam was led inside and outside the glovebox by glass fibers (Ocean Optics) that were connected to a cuvette holder (Ocean Optics). Thus, absorbance spectra were recorded under O_2-free conditions in quartz cuvettes. pH titrations were performed in a 3 mL cuvette with a small pH glass electrode inserted into the solution such that the electrode did not cross the beam. pH titrations were performed with dilute HOAc or KOH solutions, and the actual pH was read upon mixing.

Resonance Raman Spectroscopy. To largely deplete the protein solution of O_2, the solvent was exchanged with the respective anaerobic buffer inside the glovebox and the protein concentration was adjusted to ∼25 μM. The ferroheme species was prepared by careful titration with stoichiometric amounts of a freshly prepared $Na_2S_2O_4$ solution. To form the NO complexes, the protein solution was thereafter titrated with a DEA/NO solution in 10 mM NaOH under photometric control. The ^{15}NO complexes were prepared by incubation with $GS^{15}NO$ in the presence of catalytic amounts of CuCl.[14,a] Ambient-temperature measurements were performed in a rotating cylindrical quartz cuvette (5.5 cm diameter, ∼3 mL volume), which was closed with rubber stoppers to prevent reoxidation. The integrity of the samples was monitored by the recoding of a second spectrum right after the original measurement. In the case of a significant difference, i.e., indicating oxidation, the spectra were discarded. RR spectra were recorded with a scanning double monochromatic. The excitation line at 413.1 nm was provided by a coherent K-2 Kr^+ ion laser, and the sample was rotated throughout the measurement to minimize radiation damage.

RESULTS

Reduction of the Heme Iron of Nitrophorins with $Na_2S_2O_4$. We have shown elsewhere that the incubation of NP4 and NP7 with excess $Na_2S_2O_4$, which is a common method for the formation of ferroheme proteins, leads to protein damage because of the reduction of the two Cys−Cys disulfides contained in the protein structure.[32] Furthermore, it was previously reported that the reduced NP4 was somehow unstable,[18,33] and we had shown that this results from the presence of atmospheric O_2.[34] As a consequence, ferroheme

NPs in this study were exclusively prepared by the careful titration with stoichiometric amounts of $Na_2S_2O_4$. The preparation was monitored by UV−vis absorption spectroscopy, and the reduced compounds were handled under strictly anaerobic conditions thereafter. As one can see from Figure 1A,

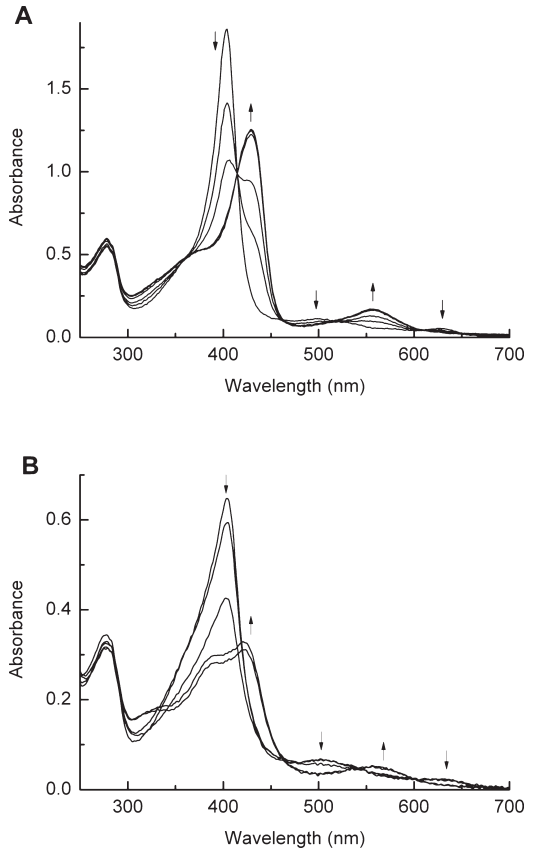

Figure 1. Reduction of (A) 12 μM NP4 and (B) 8.6 μM NP7 with $Na_2S_2O_4$ in 100 mM MOPS/NaOH and 50 mM NaCl (pH 7.5) monitored by UV−vis absorption spectroscopy under anaerobic conditions.

the titration of NP4 with $Na_2S_2O_4$ under anaerobic conditions leads to a shift of the Soret band absorption maximum from 403 to 429 nm and the appearance of a broad Q-band at ~557 nm, which is in good agreement with the previously reported data.[18] The spectral conversion is accompanied by good isosbestic behavior. In contrast, when the same experiment was performed with NP7 (see Figure 1B), two Soret band absorption maxima were found at 422 and 388 nm and a broad Q-band with a maximum at ~560 nm was obtained. Furthermore, the titration does not show isosbestic behavior, thus indicating the formation of more than one heme species.

Other ferroheme proteins with a proximal His, for example, sperm whale deoxyMb, exhibit a similarly blue-shifted Soret band when His coordination is lost[35,36] (compare in Table 1). This can happen particularly under acidic conditions; for example, at pH <4, deoxyMb undergoes a loss of secondary structure, which leads to a weakening of the Fe^{II}−His bond causing a Soret band shift from 434 to 383 nm. At this low pH, protonation of the proximal His N^{τ} atom competes with Fe^{II} coordination. However, in the case of NP7, the pH of 7.5 (Figure 1B) largely exceeds the typical pK_a of the His side chain (~6.0), and therefore, the reaction upon reduction may be

Scheme 1. Effect of One-Electron Reduction on the Coordination Environment of the Heme Iron in NP7

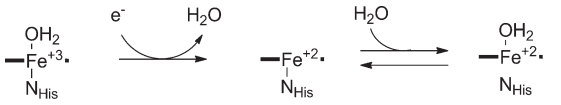

better described by an equilibrium depicted in Scheme 1. Furthermore, in contrast to Mb, of which the Soret band maximum at low pH is similar to the spectrum of free reduced hemin with absorbance maxima at 383 and ~581 nm (see Figure S2 of the Supporting Information), the absorption spectrum of NP7 at neutral pH is significantly different, which strongly indicates the integrity of the protein−heme complex.

Spectroscopic Characterization of NP4- and NP7-[Fe^{II}]. For the detailed elucidation of the coordination sphere of the single NP4[Fe^{II}] species and the two (or more) NP7[Fe^{II}] species observed in the UV−vis spectrum (Figure 1), RR spectra in the high-frequency range (1200−1650 cm^{-1}) were recorded at ambient temperature where the chromophore was excited into the Soret band at 413.1 nm. The resulting spectra are displayed in Figure 2 together with those of the

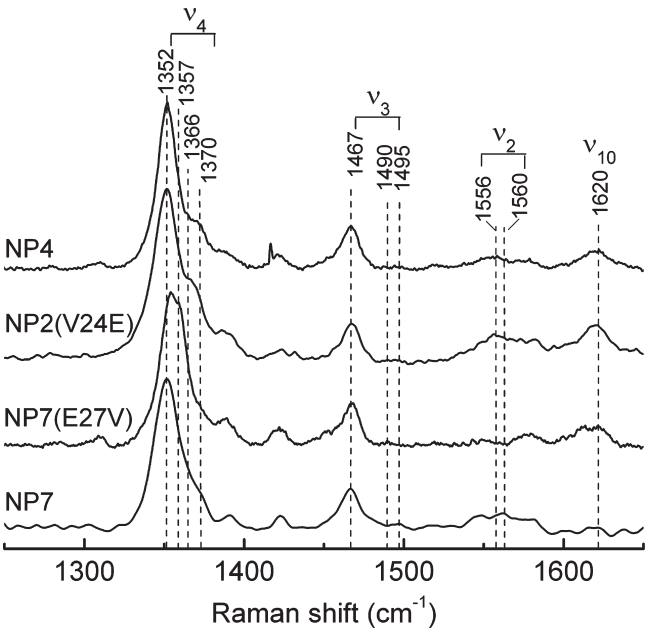

Figure 2. High-frequency region of the RR spectra of ~25 μM NP4[Fe^{II}], NP2(V24E)[Fe^{II}], NP7(E27V)[Fe^{II}], and NP7[Fe^{II}] in 100 mM MOPS/NaOH and 50 mM NaCl (pH 7.5) recorded at ambient temperature (λ_{ex} = 413.1 nm).

mutant proteins NP2(V24E)[Fe^{II}] and NP7(E27V)[Fe^{II}], which will be discussed later. The high-frequency region of the RR spectra of heme proteins includes information about the Fe coordination sphere and the spin state.[37,38] In Table 1, the Raman shift frequencies of selected resonances with diagnostic potential for the assignment of the oxidation state and spin state are summarized in comparison with those of several other ferroheme protein representatives.

The most prominent core-size marker band in the high-frequency region of the RR spectra of heme proteins is the oxidation state marker ν_4 that indicates the presence of a ferric (1370−1375 cm^{-1}) or ferrous iron oxidation state (1350−1375 cm^{-1}).[37,39−42] In NP4, the ν_4 of 1352 cm^{-1} clearly confirms the +2 oxidation state of the iron, although the appearance of a

Table 1. Comparison of the Electronic Absorption Maxima and Heme Raman Shifts of Ferrous Nitrophorins and Other Ferrous Heme Proteins with Proximal His Ligands Recorded at Room Temperature

		absorption maximum (nm)			Raman shift (cm^{-1})					
Fe^{II} protein	pH	λ_{Soret}	λ_{β}	λ_{α}	ν_4	ν_3	ν_2	Fe^{II} axial ligands	coordination number and spin state[a]	ref
NP1	7.5				1353	1467		His	5cHS	45
NP2(V24E)	7.5	425		556	1352	1467	1556	His	5cHS	tw[b]
NP4	7.5	429		556	1352	1467	1556	His	5cHS	tw[b]
NP7	7.5	422		561	1352	1467	1560	His	5cHS	tw[b]
		388			1366	1495		H_2O	5cHS	
NP7	5.5	386		574	1366	1491	1555	H_2O	5cHS	tw[b]
					1370	1504	1560	none	4cIS	
NP7	10.5	422	527	577	1355	1488	1576	His/OH^-	6cLS	tw[b]
NP7(E27V)	7.5	427		560	1354	1468		His	5cHS	tw[b]
					1357	1490		His/OH^-	6cLS	
NP7(E27Q)	7.5	422		560				His	5cHS	tw[b]
		392						H_2O	5cHS	
$NP7_{sym}$	7.5	410		~545				His	5cHS	tw[b]
Mb[c]	6.9	435		555	1354	1472	1563	His	5cHS	35
Mb[c]	3.8	426		546	1357	1495	1565	H_2O	5cHS	35
		383			1371	1504		no	4cIS	
cyt c'[d]	7.0				1352	1469	1577	His	5cHS	49
cyt c'[d]	12.0				1358	1488	1592	His/Lys	6cLS	49
cyt c'[e]	12.4				1360	1494	1585	His/Lys	6cLS	48
hHO-1(H25A)[f]	7.4	426	551	587	1357	1471	1562	?	5cHS	47
					1368	1500		none	4cIS	
*Vc*H-NOX[g]	7.5	429	568		1354	1471	1561	His	5cHS	108
*Tt*H-NOX[h]	7.5	431	565		1354	1471	1575	His	5cHS	108
NPAS2 bHLH-PAS-A[i]	8.0	426	530	559	1359	1471	1555		5cHS	109
						1493	1582		6cLS	
HRI[j]	8.0	426	531	560				His/?	6cLS	110
reduced hemin	7.5	381		~581						tw[b]

[a]HS, high-spin; LS, low-spin; IS, intermediate-spin. [b]This work. [c]From sperm whale. [d]From *Chromatium vinosum*. [e]From *Rhodospirillum rubrum*. [f]H25A mutant of human liver heme oxygenase. [g]H-NOX domain from *Vibrio cholerae*. [h]H-NOX domain from *Thermoaerobacter tengcongensis*. [i]N-Terminal basic helix−loop−helix (bHLH) motif of the first PAS (PAS-A) domain of NPAS2. [j]Heme-regulated eukaryotic initiator factor 2α kinase.

small shoulder at ~1370 cm^{-1} may indicate the presence of a small amount of ferric protein, i.e., developing from air oxidation during the recording of the spectra. Another important feature seen in Figure 2 is the so-called spin-state marker ν_3 that appears at 1467 cm^{-1}. The ν_3 porphyrin skeletal mode is well established to be sensitive to the heme core size, which changes with the spin state of the iron depending on the oxidation state, i.e., 1460−1470 cm^{-1} for a 5cHS Fe^{II} and 1490−1510 cm^{-1} for a 5cLS or 6cLS Fe^{II},[41−43] thus assigning NP4[Fe^{II}] as a His-liganded 5cHS. Comparison with the spectral features of deoxyMb also shows that the ν_2 and ν_{10} bands at 1556 and 1620 cm^{-1}, respectively, further support this assignment.[35,36,44] This is in contrast to the previous report about the NP4[Fe^{II}] X-ray structure at pH 7.5 [Protein Data Bank (PDB) entry 1YWD] where electron density was found on the distal site of the heme iron that was modeled as an O atom, i.e., water.[18] However, the release of water from the heme is typical upon reduction of Fe^{III} to Fe^{II} as was shown for many heme proteins, including NP1[Fe^{II}][45] (compare in Table 1).

Also in the case of NP7[Fe^{II}], the oxidation state marker ν_4 at 1352 cm^{-1} is well in the range of a ferrous heme; however, significant broadening of the band is noticed (Figure 2). This may be a consequence of the appearance of two or more different coordination environments on the iron, which is inferred already from the UV−vis spectrum (Figure 1). The ν_3 of 1467 cm^{-1}, like that for NP4[Fe^{II}], reflects a major fraction of His-liganded NP7[Fe^{II}]. Similar to the NP4 sample, a small fraction of reoxidized heme can be attributed to the shoulder at ~1373 cm^{-1}[146] (λ_{Soret} = 404 nm).[30] However, an additional shoulder at ~1366 cm^{-1}, in agreement with the absorption spectrum, can be attributed to the presence of another ferroheme species, i.e., 5c $Fe^{II}-OH_2$. This was also observed for deoxyMb at pH 3.8 where protonation of the proximal His leads to the breakage of the $Fe-N_{His}$ bond.[35,36]

It was observed by absorption spectroscopy that a decrease in pH causes the Soret band ratio to shift toward the 386 nm species (see below). Figure 3 displays the RR spectrum at pH 4.0 where the absorption spectrum exhibits only the Soret band at 386 nm. In some cases, the ν_{Fe-His} stretching mode was observed at ~220 cm^{-1}, which is diagnostic for the presence of the Fe−His bond.[35,41,47] However, extensive background Raleigh scattering sometimes does not allow the observation of this very weak mode,[45] which is unfortunately also the case for NP4 and NP7. Nevertheless, the loss of the $Fe-N_{His}$ bond is indicated by the disappearance of the ν_4 band at 1352 cm^{-1}. Instead, a broad ν_4 band with a maximum at 1370 cm^{-1} is obtained (see below). At the same time, the broadening of ν_4 can be attributed to an underlying species at 1366 cm^{-1} that was also seen at pH 7.5 (see above), which agrees well with the existence of the water-on complex. This is further confirmed by the ν_3 of 1491 cm^{-1} and the ν_{10} of 1635 cm^{-1}. The appearance of the strong ν_4 at 1370 cm^{-1} may indicate a ferric heme.

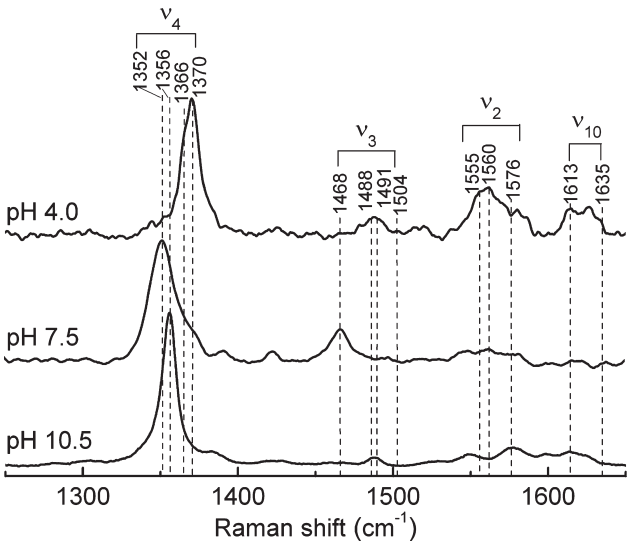

Figure 3. High-frequency range of the RR spectra (λ_{ex} = 413.1 nm) of NP7[Fe^{II}] at pH 4.0 (100 mM NaOAc/HOAc), pH 7.5 (100 mM MOPS/NaOH), and pH 10.5 (100 mM $NaHCO_3$/NaOH) recorded at ambient temperature.

However, oxidation can be ruled out on the basis of the absorption spectrum recorded after the RR measurement (data not shown). To interpret the spectrum, the novel ν_3 = 1504 cm^{-1} band has to be taken into account; by analogy to deoxyMb and the H25A mutant of hHO-1, it can be attributed to the presence of a 4c intermediate-spin (4cIS) ferrous heme.[47]

In addition to the low-pH sample, RR spectra of NP7[Fe^{II}] at pH 10.5 were also recorded (Figure 3). Inspection of core marker bands ν_4, ν_3, and ν_2 at 1356, 1488, and 1576 cm^{-1}, respectively, confirms the formation of a 6cLS Fe^{II} complex, which is well in agreement with the corresponding absorption spectrum (see below). In the case of σ-type interacting Fe^{II} ligands, the ν_3 and ν_4 bands typically appear at lower frequencies compared to π-backbonding ligands (ν_3 = 1494−1510 cm^{-1}; ν_4 = 1360−1372 cm^{-1}).[48] Many heme proteins contain a potential distal ligand; for example, in cyt *c*′, a Lys coordinates as a sixth ligand at elevated pH (so-called type n ferrocytochrome *c*′), whereas under moderate-pH conditions, the iron remains 5c (so-called type a ferrocytochrome *c*′).[48,49] In contrast, the distal pocket of NPs does not provide a residue with the ability to coordinate to the heme; thus, it can be concluded that an N_{His}−Fe^{II}−OH^- hydroxo complex is formed at elevated pH.

pH Titration of NP7[Fe^{II}]. The preceding experimental information was used to perform a pH titration on NP7[Fe^{II}] monitored by absorption spectroscopy. The experiment was conducted between pH 10.0 and 3.8, and the resulting spectra are depicted in Figure 4. Within these pH borders, the changes were fully reversible, which indicates the integrity of the protein. The hydroxo complex shows a strong Soret band absorption at 422 nm and the appearance of two sharp Q-bands at 557 nm (α-band) and 527 nm (β-band), which is characteristic for LS heme complexes. The plot of the Soret band absorption maximum versus pH exhibits two major transitions where the plot of the α-band absorbance versus pH exhibits only a single transition. Because this spectral change is attributed to the disappearance of the LS complex, i.e., N_{His}−Fe^{II}−OH^- + H^+ ⇆ N_{His}−Fe^{II} + H_2O, when the pH is decreased,

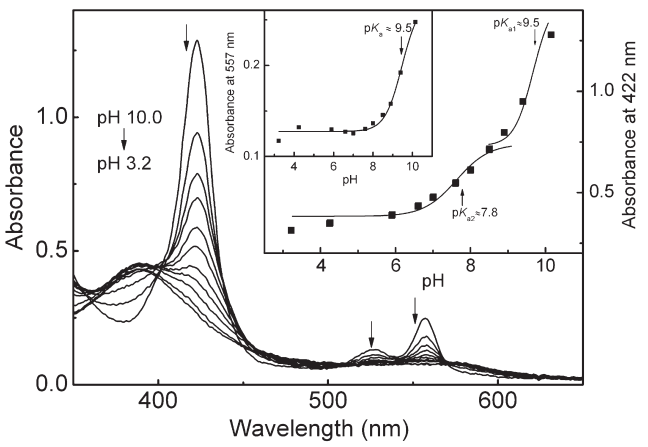

Figure 4. pH titration of NP7[Fe^{II}] monitored by UV−vis spectroscopy. The insets show the plots of the absorbancies at 422 and 557 nm versus pH.

the plot is used to determine the pK_a of the first transition (i.e., $pK_{a1} \approx 9.5$). The second transition was then fit in the ΔA_{422} versus pH plot, yielding a pK_{a2} of ≈7.8. This process is fully reversible within the pH boundaries applied.

The pH dependence of the axial heme coordination in NP7 is summarized in Scheme 2.

Scheme 2. pH Dependence of the Heme Coordination in NP7[Fe^{II}]

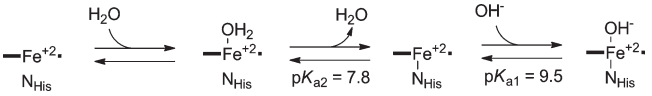

Absorption Spectra of Related Mutant Proteins. Mutant proteins NP7(E27V), NP7(E27Q), and NP2(V24E) were previously produced and their ferric oxidation states partly characterized.[31,50] Glu27 resembles the position of Val24 in NP2 and -3 or Val25 in NP1 and -4 and has a subtle influence on the heme properties. Thus, the E27V mutation in NP7 increases its level of similarity to *wt* NP1−4, whereas the V24E mutation in NP2 increases its level of similarity to *wt* NP7. NP7(E27Q) was created as a charge-depleted mutant of *wt* NP7. In addition, a novel mutant NP4(D70A) was engineered and for the first time recombinantly expressed.

Upon reduction of NP4(D70A), NP2(V24E), and NP7(E27V) with stoichiometric amounts of $Na_2S_2O_4$ under anaerobic conditions, isosbestic spectral change similar to NP4 was observed (data not shown). Figure 5 displays the resulting absorption spectra of NP4(D70A)[Fe^{II}], NP2(V24E)-[Fe^{II}], NP7(E27V)[Fe^{II}], and NP7(E27Q)[Fe^{II}] in comparison to those of *wt* NP4[Fe^{II}] and *wt* NP7[Fe^{II}] at pH 7.5. In summary, among this set of proteins, NP7(E27Q)[Fe^{II}] is the only protein that exhibits a Soret band splitting comparable to that of *wt* NP7[Fe^{II}], though the high-energy band maximum is shifted ∼4 nm toward the red. In contrast, the NP7(E27V)-[Fe^{II}] mutant not only lacks the high-energy Soret band but also shifts the low-energy Soret band maximum ∼5 nm to the red. The Q-band maxima of all NP7 types of proteins are shifted to the blue by 6−8 nm. The Soret band maximum is comparable to the 427 nm value of NP7(E27V), though it varies between 425 and 429 nm. Thus, these spectroscopic data fit well to the previous proposal that the presence of Glu27 is crucial for the special functionality of NP7; however, Glu27 can

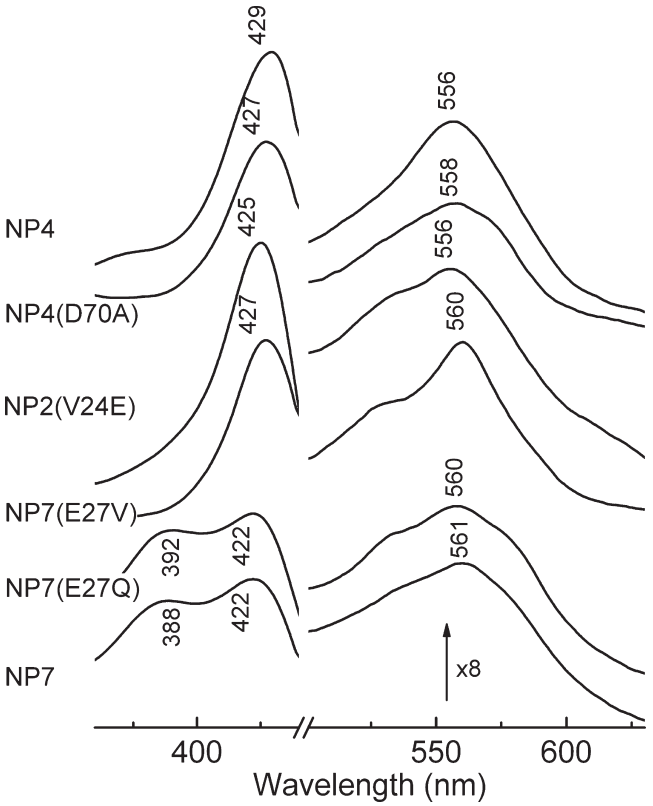

Figure 5. Comparison of the UV−vis absorption spectra of the Soret band and Q-band region of NP4[Fe^{II}], NP4(D70A)[Fe^{II}], NP2-(V24E)[Fe^{II}], NP7(E27V)[Fe^{II}], NP7(E27Q)[Fe^{II}], and NP7[Fe^{II}] in 100 mM MOPS/NaOH and 50 mM NaCl (pH 7.5).

be substituted with Gln without a significant spectral change, indicating that the steric effect of the residue is more important than the charge. Nevertheless, the preparation of NP7(E27Q) yields only small amounts of protein and tends to precipitate at elevated concentrations, indicating that the charge of Glu27, though not crucial for the properties of the heme environment, is essential for protein folding.[31] However, comparison of the protein aromate absorbance at 280 nm with the Soret band absorbance indicates a filling of NP7(E27Q) comparable to that of the *wt*.

Resonance Raman Spectra of Related Mutant Proteins. The instability of most of the mutants also does not allow the recording of RR spectra, which requires relatively high protein concentrations. However, as one can see from Figure 2, NP7(E27V)[Fe^{II}] and NP2(V24E)[Fe^{II}] behave much like *wt* NP4[Fe^{II}] and NP7[Fe^{II}], and the respective Raman shifts are listed in Table 1. Overall, all spectra look very similar, indicating that the major species observed is the 5c His-on species, a finding supported well by the absorption spectra. However, the ν_4 band of NP7(E27V)[Fe^{II}] is rather broad, and the shoulder at 1357 cm^{-1} can be assigned to a significant fraction of the hydroxo species, similar to the spectrum of NP7[Fe^{II}] at higher pH values (Figure 3). This is supported by the appearance of the weak ν_3 band at 1490 cm^{-1}. Furthermore, like in NP4[Fe^{II}] and NP7[Fe^{II}], the shoulder at ~1370 cm^{-1} is attributed to a minor fraction of oxidized material.

Absorption Spectra of NP4- and NP7[Fe^{II}−NO] and Corresponding Mutant Proteins. The previous studies were accompanied by the examination of the ferroheme nitrosyl complexes. Fe^{II} porphyrins form very tight complexes with NO where NO exhibits a strong negative *trans* effect on the proximal ligand[51,52] that makes it hard to prepare good synthetic models of 6c {FeNO}^{7} complexes,[53] although few such complexes were reported.[54,55] In contrast, in proteins the His ligation is typically preserved upon NO binding. However, a number of ferroheme proteins, in particular those that are involved in NO signaling, lose His coordination upon NO binding. Prominent examples are the CooA from *Rhodospirillum rubrum*,[56] mammalian sGC,[57] and the neuronal PAS protein 2.[58] However, the structural factors that determine the weakening or strengthening of the *trans* bond are not clear, although it is important to understand the structure−function relationships of such proteins, not at least because of the physiological importance and pharmacological potential associated with sGC.[59]

In the case of NP7[Fe^{II}], because of the already weakened N_{His}−Fe^{II} bond, the loss of the coordination upon NO binding is expected. It was previously reported that NP4[Fe^{II}−NO] is a His-on species.[18] In marked contrast, the absorption spectrum of NP7[Fe^{II}−NO] displayed in Figure 6 indicates that this form

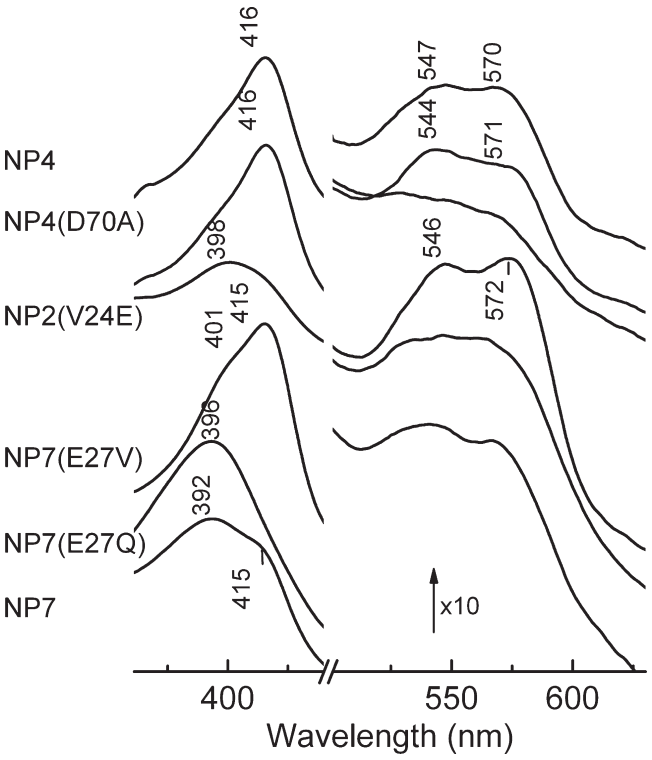

Figure 6. UV−vis absorption spectra of *wt* NP4[Fe^{II}−NO] and *wt* NP7[Fe^{II}−NO] and corresponding mutant proteins in 100 mM MOPS/NaOH and 50 mM NaCl (pH 7.5).

comprises mostly a 5c species (392 nm), although a significant amount of the Soret band absorption from the His-on species can be seen (~415 nm). Interestingly, the E27Q mutation in NP7 leads to only the His-off species. On the other hand, insertion of Val27 into NP7 reverses this effect, and the absorption spectrum displays mainly the His-on species, though a small contribution is assigned to the His-off species.

In contrast to the mutations of Glu27 in NP7, mutation of Asp70, i.e., NP4(D70A), does not alter the behavior of NP4, which agrees well with the previous finding for NP4(D70A)-[Fe^{II}] (see above). To our surprise, though, NP2(V24E)[Fe^{II}−NO] completely loses the N_{His}−Fe^{II} coordination.

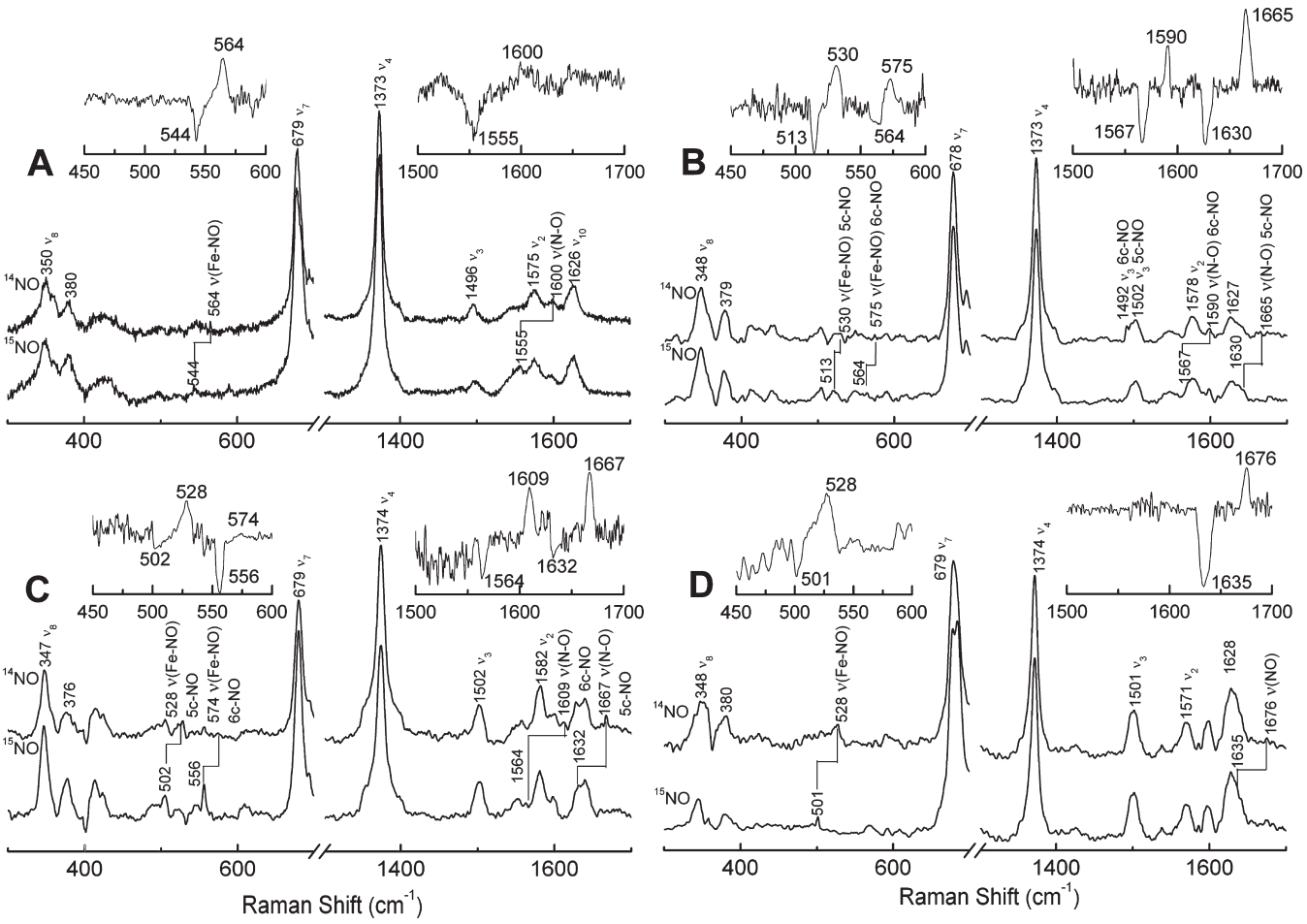

Figure 7. Comparison of the RR spectra of (A) NP4[Fe^{II}–NO], (B) NP7(E27V)[Fe^{II}–NO], (C) NP7[Fe^{II}–NO], and (D) NP2(V24E)[Fe^{II}–NO] in 100 mM MOPS/NaOH and 50 mM NaCl (pH 7.5) at ambient temperature (λ_{ex} = 413.1 nm).

Resonance Raman Spectra of NP4- and NP7[Fe^{II}–NO] and Corresponding Mutant Proteins. Similar to the previous assignment of the coordination state of the unliganded NPs, the absorption spectra were accompanied by the recording of RR spectra. For the unambiguous assignment of the ν_{Fe-NO} and ν_{N-O} stretch vibrations, samples with ^{14}NO and ^{15}NO were measured. The resulting RR spectra of NP4[Fe^{II}–NO], NP7[Fe^{II}–NO], NP2(V24E)[Fe^{II}–NO], and NP7(E27V)[Fe^{II}–NO] were recorded, and they are presented in Figure 7. The corresponding Raman shifts are summarized in Table 2 together with the corresponding data of relevant proteins from the literature.

The RR spectrum of NP4[Fe^{II}–NO] at pH 7.5 is depicted in Figure 7A. In the high-frequency region of the RR spectra, core-size marker bands, ν_4, ν_3, and ν_2 at 1373, 1496, and 1575 cm^{-1}, respectively, are consistent with those reported for 6c ferrous heme–NO complexes.[60−65] The Fe^{II}–NO stretching frequency is sensitive to heme coordination number, while a 5c heme–NO stretch typically falls between 510 and 530 cm^{-1}[66] and a 6c heme–NO stretch between 530 and 590 cm^{-1}.[55] The ν_{Fe-NO} for NP4[Fe^{II}–NO] is 564 cm^{-1} and shifts down to 544 cm^{-1} with ^{15}NO. NP4(D70A)[Fe^{II}–NO] also has a 6c heme as judged from the UV–vis absorption spectrum. The broad Soret band has a maximum at ~400 nm for NP7[Fe^{II}–NO] and NP7(E27Q)[Fe^{II}–NO] and is consistent with those reported for 5c ferrous heme–NO complexes.[56,64,67−69] This is further confirmed by the RR spectrum. The core-size marker bands (Figure 7C), ν_4, ν_3, and ν_2 at 1374, 1502, and 1582 cm^{-1}, respectively, identify NP7[Fe^{II}–NO] as a 5c ferrous heme–NO complex.[70,71] The ν_{Fe-NO} mode for NP7[Fe^{II}–NO] appears at 528 cm^{-1}, which is also very characteristic for a 5c ferrous heme–NO complex. As mentioned above, the UV–vis spectrum (Figure 6) indicates a small fraction of the 6c His-on species, the concentration of which is too small, compared to that of the 5c His-off species, to detect the corresponding Raman shift in the core-size marker bands. However, the much better resolved ν_{Fe-NO} and ν_{N-O} modes appear at 574 and 1609 cm^{-1}, respectively, which is confirmed by the spectrum of the ^{15}NO-labeled species.

NP7(E27V)[Fe^{II}–NO] has a Soret band maximum at 415 nm and a shoulder at 401 nm, which suggests the coexistence of 6c and 5c ferrous heme–NO complexes. This can be confirmed by the RR spectrum (Figure 7B): for the 6c NO complex, ν_3 = 1492 cm^{-1} and ν_{Fe-NO} = 550 cm^{-1}, and for the 5c NO complex, ν_3 = 1502 cm^{-1} and ν_{Fe-NO} = 530 cm^{-1}.

In contrast to the three previously reported proteins, NP2(V24E)[Fe^{II}–NO] did not exhibit any signature of the 6c His-on form in the UV–vis spectrum. Accordingly, the RR spectra provide only the ν_{Fe-NO} and ν_{N-O} modes at 528 and 1676 cm^{-1}, respectively, that correspond to the 5c His-off species (Figure 7D). The core-size marker bands all agree well with this interpretation.

Ferroheme NP7 Reconstituted with Symmetric Heme. A significant lack of symmetry in protoporphyrin IX

Table 2. Comparison of the Absorption Maxima and Heme Raman Shifts of the Nitrosyl Complexes of Ferrous Nitrophorins with Those of the Nitrosyl Complexes of Other His-Liganded Ferrous Heme Proteins Recorded at Room Temperature

		absorption maximum (nm)			Raman shift (cm^{-1})					
protein	pH	λ_{Soret}	λ_{β}	λ_{α}	ν_4	ν_3	ν_2	ν_{Fe-N}	ν_{N-O}	ref
					6cNO[a]					
NP1	8.0	416							1611[b]	10
NP2(D1A)	7.5	414								8
NP4	7.5	416	547	570	1373	1496	1575	564	1600	tw[c]
NP4(D70A)	7.5	416	544	571						tw[c]
NP7(E27V)	7.5	415	546	572	1373	1496	1571	575	1590	tw[c]
NP7	7.5	415						574	1609	tw[c]
Mb[d]	7.4	421			1375	1500	1583	558	1613	60
Mb[e]	7.0							552	1612	93
Mb(H64L)[e]	7.0							563	1635	93
Mb(H64I)[e]	7.0							558	1638	93
Cygb[f]	8.0				1376	1502	1574	569	1604	61
Ngb[g]	8.0				1375	1498	1572	573	1600	61
FixLN[h]	7.8	420	546	578	1373	1498	1575	558		62
BjFixLH[i]	7.0					1498	1575	568	1634	63
AXCP[j]	8.9	415	540	575	1375	1504	1596	579	1624	64
RCCP[k]	7.0	414	540	570	1377	1506	1598	569	1625	65
*Tt*H-NOX[l]	7.5	420	545	575	1371	1496	1580	553	1655	108
					5cNO[m]					
NP2(V24E)	7.5	398			1374	1501	1571	528	1675	tw[c]
NP7	7.5	392	540	572	1373	1504	1583	528	1667	tw[c]
NP7(E27V)	7.5	401	546	572	1373	1502	1581	530	1665	tw[c]
NP7(E27Q)	7.5	396	540	572						tw[c]
$NP7_{sym}$	7.5	387	525	562						tw[c]
NP2(D1A/D29A)	5.5	398								8
	7.5	400[n]								8
NP2(D1A/D36A)	5.5	398								8
	7.5	400[o]								8
NP4(D30A)	5.5	407[o]								8
	7.5	404								8
sGC_2[p]	7.4	398	537	572	1375	1509	1584	525	1677	67, 68
*Vc*H-NOX[q]	7.5	398	537	572	1372	1505	1580	525	1677	108
CooA[r]	7.4	399	544	572	1376	1506	1582	523	1672	56
CLOCK PAS-A[s]	7.1	396	541	577	1374	1508	1588	525	1668	69
AXCP[j]	8.9	395	539	565	1373	1506	1592	526	1661	64
NPAS2 bHLH-PAS-A[t]	8.0	394			1376	1508	1584	523	1670	109
HRI[u]	8.0	398	538					524	1677	110

[a]Six-coordinate nitrosyl complexes, proximal His bound. [b]Determined by FT-IR spectroscopy. [c]This work. [d]From horse heart. [e]Recombinant human myoglobin. [f]Human cytoglobin. [g]Human neuroglobin. [h]FixLN, a membrane-bound protein from soil bacterium *Rhizobium meliloti*. [i]BjFixLH, the heme-binding domains of *Bradyhizobium japonicum* FixL. [j]AXCP, *Alcaligenes xylosoxidans* cytochrome *c*′, measured at 90 K. [k]RCCP, *Rhodobacter capsulatus* cytochrome *c*′. [l]H-NOX domain from *T. tengcongensis*. [m]Five-coordinate nitrosyl complexes. [n]Shoulder at ∼413 nm. [o]Shoulder at ∼415 nm. [p]From bovine lung. [q]H-NOX domain from *V. cholerae*. [r]CooA, CO oxidation activator protein from *R. rubrum*. [s]CLOCK PAS-A, mammalian circadian protein CLOCK. [t]N-Terminal basic helix−loop−helix (bHLH) motif of the first PAS (PAS-A) domain of NPAS2. [u]Heme-regulated eukaryotic initiator factor 2α kinase.

is achieved by the particular pattern of substituents at the aromatic core, as shown in Scheme 3. As a consequence, the cofactor can orient inside a protein heme pocket in two different orientations, **A** and **B**, a phenomenon that has been termed "heme rotational disorder" (see Scheme 3). Using NMR, it was shown that NP1 and -4 have no preference for one orientation (≈1:1 **A**:**B**) whereas NP2 and -3 exhibit a preference for the **B** orientation.[13,72−74,b] In contrast, using ^{1}H NMR and circular dichroism (CD) spectroscopy, NP7 was found to be the only member of the NP family that stabilizes the heme **A** orientation.[14,31] By use of the mutants NP7(E27V) and NP7(E27Q), which were also applied in this study, it was determined that Glu27 in NP7 is responsible for the formation of the **A** orientation. NP7 is the only NP that exhibits a Glu residue at this position where NP1−4 have a Val (see Figure S1 of the Supporting Information). Consequently, insertion of this residue into NP2, i.e., NP2(V24E), results in the **A** orientation.[31,50] An examination of the protein structure suggests that the steric demand of Glu27 causes repulsion of the cofactor.

To understand the extent to which the vinyl groups of the cofactor influence the steric interaction with the NPs, we reconstituted NP7 with symmetric heme. The absorbance spectrum of the complex is shown in Figure 8 together with the spectra of the ferroheme species and the Fe^{II}−NO complex. When compared to the native form, all species show absorbance spectra with their maxima shifted ∼10 nm to the

Scheme 3. Heme *b* Nomenclature and Heme Orientation inside the Pocket of NP2[a]

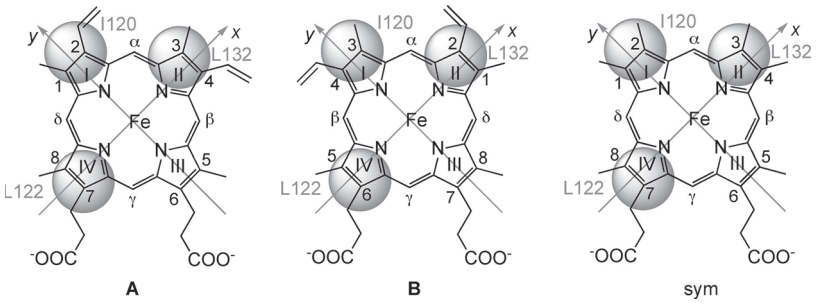

[a]The heme pocket of NP2 is indicated by the three circles corresponding to the positions of the three aliphatic side chains pointing from the top of the distal pocket onto the heme plane. The two possible heme orientations are indicated as **A** and **B**. The "symmetric heme" (2,4-dimethyldeuterohemin) used in this study is designated sym.

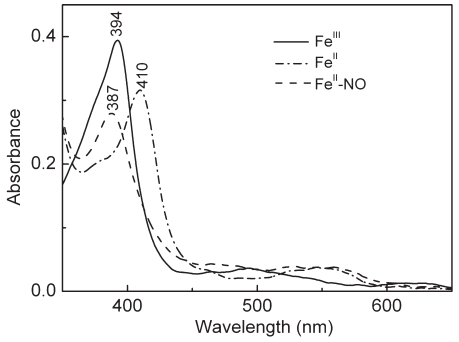

Figure 8. Absorption spectrum of NP7 reconstituted with symmetric heme in +3 and +2 iron oxidation states and of the ferroheme−nitrosyl complex. Spectra were recorded at pH 7.5.

blue. This is expected because of the smaller π-electron system and was also observed for other heme proteins.[27] More importantly, where the position of the Soret bands of unliganded ferriheme and ferroheme forms suggests the presence of the His-on case, the Soret band position of $NP7_{sym}[Fe^{II}–NO]$ corresponds to a 5c species, i.e., His-off.

DISCUSSION

Fe^{II}–His Bond Breakage Observed in NP7. The breakage of the Fe^{II}–His bond in the case of the unliganded *wt* NP7[Fe^{II}] and NP7(E27Q)[Fe^{II}] at neutral pH is a remarkable case in the sense that the Fe^{II}–His60 bond is so weak that it breaks, at least in part, already in the 5cHS state, which is then in equilibrium with the 5cHS state with a water on according to Scheme 1. Table 3 summarizes the results of this study with respect to the stability of the Fe^{II}–His bond in NPs at pH 7.5. To the best of our knowledge, the heme c_n (or heme *x*) in the cytochrome b_6f complex is the only naturally occurring example of a heme without a direct iron−side chain ligation, i.e., a 5c water complex.[75,c] The only other example of a His-liganded ferroheme with a His-on:His-off ratio similar to those of NP7 and NP7(E27Q) is AXCP and a couple of proximal and distal site mutants thereof.[76] Therefore, in this study, we address the factors that contribute to the destabilization of this interaction in NP7[Fe^{II}]. Unfortunately, for NP7, an experimental structure is currently not available; however, because of the high degree of amino acid sequence identity with NP2 (62%) and the absence of residue shifts in the sequence alignment, a highly reliable homology model of NP7 is available.[14]

Table 3. Summary of the Coordination Geometry Observed in Ferroheme NPs and NP Mutants at pH 5.5 and 7.5

	coordination of the proximal His			
	Fe^{II}		Fe^{II}–NO	
protein	pH 5.5	pH 7.5	pH 5.5	pH 7.5
*wt*NP7[a]	off	on/off	off	off(/on)
wt NP4[18 a]	on	on	on	on
NP7(E27V)[a]	on	on	on(/off)	on(/off)
NP7(E27Q)[a]	off	on/off	off	off
NP2(V24E)[a]	on	on	off	off
NP4(D70A)[a]	on	on	on	on
$NP7_{sym}$[a]		on		off
NP2(D1A)[8]			off	on
NP2(D1A/D29A)[8]			off	off(/on)
NP2(D1A/D36A)[8]			off	off(/on)

[a]This work.

Figure 9 illustrates the proximal site arrangement in NP7 in comparison to NP4 by representing the residues involved by the van der Waals radii of the respective atoms. It is obvious that the arrangement of the residues in the neighborhood of the proximal His60 in NP7 is very dense versus the spatial arrangement of Glu27, Phe43, and His60 compared to the arrangement in NP4 with the much smaller residues Val25, Ala41, and His58.[d] This suggests that the polar and bulky Glu27 cannot orient differently and mediates a certain tension via Phe43 to the proximal His60. In agreement with this hypothesis, the displacement of Glu27 in NP7, i.e., NP7-(E27V), retrieves the heme coordination whereas the sterically similar Gln, i.e., NP7(E27Q), shows a behavior similar to that of the *wt*, indicating that the size rather than the charge of Glu27 is responsible for the effects described herein.

The reverse insertion of Glu into NP2, i.e., NP2(V24E), is not sufficient for the destabilization of the Fe^{II}–His bond because the Phe residue, mediating the tension between Glu27 and $His_{proximal}$ in NP7, is missing in NP2(V24E), which has a Ser40 instead. However, the Fe^{II}–His bond in NP2(V24E)-[Fe^{II}] breaks completely upon NO binding (Table 3). The negative *trans* effect of NO decreases the affinity of axial N-donor ligands due to a competition of the π^* orbital of NO and the σ orbital of the N-donor for the d_{z^2} orbital of iron. Thus, the presence of Glu24 in NP2(V24E) creates enough tension for the Fe^{II}–His labilization so that together with the electronic weakening of the NO the proximal bond is broken. These effects may be summarized by Scheme 4 in which the

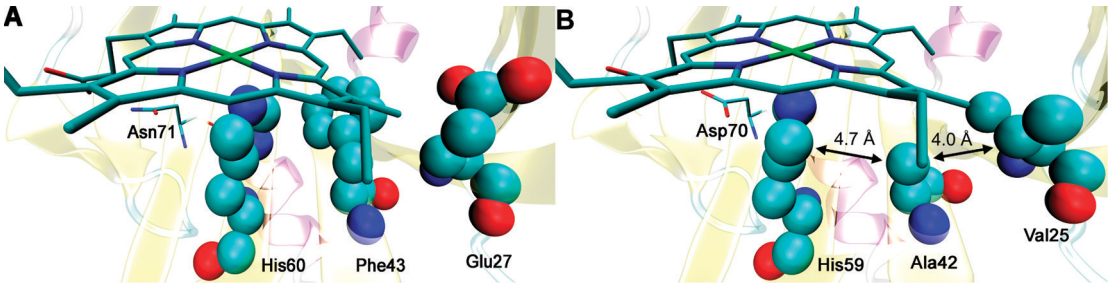

Figure 9. Representation of the spatial arrangement of the proximal heme site in (A) NP7 (homology model[14]) and (B) NP4 (PDB entry 1NP4). Residues Glu27, Phe43, and His60 (A) and Val25, Phe41, and His58 (B) are displayed in their van der Waals radii. In both structures, the heme is displayed in the **A** configuration (compare to Scheme 3). This figure was created with VMD version 1.8.7[111] and rendered with POV-Ray version 3.62 (http://www.povray.org/).

Scheme 4. Tentative Scheme of the Forces Directed to the Heme Cofactor and the Proximal His in NP7 and NP2(V24E) in Comparison to the Situation in Standard Nitrophorins[a]

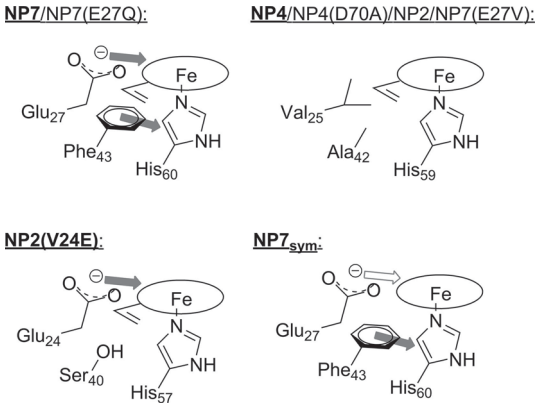

[a]The amino acid numberings correspond to the proteins in bold.

tension created on the Fe^{II}–$His_{proximal}$ bond in NP7 and NP7(E27Q) is depicted as two potential forces indicated by arrows: (i) mediation through Phe43 as described previously and (ii) directly onto the heme plane. In NP2(V24E), the mediation through Phe does not exist, but some tension remains. In contrast, in NP4, NP2, NP7(E27V), and others, no such mechanism exists.

It was previously reported that Glu27 plays a crucial role in the heme properties in NP7, in particular with respect to the orientation of the heme plane inside the pocket,[31,50] which already indicated the very dense situation inside the heme pocket of NP7 (compare to Figure 9). In contrast to NP7, all other NPs exhibit Val24 or -25 (NP2 and -3 or NP1 and -4, respectively) instead. Insertion of the Glu residue into NP2, i.e., NP2(V24E), reverses the heme orientation from **B** to **A** (compare to Scheme 3).[31,50] In contrast, insertion of Val into NP7, i.e., NP7(E27V), reverses the heme orientation from **A** to **B**. In this work, it was shown that both NP7(E27V) and NP7(E27V)[Fe^{II}–NO] do not labilize the Fe^{II}–His60 bond, whereas NP2(V24E)[Fe^{II}–NO] breaks the Fe^{II}–His57 bond. Therefore, the question of the extent that the heme orientation may be involved in His–Fe bond breakage arises.

The insertion of a symmetric heme (compare to Scheme 3) into NP7 shows that the Fe^{II}–His60 bond is indeed preserved in the unliganded situation, demonstrating that the absence of the vinyl group in $NP7_{sym}$ provides enough space for a better fitting into the heme pocket; thus, at least some of the tension from the proximal iron bond is released. On the other hand, $NP7[Fe^{II}–NO]_{sym}$ is a His-off species and, therefore, behaves very much like NP2(V24E). In this case, the force on the $His_{proximal}$ is mediated through Phe43, and a relaxation in the Glu27–heme arrangement is obtained. Furthermore, the influence of the heme vinyl(s) on Fe^{II}–His bond stability demonstrates that the heme orientation matters for the heme properties.

Comparison of NP–NO Five-Coordination with the Behavior of Other Heme Proteins. The molecular mechanisms involved in the biological production, distribution, and sensing of the mammalian signaling molecule NO are currently being investigated. A major key player is the ferroheme protein sGC, which is activated upon coordination of NO to the heme iron and subsequently produces the second-messenger cGMP.[21,77,78] The signal of the NO coordination is mediated through the breakage of the proximal Fe^{II}–His bond as a consequence of the strong negative *trans* effect of NO.[21,79] The resulting conformational change is the trigger for the increase in the level of cGMP formation. However, loss of 6c at ferrohemes upon NO binding occurs rarely in His-coordinated heme proteins, which is in contrast to ferroheme model complexes in which the weak N-base ligands are typically released upon NO binding (K_{eq} = 10–50 M^{-1}).[79] Thus, the entropy gained by the formation of the protein–heme complex compensates for the small free energy of the Fe^{II}–His coordination in most heme protein cases, but what then determines if a Fe^{II}–His bond upon NO binding to a heme inside a protein pocket is broken?

Unfortunately, the structure of the heme domain of sGC is not known, so that structure–function relationships are vague and require comparison with those of proteins with similar features. Furthermore, the binding of NO to sGC may not include only the simple two-step mechanism of (i) NO binding and (ii) His release; it is a matter of debate that by a yet unknown mechanism NO may bind to the proximal iron site according to Scheme 5.[e] While many His-ligated heme proteins

Scheme 5. Mechanism of the Binding of NO to Ferroheme sGC

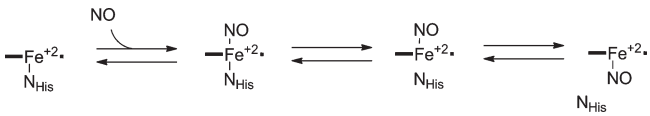

form a 5c Fe^{II}–NO complex only at fairly low pH (e.g., cytochrome *c* at pH 2.0[80] or Mb–NO at pH 4[81]), there are a

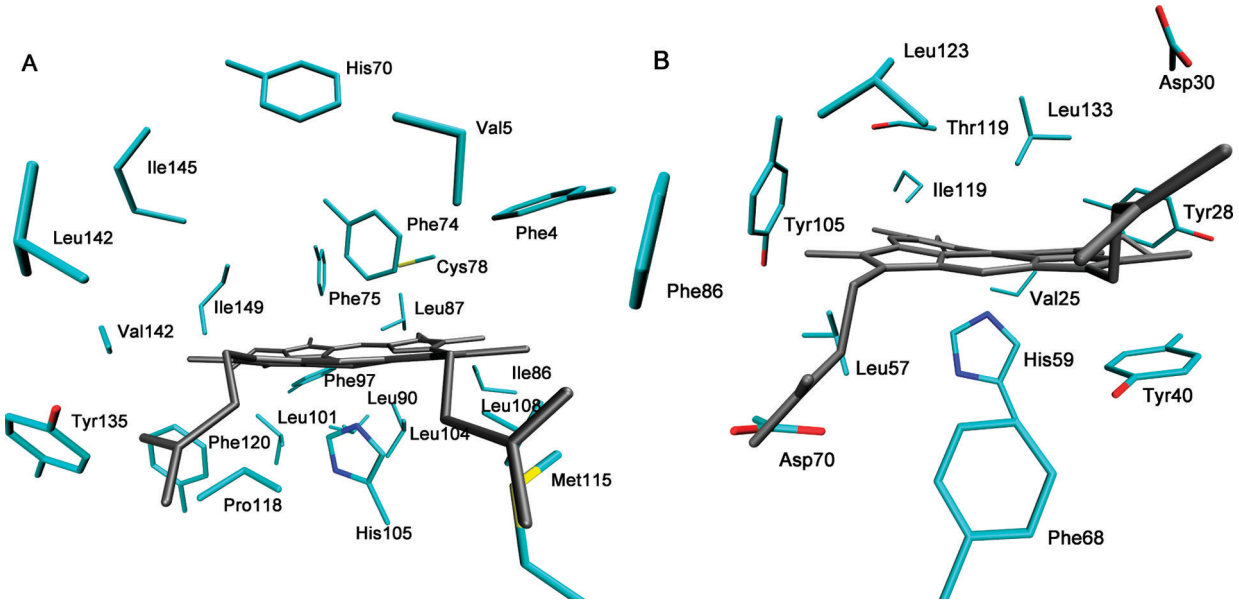

Figure 10. (A) Heme pocket of sGC in comparison with that of (B) NP4. For human sGC, a homology model was used. For NP4, the X-ray structure from PDB entry 1NP4 was used. Figures were prepared with VMD version 1.8.7[111] and rendered with POV-Ray version 3.62 (http://www.povray.org/).

few examples of proteins that break the His N^{τ}–Fe^{II} bond even at approximately neutral pH. To the best of our knowledge, the few examples of non-sGC proteins include CooA, CLOCK PAS-A, the H-NOX domains of *T. tengcongensis*,[82] and the cytochrome *c*′ compounds from various species.[83−85] In particular, the cytochrome *c*′ proteins, originating from bacteria with yet uncertain function, have been studied in the past as models for sGC, and a great advantage is the availability of crystallographic structures of the protein from *A. xylosoxidans*, often termed AXCP.[86] Insights came also from the study of human serum albumin (HSA) and the proximal His deletion mutant H93G of sperm whale Mb [Mb(H93G)] in a complex with ImH, which have been used as model proteins.[87] [A surprisingly different case is heme b_3 of nitric oxide reductase (NoR) that appears His-off in the Fe^{III} state and establishes the Fe–His bond upon reduction to Fe^{II} or NO binding to Fe^{III}.[88]]

On the basis of the results obtained by spectroscopic and crystallographic investigations, the His N^{τ}–Fe^{II} bond weakening in sGC and sGC model proteins was attributed to effects inside the proximal and distal heme pocket. On the distal site, a stabilization of the NO complex by the heme pocket residues was proposed. For example, in Mb the distal His64 residue is able to form an H-bond with NO coordinated to the heme Fe^{II}. However, investigations of the Mb(H64L) and Mb(H64I) mutants by vibrational spectroscopy in combination with DFT calculations revealed a weak interaction of the His–N···N–O bond.[89]

On the proximal site, the influence of certain residues has also been considered. A recent extensive crystallographic and spectroscopic investigation of AXCP and mutant proteins of Arg124 revealed a major contribution of this residue to the affinity and orientation of NO. However, Arg124 forms an H-bond to the proximal NO and stabilizes it, so that the contribution to $His_{proximal}$ at present cannot be estimated. It is also surprising that the large variety of mutants that have been created, i.e., AXCP(R124E), AXCP(R124F), AXCP(R124K), and AXCP(R124Q), exhibit only minor alterations in the NO binding behavior compared to that of the *wt* protein, and that only AXCP(R124A) keep the NO at the distal site.

Recently, an energy-optimized homology model of the human sGC heme domain based on *Ns*H-NOX (PDB entry 2O09)[90] was reported.[91,f] Comparison of the distal heme pockets of sGC with those of NP4 (Figure 10) indicates only aliphatic and aromatic side chains in the vicinity of the heme pocket, in both cases rather densely packed. In contrast, AXCP reveals the Arg124 residue that is able to H-bond to N^{τ} of the proximal His120.[86] Furthermore, it forms an H-bond to NO when the 5c complex at the distal side is formed and, therefore, stabilizes this complex. Whereas such a residue is missing in both sGC and NPs, the latter exhibits a $His_{proximal}$ N^{τ}···water···Asp/Asn network. In NP4, His59 forms an H-bond to the side chain of Asp70 via a water, i.e., His59 H···water···Asp70. However, removal of Asp70 [NP4(D70A)] did not lead to a significant change in the spectroscopic features; in particular, the His-on:His-off ratio was not affected. Thus, it can be concluded that the respective H-bond is not responsible for the stabilization of the Fe^{II}–His bond. It should be noted that, whereas in NP1 Asp70 is also present, in NP2 it is represented by Asn68.[g] However, in both proteins, the Fe^{II}–His bond does not break upon NO binding.[8,33] Inspection of the sGC model structure drew our attention to Asp102 in the case of sGC, which is also present in the *Ns*H-NOX structure. Like in the NPs, $His_{proximal}$ N^{τ} is coordinated to Asp102 via a water; thus, the arrangement likely exists in sGC. On the basis of the data derived from NPs, it can be concluded that the presence or absence of this network may not be important for Fe^{II}–$His_{proximal}$ bond breakage.

ν_{N-O} versus ν_{Fe-N} Anticorrelation in Nitrophorins. Another factor associated with His–Fe bond breakage is the His–Fe bond strength, determination of which can be best estimated by RR spectroscopy where the weak ν_{Fe-His} vibration appears typically in the range of 200–250 cm^{-1}.[92] However, whereas this vibration has been obtained for many proteins, it was, unfortunately, not possible to obtain the vibration with certainty for the nitrophorins even when the excitation wavelength was

shifted to 441.6 nm, which typically enhances this mode. Such difficulty was also reported for other heme proteins, for example, CLOCK PAS-A.[69] However, in a comparative study of AXCP and RCCP, it has been recently pointed out that the Fe–$His_{proximal}$ bond strength may not play such a critical role in bond breaking.[65]

Backdonation of the Fe^{II} d_π electrons to the NO π^* orbital is the reason for the negative correlation between the ν_{Fe-N} and ν_{N-O} vibrations.[55,66,93] The correlation of the 5c adducts is linear with a slope of −0.40, whereas the slope of the correlation of the 6c complexes is −1.0 (developed using heme model compounds).[55,66] Both lines are indicated in the plot in Figure 11 together with the ν_{Fe-N}/ν_{N-O} pairs reported herein

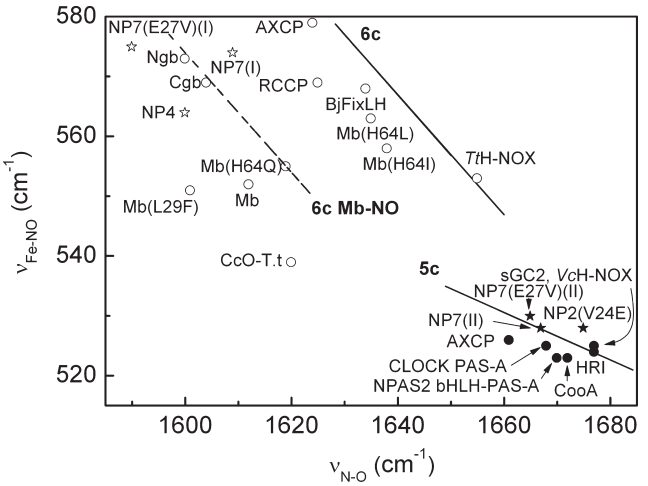

Figure 11. ν_{Fe-NO}/ν_{N-O} correlation plot for the data from heme protein Fe^{II}–NO complexes. The backbonding correlations for the 5c and 6c Fe^{II}–NO porphyrinates and 6c-Mb-NO are from literature.[55,66,93] References for protein complexes are listed in Table 2. The proteins investigated in this study are denoted with stars. Other proteins are denoted with circles. 5c NO complexes are denoted with filled symbols, and 6c NO complexes are denoted with empty symbols.

and a selection of ν_{Fe-N}/ν_{N-O} pairs from proteins. The three 5c complexes reported here, NP7[Fe^{II}–NO], NP7(E27V)[Fe^{II}–NO], and NP2(V24E)[Fe^{II}–NO], fall on this line, which is the case for all the 5c proteins identified so far. The amount of structural data in the case of proteins and model compounds is very limited for the 5c complexes. The variation of model hemes is limited to the variation of substituents at the porphyrin core, and it was demonstrated that the metal–ligand backbonding strength correlates well with the electron withdrawing capabilities of the porphyrin core substituent.[66] However, in the protein examples discovered so far, the macrocycle consists of ppIX; thus, variations in the backbonding must derive from (i) the ligand environment and/or (ii) the heme deformation. However, the only example, to the best of our knowledge, of a 5c protein complexed X-ray structure is reported for AXCP and a number of its mutants.[94] Unfortunately, characterization of the vibrational modes of the Fe–N–O moiety has only been reported for *wt* AXCP. Furthermore, although the proteins fall generally well on the linear correlation, among the heme proteins reported, AXCP is something of an outlier with unusually weak Fe–N and N–O bonds, a fact also reflected in the long Fe–N (2.04 Å) and N–O (1.17 Å) distances (PDB entry 1E85).[86] For comparison, in [Fe(TPP)(NO)] (TPP is 5,10,15,20-tetraphenyl-21*H*,23*H*-porphyrin), the distances are as follows: 1.717 Å for Fe–N and 1.122 Å for N–O.[95] The latter is also characterized by bond angle ∠(Fe–N–O) of 149.2°, which is in good agreement with the {FeNO}^{7} electronic structure, whereas in AXCP, ∠(Fe–N–O) = 125°, which can be attributed to a negative charge density on the NO ligand. In AXCP, the nearby Arg124 was attributed to a particular role in the stabilization of the NO complex through the positive charge on the guanidine group (Arg124 N^ω–NO distance of 3.8 Å).[86] However, comparison of the X-ray structures shows that the Fe–NO bond strongly depends on the charge of residue 124, i.e., Fe–NO distance between 1.81 and 1.93 Å with polar side chain Glu124, Lys124, or Gln124, but 1.73 or 1.75 Å with Phe124 or Ala124, respectively.[94] A similar trend in bond distance was observed for the 6c NO complexes of Mb and its distal site mutant Mb(H64L) based on the ν_{Fe-N} increase (see Figure 11).[75] In contrast, the 5c components of NP7(E27V) and NP7 fit well to the line but are located at the upper end, which reflects greater backbonding character as compared to, for example, that of CooA or sGC. It cannot currently be determined if the NO in 5c NP complexes remains bound to the distal side or moves, like in AXCP (compare Scheme 5), upon loss of the Fe–His bond to the proximal side. A characteristic of the NP distal side is the presence of many aliphatic side chains, which would reduce the polarization of the NO ligand and therefore strengthen Fe–NO backbonding. This interpretation is supported by the fact that the slightly more polar heme pocket of *wt* NP7 has a decreased level of backbonding compared to that of NP7(V24E). On the other hand, the ν_{Fe-N}/ν_{N-O} correlation of NP2(V24E) reflects less backbonding character.

In the case of 6c ferrous NO/His heme proteins, it was previously noticed that the ν_{Fe-N}/ν_{N-O} pairs are much more scattered from the ideal line of model hemes than in the case of the 5c complexes,[55] but also in comparison to those of the well-behaving 6c Fe^{II}–CO complexes.[96] The deviation was attributed to the affection of ∠(Fe–N–O), which should be 142° based on calculations. Hydrogen bonding from His64 in Mb to the NO would potentially strengthen the Fe^{III}–NO^- character,[55] whereas the description of the Fe^{II}–NO center as {FeNO}^{7} provides room to understand the entity as resonances of Fe^{I}–NO^+ ↔ Fe^{II}–NO ↔ Fe^{III}–NO^-.[79] Ngb and Cygb have a similar distal His like Mb, and the distal Cu^+ in CcO creates a similar situation. It was previously determined that many of the 6c NO protein species fall on an alternate line that is parallel to the line derived from model hemes (Figure 11). This was attributed to a stabilization of the Fe^{III}–NO^- mesomeric form by H-bonding of a His residue to N_{NO}, i.e., stabilization of the significant negative charge located at N_{NO}. As a consequence, angle ∠(Fe–N–O) is expected to become significantly less than 140°, which is the ideal case for the Fe^{II}–NO complex, which was confirmed with model hemes.[53,97−99] In the case of Mb, this could not be confirmed crystallographically because, for reasons currently not understood, different Mb[Fe^{II}–NO] crystal structures[100−102] reveal different angles (112–144°)[103] and interatom distances (1.86–2.13 Å Fe–N and 1.17–1.20 Å N–O). On the other hand, this interpretation is supported by the replacement of His64 in Mb with Leu or Ile, which brings the ν_{Fe-N}/ν_{N-O} pair back toward the regular 6c line (see Figure 11).[60,93] However, both experimental and theoretical studies have suggested that the H-bond is likely weak in the case of NO (3–4 kcal/mol), so that the effect seen in vibrational spectroscopy may be more likely due to a polarization of the π/π^* orbitals of the NO.[79,104,105]

As one can see from Figure 11, NP4[Fe^{II}–NO], 6c-NP7[Fe^{II}–NO], and NP7(E27V)[Fe^{II}–NO] fall well on the 6c Mb–NO line. This is interesting because in contrast to the globins, the NPs do not provide a H^+-donating group in the distal pocket. In fact, in the available crystal structures of NP nitrosyls, the closest possible H^+ donor is a water molecule with an O_{water}–O_{NO} distance between 3.7 and 4.1 Å, which should be too week to significantly influence the {FeNO}^{7} entity. Moreover, whereas in the case of NP1[Fe^{II}–NO] the bond angle is indeed 120°, in the high-resolution structures of NP4[Fe^{II}–NO] an angle of 141° or 144° was obtained. (A collection of the available crystal structures of NP nitrosyls is available in Table S1 of the Supporting Information.) Why then do NP4 and NP7 fall on the 6c Mb–NO line?

In this respect, the ferroheme nitrosyl complex of Mb was compared to the oxyMb form,[60,81] which has significant Fe^{III} character, i.e., Fe^{III}–O_2^-, because of an H-bond between His64 and O_2.[106] Studies of the reaction of NP4[Fe^{II}] and NP7[Fe^{II}] with O_2 revealed a very rapid oxidation[34] that can even lead to porphyrin bleaching.[19,32,107] These effects can be best explained by the reaction via the Fe^{III}–O_2^- intermediate. However, while NPs do not provide a H^+ donor in the distal pocket, stabilization of the Fe^{III} state is performed by (i) the localization of numerous carboxylate side chains[8] near the heme pocket and (ii) ruffling of the macrocycle induced by the pocket architecture,[9] which is reflected in the low reduction potentials of the NPs.[6,14] Thus, whereas in the case of oxyMb the Fe^{III} character is induced to the complex upon O_2 binding, the tendency for Fe^{III} formation is an immanent character of NP hemes. However, although this effect is induced for both proteins by different mechanisms, the Fe^{III} character in the {FeNO}^{7} complexes of both proteins may be induced by the same mechanisms as in the O_2 complexes; this may explain why both proteins have a strengthened Fe–N_{NO} bond and thus fall on the 6c Mb–NO line. It is interesting to note that the NP7(E27V)[Fe^{II}–NO]/NP7[Fe^{II}–NO] pair behaves like the Mb[Fe^{II}–NO]/Mb(H64L/I)[Fe^{II}–NO] pair with respect to the large change in ν_{Fe-N} (−19 cm^{-1} vs −23 cm^{-1}), thus reflecting a similar trend in the affection of the Fe^{II}–N_{NO} bond. It should be mentioned that recently the usual interpretation of the lower of the two isotopically sensitive Raman bands of ferroheme nitrosyls as an Fe–N stretch vibration was called into question using nuclear resonance vibrational spectroscopy (NRVS).[79,105] According to these studies, the band may rather reflect the δ_{Fe-N-O} bending vibration and, therefore, reflect both bond angles and bond lengths, which may account for the bad anticorrelation observed in the case of the ferroheme nitrosyls.

In summary, the results obtained in this study reveal the strong tension that the steric demand of neighboring side chains can place on a proximal His–Fe bond in ferroheme proteins. The results are summarized in Scheme 5. Thus, in the case of the very dense arrangement in the heme pocket of NP7, the Glu27 residue, but also Gln27 in NP7(E27Q), together with Phe43 puts a strain on the proximal His, which is responsible for bond breakage. This is indicated by the exchange of Glu27 with Val, which abolishes this behavior. In addition, Glu27 also puts strain on the heme cofactor mediated through the heme vinyls, so that even in the absence of the Phe, insertion of the Glu residue can force the Fe–His bond breakage, as shown with NP2(V24E)[Fe^{II}–NO]. Similarly, removal of the heme vinyls in NP7, i.e., $NP7_{sym}$, breaks the bond more easily than NP7(E27V) does, but $NP7_{sym}$ is more stable than *wt* NP7. Hence, the proteins of this study may be arranged as follows with respect to Fe^{II}–$His_{proximal}$ stability: NP7 ≈ NP7(E27Q) < NP2(V24E) ≈ $NP7_{sym}$ < NP7(E27V) < NP4 ≈ NP4(D70A). By analogy, in the discussion of the question of why the Fe^{II}–$His_{proximal}$ bond breaks in the case of sGC, the steric tension may have been underestimated so far. This study shows that this effect in combination with others, the most important of which certainly is the negative *trans* effect of NO, can play an important role in understanding sGC function.

■ ASSOCIATED CONTENT

Ⓢ Supporting Information

Amino acid sequence alignment of the *R. prolixus* nitrophorins (Figure S1), absorbance spectra of free heme (Figure S2), and summary of the geometry of the Fe–N–O entity in crystal structures of nitrosyl complexes of nitrophorins (Table S1). This material is available free of charge via the Internet at http://pubs.acs.org.

■ AUTHOR INFORMATION

Corresponding Author

*Telephone: +49 (0)208 306 3671. Fax: +49 (0)208 306 3951. E-mail: mknipp@mpi-muelheim.mpg.de.

Funding

This work was financially supported by the Max Planck Society (MPG) and by the Deutsche Forschungsgemeinschaft (DFG), Grants KN 951/1-1 and -2 (to M.K.).

■ ACKNOWLEDGMENTS

The technical assistance of Johanna J. Taing, Robin L. Kosinsky, Jan Hanis, and Marion Stapper is gratefully acknowledged. Dr. Xiangshi Tan, Department of Chemistry and Institutes of Biomedical Sciences, Fudan University, Shanghai (China) is acknowledged for providing the coordination files of the homology model of the sGC heme domain.

■ ABBREVIATIONS

4c, four-coordinate; 5c, five-coordinate; 6c, six-coordinate; AXCP, cytochrome *c*′ from *A. xylosoxidans*; CcO, cytochrome *c* oxidase; CooA, CO oxidation activator protein; Cygb, cytoglobin; cyt *c*′, cytochrome *c*′; DEA/NO, diethylammonium 2-(*N*,*N*-diethylamino)diazenolate-2-oxide; $GS^{15}NO$, *S*-[^{15}N]-nitrosoglutathione; Hb, hemoglobin; HO-1, heme oxygenase 1; HS, high-spin; IS, intermediate-spin; LS, low-spin; MALDI, matrix-assisted laser desorption ionization; Mb, myoglobin; MOPS, 3-(*N*-morpholino)propanesulfonic acid; Ngb, neuroglobin; NOX, nitrogen- and oxygen-sensing; NP, nitrophorin; $NP7_{sym}$, NP7 reconstituted with the "symmetric heme" 2,4-dimethyldeuterohemin; ppIX, protoporphyrin IX; RCCP, cytochrome *c*′ from *R. capsulatus*; TOF, time-of-flight; sGC, soluble guanylate cyclase; SHE, standard hydrogen electrode; TPP, 5,10,15,20-tetraphenyl-21*H*,23*H*-porphyrin; *wt*, wild-type.

ADDITIONAL NOTES

[a]In the presence of Cu^I, GSNO releases NO according to the equation 2GS–NO → GS–SG + 2NO.

[b]This phenomenon was observed in many heme *b* proteins and is often termed heme rotational disorder.

[c]The function of heme c_n is not known. The iron is coordinated by a water or OH^-, which is H-bonded to an Asp side chain.[1]

[d]It should be noted that at present there is no experimental structure of NP7 published. However, a very reliable homology model was built on the basis of the sequence identity with the crystal structure of NP2 (62%). The alignment of the NP2 and NP7 sequences does not have any gaps. The highly similar backbone structure in combination with the compactness of the structure of the heme pocket strongly suggests a very similar local arrangement of the side chains.
[e]At present, it is not possible to decide if the NO binds to the distal or to the proximal iron site of the 5c ferrous NPs.
[f]The coordination file of this model was kindly provided to us by X. Tan, Department of Chemistry and Institutes of Biomedical Sciences, Fudan University, Shanghai, China.
[g]The different numbering of the residues of the different NPs is due to shifts that originate from the sequence alignment (see Figure S1 of the Supporting Information).

REFERENCES

(1) Kurisu, G., Zhang, H., Smith, J. L., and Cramer, W. A. (2003) Structure of the cytochrome b_6f complex of oxygenic photosynthesis: Tuning the cavity. *Science 302*, 1009−1014.
(2) Ribeiro, J.M. C., and Francischetti, I. M. B. (2003) Role of arthropode saliva in blood feeding: Sialome and post-sialome perspectives. *Annu. Rev. Entomol. 48*, 73−88.
(3) Ignarro, L. J. (1990) Biosynthesis and metabolism of endothelium-derived nitric oxide. *Annu. Rev. Pharmacol. Toxicol. 30*, 535−560.
(4) Soares, A. C., Carvalho-Tavares, J., Gontijo, N. d. F., dos Santos, V. C., Teixeira, M. M., and Pereira, M. H. (2006) Salivation pattern of *Rhodnius prolixus* (Reduviidae; Triatominae) in mouse skin. *J. Insect Physiol. 52*, 468−472.
(5) Weichsel, A., Andersen, J. F., Champagne, D. E., Walker, F. A., and Montfort, W. R. (1998) Crystal structures of a nitric oxide transport protein from a blood-sucking insect. *Nat. Struct. Biol. 5*, 304−309.
(6) Walker, F. A. (2005) Nitric oxide interaction with insect nitrophorins and thoughts on the electron configuration of the $\{FeNO\}^6$ complex. *J. Inorg. Biochem. 99*, 216−236.
(7) Hoshino, M., Maeda, M., Konishi, R., Seki, H., and Ford, P. C. (1996) Studies on the reaction mechanism for reductive nitrosylation for ferrihemoproteins in buffer solutions. *J. Am. Chem. Soc. 118*, 5702−5707.
(8) Berry, R. E., Shokhirev, M. N., Ho, A. Y. W., Yang, F., Shokhireva, T. K., Zhang, H., Weichsel, A., Montfort, W. R., and Walker, F. A. (2009) Effect of mutation of carboxyl side-cahin amino acids near the heme on the midpoint potentials and ligand binding constants of nitrophorin 2 and its NO, histamine, and imidazole complexes. *J. Am. Chem. Soc. 131*, 2313−2327.
(9) Shokhireva, T. K., Berry, R. E., Uno, E., Balfour, C. A., Zhang, H., and Walker, F. A. (2003) Electrochemical and NMR spectroscopic studies of distal pocket mutants of nitrophorin 2: Stability, structure, and dynamics of axial ligand complexes. *Proc. Natl. Acad. Sci. U.S.A. 100*, 3778−3783.
(10) Ding, X. D., Weichsel, A., Andersen, J. F., Shokhireva, T. K., Balfour, C., Pierik, A. J., Averill, B. A., Montfort, W. R., and Walker, F. A. (1999) Nitric oxide binding to the ferri- and ferroheme states of nitrophorin 1, a reversible NO-binding heme protein from the saliva of the blood-sucking insect, *Rhodnius prolixus*. *J. Am. Chem. Soc. 121*, 128−138.
(11) Enemark, J. H., and Feltham, R. D. (1974) Principles of structure, bonding, and reactivity for metal nitrosyl complexes. *Coord. Chem. Rev. 13*, 339−406.
(12) Berry, R. E., Ding, X. D., Shokhireva, T. K., Weichsel, A., Montfort, W. R., and Walker, F. A. (2004) Axial ligand complexes of the *Rhodnius* nitrophorins: Reduction potentials, binding constants, EPR spectra, and structures of the 4-iodopyrazole and imidazole complexes of NP4. *J. Biol. Inorg. Chem. 9*, 135−144.
(13) Berry, R. E., Shokhireva, T. K., Filippov, I., Shokhirev, M. N., Zhang, H., and Walker, F. A. (2007) The effect of the N-terminus on heme cavity structure, ligand equilibrium and rate constants and reduction potentials of nitrophorin 2 from *Rhodnius prolixus*. *Biochemistry 46*, 6830−6843.
(14) Knipp, M., Yang, F., Berry, R. E., Zhang, H., Shokhirev, M. N., and Walker, F. A. (2007) Spectroscopic and functional characterization of nitrophorin 7 from the blood-feeding insect *Rhodnius prolixus* reveals an important role of its isoform-specific N-terminus for proper protein function. *Biochemistry 46*, 13254−13268.
(15) Traylor, T. G., and Sharma, V. S. (1992) Why NO? *Biochemistry 31*, 2847−2849.
(16) Nienhaus, K., Maes, E. M., Weichsel, A., Montfort, W. R., and Nienhaus, G. U. (2004) Structural dynamics controls nitric oxide affinity in nitrophorin 4. *J. Biol. Chem. 279*, 39401−39407.
(17) Benabbas, A., Ye, X., Kubo, M., Zhang, Z., Maes, E. M., Montfort, W. R., and Champion, P. M. (2010) Ultrafast dynamics of diatomic ligand binding to nitrophorin 4. *J. Am. Chem. Soc. 132*, 2811−2820.
(18) Maes, E. M., Roberts, S. A., Weichsel, A., and Montfort, W. R. (2005) Ultrahigh resolution structures of nitrophorin 4: Heme distortion in ferrous CO and NO complexes. *Biochemistry 44*, 12690−12699.
(19) Ribeiro, J. M. C. (1996) Salivary thiol oxidase activity of *Rhodnius prolixus*. *Insect Biochem. Mol. Biol. 26*, 899−905.
(20) Daff, S. (2010) NO synthase: Structures and mechanisms. *Nitric Oxide 23*, 1−11.
(21) Poulos, T. L. (2006) Soluble guanylate cyclase. *Curr. Opin. Struct. Biol. 16*, 736−743.
(22) Gladwin, M. T., Grubina, R., and Doyle, M. P. (2009) The new chemical biology of nitrite reactions with hemoglobin: R-state catalysis, oxidative denitrosylation, and nitrite reductase/anhydrase. *Acc. Chem. Res. 42*, 157−167.
(23) Basu, S., Grubina, R., Huang, J., Conradie, J., Huang, Z., Jeffers, A., Jiang, A., He, X., Azarov, I., Seibert, R., Mehta, A., Patel, R., King, B. S., Hogg, N., Ghosh, A., Gladwin, M. T., and Kim-Shapiro, D. B. (2007) Cataclytic generation of N_2O_3 by the concerted nitrite reductase and anhydrase activity of hemoglobin. *Nat. Chem. Biol. 3*, 785−794.
(24) Creutz, C., and Sutin, N. (1973) Reduction of ferricytochrome *c* by dithionite ion: Electron transfer by parralel adjacent and remote pathways. *Proc. Natl. Acad. Sci. U.S.A. 70*, 1701−1703.
(25) Knipp, M., Braun, O., and Vašák, M. (2005) Searching for DDAH inhibitors: *S*-Nitroso-L-homocysteine is a chemical lead. *J. Am. Chem. Soc. 127*, 2372−2373.
(26) Braun, O., Knipp, M., Chesnov, S., and Vašák, M. (2007) Specific reactions of *S*-nitrosothiols with cysteine hydrolases: A comparative study between dimethylargininase-1 and CTP synthetase. *Protein Sci. 16*, 1522−1534.
(27) Neya, S., Suzuki, M., Hoshino, T., Ode, H., Imai, K., Komatsu, T., Ikezaki, A., Nakamura, M., Furutani, Y., and Kandori, H. (2010) Molecular insights into intrinsic heme distortion in ligand binding in hemoprotein. *Biochemistry 49*, 5642−5650.
(28) Hintz, M. J., and Peterson, J. A. (1980) The kinetics of reduction of cytochrome $P\text{-}450_{cam}$ by the dithionite anion monomer. *J. Biol. Chem. 255*, 7317−7325.
(29) Wang, W., and Malcolm, B. A. (1999) Two-stage PCR protocol allowing introduction of multiple mutations, deletions and insertions using QuikChange Site-Directed Mutagenesis. *BioTechniques 26*, 680−682.
(30) Knipp, M., Zhang, H., Berry, R. E., and Walker, F. A. (2007) Overexpression in *Escherichia coli* and functional reconstitution of the liposome binding ferriheme protein nitrophorin 7 from the blood sucking bug *Rhodnius prolixus*. *Protein Expression Purif. 54*, 183−191.
(31) Yang, F., Zhang, H., and Knipp, M. (2009) A one-residue switch reverses the orientation of a heme *b* cofactor. Investigations on the ferriheme NO transporters nitrophorin 2 and 7 from the blood-feeding insect *Rhodnius prolixus*. *Biochemistry 48*, 235−241.

(32) Knipp, M., Taing, J. J., and He, C. (2011) Reduction of the lipocalin type heme containing protein nitrophorin: Sensitivity of the fold-stabilizing cysteine disulfides toward routine heme-iron reduction. *J. Inorg. Biochem.*, DOI: doi: 10.1016/j.jinorgbio.2011.07.009.

(33) Andersen, J. F., Ding, X. D., Balfour, C., Shokhireva, T. K., Champagne, D. E., Walker, F. A., and Montfort, W. R. (2000) Kinetics and equilibria in ligand binding by nitrophorins 1−4: Evidence for stabilization of a nitric oxide-ferriheme complex through a ligand-induced conformational trap. *Biochemistry 39*, 10118−10131.

(34) Knipp, M., and He, C. (2011) Nitrophorins: Nitrite disproportionation reaction and other novel functionalities of insect heme-based nitric oxide transport proteins. *IUBMB Life 63*, 304−312.

(35) Palaniappan, V., and Bocian, D. F. (1994) Acid-induced transformations of myoglobin. Characterization of a new equilibrium heme-pocket intermediate. *Biochemistry 33*, 14264−14274.

(36) Tang, Q., Kalsbeck, W. A., Olson, J. S., and Bocian, D. F. (1998) Disruption of the heme iron-proximal histidine bond requires unfolding of deoxymyoglobin. *Biochemistry 37*, 7047−7056.

(37) Spiro, T. G., and Li, X.-Y. (1988) Resonance Raman spectroscopy of metalloporphyrins. In *Resonance Raman Spectra of Heme and Metalloproteins* (Spiro, T. G., Ed.) 1st ed., pp 1−38, John Wiley & Sons, New York.

(38) Spiro, T. G., and Czernuszewicz, R. S. (2000) Resonance Raman Spectroscopy. In *Physical Methods in Bioinorganic Chemistry: Spectroscopy and Magnetism* (Que, L., Jr., Ed.) 1st ed., pp 59−119, UniversityScience Books, Sausalito, CA.

(39) Maes, E. M., Walker, F. A., Montfort, W. R., and Czernuszewicz, R. S. (2001) Resonance Raman spectroscopic study of nitrophorin 1, a nitric oxide-binding heme protein from *Rhodnius prolixus*, and its nitrosyl and cyano adducts. *J. Am. Chem. Soc. 123*, 1164−1172.

(40) Kincaid, J. R. (2000) Resonance Raman spectra of heme proteins and model compounds. In *The Porphyrin Handbook* (Kadish, K. M., Smith, K. M., and Guilard, R., Eds.) 1st ed., pp 225−291, Academic Press, San Diego.

(41) Andersson, L. A., Mylrajan, M., Sullivan, E. P. Jr., and Strauss, S. H. (1989) Modeling low-pH hemoproteins. *J. Biol. Chem. 264*, 19099−19102.

(42) Kitagawa, T., Kyogoku, Y., Iizuka, T., and Saito, M. I. (1976) Nature of the iron-ligand bond in ferrous low spin hemoproteins studied by resonance Raman scattering. *J. Am. Chem. Soc. 98*, 5169−5173.

(43) Spiro, T. G., Stong, J. D., and Stein, P. (1979) Porphyrin core expansion and doming in heme proteins. New evidence from resonance Raman spectra of six-coordinate high-spin iron(III) hemes. *J. Am. Chem. Soc. 101*, 2648−2655.

(44) Sage, J. T., Morikis, D., and Champion, P. M. (1991) Spectroscopic studies of myoglobin at low pH: Heme structure and ligation. *Biochemistry 30*, 1227−1237.

(45) Vetter, S. W., Terentis, A. C., Orsborne, R. L., Dawson, J. H., and Goodin, D. B. (2009) Replacement of the axial histidine heme ligand with cysteine in nitrophorin 1: Spectroscopic and crystallographic characterization. *J. Inorg. Biol. Chem. 14*, 179−191.

(46) He, C., and Knipp, M. (2009) Formation of nitric oxide from nitrite by the ferriheme *b* protein nitrophorin 7. *J. Am. Chem. Soc. 131*, 12042−12043.

(47) Sun, J., Loehr, T. M., Wilks, A., and Ortiz de Montellano, P. R. (1994) Identification of histidine 25 as the heme ligand in human liver heme oxygenase. *Biochemistry 33*, 13734−13740.

(48) Kitagawa, T., Ozaki, Y., Kyogoku, Y., and Horio, T. (1977) Resonance Raman study of the pH-dependent and detergent-induced structural alterations in the heme moiety of *Rhodospirillum rubrum* cytochrome *c*′. *Biochim. Biophys. Acta 495*, 1−11.

(49) Hobbs, J. D., Larsen, R. W., Meyer, T. E., Hazzard, J. H., Cusanovich, M. A., and Ondrias, M. R. (1990) Resonance Raman characterization of *Chromatium vinosum* cytochrom *c*′. Effect of pH and comparison of equilibrium and photolyzed cabron monoxide species. *Biochemistry 29*, 4166−4174.

(50) Yang, F., Knipp, M., Shokhireva, T. K., Berry, R. E., Zhang, H., and Walker, F. A. (2009) A ^{1}H and ^{13}C NMR spectroscopic study of the ferriheme resonances of three low-spin complexes of wild-type nitrophorin 2 and nitrophorin2(V24E) as a function of pH. *J. Biol. Inorg. Chem. 14*, 1077−1095.

(51) Decatur, S. M., Franzen, S., DePillis, G. D., Dyer, R. B., Woodruff, W. H., and Boxer, S. G. (1996) *Trans* effect in nitric oxide binding to myoglobin cavity mutant H93G. *Biochemistry 35*, 4939−4944.

(52) Ford, P. C. (2010) Reactions of NO and nitrite with heme models and proteins. *Inorg. Chem. 49*, 6226−6239.

(53) Praneeth, V. K. K., Näther, C., Peters, G., and Lehnert, N. (2006) Spectroscopic properties and electronic structure of five- and six-coordinate iron(II) porphyrin NO complexes: Effect of the axial N-donor ligand. *Inorg. Chem. 45*, 2795−2811.

(54) Scheidt, W. R., and Ellison, M. K. (1999) The synthetic and structural chemistry of heme derivatives with nitric oxide ligands. *Acc. Chem. Res. 32*, 350−359.

(55) Ibrahim, M., Xu, C., and Spiro, T. G. (2006) Differential sensing of protein influences by NO and CO vibrations in heme addcuts. *J. Am. Chem. Soc. 128*, 16834−16845.

(56) Reynolds, M.F., Parks, R. B., Burstyn, J. N., Shelver, D., Thorsteinsson, M. V., Kerby, R. L., Roberts, G. P., Vogel, K. M., and Spiro, T. G. (2000) Electronic absorption, EPR, and resonance Raman spectroscopy of CooA, a CO-sensing transcription activator from *R. rubrum*, reveals a five-coordinate NO-heme. *Biochemistry 39*, 388−396.

(57) Tomita, T., Ogura, T., Tsuyama, S., Imai, Y., and Kitagawa, T. (1997) Effects of GTP on bound nitric oxide of soluble guanylate cyclase probed by resonance Raman spectroscopy. *Biochemistry 36*, 10155−10160.

(58) Mukaiyama, Y., Uchida, T., Sato, E., Sasaki, A., Sato, Y., Igarashi, J., Kurokawa, H., Sagami, I., Kitagawa, T., and Shimizu, T. (2006) Spectroscopic and DNA-binding characterization of the isolated heme-bound basic helix-loop-helix-PAS-A domain of neuronal PAS protein 2 (NPAS2), a transcription activator associated with circadian rythms. *FEBS J. 273*, 2528−2539.

(59) Schade, D., Kotthaus, J., and Clement, B. (2010) Modulating the NO generating system from a medicinal chemistry perspective: Current trends and therapeutic options in cardiovascular disease. *Pharmacol. Ther. 126*, 279−300.

(60) Tomita, T., Hirota, S., Ogura, T., Olson, J. S., and Kitagawa, T. (1999) Resonance raman investigation of Fe-N-O structure of nitrosylheme in myoglobin and its mutants. *J. Phys. Chem. B 103*, 7044−7054.

(61) Sawai, H., Makino, M., Mizutani, Y., Ohta, T., Sugimoto, H., Uno, T., Kawada, N., Yoshizato, K., Kitagawa, T., and Shiro, Y. (2005) Structural characterization of the proximal and distal histidine environment of cytoglobin and neuroglobin. *Biochemistry 44*, 13257−13265.

(62) Lukat-Rodgers, G. S., and Rodgers, K. R. (1997) Characterization of ferrous FixL-nitric oxide adducts by resonance raman spectroscopy. *Biochemistry 36*, 4178−4187.

(63) Tomita, T., Gonzalez, G., Chang, A. L., Ikeda-Saito, M., and Gilles-Gonzalez, M. A. (2002) A comparative resonance Raman analysis of heme-binding PAS domains: Heme iron coordination structures of the *Bj*FixL, *Ax*PDEA1, *Ec*Dos, and *Mt*Dos proteins. *Biochemistry 41*, 4819−4826.

(64) Andrew, C. R., George, S. J., Lawson, D. M., and Eady, R. R. (2002) Six- to five-coordinate heme-nitrosyl conversion in cytochrome *c*′ and its releveance to guanylate cyclase. *Biochemistry 41*, 2353−2360.

(65) Andrew, C. R., Kemper, L. J., Busche, T. L., Tiwari, A. M., Kecskes, M. C., Stafford, J. M., Croft, L. C., Lu, S., Moënne-Loccoz, P., Huston, W., Mior, J. W. B., and Eady, R. R. (2005) Accessibility of the distial heme face, rather than Fe-His bond strength, determines the heme-nitrosyl coordination number of cytochromes *c*′: Evidence from spectroscopic studies. *Biochemistry 44*, 8664−8672.

(66) Vogel, K. M., Kozlowski, P. M., Zgierski, M. Z., and Spiro, T. G. (1999) Determinants of the FeXO (X = C, N, O) vibrational frequencies in heme adducts from experiment and density functional theory. *J. Am. Chem. Soc. 121*, 9915−9921.

(67) Deinum, G., Stone, J. R., Babcock, G. T., and Marletta, M. A. (1996) Binding of nitric oxide and carbon monoxide to soluble guanylate cyclase as observed with resonance Raman spectroscopy. *Biochemistry 35*, 1540−1547.

(68) Stone, J. R., and Marletta, M. A. (1994) Soluble guanylate cyclase from bovine lung: Activation with nitric oxide and carbon monoxide and spectral characterization of the ferrous and ferric states. *Biochemistry 33*, 5636−5640.

(69) Lukat-Rodgers, G. S., Correia, C., Botuyan, M. V., Mer, G., and Rodgers, K. R. (2010) Heme-based sensing by the mammalian circadian protein CLOCK. *Inorg. Chem. 49*, 6349−6365.

(70) Vogel, K. M., Hu, S., Spiro, T. G., Dierks, E. A., Yu, A. E., and Burstyn, J. N. (1999) Variable forms of soluble guanylyl cyclase: Protein-ligand interactions and the issue of activation by carbon monoxide. *J. Biol. Inorg. Chem. 4*, 804−813.

(71) Yu, A. E., Hu, S., Spiro, T. G., and Burstyn, J. N. (1994) Resonance Raman Spectroscopy of Soluble Guanylyl Cyclase Reveals Displacement of Distal and Proximal Heme Ligands by NO. *J. Am. Chem. Soc. 116*, 4117−4118.

(72) Shokhireva, T. K., Smith, K. M., Berry, R. E., Shokhirev, N. V., Balfour, C. A., Zhang, H., and Walker, F. A. (2007) Assignment of the ferriheme resonances of the high-spin forms of nitrophorins 1 and 4 by ^{1}H NMR spectroscopy: Comparison to structural data obtained from X-ray crystallography. *Inorg. Chem. 46*, 170−178.

(73) Shokhireva, T. K., Weichsel, A., Smith, K. M., Berry, R. E., Shokhirev, N. V., Balfour, C. A., Zhang, H., Montfort, W. R., and Walker, F. A. (2007) Assignment of the ferriheme resonances of the low-spin complexes of nitrophorins 1 and 4 by ^{1}H and ^{13}C NMR spectroscopy: Comparison to structural data obtained from X-ray crystallography. *Inorg. Chem. 46*, 2041−2056.

(74) Shokhireva, T. K., Berry, R. E., Zhang, H., Shokhirev, M. N., and Walker, F. A. (2008) Assignment of ferriheme resonances for high- and low-spin forms of nitrophorin 3 by ^{1}H and ^{13}C NMR spectroscopy and comparison to nitrophorin 2: Heme pocket structural similarities and differences. *Inorg. Chim. Acta 361*, 925−940.

(75) Baniulis, D., Yamashita, E., Zhang, H., Hasan, S., and Cramer, W. A. (2008) Structure-function of the cytochrome b_6f complex. *Photochem. Photobiol. 84*, 1349−1358.

(76) Barbieri, S., Murphy, L. M., Sawers, R. G., Eady, R. R., and Hasnain, S. S. (2008) Modulation of NO binding to cytochrome *c*′ by distal and proximal haem pocket residues. *J. Biol. Inorg. Chem. 13*, 531−540.

(77) Sharma, V. S., and Madge, D. (1999) Activation of soluble guanylate cyclase by carbon monoxide and nitric oxide: A mechanistic model. *Methods 19*, 494−505.

(78) Hobbs, A. J. (1997) Soluble guanylate cyclase: The forgotten sibling. *Trends Pharmacol. Sci. 18*, 484−491.

(79) Goodrich, L. E., Paulat, F., Praneeth, V. K. K., and Lehnert, N. (2010) Electronic structure of heme-nitrosyls and its significance for nitric oxide reactivity, sensing, transport, and toxicity in biological systems. *Inorg. Chem. 49*, 6293−6316.

(80) Yoshimura, T., and Siuzuki, S. (1988) The pH dependence of the stereochemistry around the heme group in NO-cytochrome *c* (horse heart). *Inorg. Chim. Acta 152*, 241−249.

(81) Duprat, A. F., Traylor, T. G., Wu, G.-Z., Coletta, M., Sharma, V. S., Walda, K. N., and Magde, D. (1995) Myoglobin-NO at low pH: Free four-coordinate heme in the protein pocket. *Biochemistry 34*, 2634−2644.

(82) Pellicena, P., Karow, D. S., Boon, E. M., Marletta, M. A., and Kuriyan, J. (2004) Crystal structure of an oxygen-binding heme domain related to soluble guanylate cyclases. *Proc. Natl. Acad. Sci. U.S.A. 101*, 12854−12859.

(83) Suzuki, S., Yoshimura, T., Nakahara, A., Iwasaki, H., Shidara, S., and Matsubara, T. (1987) Electronic and magnetic circular dichroism spectra of pentacoordinate nitrosylhemes in cytochromes *c*′ from nonphotosynthetic bacteria and their model complexes. *Inorg. Chem. 26*, 1006−1008.

(84) Iwasaki, H., Yoshimura, T., Suzuki, S., and Shidara, S. (1991) Spectral properties of *Achromobacter xylosoxidans* cytochrome *c*′ and their NO complexes. *Biochim. Biophys. Acta 1058*, 79−82.

(85) Yoshimura, T., Fujii, S., Kamada, H., Yamaguchi, K., Suzuki, S., Shidara, S., and Takakuwa, S. (1996) Spectroscopic characterization of nitrosylheme in nitric oxide complexes of ferric and ferrous cytochrome *c*′ from photosynthetic bacteria. *Biochim. Biophys. Acta 1292*, 39−46.

(86) Lawson, D. M., Stevenson, C. E. M., Andrew, C. R., and Eady, R. R. (2000) Unprecedented proximal binding of nitric oxide to heme: Implications for guanylate cyclase. *EMBO J. 19*, 5661−5671.

(87) Kharitonov, V. G., Sharma, V. S., Magde, D., and Koesling, D. (1997) Kinetics of nitric oxide dissociation from five- and six-coordinate nitrosyl hemes and heme proteins, including soluble guanylate cyclase. *Biochemistry 36*, 6814−6818.

(88) Pinakoulaki, E., Gemeinhardt, S., Saraste, M., and Varotsis, C. (2002) Nitric-oxide reductase: Structure and properties of the catalytic site from resonance Raman scattering. *J. Biol. Chem. 277*, 23407−23413.

(89) Xu, C., and Spiro, T. G. (2008) Ambidentate H-bonding by heme-bound NO: Structural and spectral effects of -O versus -N H-bonding. *J. Biol. Inorg. Chem. 13*, 613−621.

(90) Ma, X., Sayed, N., Beuve, A., and van den Akker, F. (2007) NO and CO differentially activate soluble guanylate cyclase via a heme pivot-bend mechanism. *EMBO J. 26*, 578−588.

(91) Zhong, F., Wang, H., Ying, T., Huang, Z.-X., and Tan, X. (2010) Efficient expression of human soluble guanylate cyclase in *Escherichia coli* and its signaling-related interaction with nitric oxide. *Amino Acids 39*, 399−408.

(92) Kitagawa, T. (1988) in *Biological Applications of Raman Spectroscopy* (Spiro, T. G., Ed.) pp 97−131, John Wiley & Sons, New York.

(93) Coyle, C. M., Vogel, K. M., Rush, T. S. III, Kozlowski, P. M., Williams, R., Spiro, T. G., Dou, Y., Ikeda-Saito, M., Olson, J. S., and Zgierski, M. Z. (2003) FeNO structure in distal pocket mutants of myoglobin based on resonance Raman spectroscopy. *Biochemistry 42*, 4896−4903.

(94) Hough, M. A., Antonyuk, S. V., Barbieri, S., Rustage, N., McKay, A. L., Servid, A. E., Eady, R. R., Andrew, C. R., and Hasnain, S. S. (2011) Distal-to-proximal NO conversion in hemoproteins: The role of the proximal pocket. *J. Mol. Biol. 405*, 395−409.

(95) Scheidt, W. R., and Frisse, M. E. (1975) Nitrosylmetalloporphyrins. II. Synthesis and molecular sterochemistry of nitrosyl-$\alpha,\beta,\gamma,\delta$-tetraphenylporphinatoiron(II). *J. Am. Chem. Soc. 97*, 17−21.

(96) Spiro, T. G., and Wasbotten, I. H. (2005) CO as a vibrational probe of heme protein active sites. *J. Inorg. Biochem. 99*, 34−44.

(97) Wyllie, G. R. A., Schulz, C. E., and Scheidt, W. R. (2003) Five- to six-coordination in (nitrosyl)iron(II) porphyrinates: Effects of binding the sixth ligand. *Inorg. Chem. 42*, 5722−5734.

(98) Scheidt, W. R., and Piciulo, P. L. (1976) Nitrosylmetalloporphyrins. III. Synthesis and molecular stereochemistry of nitrosyl-$\alpha,\beta,\gamma,\delta$-tetraphenylporphinato(1-methylimidazole)iron(II). *J. Am. Chem. Soc. 98*, 1913−1919.

(99) Silvernail, N. J., Pavlik, J. W., Noll, B. C., Schulz, C. E., and Scheidt, W. R. (2008) Reversible NO motion in crystaline [Fe(porphy)(1-MeIm)(NO)] derivatives. *Inorg. Chem. 47*, 912−920.

(100) Copeland, D. N., Soares, A. S., West, A. H., and Richter-Addo, G. B. (2006) Crystal structures of the nitrite and nitric oxide complexes of horse heart myoglobin. *J. Inorg. Biochem. 100*, 1413−1425.

(101) Brucker, E. A., Olson, J. S., Ikeda-Saito, M., and Phillips, G. N. Jr. (1998) Nitric oxide myoglobin: Crystal structure and analysis of ligand geometry. *Proteins: Struct., Funct., Genet. 30*, 352−356.

(102) Copeland, D. N., West, A. H., and Richter-Addo, G. B. (2003) Crystal structure of ferrous horse heart myoglobin complexed with nitric oxide and nitrosoethane. *Proteins: Struct., Funct., Genet. 53*, 182−192.

(103) A study of multiple scattering analysis of XAFS data from a frozen solution of Mb[Fe^{II}-NO] yielded 150°: Rich, A. M.,

Armstrong, R. S., Ellis, P. J., and Lay, P. A. (1998) Determination of the Fe−Ligand Bond Lengths and Fe−N−O bond angles in horse heart ferric and ferrous nitrosylmyoglobin using multiple-scattering XAFS analyses. *J. Am. Chem. Soc. 120*, 10827−10836.

(104) Tangen, E., Savadberg, A., and Ghosh, A. (2005) Toward modeling H-NOX domains: A DFT study of heme-NO complexes as hydrogen bond acceptors. *Inorg. Chem. 44*, 7802−7805.

(105) Lehnert, N., Sage, J. T., Silvernail, N., Scheidt, W. R., Alp, E. E., Sturhahn, W., and Zhao, J. (2010) Oriented single-crystal nuclear resonance vibration spectroscopy of [Fe(TPP)(MI)(NO)]: Quantitative assessment of the *trans* effect of NO. *Inorg. Chem. 49*, 7197−7215.

(106) Sigfridsson, E., and Ryde, U. (1999) On the significance of hydrogen bonds for the discrimination between CO and O_2 by myoglobin. *J. Biol. Inorg. Chem. 4*, 99−110.

(107) Ribeiro, J.M. C. (1998) *Rhodnius prolixus* salivary nitrophorins display heme-peroxidase activity. *Insect Biochem. Mol. Biol. 28*, 1051−1057.

(108) Karow, D. S., Pan, D., Tran, R., Pellicena, P., Presley, A., Mathies, R. A., and Marletta, M. A. (2004) Spectroscopic characterization of the soluble guanylate cyclase-like heme domains from *Vibrio cholerae* and *Thermoanaerobacter tengcongensis*. *Biochemistry 43*, 10203−10211.

(109) Mukaiyama, Y., Uchida, T., Sato, E., Sasaki, A., Sato, Y., Igarashi, J., Kurikawa, H., Sagami, I., Kitagawa, T., and Shimizu, T. (2006) Spectroscopic and DNA-binding characterozation of the isolated heme-bound basic helix-loop-helix-PAS-A domain of neuronal PAS protein 2 (NPAS2), a transcription activator protein associated with circadian rythms. *FEBS J. 273*, 2528−2539.

(110) Igarashi, J., Sato, A., Kitagawa, T., Yoshimura, T., Yamauchi, S., Sagami, I., and Shimizu, T. (2004) Activation of heme-regulated eukaryotic initiator factor 2α kinase by nitric oxide is induced by the formation of a five-coordinate NO-heme complex. Optical absorption, electron spin resonance, and resonance Raman spectral studies. *J. Biol. Chem. 279*, 15752−15762.

(111) Humphrey, W., Dalke, A., and Schulten, K. (1996) VMD: Visual Molecular Dynamics. *J. Mol. Graphics 14*, 33−38.

Breaking the Proximal Fe^{II}–N_{His} Bond in Heme Proteins through Local Structural Tension: Lessons from the Heme *b* Proteins Nitrophorin 4, Nitrophorin 7, and Related Site-Directed Mutant Proteins

Chunmao He,[†] Saburo Neya,[‡] Markus Knipp*[,†]

[†] *Max-Planck-Institut für Bioanorganische Chemie, Stiftstrasse 34-36, D-45470 Mülheim an der Ruhr, Germany*

[‡] *Department of Physical Chemistry, Graduate School of Pharmaceutical Sciences, Chiba University, Image-Yayoi, Chiba 263-8522, Japan*

* Supporting Information *

* To whom correspondence should be addressed: Telephone: +49 (0)208 306 3671. Fax: +49 (0)208 306 3951. E-mail: mknipp@mpi-muelheim.mpg.de.

Figure S1: Amino acid sequence alignment of *R. prolixus* NP1 (Swiss-Port entry Q26239), NP2 (Swiss-Port entry Q26241), NP3 (Swiss-Port entry Q94733), NP4 (Swiss-Port entry Q94734), and NP7 (Swiss-Prot entry Q6PQK2) (*1*). The total sequence identity among all 5 protein sequences amount to 33% (indicated by '*'). The proximal His is indicated by '#'. An initial Met residue (in grey) results in case of the recombinantly expressed proteins of NP1, NP2, NP3, and NP7 is not present in the mature proteins *in vivo* (*2, 3*). Residues of relevance to this study are highlighted in color.

```
     0         10         20         30         40         50         60
NP1: M    KCTKNAL AQTGFNKDKY FNGDVWYVTD YLDLEPDDVP KRYCAALAAG TASGKLKEAL (57)
NP2: M    DCSTNIS PKQGLDKAKY FSG-KWYVTH FLDKDP-QVT DQYCSSFTPR ESDGTVKEAL (55)
NP3: M    DCSTNIS PKKGLDKAKY FSG-TWYVTH YLDKDP-QVT DPYCSSFTPK ESGGTVKEAL (55)
NP4:      ACTKNAI AQTGFNKDKY FNGDVWYVTD YLDLEPDDVP KRYCAALAAG TASGKLKEAL (57)
NP7: M LPGECSVNVI PKKNLDKAKF FSG-TWYETH YLDMDP-QAT EKFCFSFAPR ESGGTVKEAL (58)
          *  *         * *  * *  ** *   **  *        *          *  ****

       #      70         80         90        100        110        120
NP1:   YHYDPKTQDT FYDVSELQEE SPG-KYTANF KKVEKNGNVK VDVTSGNYYT FTVMYADDSS (116)
NP2:   YHYNANKKTS FYNIGEGKLE SSGLQYTAKY KTVDKKKAVL KEADEKNSYT LTVLEADDSS (115)
NP3:   YHFNSKKKTS FYNIGEGKLG SSGVQYTAKY NTVDKKRKEI EPADPKDSYT LTVLEADDSS (115)
NP4:   YHYDPKTQDT FYDVSELQVE SLG-KYTANF KKVDKNGNVK VAVTAGNYYT FTVMYADDSS (116)
NP7:   YHFNVDSKVS FYNTGTGPLE SNGAKYTAKF NTVDKKGKEI KPADEKYSYT VTVIEAAKQS (118)
       **         **         *    ***     * *              **  **  *   *

              130        140        150        160        170        180
NP1:   ALIHTCLHKG NKDLGDLYAV LNRNKDTNAG DKVKGAVTAA SLKFSDFIST KDNKCEYDNV (176)
NP2:   ALVHICLREG SKDLGDLYTV LTHQKDAEPS AKVKSAVTQA GLQLSQFVGT KDLGCQYD-D (174)
NP3:   ALVHICLREG PKDLGDLYTV LSHQKTGEPS ATVKNAVAQA GLKLNDFVDT KTLSCTYD-D (174)
NP4:   ALIHTCLHKG NKDLGDLYAV LNRNKDAAAG DKVKSAVSAA TLEFSKFIST KENNCAYDND (176)
NP7:   ALIHICLQED GKDIGDLYSV LNRNKNALPN KKIKKALNKV SLVLTKFVVT KDLDCKYD-D (177)
       ** * **     ** **** * *   *         * *           *  * *   * **

NP1:   SLKSLLTK (184)
NP2:   QFTSL    (179)
NP3:   QFTSM    (179)
NP4:   SLKSLLTK (184)
NP7:   KFLSSWQK (185)
          *
```

Figure S2: Absorption spectra of hemin dissolved in 100 mM NaOH recorded immediately after dilution in 100 mM NaH_2PO_4/NaOH (pH 7.5) (*black trace*). Afterwards, the hemin was reduced with $Na_2S_2O_4$ (*red trace*) and finally DEA/NO was added (*blue trace*).

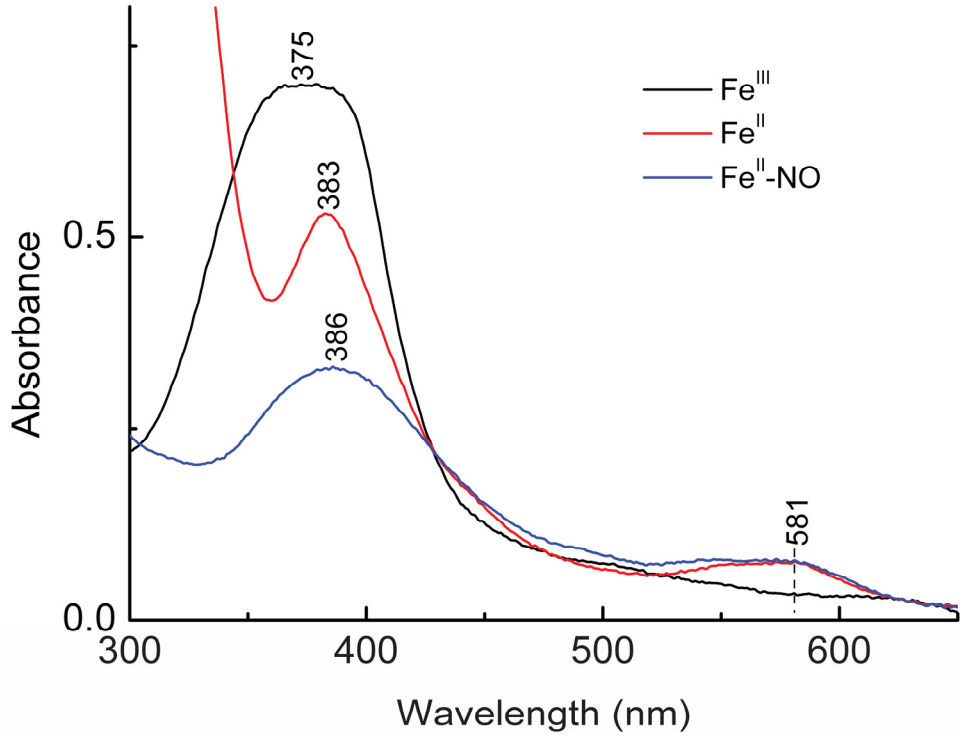

Table S1: Summary of the geometry of the Fe–N–O entity in crystal structures of nitrosyl complexes of nitrophorins.

Protein	PDB code	pH	Resolution (Å)	Fe↔N[a] (Å)	N↔O[b] (Å)	∠(Fe–N–O)[c]	N_{NO}↔O_{water}[d] (Å)
NP1	4NP1 (*4*)[e]	7.5	2.3	2.0	1.3	120°	-
NP2	1T68 [e]	7.5	1.45	1.93	1.38	133°	4.11
NP4	1X8N (*5*)[f]	7.4	1.08	1.71	1.20	144°	3.80
	1KOI (*6*)[g]	5.6	1.08	1.66	1.14	155°	3.71
	1X8O (*5*)[g]	5.6	1.01	1.69	1.09	159°	3.88
	1YWB (*7*)[f]	5.6	0.97	1.73	1.15	141°	3.78

[a] Distance between heme iron and NO nitrogen. [b] Interatomic distance in the Fe bound NO. [c] Angel of the Fe–N–O entity. [d] Distance between the NO oxygen and the closest water molecule. [e] Photoreduced ferroheme form. [f] Chemically ferroheme form. [g] Ferriheme form.

References

(1) Knipp, M., Yang, F., Berry, R. E., Zhang, H., Shokhirev, M. N., and Walker, F. A. (2007) Spectroscopic and functional characterization of nitrophorin 7 from the blood-feeding insect *Rhodnius prolixus* reveals an important role of its isoform-specific N-terminus for proper protein function. *Biochemistry 46*, 13254-13268.

(2) Berry, R. E., Shokhireva, T. K., Filippov, I., Shokhirev, M. N., Zhang, H., and Walker, F. A. (2007) The effect of the N-terminus on heme cavity structure, ligand equilibrium and rate constants and reduction potentials of nitrophorin 2 from *Rhodnius prolixus*. *Biochemistry 46*, 6830-6843.

(3) Knipp, M., Zhang, H., Berry, R. E., and Walker, F. A. (2007) Overexpression in *Escherichia coli* and functional reconstitution of the liposome binding ferriheme protein nitrophorin 7 from the blood sucking bug *Rhodnius prolixus Prot. Expr. Purif. 54*, 183-191.

(4) Ding, X. D., Weichsel, A., Andersen, J. F., Shokhireva, T. K., Balfour, C., Pierik, A. J., Averill, B. A., Montfort, W. R., and Walker, F. A. (1999) Nitric oxide binding to the ferri- and ferroheme states of nitrophorin 1, a reversible NO-binding heme protein from the saliva of the blood-sucking insect, *Rhodnius prolixus*. *J. Am. Chem. Soc. 121*, 128-138.

(5) Kondrashov, D. A., Roberts, S. A., Weichsel, A., and Montfort, W. R. (2004) Protein functional cycle viewed at atomic resolution: Conformational change and mobility in nitrophorin 4 as a function of pH and NO binding. *Biochemistry 43*, 13637-13647.

(6) Roberts, S. A., Weichsel, A., Qiu, Y., Shelnutt, J. A., Walker, F. A., and Montfort, W. R. (2001) Ligand-induced heme ruffling and bent NO geometry in ultra-high-resolution structures of nitrophorin 4. *Biochemistry 40*, 11327-11337.

(7) Maes, E. M., Roberts, S. A., Weichsel, A., and Montfort, W. R. (2005) Ultrahigh resolution structures of nitrophorin 4: Heme distortion in ferrous CO and NO complexes. *Biochemistry 44*, 12690-12699.

Breaking of the Fe-His bond

Chapter 8. General discussion and conclusion

Since the first report of NPs in 1993,[1] the major research interest has been devoted to the elucidation of the NO-transporting properties and histamine sequestration. Thus, NPs were mainly looked at as simple NO vehicles. In this study, the reactivity of NPs was first addressed in an extensive manner. The thesis focuses on two major aspects. One of the aspects dealt with the interaction of the ferriheme NPs with nitrite, where it was shown that an unprecedented reaction occurs. Further investigations revealed part of the reaction mechanism. Although NPs are natively ferriheme proteins, the Fe^{II} state is also interesting since the Fe^{II}-CO derivative is isoelectronic to and used as a model for {FeNO}^{6}, for example, in FT-IR and laser flash photolysis experiments.[2,3] However, there are only very few reports on the Fe^{II} state of NPs including the crystal structures of several *wt* NP4 derivatives[4] and the proposed Fe^{II} intermediate state in the reduction of NPs with low-molecular weight thiols.[5] Hence, a deeper insight into the redox properties of NPs is required.

8.1. The interaction of nitrite with nitrophorins

The results of reactivity of NP4 and NP7 with nitrite are presented in *Chapter 2* where the stoichiometry is established as presented in Eq. (1):

$$3NO_2^- + 2H^+ \xrightarrow{NP[Fe^{III}]} 2NO + NO_3^- + H_2O \qquad (1)$$

This equation resembles the stoichiometry of nitrite disproportionation reaction occurring in aqueous media at pH < 4 (see *Chapter 1.4.1*). This is the first example of such a reaction at neutral pH promoted by ferriheme proteins. The affinities of nitrite to NP4 (K_d = 66 mM) and NP7 (K_d = 5.2 mM) are comparable to those of metMb (K_d = 17 mM) and

metHb (K_d = 6.5 mM).[6] However, metMb and metHb only coordinate nitrite,[6] whereas NPs do turnover the nitrite to NO although the reaction rate is rather slow under our experimental conditions (5600 pM s^{-1} when incubating 10 µM NP7 with 1mM NO_2^- at 37 °C). Based on the results from the present thesis work, NPs are classified by IUBMB as the first example of nitrite dismutase (EC 1.7.6.1).[§§§]

Therefore, the question remains as to the biological relevance of this process given the slow reaction rate and the low nitrite affinity. Under our experimental conditions, the produced NO coordinates subsequently to NPs ($K_d^{[NP4–NO]}$ = 0.12 µM at pH 7.5),[7] which induces strong product inhibition, Eq. (2). *In vivo*, there are numerous NO reactive species R, e.g., low-molecular weight thiols, transition metals, and radicals like $O_2^{\bullet-}$, which can trap NO and regenerate NPs according to Eq. (3).

$$NO + NP[Fe^{III}] \rightleftharpoons NP[Fe^{III}\text{-}NO] \qquad (2)$$

$$NP[Fe^{III}\text{-}NO] + R \longrightarrow NP[Fe^{III}] + R\text{-}NO \qquad (3)$$

R = NO reactive species

In vitro, it was shown in this thesis that in the presence of the NO-trapping compound (R = 2-phenyl-4,4,5,5,-tetramethylimidazoline-1-oxyl 3-oxide, PTIO), several turn overs are possible. NPs can, thus act as catalysts for the reaction Eq. (1). Furthermore, it was reported that some of the NPs can also interact with other compounds *in vivo* resulting in conformational changes. For example, NP2 binds to the coagulation factor IX[8] and NP7 to the negatively charged, for example, L-α-phosphatidyl-L-serine (PS) containing phospholipid membranes.[9,10] It is possible to speculate that such interactions are capable to change the reactivities of NPs, thus increasing the effective turn-over under physiological conditions.

[§§§]Detailed information at: http://www.enzyme-database.org/query.php?ec=1.7.6.1

To further address the question by which mechanism the nitrite disproportionation reaction is accomplished, the nitrite complexes of NP4, NP7, NP4(D30N), and a new mutant protein NP4(L130R) were studied (refer to *Chapters 3*, *4*, and *5*). UV/vis, RR, and EPR spectroscopy show that the nitrite complexes of NP4 and NP7 behave similarly to the model complexes [Fe(TpivPP)(η^1-NO_2)(Py)] and [Fe(TpivPP)(η^1-NO_2)(ImH)].[11] The X-ray crystal structure of NP4–NO_2^- was solved (*Chapter 3*) and further supports the η^1-N nitro binding mode. This is the binding mode observed for most of the ferriheme proteins and model complexes. However, there is no potential H-bonding residue in the distal heme pocket of NP4–NO_2^-, which is critical for the function of many other nitrite-binding heme proteins (Table 1) (compare Figure 10 in *Chapter 1.4.2*). Moreover, protons are required for the nitrite disproportionation reaction Eq. (1). How can NPs facilitate this reaction without H-bonding residues in their distal pocket?

Table 1. Summary of the X-ray crystal structures of nitrite complexes with heme proteins.

Protein	PDB entry	Heme	Proximal ligand	Fe–NO_2^- (Å)	Fe–L (Å)	H-Bonding res., Dist. (Å)	Ref
cd$_1$ NiR[a]	1AOQ	Heme *d*$_1$	His	2.0	2.0	His345 N^{ε}, 3.2 His388 N^{ε}, 3.2	12
cc NiR[b]	2E80	Heme *c*	Lys	1.9	2.1	Arg114:N^{ω}, 2.8	13
SiRHP[c]	3GEO	Siroheme	Cys	2.0	2.4	His277:N^{ε}, 2.6 Arg82:N^{ω}, 3.2 Arg153:N^{ω}, 3.8 Lys215:N^{ε}, 2.9 Lys217:N^{ε}, 3.0	14
metHb[d]	3D7O	Heme *b*	His	2.0	2.0	His63 N^{ε}, 2.9	15
metMb[e]	2FRF	Heme *b*	His	1.9	2.1	His64:N^{ε}, 2.8	16
metMb(H64V/V67R)[e]	3HEO	Heme *b*	His	2.1	2.1	Arg67:N^{ω}, 3.2	17
Cld[f]	3Q09	Heme *b*	His	2.1	2.1	Arg183:N^{ω}, 2.7	18
NP4	3MVF	Heme *b*	His	2.0	2.0	--	19

[a] Cytochrome *cd*$_1$ nitrite reductase from *T. pantotropha*. [b] Cytochrome *c* nitrite reductase from *W. succinogenes*. [c] *E. coli* sulfite reductase hemoprotein. [d] Human methemoglobin. [e] Horse heart metmyoglobin. [f] Chlorite dismutase from *D. aromatica*.

Inspired by the work of Richter-Addo and co-workers on horse metMb, which shows that the distal H-bonding residue is key for their *O*-bound nitrito mode,[17] an Arg residue was inserted into the distal heme pocket of NP4 by Leu130 → Arg mutation. The heme cavity

of the mutant protein NP4(L130R) itself is not affected as confirmed by UV/vis, RR and EPR spectroscopy and X-ray crystallography. Different to metMb and metMb(H64V/V67R), the crystal structure of NP4(L130R)–NO_2^- reveals a similar nitrite binding mode compared to the *wt* NP4–NO_2^-, i.e., η^1-N nitro mode. The angles between the nitrite and His ligand are 6° and 18° for *wt* NP4–NO_2^- and NP4(L130R)–NO_2^-, respectively. However, the change in the UV/vis absorbance upon NO_2^- binding is much more significant in the case of NP4(L130R) compared to *wt* NP4 ($\Delta\varepsilon_{404nm}^{NP4(L130R)}$ = 12,500 M^{-1} cm^{-1} *vs.* $\Delta\varepsilon_{404nm}^{wt\ NP4}$ = 3,400 M^{-1} cm^{-1}).[19] What is the reason for the marked difference between the changes observed in solution given their similar nitrite binding mode as obtained in X-ray crystallography? The EPR spectra of wild type and NP4(L130R)–NO_2^- complexes contain two sets of LS signals, a normal rhombic (g_1 = 2.70, g_2 = 2.42, g_3 = 1.49) and a HALS type of signal (g_{max} = 3.3). The EPR spectrum of *wt* NP4–NO_2^- shows mainly the normal rhombic signal (70% of the total spins), whereas NP4(L130R)–NO_2^- shows more HALS signal (75% of the total spins). In the case of model complexes [Fe(TpivPP)(η^1-NO_2)(Py)] and [Fe(TpivPP)(η^1-NO_2)(ImH)] the NO_2^- ligand is more perpendicular oriented to the axial ligand (77° and 69°, respectively),[11] with g_{max} of 2.98 and 2.87, respectively. It is concluded that the HALS signal observed in the case of NP4 is attributed to a rotational isomer with a more perpendicular ligand orientation, which is not observed in the X-ray structure. This may be a consequence of the crystal packing. However, the reasons for the presence of a HALS type of signal are multi-factorial (see *Chapter 1.5.2.1*) and, therefore, other factors may also contribute.

The reactivity of the mutant protein NP4(L130R) toward nitrite is much slower compared to *wt* NP4. The major structural difference between the nitrite complexes of the two proteins lies in the distal heme pocket (Figure 1). In the case of *wt* NP4–NO_2^- a water net-

work that connects the Asp30 with the nitrite molecule (Figure 1a), whereas in NP4(L130R) $–NO_2^-$ this network is disrupted (Figure 1b).

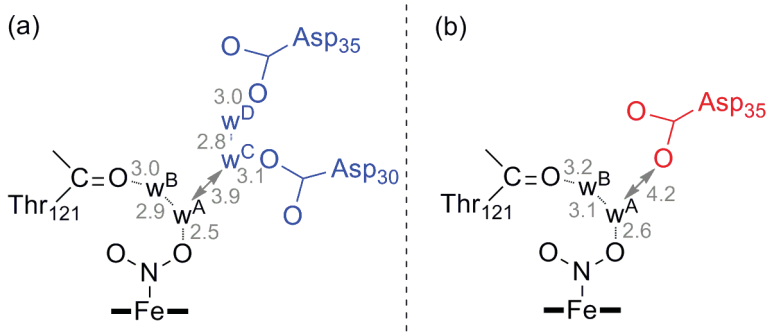

Figure 1. Schematic representation of water molecules and important side chains of the X-ray crystal structures of nitrite complexes with (a) *wt* NP4 and (b) NP4(L130R).

The ultra high resolution (0.85 Å) X-ray crystal structures of *wt* NP4 and its mutants [i.e., NP4(D30N) and NP4(D30A)] in combination with calculations postulate an unusually high pK_a of 5.5-7.4 for Asp30.[20-22] Thus, it is proposed that Asp30 may be able to donate protons through this water network that is essential for the nitrite disproportionation reaction.

According to the present study, NPs catalyze the nitrite disproportionation reaction, Eq. (1). The initial nitrite complex has been characterized through UV/vis absorption and EPR spectroscopies, X-ray crystallography, and stopped-flow kinetics. Furthermore, Asp30 can serve as the source for H^+ that is critical for this reaction. However, the trapping of the second nitrite or any other intermediate by spectroscopic and crystallographic methods did not succeed. Nevertheless, even the mechanism of the nitrite disproportionation reaction at low pH aqueous solutions is very complex and yet to be fully elucidated (Figure 2). It is likely that the first step involves protonation of nitrite to form nitrous acid.[23]

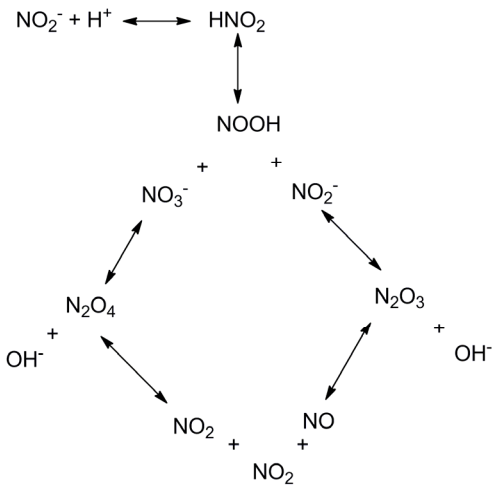

Figure 2. Proposed reaction pathways of nitrogen oxides. Adapted from ref 23.

The rate of NO production from nitrite disproportionation at physiological pH and concentration (i.e., pH 7.2-7.4 and $[NO_2^-]$ = 10-50 μM) was estimated to occur through the N_2O_3 pathway (Figure 2) with an apparent rate of 0.05-1 pM s^{-1}.[23] It increases to ~ 100 pM s^{-1} when $[NO_2^-]$ = 1 mM, which is still much slower compared to the NO production in the presence NPs (5600 pM s^{-1}, 10 μM NP7, 1mM NO_2^-).

By analogy to the initial step of nitrite disproportionation in aqueous solution, the bound nitrite on NPs may also be at first protonated, producing Fe^{III}–$[HNO_2]$, which can then further react. In studies of the nitrite complexes of Fe^{III}–porphyrin, i.e., $Fe^{III}(TPP)OClO_3$, $Fe^{III}(TTP)OClO_3$, and $Fe^{III}(OEP)OClO_3$, the compounds were not stable in organic solvents. It appeared that ferrous nitrosyl complexes were formed through single oxygen atom transfer (OAT) from a coordinated nitrite to a free nitrite according to Eq. (4):[24]

$$[Fe^{III}(P)(NO_2)(ONO)]^- + NO_2^- \longrightarrow Fe^{II}(P)(NO)(ONO)]^- + NO_3^- \qquad (4)$$

P = porphyrin

By analogy, NP[Fe^{III}–NO_2^-] may also transfer an oxygen atom to the free nitrite to form NP[Fe^{II}–NO]. Unfortunately, we were unable to trap this compound using UV/vis and

EPR spectroscopy, which may be due to its subsequent oxidation to NP[Fe^{III}–NO] by the excess nitrite present in the system according to Eq. (5).

$$NP[Fe^{II}\text{-}NO] + NO_2^- + 2H^+ \rightleftharpoons NP[Fe^{III}\text{-}NO] + NO + H_2O \qquad (5)$$

Moreover, Eq. (5) is a plausible reaction particularly in the case of NPs considering the much lower reduction potentials of NP[$Fe^{III/II}$–NO] compared to those of model complexes and heme proteins (Table 2). The reduction potential of the NO_2^-/NO redox couple is strongly pH dependent as shown in Scheme 1. In fact, it was reported that nitrite can catalyze the reductive nitrosylation of metHb, metMb, and model ferriheme compounds, which shifts the equilibrium of Eq. (5) to the left (see also *Chapter 1.4.3.3*).[25] Thus, it is reasonable to propose that in the case of NPs where the reduction potential of $Fe^{III/II}$–NO is much smaller [$E_o(NO_2^-/NO)$: ~0.37 V *vs.* $E_o(Fe^{III/II}\text{–NO})$ of NP1: 0.13 V] at pH 7.5, Fe^{II}–NO can be oxidized by nitrite to form Fe^{III}–NO.

Table 2. Reduction potentials for the nitrosyl complexes with ferriheme models and proteins[a]

Ferriheme models or proteins	Fe^{III}(TMPyP)[b]	Fe^{III}(TPPS)[c]	metHb[d]	metMb[d]	NP1[e]	NP2(D1A)[f]	NP4[g]	NP7[h]
E(V)	+0.79	+0.59	~ +0.53	+0.47	+0.13	–0.02	+0.06	+0.11

[a] Reduction potential vs SHE at 27 °C, pH 7.5; [b] TMPyP = *meso*-tetrakis(*N*-methyl-4-pridyl)porphyrinato, from ref 26; [c] TPPS = tetra(4-sulfonato-phenyl)porphyrinato, from ref 27; [d] from ref 28,29; [e] from ref 30; [f] from ref 31; [g] from ref 32,33; [h] from ref 34.

Scheme 1. Latimer diagram of nitrogen oxides in acidic and basic solution (units in V).[35]

Acidic soluion

$$HNO_3 \xrightarrow{+0.94} HNO_2 \xrightarrow{+1.00} NO \xrightarrow{+1.59} N_2O \xrightarrow{+1.77} N_2 \xrightarrow{-0.23} N_2H_5^+ \xrightarrow{+1.28} NH_4^+$$

+5 +3 +2 +1 0 -2 -3

Basic soluion

$$NO_3^- \xrightarrow{+0.01} NO_2^- \xrightarrow{-0.46} NO \xrightarrow{+0.79} N_2O \xrightarrow{+0.94} N_2 \xrightarrow{-1.16} N_2H_4 \xrightarrow{+0.10} NH_3$$

8.2. An unprecedented arginine coordination to the heme iron in NP4(L130R)

As mentioned above, the mutant protein NP4(L130R) was engineered so as to investigate the effect of an H-bonding residue in NP4 on the nitrite binding and reactivity. Surprisingly, the X-ray crystal structure of NP4(L130R) obtained at 100 K reveals an Arg130:N^{ω} coordination to the Fe with a distance of 2.1 Å (occupancy, 60%). Examples of coordination complexes with guanine ligands are very rare, in biomolecules nearly not existing. Metal complexes of guanidines have been reported for Co^{II}, $Cu^{I/II}$, Zn^{II}, Pd^{II}, Ni^{II}, Cr^{II}, Au^{I}, and Pt^{II}, where in all cases the coordination was achieved via the imine nitrogen. The only example of Arg coordination to iron is in the case of biotin synthase BioB, in which the Arg residue coordinates to one of the irons in the [Fe_2S_2] cluster.[36,37] In contrast to the X-ray crystallography data, UV/vis and RR recorded both at room temperature and in frozen solutions show a six-coordinate high spin (6cHS) ferric heme complex with H_2O as the sixth ligand. Dose-dependent X-ray irradiation on crystals observed by micro-absorbance spectroscopy that the ferric heme is readily reduced by a very low dose (0.45 MGy) of X-ray irradiation. To demonstrate the reason for this apparent disagreement, RR spectra of the chemically reduced NP4(L130R) were recorded in solution and at 77 K. Interestingly, where in solution a 5c complex is formed, the spectrum of the frozen sample is indicative of 6cLS. For an overview, see Scheme 2.

Scheme 2. Tentative reaction scheme of the binding of the internal Arg130 to NP4(L130R)[Fe^{II}].

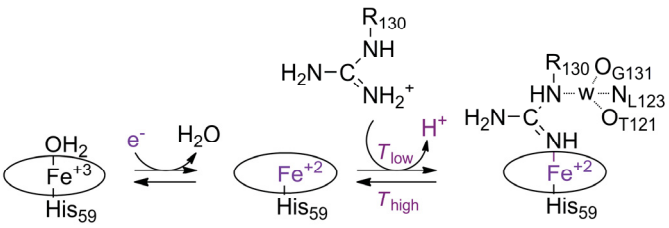

Thus, NP4(L130R) represents the first example of an Arg coordination to a metalloporphyrin.

8.3. Ferrous oxidation state of nitrophorins

As already mentioned, there is increasing interest in ferrous NPs, the first detailed investigation of the unliganded form was carried out during this thesis work. It was observed that ferroheme NPs react with O_2 at a remarkably high rate, which may be due to the low reduction potentials and the very open distal heme pocket of NPs.[38] Thus, special care should be taken when producing and handling ferroheme NPs. The effect of the routinely used reducing agent $Na_2S_2O_4$ on the Cys–Cys disulfide of NPs was first considered. It revealed that excess $Na_2S_2O_4$ indeed breaks the Cys–Cys disulfide, forming CysH/Cys^- and Cys–SO_3^- where it is not clear if (an) intermediate compound(s) (e.g., Cys–SO_2^-) may appear and to what extend other side reactions may occur. It is thus important to titrate in stoichiometry the amount of $Na_2S_2O_4$ for the reduction of NPs or other disulfide-containing heme proteins, in order to preserve their disulfides.

A detailed characterization of the ferrous oxidation state of NP4, NP7, and their related site-directed mutant was then carried out. NP4 shows the normal coordination and spin states changes upon reduction with $Na_2S_2O_4$, i.e., 6cHS for Fe^{III} and 5cHS with His as the fifth ligand for Fe^{II}. Surprisingly, in the case of NP7, addition of $Na_2S_2O_4$ lead to two Soret bands in the UV/vis absorbance spectrum at pH 7.5, one of which was attributed to the loss of the proximal His coordination as confirmed from RR. Further studies through pH titration showed that the coordination chemistry of NP7[Fe^{II}] strongly depends on the pH as indicated in Figure 3 .

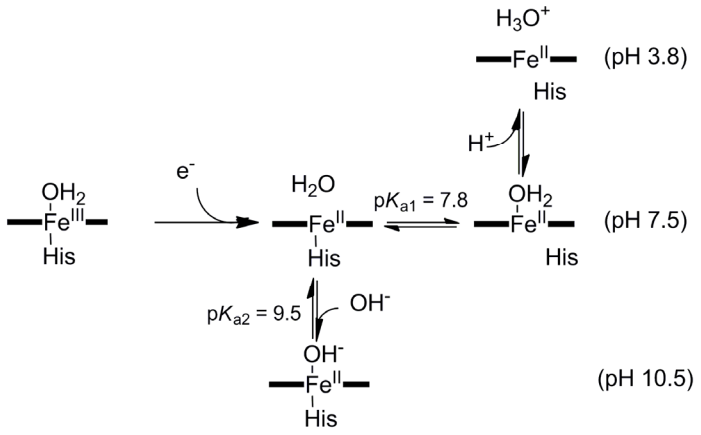

Figure 3. Effect of one-electron reduction on the coordination environment of the heme iron in NP7 at different pHs.

In order to understand the molecular mechanism for the loss of His coordination in the case of NP7[Fe^{II}] at neutral pH, various heme pocket mutant proteins, i.e., NP4(D70A), NP2(V24E), NP7(E27V), and NP7(E27Q) as well as the NP7 reconstituted with symmetric heme ($NP7_{sym}$) were studied by UV/vis and RR. The steric tension of the neighboring side chains from the Glu27 and Phe43 was identified to be responsible for the loss of the proximal His ligand in NP7[Fe^{II}].(Figure 4A).Thus, in the case of the very dense arrangement in the heme pocket of NP7, the Glu27 residue, but also Gln27 in NP7(E27Q), together with Phe43 put a strain on the proximal His, which is responsible for the bond breakage. This is supported by the exchange of Glu27 with Val, which abolishes this behavior. In addition, Glu27 also puts strain on the heme cofactor that is mediated through the heme vinyls, so that even in the absence of the Phe, insertion of the Glu residue can force the Fe–His bond breakage, as is shown with NP2(V24E)[Fe^{II}–NO]. Similarly, removal of the heme vinyls in NP7, i.e., $NP7_{sym}$, breaks the bond easier than NP7(E27V), but is more stable than *wt* NP7. Hence, the proteins may be arranged NP7 ≈ NP7(E27Q) < NP2(V24E) ≈ $NP7_{sym}$ < NP7(E27V) < NP4 ≈ NP4(D70A) with respect to the Fe^{II}–$His_{proximal}$ stability.

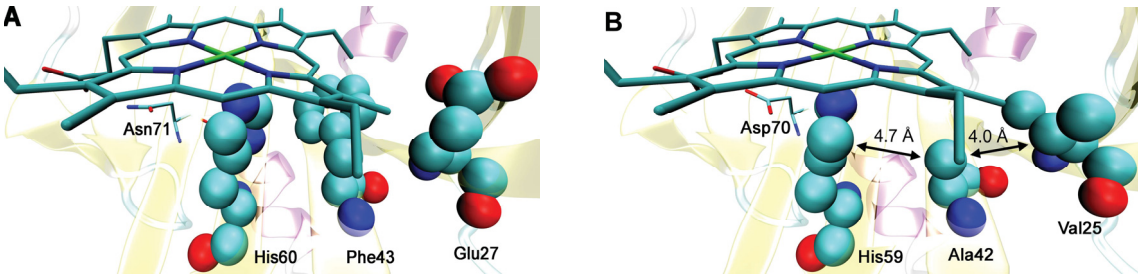

Figure 4. Representation of the spatial arrangement of the proximal heme site in (A) NP7 (homology model) and (B) NP4 (PDB code 1NP4). Reprinted with permission from He, C., Neya, S., Knipp, M. Biochemistry 2011, 50, 8559-8575. Copyright 2011 American Chemical Society.

8.4. Concluding remarks

NPs, apparent from this thesis work, are far more than just NO-transport proteins. It was shown for the first time that NPs facilitate the nitrite disproportionation reaction at neutral pH, which indicates that NPs can not only transport NO, but also may be able to produce NO once in the blood. This further expands the very diverse chemistry of heme models and proteins. It was also concluded that Asp30 may serve as a proton donor for the nitrite disproportionation reaction. The mutant protein NP4(L130R) that was generated in order to insert an H-bonding residue into the distal heme pocket, shows a very unique 6c heme in the X-ray crystal structure recorded at 100 K. This was attributed to the photoreduction by the X-ray irradiation leading to Fe^{II}, which coordinates an imine ligand much easier compared to Fe^{III}. NP4(L130R) represents the first example of an Arg coordination to a metalloporphyrin. However, the study puts the stability of crystals of ferric heme proteins against photoreduction into serious question. The studies on the ferrous oxidation state of NPs show that the routinely used reducing agent $Na_2S_2O_4$ may break the disulfide of NPs, thus it is important to use the stoichiometric amounts of $Na_2S_2O_4$ for iron reduction. The ferroheme NPs are extremely O_2 sensitive and should, therefore, be handled with care. Moreover, the very unique property of the heme pocket of NP7 was manifested in the breakage of the proximal Fe-His bond upon reduction of the Fe^{III} to Fe^{II}. There are only very few examples of His coordinated heme proteins show this be-

havior. In the case of the ferroheme protein soluble guanylate cyclase (sGC), which is the key sensor for NO in mammals, the Fe^{II}-His bond breaks upon NO binding and, thus initiates signal transduction. Unfortunately, the structure of sGC is not available and the mechanism by which the Fe^{II}-His is cleaved is not fully understood. Besides the negative *trans* effect of NO, the present study shows that steric tension may also play an important role in that event. Finally, the characterization of the ferroheme NPs is currently used as an important prerequisite information in understanding the kinetics of ultra-fast laser flash photolysis experiments of NP[Fe^{II}-CO].

8.5. References

1. Ribeiro, J. M. C., Hazzard, J. M., Nussenzveig, R. H., Champagne, D. E., and Walker, F. A. (1993) Reversible binding of nitric oxide by a salivary heme protein from a bloodsucking insect, *Science 260*, 539-541.
2. Nienhaus, K., Maes, E. M., Weichsel, A., Montfort, W. R., and Nienhaus, G. U. (2004) Structural dynamics controls nitric oxide affinity in nitrophorin 4, *J. Biol. Chem. 279*, 39401-39407.
3. Benabbas, A., Ye, X., Kubo, M., Zhang, Z., Maes, E. M., Montfort, W. R., and Champion, P. M. (2010) Ultrafast dynamics of diatomic ligand binding to nitrophorin 4, *J. Am. Chem. Soc. 132*, 2811-2820.
4. Maes, E. M., Roberts, S. A., Weichsel, A., and Montfort, W. R. (2005) Ultrahigh resolution structures of nitrophorin 4: Heme distortion in ferrous CO and NO complexes, *Biochemistry 44*, 12690-12699.
5. Ribeiro, J. M. C. (1996) Salivary thiol oxidase activity of *Rhodnius prolixus*, *Insect Biochem. Mol. Biol. 26*, 899-905.
6. Wanat, A., Gdula-Argasińska, J., Rutkowska-Żbik, D., Witko, M., Stochel, G., and van Eldik, R. (2002) Nitrite binding to metmyoglobin and methemoglobin in comparison to nitric oxide binding, *J. Biol. Inorg. Chem. 7*, 165-176.
7. Andersen, J. F., Ding, X. D., Balfour, C., Shokhireva, T. K., Champagne, D. E., Walker, F. A., and Montfort, W. R. (2000) Kinetics and equilibria in ligand binding by nitrophorins 1-4: Evidence for stabilization of a nitric oxide-ferriheme complex through a ligand-induced conformational trap, *Biochemistry 39*, 10118-10131.
8. Gudderra, N. P., Ribeiro, J. M. C., and Andersen, J. F. (2005) Structural determination of factor IX(a) binding in nitrophorin 2, a lipocalin inhibitor of the intrinsic coagulation pathway, *Journal of Biological Chemistry 280*, 25022-25028.
9. Andersen, J. F., Gudderra, N. P., Francischetti, I. M. B., Valenzuela, J. G., and Ribeiro, J. M. C. (2004) Recognition of anionic phospholipid membranes by an antihemostatic protein from a blood-feeding insect, *Biochemistry 43*, 6987-6994.
10. Andersen, J. F., Gudderra, N. P., Francischetti, I. M. B., and Ribeiro, J. M. C. (2005) The role of salivary lipocalins in blood feeding by *Rhodnius prolixus*, *Archives of Insect Biochemistry & Physiology 58*, 97-105.
11. Nasri, H., Wang, Y., Huynh, B. H., Walker, F. A., and Scheidt, W. R. (1991) Reactions of bis(nitro)($\alpha,\alpha,\alpha,\alpha$-tetrakis(*o*-pivalamidophenyl)porphinato)ferrat(III) with pyridine and imidazole. EPR and Mössbauer spectra and molecular structures of the mixed-ligand species, *Inorg. Chem. 30*, 1483-1489.

12. Williams, P. A., Fülöp, V., Garman, E. F., Saunders, N. F. W., Ferguson, S. J., and Hajdu, J. (1997) Haem-ligand switching during catalysis in crystals of a nitrogen-cycle enzyme, *Nature 389*, 406-412.
13. Einsle, O., Messerschmidt, A., Huber, R., Kroneck, P. M. H., and Neese, F. (2002) Mechanism of the six-electron reduction of nitrite to ammonia by cytochrome *c* nitrite reductase, *J. Am. Chem. Soc. 124*, 11737-11745.
14. Crane, B. R., Siegel, L. M., and Getzoff, E. D. (1997) Probing the catalytic mechanism of sulfite reductase by X-ray crystallography: Structures of the *Escherichia coli* hemoprotein in complex with substrates, inhibitors, intermediates, and products, *Biochemistry 36*, 12120-12137.
15. Yi, J., Safo, M. K., and Richter-Addo, G. B. (2008) The nitrite anion binds to human hemoglobin via the uncommon *O*-nitrito mode, *Biochemistry 47*, 8247-8249.
16. Copeland, D. N., Soares, A. S., West, A. H., and Richter-Addo, G. B. (2006) Crystal structures of the nitrite and nitric oxide complexes of horse heart myoglobin, *J. Inorg. Biochem. 100*, 1413-1425.
17. Yi, J., Heinecke, J., Tan, H., Ford, P. C., and Richter-Addo, G. B. (2009) The distal pocket histidine residue in horse heart myoglobin directs the O-binding mode of nitrite to the heme iron, *J. Am. Chem. Soc. 131*, 18119-18128.
18. Goblirsch, B. R., Streit, B. R., DuBois, J. L., and Wilmot, C. M. (2010) Structural features promoting dioxygen production by *Dechloromonas aromatica* chlorite dismutase, *J. Biol. Inorg. Chem. 15*, 879-888.
19. He, C., Ogata, H., and Knipp, M. (2010) Formation of the complex of nitrite with the ferriheme *b* β-barrel proteins nitrophorin 4 and nitrophorin 7, *Biochemistry 49*, 5841-5851.
20. Menyhárd, D. K., and Keserü, G. M. (2005) Proteonation state of Asp30 exerts crucial influence over surface loop rearrangements responsible for NO release in nitrophorin 4, *FEBS Lett. 579*, 5392-5398.
21. Weichsel, A., Andersen, J. F., Roberts, S. A., and Montfort, W. R. (2000) Nitric oxide binding to nitrophorin 4 induces complete distal pocket burial, *Nat. Struc. Biol. 7*, 551-554.
22. Swails, J. M., Meng, Y., Walker, F. A., Martí, M. A., Estrin, D. A., and Roitberg, A. E. (2009) pH-dependent mechanism of nitric oxide release in nitrophorin 2 and 4, *J. Phys. Chem. B 113*, 1192-1201.
23. Samouilov, A., Kuppusamy, P., and Zweier, J. L. (1998) Evaluation of the magnitude and rate of nitric oxide production from nitrite in biological systems, *Arch. Biochem. Biophys. 375*, 1-7.
24. Finnegan, M. G., Lappin, A. G., and Scheidt, W. R. (1990) Instability of the nitrite/iron(III) porphyrinate system, *Inorg. Chem. 29*, 181-185.

25. Fernandez, B. O., and Ford, P. C. (2003) Nitrite catalyzes ferriheme protein reductive nitrosylation, *J. Am. Chem. Soc. 125*, 10510-10511.

26. Barley, M. H., Rhodes, M. R., and Meyer, T. J. (1987) Electrocatalytic reduction of nitrite to nitrous oxide and ammonia based on the N-methylated, cationic iron porphyrin complex [FeIII(H2O)(TMPyP)]5+, *Inorg. Chem. 26*, 1746-1750.

27. Barley, M. H., and Meyer, T. J. (1986) Electrocatalytic reduction of nitrite to ammonia based on a water-soluble iron porphyrin, *J. Am. Chem. Soc. 108*, 5876-5885.

28. Hoshino, M., Ozawa, K., Seki, H., and Ford, P. C. (1993) Photochemistry of nitric oxide adducts of water-soluble iron(III) porphyrin and ferrihemoproteins studied by nanosecond laser photolysis, *J. Am. Chem. Soc. 115*, 9568-9575.

29. Hoshino, M., Maeda, M., Konishi, R., Seki, H., and Ford, P. C. (1996) Studies on the reaction mechanism for reductive nitrosylation of ferrihemoproteins in buffer solutions, *J. Am. Chem. Soc. 118*, 5702-5707.

30. Ding, X. D., Weichsel, A., Andersen, J. F., Shokhireva, T. K., Balfour, C., Pierik, A. J., Averill, B. A., Montfort, W. R., and Walker, F. A. (1999) Nitric oxide binding to the ferri- and ferroheme states of nitrophorin 1, a reversible NO-binding heme protein from the saliva of the blood-sucking insect, *Rhodnius prolixus*, *J. Am. Chem. Soc. 121*, 128-138.

31. Berry, R. E., Shokhireva, T. K., Filippov, I., Shokhirev, M. N., Zhang, H., and Walker, F. A. (2007) The effect of the N-terminus on heme cavity structure, ligand equilibrium and rate constants and reduction potentials of nitrophorin 2 from *Rhodnius prolixus*, *Biochemistry 46*, 6830-6843.

32. Berry, R. E., Ding, X. D., Shokhireva, T. K., Weichsel, A., Montfort, W. R., and Walker, F. A. (2004) Axial ligand complexes of the *Rhodnius* nitrophorins: Reduction potentials, binding constants, EPR spectra, and structures of the 4-iodopyrazole and imidazole complexes of NP4, *J. Biol. Inorg. Chem. 9*, 135-144.

33. Berry, R. E., Shokhirev, M. N., Ho, A. Y. W., Yang, F., Shokhireva, T. K., Zhang, H., Weichsel, A., Montfort, W. R., and Walker, F. A. (2009) Effect of mutation of carboxyl side-cahin amino acids near the heme on the midpoint potentials and ligand binding constants of nitrophorin 2 and its NO, histamine, and imidazole complexes, *J. Am. Chem. Soc. 131*, 2313-2327.

34. Knipp, M., Yang, F., Berry, R. E., Zhang, H., Shokhirev, M. N., and Walker, F. A. (2007) Spectroscopic and functional characterization of nitrophorin 7 from the blood-feeding insect *Rhodnius prolixus* reveals an important role of its isoform-specific N-terminus for proper protein function, *Biochemistry 46*, 13254-13268.

35. Lehnert, N., and Scheidt, W. R. (2010) Preface for the Inorganic Chemistry Forum: The Coordination Chemistry of Nitric Oxide and Its Significance for Metabolism, Signaling, and Toxicity in Biology, *Inorg. Chem. 49*, 6223-6225.

36. Fuchs, M., Meyer, F., and Ryde, U. A combined computational and experimental investigation of the [2Fe-2S] cluster in biotin synthase, *J. Biol. Inorg. Chem. 15*, 203-212.

37. Berkovitch, F., Nicolet, Y., Wan, J. T., Jarrett, J. T., and Drennan, C. L. (2004) Crystal Structure of Biotin Synthase, an S-Adenosylmethionine-Dependent Radical Enzyme, *Science 303*, 76-79.

38. Knipp, M., and He, C. (2011) Nitrophorins: Nitrite disproportionation reaction and other novel functionalities of insect heme-based nitric oxide transport proteins, *IUBMB Life 63*, 304-312.

Abbreviations

NO	Nitric Oxide	NPs	Nitrophorins
His	Histidine	Cys	Cysteine
AGP	α_1-Acid glycoprotein	ApoD	Apolipoprotein D
C8γ	Complement factor 8γ	GLY	Glycodelin
α_1m	α_1-Microglobulin	NGAL	Neutrophil gelatinase-associated lipocalin
OBP	Odorant-binding protein	PGDS	Lipocalin type prostaglandin D synthase
RBP	Retinol-binding protein	Tlc	Tear lipocalin
NOS	Nitric oxide synthase	Mb	Myoglobin
Hb	Hemoglobin	SHE	Standard hydrogen electrode
cyt c	Cytochrome c	sGC	Soluble guanylate cyclase
IR	Infrared	RR	Resonance Raman
OEP	Octaethylporphyrin	TPP	Tetraphenylporphyrin
AXCP	*Alcaligenes xylosoxidans* cytochrome *c*'	hHO	Human heme oxygenase-1
FixLH	the heme-binding domains of *Bradyhizobium japonicum* FixL	HRP	Horse radish peroxidase
NaR	Nitrate reductase	NiR	Nitrite reductase
NoR	Nitric oxide reductase	N_2OR	Nitrous oxide reductase
DFT	Density functional theory	Cld	Chlorite dismutase
RBC	Red blood cell	OAT	Oxygen atom transfer
TPPTS	3,3′,3″- Phosphinidynetris (benzenesulfonic acid) trisodium	DMS	Dimethyl sulfide

Abbreviation

GSH	Glutathione	EPR	Electron paramagnetic resonance
ppIX	Protoporphyrin IX	LUMO	Lowest unoccupied molecular orbital
HUMO	Highest occupied molecular orbital	CYP_{450}	Chytochrome P_{450}
6c	Six coordinate	5c	Five coordinate
HS	High spin	LS	Low spin
GADPH	Glyceraldehyde-3-phosphate dehydrogenase	cGMP	Guanosine 3', 5'-cyclic monophosphate
SiR	Sulfite reductase	cd_1 NiR	Cytochrome cd_1 nitrite reductase
TTP	Tetratolylporphyrin	OEP	Ocatethylporphyrin
TpivPP	*meso*-α,α,α,α-tetrakis(*o*-pivalamidophenyl) porphyrin	Py	Pyridine
ImH	Imidazole		

Appendix: Collections of PDB files of nitrophorins

PDB	Nitrophorin	Ligand	Cryst. Cond.	Space Group	Res.	Ref.
1D2U	NP4	NH_3	3.0 M Ammonium phosphate, 10 mM Tris-HCl, pH 7.5,	C(121)	1.15	Biochemistry 2001, 40, 11327-11337.
1D3S	NP4	H_2O	23% PEG 4000 20 mM Sodium citrate PH 5.6	C(121)	1.40	Nat.Struct.Mol.Biol. 2000, 7, 551-554.
1EQD	NP4	CN	PEG 4000, Sodium citrate, pH 5.6	C(121)	1.60	Nat.Struct.Mol.Biol. 2000, 7, 551-554.
1ERX	NP4	NO	PEG 4000, Sodium citrate, pH 5.6	C(121)	1.40	Nat.Struct.Mol.Biol. 2000, 7, 551-554.
1EUO	NP2	NH_3	Ammonium phosphate, Tris-HCl, pH 7.7	$P(2_1\ 2_1\ 2)$	2.00	J.Biol.Chem. 2000, 275, 30496-30503.
1IKE	NP4	Hm	PEG4000, Sodium citrate, pH 5.6	C(121)	1.50	Biochemistry 2001, 40, 11327-11337.
1IKJ	NP4	ImH	PEG-4000, Sodium citrate, pH 5.60	C(121)	1.27	Biochemistry 2001, 40, 11327-11337.
1KOI	NP4	NO	PEG 4000, Sodium Citrate, pH 5.6	C(121)	1.08	Biochemistry 2001, 40, 11327-11337.
1ML7	NP4	4-iodopyrazole	Ammonium phosphate, pH 7.5	C(121)	1.25	J.Biol.Inorg.Chem. 2004, 9, 135-144.
1NP1	NP1	Hm	2.8 M Ammonium phosphate, 0.1 M Tris.HCl, pH 7.5	$P(1\ 2_1\ 1)$	2.00	Nat.Struct.Mol.Biol. 1998, 6, 304-309.
1NP4	NP4	NH_3	2.8 M Ammonium phosphate, 0.1 M Nacacodylate, pH 5.6 (Final pH 7.5)	C(121)	1.50	Structure 1998, 6, 1315-1327.
1PEE	NP2	ImH	1.6 M sodium citrate, pH 6.5	$P(4_1\ 2_1\ 2)$	1.50	N/A
1PM1	NP2(L122V/L132V)	ImH	Sodium citrate, pH 6.5	$P(2_1\ 2_1\ 2)$	1.10	N/A
1SXU	NP4(D30N)	ImH	PEG 4000, pH 5.6	C(121)	1.40	Biochemistry 2004, 43, 6679-6690.
1SXW	NP4(D30A)	NO	Ammonium Phosphate 3.2 M, pH 5.6	C(121)	1.05	Biochemistry 2004, 43, 6679-6690.
1SXX	NP4(D129A/L130A)	NO	Ammonium Phosphate 3.2 M, pH 5.6	C(121)	1.01	Biochemistry 2004, 43, 6679-6690.
1SXY	NP4(D30N)	NH_4	Ammonium Phosphate 3.2 M, pH 7.5	C(121)	1.07	Biochemistry 2004, 43, 6679-6690.

1SY0	NP4(T121V)	NH_4	Ammonium Phosphate 3.2 M, pH 7.5	C(121)	1.15	Biochemistry 2004, 43, 6679-6690.
1SY1	NP4(T121V)	NO	Ammonium Phosphate 3.2 M, pH 5.6	C(121)	1.01	Biochemistry 2004, 43, 6679-6690.
1SY2	NP4(D129A/L130A)	NH_4	Ammonium Phosphate 2.8 M, pH 7.0	C(121)	1.00	Biochemistry 2004, 43, 6679-6690.
1SY3	NP4(D30N)	NO	Ammonium Phosphate 3.2 M, pH 5.6	C(121)	1.00	Biochemistry 2004, 43, 6679-6690.
1T68	NP2	NO	Sodium citrate, pH 7.5	$P(2_1\ 2_1\ 2)$	1.45	N/A
1U0X	NP4	Xe, NH_3	ammonium phosphate, pH 7.5	C(121)	1.45	J.Biol.Chem. 2004, 279, 39401-39407
1U17	NP1(H60C)	ImH	0.1 M potassium cacodylate pH 5.3, 2.9 M di-ammoium hydrogen phospate, pH 7.5	$P(1\ 2_1\ 1)$	1.70	N/A
1U18	NP1(H60C)	Hm	0.1 M potassium cacodylate, 2.9 M di-ammonium hydrogen phosphate, pH 7.5	$P(1\ 2_1\ 1)$	1.96	N/A
1X8N	NP4	NO	Ammonium phosphate, pH 7.4	C(121)	1.08	Biochemistry 2004, 43, 13637-13647.
1X8O	NP4	NO	Ammonium phosphate, pH 5.6	C(121)	1.01	Biochemistry 2004, 43, 13637-13647.
1X8P	NP4	NH_3	Ammonium phosphate, pH 7.4	C(121)	0.85	Biochemistry 2004, 43, 13637-13647.
1X8Q	NP4	H_2O	PEG 4000, Sodium citrate, pH 5.6	C(121)	0.85	Biochemistry 2004, 43, 13637-13647.
1YWA	NP4[Fe^{II}]	CO	2.8 M Ammonium phosphate, pH 5.6	C(121)	0.89	Biochemistry 2005, 44, 12690-12699.
1YWB	NP4[Fe^{II}]	NO	2.8 M Ammonium phosphate, pH 5.6	C(121)	0.97	Biochemistry 2005, 44, 12690-12699.
1YWC	NP4[Fe^{II}]	CO	2.8 M Ammonium phosphate, pH 7	C(121)	1.00	Biochemistry 2005, 44, 12690-12699.
1YWD	NP4[Fe^{II}]	H_2O	2.8 M Ammonium phosphate, pH 7.5	C(121)	1.08	Biochemistry 2005, 44, 12690-12699.
2A3F	NP2	H_2O	Sodium citrate, pH 6.5	$P(2_1\ 2_1\ 2)$	1.40	N/A
2ACP	NP2	H_2O	Sodium citrate, pH 6.5	$P(2_1\ 2_1\ 2)$	1.40	N/A
2AH7	NP2	H_2O	Sodium citrate, pH 6.5	$P(4_1\ 2_1\ 2)$	1.70	N/A
2AL0	NP2[Fe^{II}]	H_2O	Sodium citrate, pH 6.5	$P(4_1\ 2_1\ 2)$	1.60	N/A

2ALL	NP2(L122V/L132V)	H_2O	Sodium citrate, pH 6.5	$P(2_1\ 2_1\ 2)$	1.47	N/A
2AMM	NP2(L122V/L132V)	H_2O	Sodium citrate, pH 6.5	$P(4_1\ 2_1\ 2)$	1.90	N/A
2ASN	NP2(D1A)	ImH	Sodium citrate, pH 6.5	$P(4_1\ 2_1\ 2)$	1.70	N/A
2AT0	NP4(L133V)	NO	Ammonium phosphate, pH 5.6	C(121)	1.00	N/A
2AT3	NP4(L123V/L133V) NP4	ImH	Ammonium phosphate, imidazole, pH 5.6	C(121)	1.00	N/A
2AT5	Deuteroporphyrin IX NP4	NO	Ammonium phosphate, pH 5.6	C(121)	1.22	N/A
2AT6	Deuteroporphyrin IX NP4 2,4 Dimethyl	H_2O	Ammonium phosphate, pH 5.6	C(121)	1.22	N/A
2AT8	Deteroporphyrin IX	NO	Ammonium phosphate, pH 5.6	C(121)	1.00	N/A
2EU7	NP2(D1A)	NH_3	3.2M Ammonium phosphate, 100mM Tris HCl, pH 7.5	$P(2_1\ 2_1\ 2)$	1.20	N/A
2GTF	NP2	pyrimidine	Sodium citrate, pH 6.5	$P(4_1\ 2_1\ 2)$	1.40	N/A
2HYS	NP2	CN	89% saturated sodium citrate, 100 mM hepes, pH 7.5	$P(4_1\ 2_1\ 2)$	1.20	Inorg.Chem. 2007, 46, 2041-2056.
2NP1	NP1	NH_4	2.8 M Ammonium phosphate, 100mM Tris HCl, pH 7.5	$P(1\ 2_1\ 1)$	2.00	Nat.Struct.Mol.Biol.1998, 5, 304-399.
2OFM	Apo NP 4 NP4	--	Ammonium sulfate, pH 5.6	C(121)	1.11	Protein Sci. 2007, 16, 2076-2681.
2OFR	(V36A/D129A/L130A)	NO	Ammonium phosphate, pH 5.6	C(121)	1.00	N/A
3C76	NP4(L133V) NP4	NH_3	Ammonium phosphate, pH 7.50	C(121)	1.07	N/A
3C77	deuteroporphyrin ix NP4 2,4 dimethyl	NH_3	Ammonium phosphate, pH 7.50	C(121)	1.08	N/A
3C78	deuteroporphyrin ix	NH_3	Ammonium phosphate, pH 7.50	C(121)	0.98	N/A

Appendix

3FLL	NP4(E55Q)	NH_3	Ammonium phosphate, pH 5.6	C(121)	1.50	J.Am.Chem.Soc. 2009, 131, 2313-2327.
3MVF	NP4	NO_2^-	Ammonium phosphate, pH 7.4	C(121)	1.40	Biochemistry 2010, 49, 5481-5451.
3NP1	NP1	CN	2.8 M Ammonium phosphate, 0.1 M Tric.HCl, pH 7.5	P(1 2_1 1)	2.30	Nat.Struct.Mol.Biol. 1998, 5, 304-309.
4NP1	NP1	NO	2.8 M Ammonium phosphate, 0.1 M Tric.HCl, pH 7.5	P(1 2_1 1)	2.30	N/A
3V02	NP4(D70A)	NH_3	Ammonium phosphate, pH 7.4	*C*2	1.50	Submitted for publication
3TGA	NP4(L130R)	H_2O	Ammonium phosphate, pH 7.4	*C*2	1.30	Submitted for publication
3TGB	NP4(L130R)	ImH	Ammonium phosphate, pH 7.4	*C*2	1.40	Submitted for publication
3TGC	NP4(L130R)	NO_2^-	Ammonium phosphate, pH 7.4	*C*2	1.40	Submitted for publication

List of publications

1) Published work

Chunmao He, Saburo Neya, Markus Knipp

Breaking of Proximal Fe-His Bond in Heme Proteins through Local Structural Tension: Lessons From the Heme *b* Proteins Nitrophorin 4/7 and Related Site-Directed Mutant Proteins.

Biochemistry, **2011**, *50*, 8559-8575.

Markus Knipp, Johanna J. Taing, Chunmao He

Reduction of the Lipocalin Type Heme Containing Protein Nitrophorin - Sensitivity of the Fold-Stabilizing Cysteine Disulfides.

J. Inorg. Biochem. **2011**, *105*, 1405-1412.

Markus Knipp, Chunmao He

Nitrophorins: Nitrite Disproportionation Reaction and Other Novel Functionalities of Insect Heme-Based Nitric Oxide Transport Proteins.

IUBMB Life, **2011**, *63*, 304-312.

Chunmao He, Hideaki Ogata, Markus Knipp

Formation of the Complex of Nitrite with the Ferriheme *b* β-Barrel Proteins Nitrophorin 4 and Nitrophorin 7.

Biochemistry, **2010**, *49*, 5841-5851.

Chunmao He, Markus Knipp

Formation of Nitric Oxide from Nitrite by the Ferriheme *b* Protein Nitrophorin 7.

J. Am. Chem. Soc., **2009**, *131*, 12042-12043.

2) Submitted manuscripts

Chunmao He, Martin Fuchs, Hideaki Ogata, Markus Knipp

Guanidine-Iron Coordination in a Heme Protein: Crystallographic and Spectroscopic Characterization of the L130R Mutant of Nitrophorin 4 from *Rhodnius prolixus*.

2011, *Submitted*.

Chunmao He, Hideaki Ogata, Markus Knipp

Insertion of an H-Bonding Residue into the Distal Pocket of the Ferriheme Protein Nitrophorin 4: Effect on Nitrite–Iron Coordination and Nitrite Disproportionation.

2011, *Submitted.*

3) Conference proceedings

Chunmao He, Hideaki Ogata, Markus Knipp

The Interaction between the Ferriheme Protein Nitrophorin and Nitrite.

Proceedings of the 10th European Biological Inorganic Chemistry Conference, 2010, Thessaloniki, Greece.

Markus Knipp, Chunmao He, Hideaki Ogata

P48. Nitrite disproportionation reaction: Investigations on the mechanism of the conversion of nitrite into nitric oxide at the ferriheme center of nitrophorins at blood plasma pH.

Approaching the Clinic: Nitrite and Nitrate Pathophysiology and Therapy, 2011, Atlanta, Georgia.

Nitric Oxide, **2011**, *24, Supplement*, S33-S34.

Curriculum Vitae

CHUNMAO HE
Max-Planck-Institut für Bioanorganische Chemie
Stiftstrasse 34 - 36 / D - 45470 Mülheim an der Ruhr, Germany
Email: he@mpi-muelheim.mpg.de
Tel : +49 (0)208 306 3684

Education

09/08 – 12/11 **MAX PLANCK INSTITUTE FOR BIOINORGANIC CHEMISTRY** **MUELHEIM/GERMANY**
PhD in Chemistry. Thesis under the guidance of Dr. Markus Knipp and Prof. Dr. Wolfgang Lubitz.

09/05 – 07/08 **GUANGZHOU INSTITUTE OF CHEMISTRY, CHINESE ACADEMY OF SCIENCES** **P.R.CHINA**
Master of Science in Organic Chemistry, Jul 2008. Thesis under the guidance of Prof. Dr. Dongliang Chang.

09/01 – 07/05 **TAIYUAN UNIVERSITY OF TECHNOLOGY** **P.R.CHINA**
Bachelor of Engineering in Pharmaceutical Engineering, Jul 2005.

Publication

1. Chunmao He, Hideaki Ogata, Markus Knipp. Insertion of an H-Bonding Residue into the Distal Pocket of the Ferriheme Protein Nitrophorin 4: Effect on Nitrite–Iron Coordination and Nitrite Disproportionation. **2011**, Submitted.

2. Chunmao He, Martin Fuchs, Hideaki Ogata, Markus Knipp. Guanidine-Iron Coordination in a Heme Protein: Crystallographic and Spectroscopic Characterization of the L130R Mutant of Nitrophorin 4 from Rhodnius prolixus. **2011**, Submitted.

3. Chunmao He, Saburo Neya, Markus Knipp. Breaking of Proximal Fe-His Bond in Heme Proteins Through Local Structural Tension: Lessons From the Heme *b* Proteins Nitrophorin 4/7 and Related Site-Directed Mutant Proteins. *Biochemistry*, **2011**, *50*, 8559-8575.

4. Markus Knipp, Johanna J. Taing, Chunmao He. Reduction of the Lipocalin Type Heme Containing Protein Nitrophorin - Sensitivity of the Fold-Stabilizing Cysteine Disulfides. *J. Inorg. Biochem*. **2011**, *105*, 1405-1412.

5. Markus Knipp, Chunmao He. Nitrophorins: Nitrite Disproportionation Reaction and Other Novel Functionalities of Insect Heme-Based Nitric Oxide Transport Proteins. *IUBMB Life*, **2011**, *63*, 304-312.

6. Chunmao He, Hideaki Ogata, Markus Knipp. Formation of the Complex of Nitrite with the Ferriheme *b* β-Barrel Proteins Nitrophorin 4 and Nitrophorin 7. *Biochemistry*, **2010**, *49*, 5841-5851.

7. Chunmao He, Markus Knipp, Formation of Nitric Oxide from Nitrite by the Ferriheme *b* Protein Nitrophorin 7, *J. Am. Chem. Soc.*, **2009**, *131*, 12042-12043.

8. Chunmao He, Dongliang Chang, Jie Zhang, Asymmetric synthesis of both enantiomers of ethyl-2-hydroxy-4-phenylbutanoate, *Fine Chemicals*, **2008**, *25*, 115-118.

9. Chunmao He, Dongliang Chang, Jie Zhang, Biocatalysis method for preparing high-optical activity enantiomers of ethyl 4-cyano-3-hydroxybuturate. Chinese Patent CN 101260415 A.

10. Chunmao He, Dongliang Chang, Jie Zhang, Asymmetric reduction of α- and β-ketoesters by *B. pumilus* Phe-C3, *Tetrahedron Asymmetry*, **2008**, *19*, 1347-1351.

Conference attendance

1. Towards the Mechanism of Nitrite Disproportionation at the Ferriheme Center of Nitrophorin
   15th International Conference on Biological Inorganic Chemistry. **2011**. Vancouver.
   Oral presentation

2. Spectroscopy and X-ray crystallography on the nitrite complexes of the ferriheme protein nitrophorin 4 and site-directed mutants.
   International Symposium on "Advanced EPR Spectroscopy on Biomolecules". **2011**. Mülheim.
   Poster

3. Spectroscopic characterization of the complexes between the ferriheme *b* protein nitrophorin and nitrite
   Annual meeting of the German Biophysics Society. **2010**. Bochum.
   Poster

4. Structure induced modulation of the His:N_{ε}-Fe(II) bond in Nitrophorins
   Annual meeting of the German Biophysics Society. **2010**. Bochum.
   Poster

5. Structural features required for protein-based sensing of nitric oxide - insight from spectroscopic investigations of ferrous nitrophorins
   1st BioStruct MasterClass 2010 “Approaches to determine Protein Structures”. **2010**. Düsseldorf.
   Oral presentation

6. The interaction of nitrite with the ferriheme *b* Protein nitrophorin from the blood-sucking insect *Rhodnius prolixus*.
   10th European Biological Inorganic Chemistry Conference. **2010**. Thessaloniki.
   Poster

7. The reaction of nitrite with the ferriheme *b* Protein nitrophorin from the blood-sucking insect *Rhodnius prolixus*.
   FEBS COMBINED PRACTICAL AND LECTURE COURSE: Chemistry of Metals in Biological Systems. **2009**. Louvain-la-Neuve.
   Poster

8. Toward the understanding of the reaction mechanism of nitrophorin 7 and nitrite.
   11thJCF-Frühjahrssymposium **2009**. Essen.
   Poster

9. Asymmetric reduction of α- and β-ketoesters by *B. pumilus* Phe-C3.
   2nd International Symposium on Chemical and Molecular Sciences **2008**. Zürich.
   Oral presentation

10. Synthetic application of new bacterial alcohol dehydrogenases for asymmetric reduction of β-ketoesters containing cyano group.
    3rd International Symposium on Bioenergy and Bioprocess Engineering **2007**. Shanghai.
    Poster

Awards

1. 2010 Chinese Government Scholarship for Outstanding Self-financed Students Studying Abroad

2. 2008 First-Class Postgraduate Scholarship, Guangzhou Institute of Chemistry, Chinese Academy of Sciences